

**Detection and Imaging of 2-100 keV X-rays and Thermal
Neutrons**

Thesis submitted for the degree of
Doctor of Philosophy
at the University of Leicester

by

Okla Saleh Al-Horayess, B.Sc M.Sc. (SA)
Department of Physics and Astronomy
University of Leicester

April 1997

UMI Number: U095807

All rights reserved

INFORMATION TO ALL USERS

The quality of this reproduction is dependent upon the quality of the copy submitted.

In the unlikely event that the author did not send a complete manuscript and there are missing pages, these will be noted. Also, if material had to be removed, a note will indicate the deletion.



UMI U095807

Published by ProQuest LLC 2013. Copyright in the Dissertation held by the Author.
Microform Edition © ProQuest LLC.

All rights reserved. This work is protected against
unauthorized copying under Title 17, United States Code.



ProQuest LLC
789 East Eisenhower Parkway
P.O. Box 1346
Ann Arbor, MI 48106-1346

بِسْمِ اللّٰهِ الرَّحْمٰنِ الرَّحِیْمِ

﴿وَقَضَىٰ رَبُّكَ أَلَّا تَعْبُدُوا إِلَّا إِيَّاهُ وَبِالْوَالِدَيْنِ إِحْسَاتًا...﴾

(*And your Lord has decreed that you worship none but Him.
And that you be dutiful to your parents...*)

The Holy Quran: Surah 17, Ver. 23.

...To My Parents

Acknowledgement

Foremost, I would like to thank my supervisors Dr. Martin Turner and Dr. George Fraser, and gratefully acknowledge the guidance, support, encouragement, and valuable comments they gave me during the period of my research.

Many thanks also go to my colleagues in the XRA group, in particular Dr. J. Pearson for his co-operation. I would also like to thank Professor K. Pounds and Professor M. Ward for permitting use of the XRA group research facilities. Thanks to the technical staff, for their prompt technical support, in particular, Mr. J. Spragg, Mr. M. Waterman, and Mr. V. Brooksbank. It is pleasant duty to thank all other friends in Leicester, but with special thanks to Abdul-Wahid Saif and Aamer Bhatti. Many thanks also go to Dr. B. Ramsey from Marshal Space Flight Center, NASA, USA, who kindly provided the MS plates used in this work.

I gratefully would like to express my sincere thanks to members of my family for being the constant source of happiness and encouragement; to my father who went into God's care during the course of this work, I am sure if he was around he would be the happiest person, but I am happy that I can share the moments of happiness with my mother; to my brother Abdulrahman for his help by taking many responsibilities which enabled me to concentrate on my research; to my wife Hoda Al-Gomaiz for her invaluable patient support.

Finally, I thank King Abdul-Aziz City for Science and Technology (in Riyadh) and the Saudi Cultural Bureau (in London) through which the financial support of my study was provided.

Abstract

This work is concerned with two important types of radiation detectors, proportional counters and microchannel plates. The work on proportional counters, which represents the major part of this thesis, was carried out using a Single Wire Proportional Counter (SWPC) and Microstrip Proportional Counter (MSPC). The behaviour of both of the counters at high gas pressures was investigated using different Xenon-based gas mixtures. The results of measurements using the SWPC and MSPC were presented in terms of gas gain and energy resolution. The measured gas gain was compared with theory using the Diethorn formula. The validity and feasibility of the formula at high pressures were discussed in connection with the experimental measurements. The results showed the importance of the gas filling used and geometry of proportional counters.

The study carried out on the Microchannel Plates (MCPs) introduced a thermal neutron imaging detector based on the use of a combination of standard glass MCPs and gadolinium foil. The measurements of detection efficiency and spatial resolution of the MCP-Gd detector were reported. It was shown that such a combination produces a thermal neutron imaging detector with useful efficiency and good spatial resolution.

CONTENTS

<u>CHAPTER 1: INTRODUCTION.....</u>	<u>1</u>
1.1 IMAGING RADIATION DETECTORS.....	2
1.1.1 Proportional Counters.....	2
1.1.2 Scintillation Detectors.....	16
1.1.3 Microchannel Plates (MCPs).....	19
1.1.4 Semiconductor Detectors.....	20
1.2 SCOPE OF THE THESIS.....	23
1.2.1 Development of Xe-filled SWPC and MSPC at High Pressures.....	23
1.2.2 Thermal Neutron Imaging with MCPs.....	26
1.2.3 Organisation of the Thesis.....	27
<u>CHAPTER 2: PROPORTIONAL COUNTERS.....</u>	<u>29</u>
2.1 OPERATING PRINCIPLES.....	30
2.2 QUANTUM DETECTION EFFICIENCY.....	36
2.3 GAS GAIN.....	38
2.3.1 Gas Gain Formula.....	38
2.3.2 Measuring Gas Gain.....	42
2.4 FLUCTUATION IN THE PULSE HEIGHT.....	43
2.4.1 Fluctuation in Ionisation.....	43
2.4.2 Fluctuation in Gas Gain.....	44
2.4.3 Energy Resolution.....	46
2.5 COUNTER GAS SELECTION.....	48
2.5.1 Quenching Effect.....	49
2.5.2 Penning Mixtures.....	52

2.6 THE EFFECT OF COUNTER GAS PRESSURE.....	53
2.7 MULTI-WIRE PROPORTIONAL COUNTERS.....	55
2.7.1 Graded Density Readout.....	57
2.7.2 Disadvantages of MWPCs.....	58

CHAPTER 3: MICROSTRIP PROPORTIONAL CHAMBERS.....59

3.1 MSPCs DEVELOPMENT.....	59
3.2 OPERATING OF MSPCs.....	60
3.2.1 Electric Field Distribution in MSPCs.....	62
3.2.2 Signal Development.....	63
3.2.3 Substrate Material.....	64
3.3 GAS GAIN IN MSPCs.....	66
3.4 ENERGY RESOLUTION OF MSPCs.....	68
3.5 ADVANTAGES OF MSPCs.....	69

CHAPTER 4: THE EXPERIMENTAL PROCEDURES FOR GAS

DETECTOR EVALUATION.....72

4.1 DETECTOR DESIGN.....	72
4.1.1 The SWPC.....	72
4.1.2 The MSPC.....	74
4.2 GAS MIXTURE SELECTION.....	77
4.3 COUNTER FILL PROCEDURE.....	78
4.4 COUNTING SYSTEM ELECTRONICS.....	80
4.5 COUNTER PERFORMANCE MEASUREMENTS.....	82
4.5.1 Gas Gain Evaluation.....	82
4.5.2 Energy Resolution Evaluation.....	86

CHAPTER 5: RESULTS FROM THE SWPC.....87

5.1 GAS GAIN MEASUREMENTS AT LOW PRESSURE.....	87
5.1.1 Gain in Xe+5%CO ₂	88
5.1.2 Gas Gain in Penning Mixtures.....	89
5.2 GAS GAIN MEASUREMENTS AT HIGH PRESSURES.....	95
5.2.1 Gas Gain in The Xe+5%CO ₂ Mixture.....	95
5.2.2 Gas Gain in The Xe+5%C ₄ H ₈ Mixture.....	105
5.2.3 Gas Gain in The Xe+20%Ar Mixture.....	109
5.3 ENERGY RESOLUTION.....	114
5.3.1 The Effects of Ionisation and Excitation.....	114
5.3.2 The Effect of Anode Wire Uniformity.....	123
5.4 PRESSURE DEPENDENT DIETHORN GAS PARAMETERS.....	127

CHAPTER 6: PERFORMANCE OF A HIGH PRESSURE MSPC.....131

6.1 GAS GAIN MEASUREMENTS.....	131
6.2 ENERGY RESOLUTION MEASUREMENTS.....	139
6.3 COMPARISON WITH THE SWPC.....	147
6.3.1 Gas Gain.....	148
6.3.2 The Diethorn Parameters.....	152
6.3.3 Signal Formation.....	156
6.3.4 Breakdown Effect.....	157
6.3.5 Energy Resolution.....	158

CHAPTER 7: THERMAL NEUTRON IMAGING USING MCPs.....161

7.1 INTRODUCTION.....	161
7.2 OPERATING PRINCIPLES OF MCPs.....	163
7.2.1 Gain Factor.....	164

7.2.2 MCP Chevron Configuration.....	165
7.3 INCORPORATION OF NEUTRON-SENSITIVE ELEMENTS INTO MCP LEAD GLASS.....	166
7.3.1 Lithium Incorporation in a MCP.....	166
7.3.2 Boron Incorporation into an MCP.....	167
7.4 GADOLINIUM FOIL METHOD.....	168
7.5 DETECTOR SET-UP.....	170
7.5.1 Gamma Ray Rejection.....	172
7.5.2 Predicted Detection Efficiency.....	174
7.6 RESULTS AND DISCUSSION.....	175
<u>CHAPTER 8: SUMMARY AND CONCLUSIONS.....</u>	180
8.1 AN OVERALL SUMMARY.....	180
8.1.1 The High Pressure Xe Gas Counters.....	180
8.1.2 Thermal Neutron Imaging with a MCP.....	182
8.2 CONCLUSIONS AND SUGGESTIONS FOR FUTURE WORK.....	182
8.2.1 Gas Counter Performance.....	183
8.2.2 Thermal Neutron Imaging.....	185
APPENDIX.....	187
REFERENCES.....	192

Chapter 1

Introduction

A wide range of radiation detectors is available to modern experiments. Almost all ionising radiation detectors utilise the conversion of the detected energy into electrical signals which are then recorded and manipulated in some way. Different techniques are used in different fields. There is no perfect type of radiation detector but one may be more suited to a given application than another.

The basic characteristics of any radiation detector include: the detection efficiency, spatial resolution, temporal resolution, energy resolution, internal background, and sensitivity to the various ionising radiations. In X-ray astronomy the ideal imaging detector would combine high spatial resolution with a large useful area, excellent temporal resolution with the ability to handle large count rates, good energy resolution with unit quantum efficiency over a large bandwidth. Its output should be stable on timescales of years and its internal background of spurious signals should be negligibly low. It should be immune to damage by the in-orbit radiation environment and should require no consumables. It should be simple, rugged and cheap to construct, light in weight and have a minimal power consumption. It should have no moving parts and low output data rates [Fraser, 1989].

In practice, it is impossible to construct such a detector. It is, therefore, necessary to compromise between the desirable and acceptable limits of the performance of a detector. The following section gives a very brief description of some modern imaging X-ray detectors.

1.1 Imaging Radiation Detectors

A large contribution to the field of radiation imaging has resulted from the introduction of new detection technologies and of new, fast, cheap, reliable and highly integrated readout electronics.

With the increasing speed and decreasing cost of digital computers, demand for electronic readout imaging systems, for the different types of radiation detectors, has competitively increased. Such systems are capable of storing data in a digital form suitable to be transferred to a computer where it is easy to be processed. We must stress again that there is not a single detection technique which is ideal for all applications but, in general, many applications of imaging detectors require the detector to be of large collecting area, reasonable detection efficiency, and good energy and spatial resolutions.

1.1.1 Proportional Counters

(a) General Considerations

In general, gas filled detectors fulfil many detection tasks quite satisfactorily, and probably the most important gas detectors in the field of X-ray Astronomy are the proportional counters.

The idea of the gas proportional counter was first introduced in 1908 [Rutherford & Geiger, 1908; Geiger & Rutherford, 1912]. This was a simple cylindrical proportional counter, which later developed rapidly with the development of signal processing systems in the 1930s.

A simple proportional counter consists of a cathode and anode contained in a cylindrical chamber filled with a suitable gas (Figure 2.1 of Chapter 2). The incident photon ionises the gas atoms and produces electron-ion pairs. Under the influence of a sufficient electric field, primary electrons will be able to ionise more gas atoms.

An important process in proportional counters is the charge multiplication which occurs when the electric field is above a threshold value. Successive multiplications will result in a fast moving electron avalanche towards the anode electrode. The collected charge at the anode is proportional to the original charge, *i.e.* to the energy deposited by the incident photon.

The gas multiplication factor, or gas gain, G , can be given by the expression [Charles, 1972]:

$$G = \exp\left(-\int_r^a \alpha dx\right) \quad (1.1)$$

where α is the first Townsend coefficient, which is defined as the probability of an ionisation per unit path length [Leo, 1994], r is the radial position of avalanche onset from the anode wire, and a is the anode wire radius. Details of the operational principle of proportional counters are given in the following chapter.

Using a single noble gas in proportional counters limits the performance of such detector because of the UV photons emitted by the excited atoms of the detection gas. These photons may be of high enough energy to release electrons from the cathode surface and be a source of gas gain variation or in extreme cases, breakdown, as will be discussed in the following chapter. Therefore, a range of suitable polyatomic gases, such as Methane (CH_4), Carbon Dioxide (CO_2), Di-Methyl Ether (DME), Isobutane (C_4H_{10}), and Isobutylene (C_4H_8) are normally mixed in small quantities with noble gases, such as Ar or Xe, to absorb the radiated UV photons.

Both argon- and xenon-based gas detectors are commonly and successfully used for detection of X-ray photons with energies less than about 5 keV. These detectors have been reported to have good performance at gas pressures 2 atm or less [Kowalski *et al.*, 1992; Agrawal & Ramsey, 1988; Agrawal *et al.*, 1989].

For X-rays with energy greater than ~ 5 keV, argon gas becomes relatively transparent to the incident photons, as shown in Figure 1.1. This results in poorer detection efficiency and also poor spatial resolution. Therefore, if an efficient proportional counter for both soft and hard X-rays has to be constructed, then xenon gas mixtures will be the best choice as the counter fill [Sims *et al.*, 1982; Sood *et al.*, 1991].

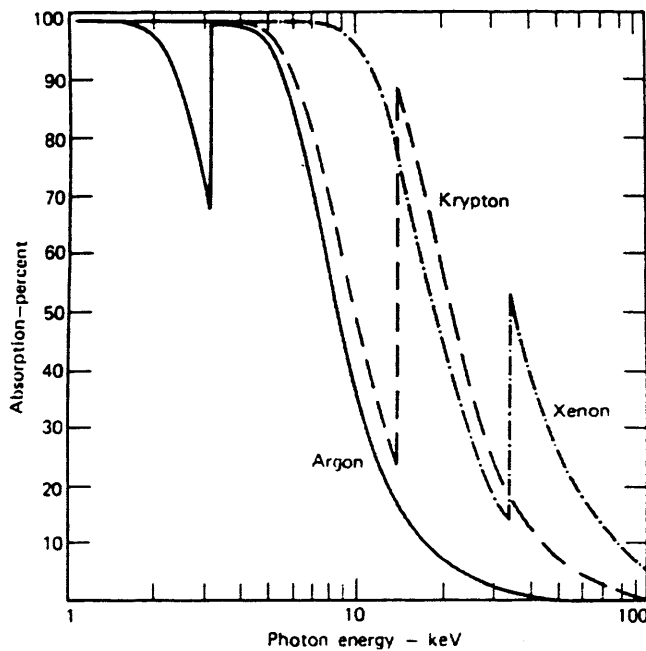


Figure 1.1: Fraction of incident photons absorbed in 5.08 cm thick gas layer of Xe, Ar, and Kr [Knoll, 1979].

New generations of proportional counter include imaging detectors which differ from the traditional counters in that the pulse is detected by position sensitive systems. These have been widely used in various applications of nuclear physics, high energy physics and X-ray astronomy because of their large detection area, simplicity of construction, absorption efficiency, background noise rejection, relatively low cost, and good energy resolution.

There are however some problems and limitations with imaging proportional counters. To realise appropriate spatial resolution for X-rays with energy $> \sim 10$ keV it is necessary to use a gas with high density or alternatively to increase the gas pressure in the counter.

Although gas counters play important roles in different fields of application [Sauli, 1992], they have a number of inherent shortcomings for many applications: the low density of the gas medium makes the interaction with incident radiation inherently inefficient, especially for photons and high energy radiations, where large detector volumes or high gas pressures would be required for good efficiency. Moreover, the finite drift mobility of positive ions produced in the gas results in a rather slow response time, of the order of milliseconds in most cases, which leads to an appreciable dead time, during which the detector may not respond to fresh incident radiation, and to a slow rise time in the charge collection pulses, again limiting the rate of detection.

The space charge effect is a serious problem which limits the use of proportional counters at high gas gains or at high count rates. This effect takes place as a result of the positive ion cloud created in the avalanche region which in turn modifies the electric field near the anode. Therefore, proportional counters, in general, suffer from an energy shift and loss of resolution as the count rate or the gas gain are increased.

When proportional counters are to be used for the detection of thermal neutrons, a conversion reaction with high thermal neutron absorption cross section, most commonly of the form (n,α) , is employed. The idea is to detect thermal neutrons via the initiation of energetic interaction. The energy which is released in the decay process, as a result of the neutron absorption, can be transferred to fast ionising particles which may then be detected [Convert & Forsyth, 1983].

The following reactions are common options for thermal neutron detection using proportional counters [Crawford, 1992]:



and



The first reaction has a much higher cross section for thermal neutrons (~3,800 b), and it can be introduced into the counter by using boron trifluoride ($^{10}\text{BF}_3$) as the counter gas, usually at pressures less than atmospheric. This reaction can also be induced in the counter by coating the inside walls of the counter [Delaney & Finch, 1992] with a thin layer of boron which should be less in thickness than the maximum range of the alpha particles. The latter method is useful when a proportional counter is to be used for both photon and neutron detection.

Using gadolinium foil as a converter has also been employed for thermal neutron imaging, [Jeavons *et al.*, 1978] (more details are given in Chapter 7 of the present work).

Some types of proportional counters commonly used as position sensitive detectors are discussed below.

(b) Single Wire Proportional Counters (SWPCs):

The simplest type of SWPC is a cylindrical chamber surrounding an axial wire, as illustrated in Figure 2.1 in Chapter 2, where the active volume is normally filled with a noble gas mixed with a simple molecular gas such as CO_2 or CH_4 which is able to absorb UV photons emitted by the excited noble gas atoms. The operating principles are described in more detail in Chapter 2.

Probably the first position measurements using a SWPC were those of Kuhlmann *et al.* (1966). These authors used a method so called the “charge division method”, which was a major step forward in imaging proportional counter technology. In this method, the counter anode wire acts as a charge division network, where the charge collected at either end of the sensitive anode wire is divided in proportion to the length of wire and is expressed as the ratio of the charge at one end to the sum of the charges from both ends. Some more details are given in Chapter 2 of the present work.

The energy resolution of a SWPC depends on the anode wire diameter and uniformity [Sakurai & Ramsey, 1992; Tokanai *et al.*, 1994]; that is, the finer is the anode wire the better is the energy resolution. Theoretically (see Section 2.4 of Chapter 2), the energy resolution of an argon- or xenon-based X-ray proportional counter can be expressed as [Fraser, 1990]:

$$R = 2.36 [(F + f) W / E_v]^{1/2} \cong 0.35 / E_v^{1/2} \quad (1.4)$$

where F is the Fano factor which is a function of the fluctuation of the number of primary electron-ion pairs, f is the variance of the avalanche size, W is the average energy required to produce an electron-ion pair, and E_v is the energy (in keV) deposited by the incident X-ray photon.

It is necessary in many applications to reduce the gas gain factor to minimise the effect of space charge which limits the energy resolution and limits the use of the counter at high gas gains or high count rates.

(c) Multi-Wire Proportional Counters (MWPCs):

In order to increase the position sensitivity of a proportional counter, one may think of enlarging the gas volume together with increasing the number of wires. This is the idea on

which MWPCs are based, *i.e.* a MWPC is a modification of the SWPC with many parallel anode wires instead of a single wire anode. The first imaging MWPC was developed by Charpak *et al.* (1968 a) at CERN. An imaging MWPC may consist of a chamber containing three planes of wires representing an anode array between two cathode arrays, as shown in Figure 1.2. The central anode plane is kept at a positive potential with respect to the two outer cathode

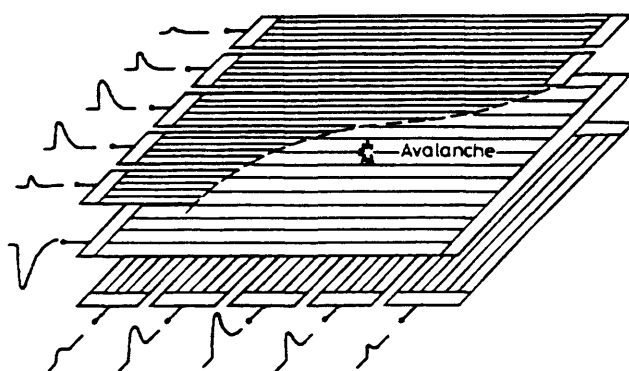


Figure 1.2: An MWPC electrode assembly [Breskin *et al.*, 1977].

planes. The wires of one cathode plane are orthogonal to those of the other. Signals induced in the several cathode wires centred on the avalanche position can be used to compute the X and Y co-ordinates of the avalanche. The electrons are attracted to the nearest anode wire, generating an electron avalanche in the high electric field, so inducing charge signals on both the anode wire and the two nearest cathodes.

The cathode wires conduct the signal to a readout system which permits measurement of the X and Y co-ordinates of the events. Various methods can be employed to locate the event along the direction of the anode wires. Charpak *et al.* (1968 b) in their early counter attached a pre-amplifier to each individual anode wire, and consequently verified that each wire acted as an independent proportional counter.

Since their introduction by Charpak *et al.* (1968 a, b), MWPCs have been employed successfully as imaging detectors on some satellite missions such as ROSAT [Aschenbach *et al.*, 1981], Spacelab 2 [Henize, 1985], and Ginga [Swinbanks, 1987; Turner & Thomas, 1989]. Studies have been carried out into the use of MWPCs on future satellite missions; *e.g.* Ubertini (1992), Gabriel (1995), and Israel (1997).

Figure 1.3 shows a schematic cross-section of the imaging proportional counter (IPC) designed earlier at the University of Leicester to operate as a high pressure MWPC. This counter was later modified for the present work by replacing its electrode assembly by a microstrip plate (see Chapters 3 and 4).

The MWPC, at least in its standard design, has two major limitations [Bellazzini & Spezziga, 1994]: (i) the spatial resolution in the direction orthogonal to the anode wires is limited by the wire spacing, typically of the order of 1mm; (ii) the rate capability is limited by

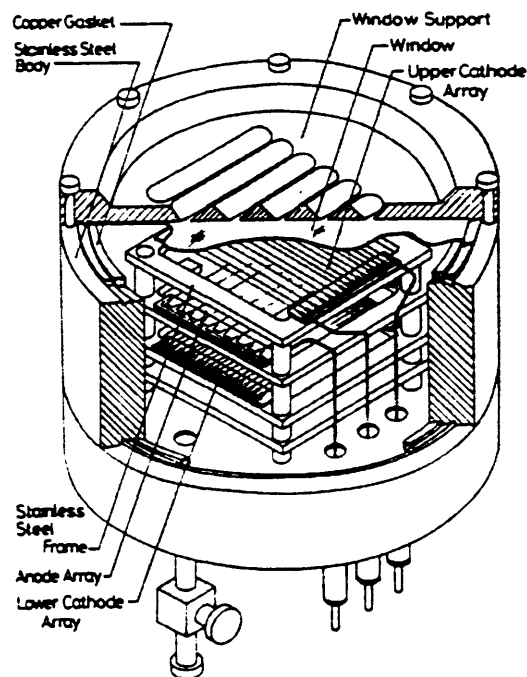


Figure 1.3: A general view of the Leicester University 9 cm x 9 cm IPC modified later for the present work [Sims *et al.*, 1981].

the long ion collection time, typically several tens of microseconds. Moreover, the energy resolution is worse than that of a SWPC because of the different response of the wires to same amount of charge. These drawbacks have been overcome partially by the introduction of gas scintillation proportional counters, and later fully by the introduction of microstrip proportional counters as will be discussed below.

(d) Gas Scintillation Proportional Counters (GSPCs)

This type of detector is based on the fact that the gas atoms can be excited by collisions with electrons drifting in a strong electric field. GSPCs basically consist of two regions [Garg, 1992]: the drift region and the light producing region. In the drift region, the reduced electric field intensity, E/p , (E is the electric field and p is the gas pressure) is low (≤ 1 V/cm-Torr). The primary electrons drift in a weak electric field towards the light producing region (or the excitation region) where the reduced electric field is higher and only excitations are produced. The excited atoms quickly de-excite by the emission of visible or UV photons, which are then detected by a photomultiplier.

These photons here are advantageous, whereas they may be very harmful to conventional proportional counters, as mentioned above and discussed in Chapter 2. The dependence of the light yield on the gas pressure in Xe GSPCs has been studied by Favata *et. al.* (1990) and has been found to be independent on gas pressure in the range ~ 0.14 -1.4 atm.

Recently, Garg (1995) has suggested a formula to predict gain factor for light yield in a single wire GSPC. His semi-empirical expression gives the light gain as a function of some parameters as voltage, anode and cathode radii, filling gas, and pressure.

The energy resolution of GSPCs is limited by fluctuations in the primary ionisation and in the photocathode electron emission. Since the fluctuations in the production of secondary

scintillation photons are very small and the amplification process is almost perfect, the degradation in the energy resolution due to the avalanche process in conventional MWPCs can be avoided. This is of significant importance for the detection of low energy X-rays.

The very first GSPCs, developed at the University of Coimbra in Portugal [Policarpo *et al.*, 1972, 1974] achieved an energy resolution given as [Fraser, 1989]:

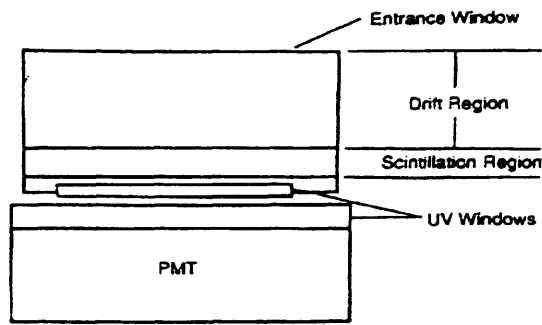
$$R \cong 0.2 / E_v^{1/2} \quad (E_v \text{ in keV}) \quad (1.5)$$

which, is a factor of two better than the equivalent figure of merit in conventional (avalanche) counters (Equation 1.4).

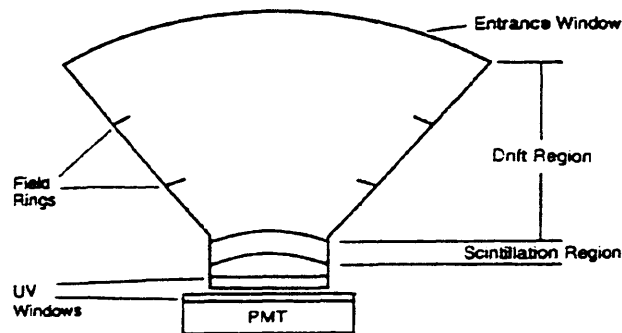
Although their energy resolution is better than that of conventional proportional counters [Hailey *et al.*, 1983], the GSPCs suffer from much poorer spatial resolution because of the further spread of electron cloud. Spatial resolution in imaging GSPCs is at best reducible to, for example, 1.0 mm fwhm at an energy of 1.49 keV [Fraser, 1990].

An attempt has been made to improve the performance of GSPCs by introducing a new counter configuration which has been called a driftless GSPC [Simon *et al.*, 1985], where the photons are absorbed directly in the scintillation region. Although such a configuration has the disadvantage that the observed light amplitude is dependent upon the depth of penetration of the observed X-ray, it has the advantage of greater simplicity of design and limited electron diffusion [Smith *et al.*, 1987]. Figure 1.4 shows various GSPC configurations, conventional and driftless geometries.

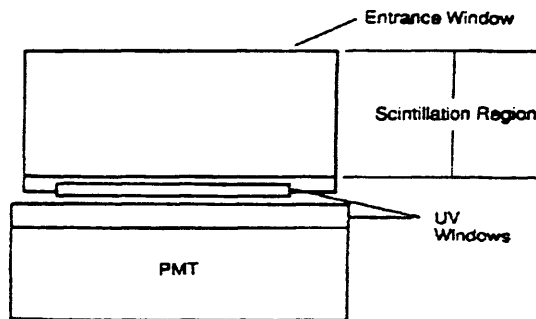
Energy resolution of GSPCs can be further improved using a pulse shaping discrimination technique [Garg *et al.*, 1993] to suppress the pulses produced by the interaction in the scintillation region.



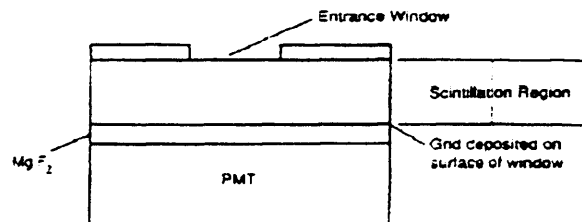
a) Conventional, Planar GSPC



b) Conventional, Spherical GSPC



c) Driftless GSPC



d) High performance, driftless GSPC

Figure 1.4: Schematic diagram shows various conventional and driftless GSPC [Smith & Bavdaz,1991]

Imaging GSPCs have been successfully employed in X-ray astronomy applications, and have been used on various satellite missions, *e.g.* EXOSAT [Peacock *et al.*, 1981; Ricci *et al.*, 1995], TENMA [Tanaka, 1984], and SAX [Scarsi, 1993]. On a recent ASCA mission, two imaging GSPCs covering the energy range from 0.7 to >10 keV with 10% detection efficiency are used. An energy resolution of 7.8% fwhm and spatial resolution of 0.5 mm fwhm at 6 keV have been achieved using these imaging detectors [Ohashi *et al.*, 1996].

(e) Micro Strip Proportional Counters (MSPCs):

The MSPC is a new approach to gas-filled detector technology. MSPCs were introduced by Oed (1988) as a form of a position sensitive neutron detector. The original idea of the MSPCs came from a desire to improve the rate capability and position resolution of the MWPC [Ramsey, 1992]. In contrast with MWPCs, the anode and cathode electrodes are deposited onto a rigid semiconducting or insulating substrate using standard microlithography techniques. More details of this novel type of detector are given in Chapter 3 of this work.

Briefly, the main advantage of MSPC over MWPC is its extremely fine, precise, uniform, and narrowly spaced anodes and cathodes. These offer a uniform gas gain, excellent energy and spatial resolutions, fast charge collection time, high count rate capability, and low operating voltage [Budtz-Jorgensen *et al.*, 1994].

A problem with MSPCs was reported in the early work of Oed (1988). The problem is connected with charging up of the insulating substrate that can modify the electric field and hence the gas gain. This has been solved in the work of Oed by applying a positive potential to the back side of the microstrip plate to repulse the positive ions away from the upper surface towards the cathode strips.

Since the introduction of MSPCs in 1988, many independent groups have intensively studied such counters and reported encouraging results at atmospheric pressures. Examples of these results have been given by Budtz-Jorgensen *et al.* (1989), Angelini *et al.* (1992), Ramsey (1992), Bateman & Connolly (1993a, b), and Bouclier *et al.* (1995).

Energy resolution of 12 % for 5.9 keV at a gas gain of 10^4 , spatial resolution of $30\mu\text{m}$ (rms), and rate capability of $> 5 \times 10^5$ counts $\text{mm}^{-2} \text{sec}^{-1}$ are some examples of already reported results. Angelini *et al.* (1990) have reported energy resolutions of less than 11% fwhm at 5.9 keV and 5.5% fwhm at 22 keV using an MSPC with $3\mu\text{m}$ anodes in an Ar-ethane mixture.

A new configuration presented as an improvement to the MSPC has been proposed by Angelini *et al.* (1993a) to provide a two-dimensional detector and to avoid the charging up problem. A schematic diagram of this detector is shown in Figure 1.5. It has been called the Micro-Gap Chamber (MGC) because of its most striking feature of the very small anode-cathode gap (a few μm), and the true possibility of an anode pitch ranging from 1 mm down to $50\mu\text{m}$. This detector has a different electrode configuration in which the cathode strips are replaced with a metal layer deposited onto a substrate. The anode strips are separated from the cathode by very thin insulating strips. The anode-cathode gap is only a few microns, so the speed of avalanche charge collection of this detector is comparable (~ 10 ns) with that of solid state detectors.

More recently a new approach to the MSPC has been introduced by Biagi and Jones (1995) and called the microdot gas detector. A schematic of one of the cell geometry/pixel structures is shown in Figure 1.6. This has been proposed to increase the maximum gas gain to greater than 2×10^4 and to be intrinsically more suitable for 2-dimensional imaging purposes than the MSPCs and MGPCs.

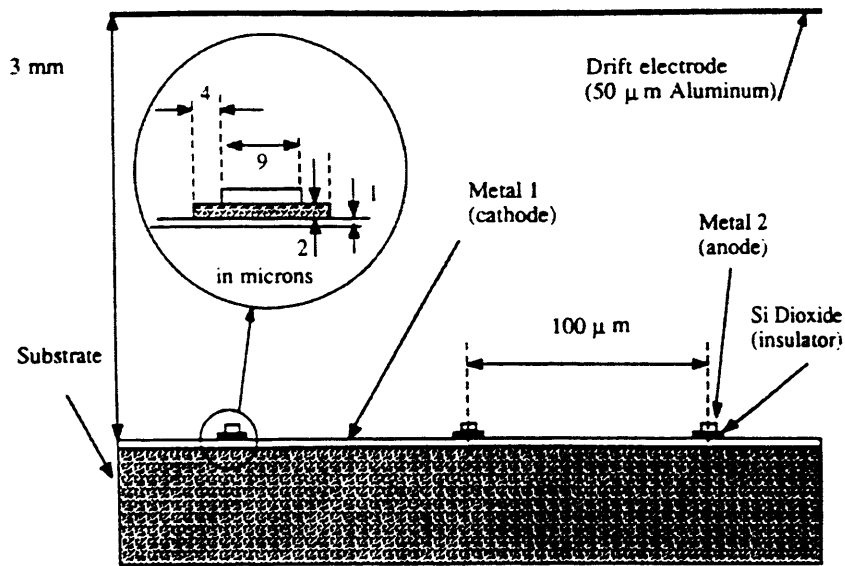


Figure 1.5: The MGPC [Angelini *et al.*, 1993a].

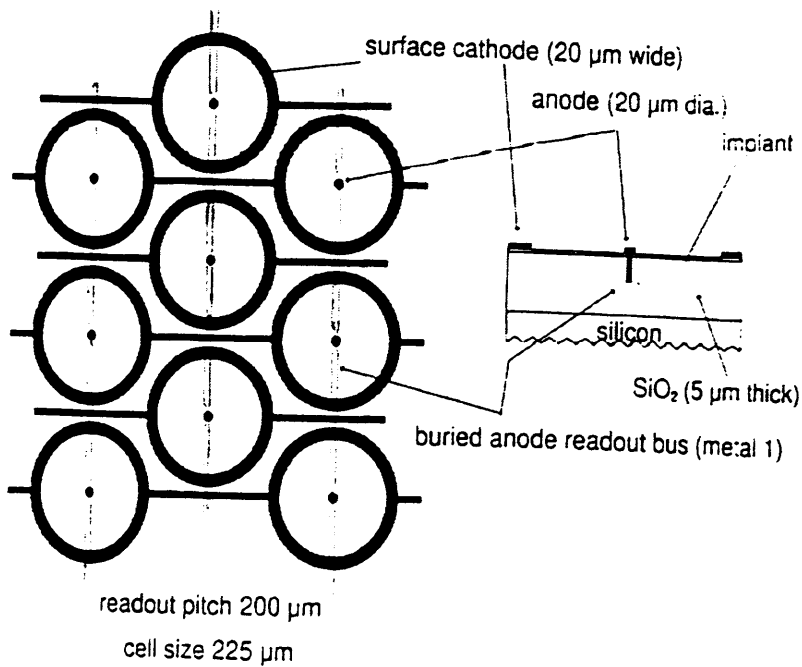


Figure 1.6: Views of a microdot cell from above and in cross section through the substrate [Biagi *et al.*, 1995].

The structure of a microdot gas detector is inherently pixel-like and is probably most suited to experiments operating in very high rate environment [Biagi *et al.*, 1995].

A recent development of a MSPC of an active area of 30 cm x 30 cm is being carried out at NASA-Marshall Space Flight Centre, USA [Ramsey *et al.*, 1996]. This counter has been designed to be the main part of a large-area coded-mask telescope for hard X-ray astronomy, on the first flight of a high-altitude balloon which is scheduled for Spring 1997.

An imaging MSPC is also planned as a candidate for the X-ray monitor for the International Gamma-Ray Astrophysical Laboratory, INTEGRAL [Budtz-Jorgensen *et al.*, 1994; Winkler, 1996].

1.1.2 Scintillation Detectors

A scintillation detector consists of a scintillation material coupled to one or more photomultiplier tubes. It makes use of the fact that some materials when struck by radiation, emit a small flash of optical light, or a scintillation. The atoms of the scintillator are excited to higher atomic levels. These atoms will decay to their ground state with the emission of a photon. When photons of the emitted light are guided to collide with a photocathode of a photomultiplier, electrons will be emitted from the photocathode, attracted by a series of dynodes where they are amplified (by a factor of $\sim 10^6$), and finally collected as electrical pulses which can then be analysed and counted to give information concerning the incident radiation.

Probably the earliest example of the use of scintillators for radiation detection was in the spintharoscope invented by Crookes in 1903 [Leo, 1994]. This instrument consisted of a ZnS screen which produced weak scintillations when struck by α particles; the human eye was used to record these scintillations. Such instruments were tedious to use, and with the invention of the gaseous ionisation detectors, optical scintillation counters fell into disuse. By 1944,

however, it was possible to detect and count the weak scintillations after the introduction of the photomultiplier tubes which led to the development of modern scintillation detectors.

The number of emitted photons from the excited atoms of a scintillator at time t can simply be given by:

$$n = n_0 e^{-\frac{t}{\tau}} \quad (1.6)$$

where n_0 is total number of emitted photons and τ is the decay constant.

The scintillator material could be an organic crystal, organic liquid, plastic, inorganic crystal, a pure gas, or glass [Leo, 1994]. The most common scintillation materials used for gamma or X-rays are NaI(Tl) and CsI(Tl) crystals. In general, an ideal detector scintillator should possess the following properties [Knoll, 1979]:

- 1) High efficiency for conversion of excitation energy to fluorescent radiation.
- 2) Linear conversion- the emitted light intensity should be proportional to the deposited energy over as wide a range as possible.
- 3) Transparency to the wavelength of its own fluorescent radiation so as to allow transmission of the light.
- 4) A refraction index with a value near to that of glass (~ 1.5) to permit efficient coupling of the scintillation light to a photomultiplier.
- 5) A short decay time of the induced luminescence so that fast signal pulses can be generated.

In addition, the scintillation material should be of good optical quality and available to manufacture in sizes large enough to be of interest as a practical detector.

A configuration of a scintillator, a photocathode, and an array of photomultipliers can be used as a position sensitive detector. A more sophisticated imaging scintillation detector has

been constructed [Hoftiezer, 1977] by using what is called a hodoscope, where scintillation strips are connected to photomultiplier tubes through light guides. Illustration of a scintillator hodoscope is shown in Figure 1.7.

Scintillation detectors have high counting rate capability because of the fast charge collection. They have high detection efficiencies which can approach unity with some scintillators for X-rays in the 20 - 100 keV range.

The energy resolution of scintillation detectors is controlled by three factors: the excitation process and hence photon emission from the scintillator, the light collection and guidance, and the electron emission from the photocathode. Energy resolution of scintillation detectors for X-rays is poor compared to that of proportional counters or solid state detectors.

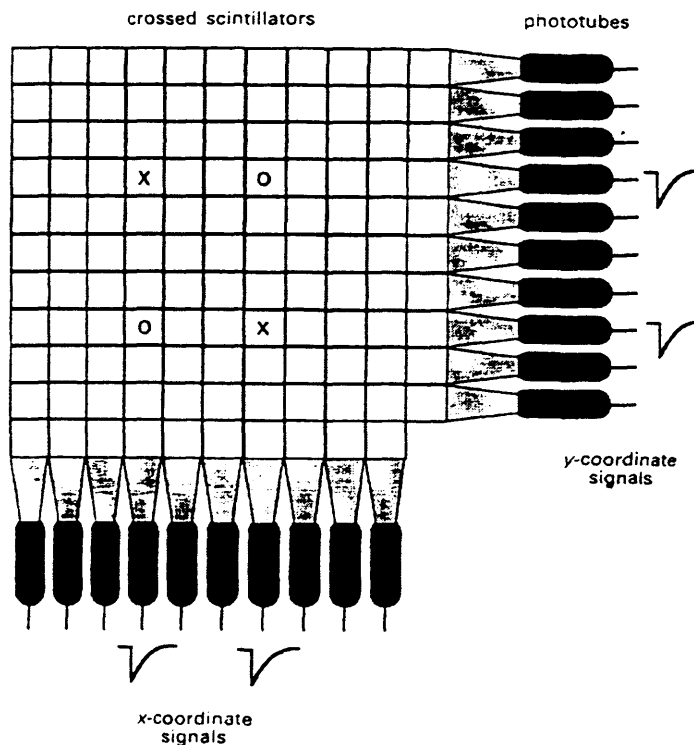


Figure 1.7: A scintillator hodoscope with two crossed planes of scintillators [Gilmore, 1992].

For thermal neutron detection, scintillation detectors with plastic or glass crystals loaded with lithium (Li) or boron (B), are used and can be of 100% efficiency. This is based on utilising an (n, α) reaction such as those of Equations 1.3 and 1.4.

One of the applications of conventional scintillation detectors in X-ray astronomy is that of the NASA's X-ray Timing Explorer (XTE) mission which was launched into the low earth orbit in late 1995. One of the imaging detectors used in this mission consisted of a group of NaI scintillation detectors grouped into two independent clusters [Gruber *et al.*, 1996].

1.1.3 Microchannel Plates (MCPs)

An MCP is a fast detector which works by means of electron multiplication. The first MCPs were built in the early 1960s as a further development of the single channel electron multiplier. In an MCP (more details are given in Chapter 7), millions of tiny single channels made of a special lead glass and are packed parallel to each other. The front and rear face of the MCP are coated with a metallic layer in order to provide electric contact to each channel. When a MCP is placed in vacuum and a voltage is applied between the surfaces, each channel becomes a continuous-dynode electron multiplier and a gain of $\sim 10^4$ can be obtained with a standard MCP. Higher gains ($10^6 - 10^8$) can be obtained by using one of a number of multi-stage MCP configurations. The gain of MCPs is known to degrade with extended use. This drop in gain is related to the amount of abstracted charge removed from the MCP [Lees, 1989].

Channels of a MCP are usually manufactured in a cylindrical geometries. Square or rectangular pores have also been proposed [Asam, 1978; Wilkins *et al.*, 1989]. Fraser *et al.* (1991) have made measurements of gain and quantum detection efficiency of MCPs with square pores. These authors have shown that the detection efficiency of a bare square-pore MCP is very high compared with a conventional MCP.

Advantages of MCPs include flexibility of their structure, which can be shaped according to the application of interest, high count rate capability, and good spatial resolution. On the other hand, their disadvantages include low detection efficiency for soft X-rays which decreases with increase of photon energy and varies strongly with angle of incidence. Other disadvantages are the extremely poor energy resolution, and the difficulty of fabricating large area detectors.

An example of MCP application in X-ray astronomy is the High Resolution Imager [Zombeck *et al.*, 1995] of ROSAT.

MCPs can be used for the detection and imaging of thermal neutrons in different ways such as MCP-Gd foil method, investigated in detail in Chapter 7 of the present work.

1.1.4 Semiconductor Detectors

This type of detector is based on the use of crystalline semiconductor material and operates like a gas ionisation chamber. The most successful semiconductor detectors are made of silicon (Si) and germanium (Ge). Development of these instruments first began in the late 1950s with small germanium surface barrier devices with gold electrodes.

The charge carriers in semiconductor (or solid state) detectors are electrons and holes which are produced by the incident radiation. Both negatively and positively charged carriers are free to move, in opposite directions, under the influence of an applied electric field. The required average energy to create an electron-hole in silicon or germanium is about 3 eV, whereas the average energy to create an electron-ion pair in xenon gas is about 22 eV, and about 35 eV in air. Therefore, the primary charge created in silicon or germanium is about seven times greater than that in xenon. Moreover, these detectors have greater stopping power than 1 bar gas detectors because of their greater density.

Excellent energy resolution is the most obvious feature of this type of detector compared to other detectors. It is given by, in the limit of negligible electronic noise:

$$R = \Delta E_v / E_v = 2.35 \sqrt{FW / E_v} = 0.05 / E_v^{1/2} \quad (E_v \text{ in keV}) \quad (1.7)$$

The Fano factor F for silicon and germanium is around 0.12 [Leo, 1994]. The X-ray energy response of silicon, in terms of W and F , has been studied at constant detector temperature by Fraser *et al.* (1994). These authors have found that W is an increasing function of X-ray energy for $E_v < 0.5$ keV, while F is predicted to increase slowly with E_v .

New ideas in the field of solid state detectors include imaging structures, with low output capacitance, such as Charge-Coupled Devices (CCDs) [Klanner, 1985; Janesick & Blouke, 1987] and Silicon Drift Chambers [Gatti & Rehak, 1984; Sumner *et al.*, 1988].

A CCD (Figure 1.8) is a silicon device consisting, essentially, of a two-dimensional array of metal-oxide-silicon (MOS) capacitors formed by the deposition of parallel linear electrodes on

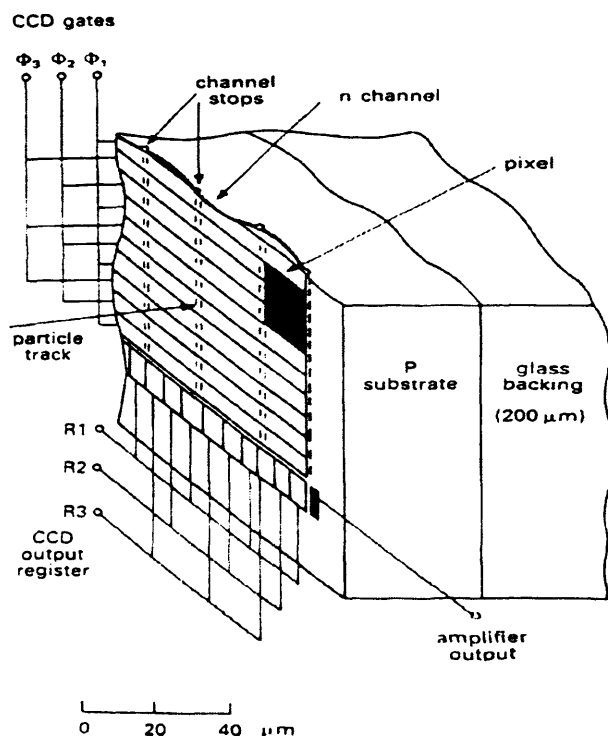


Figure 1.8: A CCD two-dimensional imaging detector [Damerell *et al.*, 1981].

to the oxidised surface of a silicon wafer. The array consists of tiny potential wells each covering a small surface of area (typically $20 \times 20 \mu\text{m}^2$). Electrons are the majority charge carriers in most CCDs, and if an X-ray is absorbed in the depletion layer, the charge carriers thereby liberated will be captured in these wells. This charge information is then readout by successively shifting the charge from one well to the next until it reaches the output node.

The X-ray detection efficiency of CCD is dependent on the thickness of the active depletion layer in the silicon, typically less than $40 \mu\text{m}$. The CCD detection efficiency drops sharply above 8 keV , but by utilising an “edge-on” illumination geometry, CCDs can detect X-rays up to 100 keV with reasonable efficiency and good energy resolution [Castelli & Fraser, 1996].

The silicon drift chamber has an electrode structure which is less complex than that of a CCD and because the drift chamber is necessarily depleted throughout its $300 \mu\text{m}$ depth, the X-ray bandwidth of the former device should be much broader [Fraser, 1989].

In general, in addition to the excellent energy resolution of semiconductor detectors, they have some other advantages including good detection efficiency, energy linearity, insensitivity to magnetic fields, and fast pulse rise time.

A disadvantage of this type of detectors is their requirement for cooling to very low temperatures ($\sim -100^\circ \text{C}$) before they can be operated to reduce their background thermal noise. Therefore, investigations have been carried out to find an alternative “room temperature” materials. New solid state materials, such as mercuric iodide (HgI_2) and cadmium telluride (CdTe), have been investigated for room temperature operation [Schieber & van den Berg 1983; Cuzin 1987].

CCDs have been selected in various imaging applications because of their high spatial resolution. An example of such an application in X-ray astronomy is the X-ray Multi Mirror

(XMM) mission of the European Space Agency (ESA) planned to be launched by the end of this century [Soltau *et al.*, 1996].

1.2 Scope of the Thesis

This work is aimed at developing efficient neutral radiation detectors needed in many fields such as X-ray astronomy, high energy physics, and radiography. The work was carried out mainly on gas counters and partially on microchannel plates (MCPs). The work on gas counters had the aim of investigating properties of proportional counters at high gas pressures to develop an efficient imaging detector for X-rays in the energy range ~ 10 to 100 keV. The aim of the work on MCPs was to develop a novel Gd/MCP thermal neutron imaging detector. The work carried out in these two areas is reviewed in the next two sections.

1.2.1 Development of Xe-Filled SWPC and MSPC at High Pressures

Proportional counters have been used successfully and efficiently in many applications using xenon (Xe) or argon (Ar) gas mixtures. The preferable gas filling is the one which has high detection efficiency, high gain (*i.e.* low working voltage), good proportionality, and low cost. Xe and Ar have been found to be the best choices among other noble gases.

The X-ray Astronomy Group of the Department of Physics and Astronomy at Leicester University has been involved in the development of Xe imaging proportional counters for the past couple of decades. Most previous work on proportional counters within the group has been mainly carried out at pressures of up to 2 atmospheres (atm) [Sims *et al.*, 1981; Smith & Turner, 1982; Thomas & Turner, 1984; Turner & Thomas, 1989].

Few studies are available on xenon gas wire proportional counters at gas pressures greater than 2 atm. Ultra-high-pressure xenon and argon-filled counters were investigated by a group at

the University of New South Wales, Australia [Manchanda *et al.*, 1990; Sood *et al.*, 1991; Ye *et al.*, 1993; Sood *et al.*, 1994]. The first paper of this group was concerned with argon-methane mixtures at pressures of up to ~ 27 atm. An important comparison, reported in the same work, has been made between the detection efficiency of a Xenon-methane counter at ~ 3.5 atm and an argon-methane counter at ~ 27 atm. The detection efficiency of the xenon counter was found to be higher for a wide range of photon energies (> 200 keV). A later paper was concerned with xenon-methane counter at pressures of up to 17 atm. At a gas gain of $\sim 10^3$ these authors have reported energy resolutions of $\sim 6\%$ and 12% for 60 keV photons, at pressures of 1 and 13.5 atm respectively, using Xe+2%CH₄.

Another research group at the NASA Marshall Space Flight Centre, USA [Sakurai *et al.*, 1991], has investigated the performance of a similar single wire counter using the same mixture (Xe+2%CH₄) at pressures of up to 10 atm. These authors have reported energy resolutions, at a gas gain of ~ 100 , of 7.7 % and 9.8% for 22 keV, and 5.1 % and 7.3 % for 60 keV at pressures of 1 and 10 atm respectively.

More investigations seem to be necessary to further understand the influence of increasing pressure in xenon-based proportional counters and the corresponding changes in connection with the type of quenching, in particularly with Xe Penning mixtures (discussed in Chapter 2).

Little attention has so far been paid to investigations of the behaviour of MSPCs at high pressures. Angelini *et al.* (1993b) have reported results obtained from a glass substrate MSPC with 5 μm anodes, 125 μm anode pitch, 30 μm cathodes, and 45 μm anode-cathode spacing. Using Xe+10%CH₄ at pressures of up to ~ 6 atm, these authors have achieved gas gains up to $\sim 10^4$ and an energy resolution of $\sim 20\%$ for 22 keV X-rays.

Using same gas mixture at same pressure range, Minakov *et al.* (1993) have used MSPCs of two different glass substrates with different anode strip widths (3, 5, 7, and 10 μm), 200 μm

anode pitch, and 60 μm cathode strips. With the 3 μm width anode strips, they have reported gas gains up to $\sim 10^4$ and an energy resolution of $\sim 8\%$ for 22 keV X-rays.

More recently, Fraga *et al.* (1996) have tried different gas mixtures, including Xe-CO₂, in an MSPC and MGPC at pressures of up to ~ 6 atm. Their results have been obtained using an MSPC with 8 μm anodes, 10³ μm pitch, and 400 μm cathodes, and an MGPC with 9 μm anodes, 200 μm pitch, and 3 μm anode-cathode gap. Their results with Xe+14% CO₂ in MSPC are not encouraging, whereas with 10%CO₂ in an MGPC they have reported a reasonable energy resolution, 15 % for 22 keV X-rays at a pressure of ~ 6 atm and a gas gain of ~ 100 . For Xe+10%CH₄, at the same pressure and nearly the same gain, they have reported an energy resolution of 12%.

The present work is concerned with the performance of Xe-based gas proportional counters at high pressures up to 10 atm to probe the possibility of achieving an efficient X-ray imaging detector with good performance for the X-ray energy range up to ~ 100 keV. The high pressure SWPC and MSPC have been designed by the X-ray Astronomy Group of the Department of Physics and Astronomy at Leicester University to be operated at pressures up to 10 atm.

The performance investigations of the counters studied included gas gain, energy resolution, and proportionality. These characteristics were obtained using a prototype SWPC and a MSPC. The data obtained with the SWPC were used as a reference for investigations of the MSPC.

The microstrip plates used in the present work were with Corning 7740 glass substrates having 10 μm anode strips, 10³ μm pitch, and 390 μm cathode strips. They were kindly provided by Dr. B Ramsey from Marshall Space Flight Center, NASA, USA.

Significant results were obtained for the MSPC using Xe+5%CO₂ at pressures up to 5 atm, although the plates were received in moderate condition and were very fragile- most of them

were damaged during our experiments and eventually the programme was curtailed due to lack of good plates.

Carbon-Dioxide is a low cost gas, it has no polymerisation problems, and it has a relatively high ionization potential. Therefore, we preferred to use the mixture Xe+5%CO₂ and selected it as a reference mixture. Other mixtures studied at high pressure were Xe+20%Ar and Xe+5% Isobutylene (C₄H₈) as the former represents a noble gas-Penning mixture whereas the latter represents an organic gas quenching mixture, also exhibiting the Penning effect.

1.2.2 Thermal Neutron Imaging with MCPs

There are applications (focused small-angle scattering, diffraction profile analysis, microscopy [Kurz *et al.*, 1988]) in neutron physics which require the development of 2-dimensional, position-sensitive long-wavelength neutron detectors with spatial resolution much less than 1 mm fwhm.

The use of MCPs as thermal neutron imaging counters has not been satisfactorily investigated to date. One previous attempt to use MCP technology in neutron detection employed a gadolinium neutron-beta converter coupled to a MCP image intensifier with phosphor-screen readout [Chalmeton, 1973].

In recent work at Leicester University [Fraser & Pearson, 1990], the principle of direct detection of thermal neutrons using a MCP has been tested. The authors have considered, both theoretically and experimentally, the combination of (n, α) capture conversion and electron multiplication within a channel plate structure containing lithium. Their conclusion was that the production of lead glasses with much higher lithium concentrations (or including boron) might produce a thermal neutron detector combining useful efficiency and channel-pitch-limited (~ 15

μm) spatial resolution. Construction of such MCP-based detection system requires a high cost glass development, which is, however, now underway in the United States.

In the present work, a simple alternative method involves the detection, using MCPs of standard glass composition, of the internal conversion electrons from a thin gadolinium foil. The first measurements of such a low cost MCP-Gd detector were presented. These include the detection efficiency, pulse height resolution, and imaging properties.

1.2.3 Organization of the Thesis

Chapters 2 to 6 are related to the work on gas counters, whereas Chapter 7 is concerned with the MCP work. The contents of the thesis can be summarised as follows:

Chapter 2 describes in detail the operating principles of proportional counters, and the most important factors which affect behaviour of such counters. It provides details of commonly used gases in proportional counters and the factors controlling the selection of a gas mixture. Gas gain and energy resolution of proportional counters are the main parameters of interest in the gas counter work and factors affecting these parameters are given with an attention to those taking place at high pressures. A description of the Diethorn equation [Diethorn 1956], which has been adopted here for predicting gas gain in both counters, and definitions of some important terms in the gas counter technology are also given in this chapter.

Chapter 3 reviews MSPCs. Principles of MSPC operation are given in comparison with those of ordinary SWPCs and MWPCs. The well known advantages of MSPCs and some disadvantages are summarised.

Chapter 4 gives details of the experimental set-up and measurement techniques used to evaluate the performance of the gas counters. Details of the SWPC and the MSPC are given

together with a description of the counting electronics used with both counters. Gas filling procedures and factors controlling the selection of gas mixtures are also given.

Chapter 5 presents the results obtained from the SWPC, utilising selected xenon-based mixtures, at pressures up to 10 atm. Different Xe/Ar Penning mixtures were first tested at 2 atm, and gas gains were then compared with those predicted by Diethorn formula. The rest of the chapter presents the behaviour of the SWPC at high pressure in terms of the gas gain and energy resolution, and the effect of high pressure on some effective parameters is investigated. The work in this chapter is being prepared for publication.

Chapter 6 presents the results obtained from the MSPC using Xe+5%CO₂ gas mixture at pressures up to 5 atm. The measured gas gain is compared with the predicted gain which was calculated using Diethorn formula. The effective cathode radius in this case was calculated using the Diethorn gas constants obtained for the same mixture in the SWPC. The effective cathode radius of the MSPC was roughly estimated to be as the spacing between centres of anode and cathode widths. A comparison between the SWPC and the MSPC is also given in terms of some important features. The results of this chapter in connection with some parts of Chapter 5, are also being prepared for publication.

Chapter 7 gives details of the thermal neutron imaging study including a description of the experimental set-up and experience of the XRA group at Leicester University in this field. The results reported in this chapter have been published [Fraser *et al.*, 1993].

Chapter 8 summarises the general conclusions extracted from both parts of the work. These are given together with suggestions in some areas which require further investigation.

Chapter 2

Proportional Counters

The proportional counter is one of the most common radiation detectors in many fields. The proportional counter, in principle, is an extension of the ion chamber in which a higher field strength is used and internal amplification takes place. It differs from the ionisation chamber, in which the signal charge is equal to the energy deposited divided by the energy required to create an ion-electron pair, and from the Geiger-Muller counter, where response is independent of energy deposited.

One of the main advantages of proportional counters is their energy resolution, i.e. the ability of the counter to distinguish between two input energies. Energy resolution is usually given in terms of the Full Width at Half Maximum (FWHM) of the output pulse height distribution, ΔE , and is a function of the energy deposited in counter.

For X-rays with energy of ~ 2 -100 keV, which is the energy range of our interest, the proportional counters are superior in their energy resolution compared to ion chambers. This is because of the small number of ion-electron pairs produced by the X-ray photon with such an energies which in turn necessitate the amplification process, i.e. the proportional mode.

Proportional counters are often filled with a suitable gas at a pressure of one atmosphere or higher depending on energy range of interest. The gas pressure is one of the most important factors which affect the counter performance and determine its construction.

In this chapter, the operating principles of proportional counters and performance affecting parameters are explained. A brief account of the development of these counters to fulfil the demands of imaging applications is also given.

2.1 Operating Principles

A simple X-ray Single Wire Proportional counter (SWPC) consists of a cylindrical chamber with a single wire passing through its centre (Figure 2.1). X-rays are allowed to enter the active volume through a thin window. The active volume is the volume where the incident X-ray photons undergo collisions with the gas atoms. This geometry is filled with a suitable gas at a pressure usually higher than 1 atm. The cathode surrounding the very thin (typically $\sim 20\text{--}40\ \mu\text{m}$ diameter) axial wire is normally grounded.

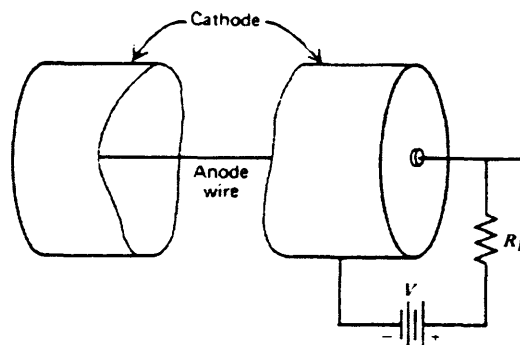


Figure 2.1: A cylindrical proportional counter. R_L is a load resistance [Knoll, 1979].

Photons which enter the active volume of a gas counter will interact with the gas atoms and molecules and release energy in the form of ionisation or excitation. At energies below ~ 100 keV, the photoelectric reaction is dominant. In the photoelectric reaction, the incident photon is absorbed and it loses all of its energy by giving that energy to a well bound electron which in turn leaves the atom. This electron is called the photoelectron which in principle can be emitted from any shell whose binding energy is less than that of the incident photon, but most probably

it will be the shell with binding energy closest to that of the photon. As a result of the atomic relaxation, an X-ray photon will be released.

The excitation energy may instead be transferred directly to one of the outer electrons. This electron, which is called an Auger electron, will be emitted with energy equal to the difference between the excitation energy and its binding energy. The probability of this alternative depends on the atomic number, and is more likely at lower Z .

The electrons and ions created in the ionisation events are free in their motion, and as a result of that free motion they collide with the molecules of the counter gas. The mean free path, λ , which is defined as the average distance travelled by an electron or ion in the gas before an interaction takes place, is equal to $1/\mu$ [Tsoufanidis, 1983], *i.e.* the mean free path of electrons or ions in a certain gas medium is inversely proportional to the number of gas molecules per unit volume.

The mean free path of electrons, λ_e , is considerably larger than that of ions. It is related to the ions mean free path, λ_{ion} , by [Kleinknecht, 1986]:

$$\lambda_e = 5.66 \lambda_{ion} \quad (2.1)$$

which is approximately fulfilled by most gases.

If an electric field, E , is applied between anode and cathode, then the electrons will drift in the opposite direction to E and the positive ions will drift in the direction of E . Electrons are collected long before the positive ions have moved away from the anode, which remains electrically neutral. It is only when these ions begin to move away that a negative charge pulse is observed by the signal processing circuit. Hence it is the movement of the positive ions that determines the pulse shape, *i.e.* the collection of electrons have a negligible contribution to the measured signal on the anode [Sanada, 1982; Tait, 1980].

The large mass and large cross-section of the positive ions for scattering make them drift slowly, with many collisions. The average drift velocity, v , will increase with the electric field strength, E , and will decrease as the gas pressure, p , is increased. An increase in the pressure will lead to a shorter mean free path during which the ion is accelerated before it loses its energy in a collision.

The average drift velocity, v , of the positive ions may be given by [Gilmore, 1992]:

$$v = \mu^+ E/p \quad (2.2)$$

where μ^+ is the positive ion mobility and p is the gas pressure. The term E/p is called the reduced electric field, S .

In ionisation chambers the electric field is just enough for the primary electrons to be collected at the anode, but in proportional counters the applied electric field is set to be strong enough to further accelerate electrons to gain sufficient energy between collisions so that they cause ionisation and hence produce secondary pairs. As the voltage is increased, a threshold field at which gas multiplication begins is reached, that is the charge in the counter begins to multiply, and the observed pulse amplitude will increase. Each primary electron finally generates a large number of electrons, or an avalanche, which is some times called Townsend avalanche. The total number of electrons in the avalanche is proportional to the number of primary electrons, and hence is dependent on the energy of the initial incident photon.

If the applied voltage is increased still further, the free electrons will move faster and quickly be collected. The positive ions move much more slowly, and therefore, each pulse within the counter creates a cloud of positive ions near the anode. If the concentration of these ions is sufficiently high, they represent a space charge which can significantly alter the shape of the electric field within the detector, as discussed below.

If the applied voltage is made sufficiently high, the space charge created by positive ions can become completely dominant in determining the subsequent history of the pulse. This finally leads to a situation where each output pulse from the detector is of the same amplitude, and no longer reflects any properties of the incident radiation. This is the “Geiger-Mueller” region of operation, as shown in Figure 2.2.

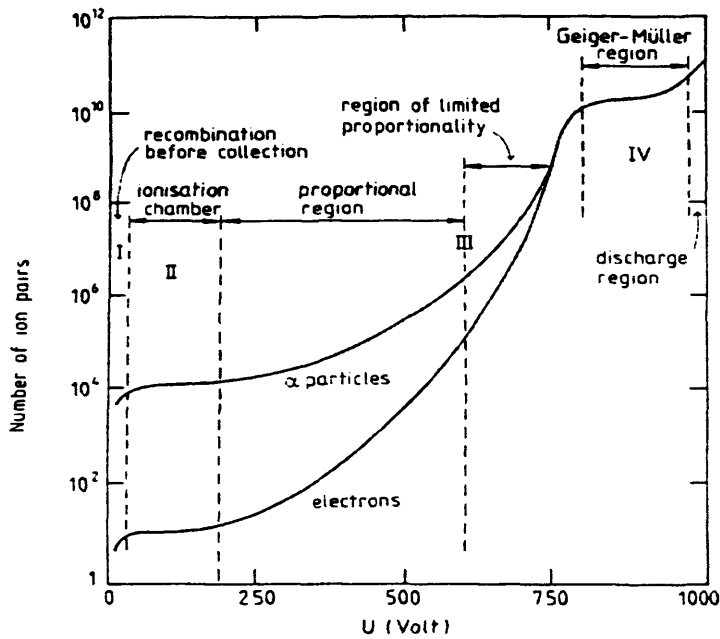


Figure 2.2: The different regions of operation of gas counters as resulted from detection of radiation of 1 and 2 MeV energies [Kleinknecht, 1986].

In case of a proportional counter of cylindrical geometry, the electric field is non-linear and it is a function of (V/r) , where V is the applied potential, and r is the radial distance from the anode. The electric field can be described by the equation:

$$E = \frac{V}{r \ln(b/a)} \quad (2.3)$$

where a and b are the anode and cathode radii respectively. Therefore, the reduced electric field for a cylindrical counter is:

$$S = V / rp \ln(b / a) \quad (2.4)$$

The electric field is inversely proportional to r (Equation 2.3), *i.e.* it is relatively weak at large r but becomes intense very close to the anode wire (at a distance of a few wire diameters). Therefore, the electric field far away from the anode wire is just sufficient for drifting the primary cloud, and almost all of the ion pairs are generated inside the critical radius and very close to the surface of the anode wire, regardless of where the original e-ion pairs are formed. The critical radius around anode wire, which can be called the avalanche region, is the region of the strongest electric field (Figure 2.3) where electron multiplication takes place. Increasing the applied voltage on the anode wire implies an increase in the avalanche region around it which results in a growth in the number of electrons produced per primary ionisation.

The theoretical analysis of Wilkinson (1950) and Sharp (1955) on the time development of the pulse from a cylindrical proportional counter has shown that the collected charge at time t can be expressed as [Gott and Charles, 1969]:

$$q(t) = q_{\max} C \ln(1 + t / t_0) \quad (2.5)$$

where:

t is the time from the start of the multiplication;

q_{\max} is final amount of charge in the avalanche;

C is the counter capacity per unit length $= \frac{1}{2 \ln(b / a)}$, where b and a are the cathode and anode radii respectively;

$t_0 =$ the characteristic time $= \frac{a^2}{4 C V_a \mu^+}$, with $V_a =$ anode voltage and μ^+ is the positive ion mobility.

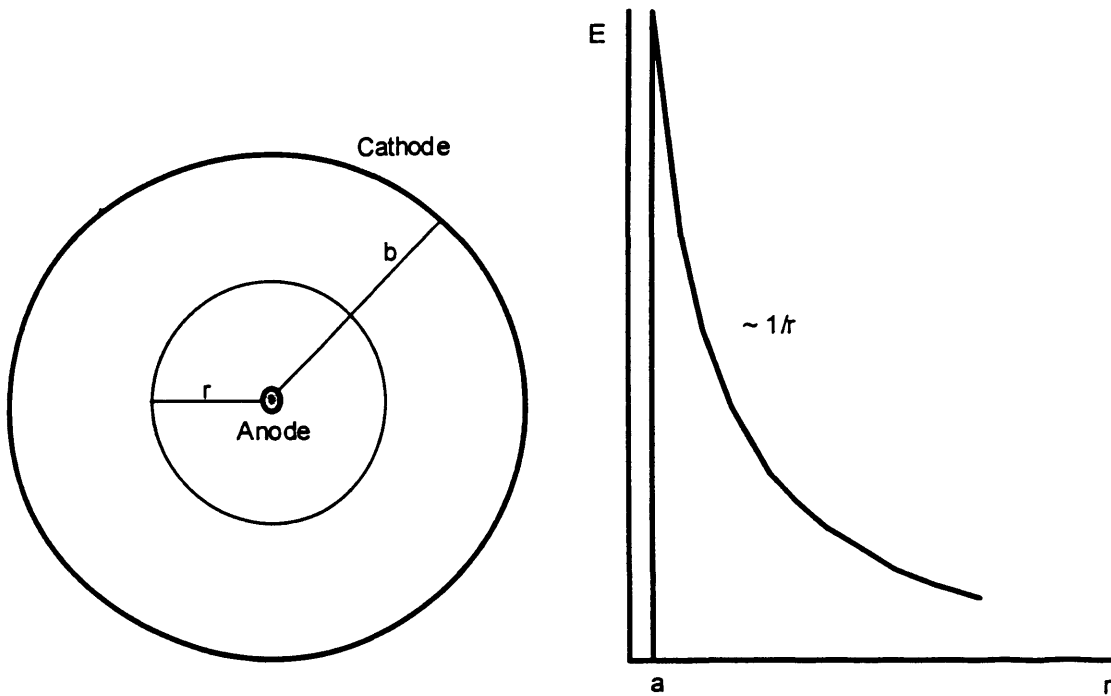


Figure 2.3: SWPC and the distribution of electric field around the anode wire [Sauli, 1977].

As the positive ions reach regions with a lower electric field, their motion is decreased and the signal rises correspondingly slowly. Therefore, the rate with which the signal pulse height increases is fast in the beginning and starts to be slower until the pulse height reaches its maximum value. However, the total drift time of a conventional proportional counter is relatively very long. It is, therefore, normal practice to limit the time response by differentiating the signal, because half of the signal is developed after just one thousandth of the total time. For a charge-sensitive preamplifier with shaping constant $\tau <$ the total drift time, the total collected charge becomes [Ye *et al.*, 1993]:

$$q(\tau) = q_{\max} C \ln\left(1 + \frac{\tau}{t_0}\right) \quad (2.6)$$

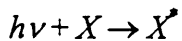
The pulse height measured at the output of the charge-sensitive preamplifier is a linear function of the input charge $q(\tau)$. Because of the logarithmic dependence of the integrated

charge on the value of the shaping time constant τ , gas gain measured by the pulse matching method can differ from the true value (see Chapter 4). The difference between the pulse height of the signal before and after shaping is known as the “ballistic deficit”.

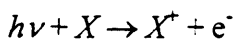
2.2 Quantum Detection Efficiency

When an X-ray photon, with energy $h\nu$ in the range ~ 10 - 100 keV, enters the active volume of a proportional counter filled with xenon ($Z=54$), the photoelectric interaction predominates.

The gas atoms may be excited or ionised by the incident X-ray photon depending on the photon energy. In case of excitation, the photon energy must correspond with the discrete energies of the excited states of the gas atom X [Rice-Evans, 1974]:



If the photon energy is greater than the ionisation potential of the gas atoms, photoionisation may occur:



As a result of ionisation of the gas atoms, a number of electron-ion pairs are produced. This number, n_0 , is given by:

$$n_0 = h\nu/W \tag{2.7}$$

where $h\nu$ is the photon energy and W is the average energy required to create an ion-electron pair. The average energy W is needed to be low in order to have a large n_0 . Table (2.1) lists values of W for some gases commonly used in proportional counters. It is clear that xenon has the lowest W amongst gases with single atom.

Table 2.1: Average energy (in eV) required to produce an ion pair in some gases [Manchanda *et al.*, 1990; Leo, 1994].

Hydrogen (H ₂)	37
Helium (He)	41
Nitrogen (N ₂)	35
Neon (Ne)	36
Argon (Ar)	26
Krypton (Kr)	24
Xenon (Xe)	22
Carbon dioxide (CO ₂)	33
Methane (CH ₄)	28
Isobutane (C ₄ H ₁₀)	23
Isobutylene (C ₄ H ₈)	21

If a photon beam is of intensity I_0 , and traverses a layer of gas of depth d or of mass depth $D = \rho d$, the intensity emerging from the layer can be written as:

$$I = I_0 e^{-\mu d} = I_0 e^{-(\mu/\rho)D} \quad (2.8)$$

where μ and μ/ρ are the linear absorption coefficient and mass absorption coefficient of the gas, respectively.

Irrespective of internal geometry, the quantum detection efficiency, Q , of any gas proportional counter may be written in the form [Fraser, 1989]:

$$Q = T_w \exp(-x_w \mu_w) [1 - \exp(-d \mu_g)] \quad (2.9)$$

where T_w is the geometric transmission of the window support, x_w is the window thickness, d is the drift region volume depth, and μ_w and μ_g are the linear absorption coefficients of the window material and of the gas, respectively.

Quantum detection efficiency of a proportional counter, therefore, decreases for low photon energies because of the absorption in the counter window, and for high photon energies because of the decrease in the photoelectric absorption cross section [Ouseph, 1975].

An important aspect of an imaging proportional counter's performance is the penetration of the X-ray beam into the detector, and consequently their detection efficiency (*i.e.* the greater the penetration, the less their efficiency). Any gas filling used has to have an adequate stopping power, which normally implies a high density (see Section 2.6 below).

2.3 Gas Gain

As mentioned in Section 2.1 above, if the electric field is sufficiently strong, the electrons may gain enough energy to excite or ionise gas atoms. When the energy of an electron exceeds the first ionisation potential of the counter gas, then a collision with a gas atom will produce an electron-ion pair.

2.3.1 Gas Gain Formula

At a constant anode potential, the gas gain, G , of the detector will be constant. It can be simply written as:

$$G = n / (hv/W) \quad (2.10)$$

where n is the final number of electrons, hv is the incident photon energy, and W is the energy required to produce an electron-ion pair, as mentioned in the above text. The probability of

producing an ion pair by a primary electron may be expressed in terms of a cross-section, σ_i , for ionisation of the atoms.

The probability that an electron will have an ionisation collision in distance dr can be given by $N \sigma_i dr$, where N is the number of atoms per unit volume. The increase in the number of electrons, n after dr is then given by [Gilmore, 1992]:

$$dn = n N \sigma_i dr \quad (2.11)$$

The product $N \sigma_i$ is the number of electron-ion pairs formed by an electron along a path of unit distance. It is referred to as the first Townsend coefficient, α , mentioned earlier in Equation 1.1 of Chapter 1. The larger the value of α the more collisions there are in a given distance, so Equation (2.11) can be written for the increase, dn , in the number of electrons as:

$$dn = n \alpha(r) dr \quad (2.12)$$

The number of electrons after a distance r will, therefore, be:

$$n = n_0 \exp\left(\int_0^r \alpha(r) dr\right) \quad (2.13)$$

where n_0 is the number of electrons present initially. If α is constant this will give the charge multiplication, or gas gain, G , to be:

$$G = n/n_0 = \exp(\alpha r) \quad (2.14)$$

This equation ideally gives the gas gain in a parallel-plate avalanche chamber where r here represents the depth of the avalanche region [Fraser, 1989].

The Townsend coefficient depends on the electric field strength and on the mean free path of the electrons and therefore on the gas type and pressure. Changes in gas pressure, temperature, voltage, ..etc. are the main source of gain variations.

Many authors have developed expressions for predicting the gas gain in SWPCs. Most formulae of gas gain have been derived from the simple expression first suggested by Townsend (1915), which is mentioned above (Equation 2.14). Each of these formulae fits measured data at various gas and counter conditions. An early work is that of Rose and Korff (1941) who suggested a gas gain formula to accompany their measurements. Other gas gain formulae have been published by: Khristove (1947), Diethorn (1956), Ward (1958), Williams and Sara (1962), Zastawny (1966), Charles (1972), Kowalski (1985), Aoyama (1985), Kowalski (1986), Akande (1992), and Uozumi *et al.* (1993).

The Diethorn formula is one of the most widely used formulae, and was derived by Diethorn (1956). Derivation of the formula has also been given elsewhere by a slightly different method [Delaney & Finch, 1992]. The Diethorn formula is based on the assumption that α is proportional to E . This formula can be expressed as:

$$\ln G = \frac{\ln 2}{\ln(b/a)} \frac{V}{\Delta V} \ln \frac{V}{\ln(b/a) a K p} \quad (2.15)$$

where V is the applied voltage, a is the anode radius, b is the cathode radius, p is the counter gas pressure, ΔV corresponds to the potential difference through which an electron moves between successive ionising events, and K is the critical value of E/p below which multiplication cannot occur.

According to Diethorn (1956), the constants ΔV and K are determined only by the properties of the counter fill gas. Table (2.2) gives values of ΔV and K obtained for some common gas mixtures by sets of experiments at different gas pressures.

In the present work, Diethorn gas constants for Xe+5%CO₂, Xe+5%Isobutylene(C₄H₈), and Xe+20%Ar mixtures were calculated (in Chapter 5) using data from a set of experiments at different gas pressures up to 10 atm.

Table 2.2: Diethorn gas constants ΔV and K for some gas mixtures.

Gas Mixture	$K \times 10^4$ (V/cm.atm)	ΔV (V)	Ref.
CH ₄	5.64	40.3	a
Xe+5%CO ₂	3.66	31.4	b
Xe+10%CH ₄	3.62	33.9	b
P-10 (Ar+10%CH ₄)	4.80	23.6	c
P-5 (Ar+5%CH ₄)	4.50	21.8	c
C ₃ H ₈ (propane)	10.0	29.5	c
He+4% i-C ₄ H ₁₀	1.48	27.6	c
15%Xe+75%Ar+10%CO ₂	5.10	20.2	c
19.9%Xe+69.4%Ar+10.7%CH ₄	5.45	20.3	c
24.7%Xe+64.6%Ar+10.7%CO ₂	6.00	18.3	c

a Diethorn (1956).

b Hendricks (1972).

c Wolff (1973).

In almost all calculations used to derive gain formulae by the authors mentioned above, the space charge effect, the recombination of ions and electrons, and negative ion formation were neglected.

As mentioned in Section 2.1, the self-induced space charge effect is a harmful phenomenon which develops in the avalanche region as a result of the slowly moving positive ions drifting

toward the cathode. This causes significant reduction of gas gain at high gain values or at high count rate which in turn affects the energy linearity of the proportional counter [Mori *et al.*, 1982; Mathieson, 1986; Mathieson & Smith, 1992].

The principle in affecting the gas gain is that the avalanche will continue to grow, with increasing voltage, until a sufficient number of positive ions have been created which in turn reduce the field below the point at which gas multiplication can take place. The primary electrons which arrive at the multiplication region after previous avalanches find a weaker field and are multiplied by a gain which depends on the total number of avalanches. The magnitude of the space charge is a function of the primary ionisation and the gas gain, G . If the primary ionisation is very small, the value of G may reach 10^5 to 10^6 before the space charge can affect the proportionality. On the other hand, if the primary ionisation is too strong, the critical value of G is smaller [Tsoulfanidis, 1983].

One, therefore, should operate a proportional counter at low gas gains where such space charge effects will not be important and the final signal will be proportional to the initial ionisation.

2.3.2 Measuring Gas Gain

A common method of measuring gas gain in a proportional counter is the so called “pulse matching method”. This method is quite old and was used by Rose and Korff (1941) to make their initial gas gain measurements. The principle of this method is to use a precision pulse generator to match on an oscilloscope the pulse amplitude from monoenergetic X-rays falling on the proportional counter [Hendricks, 1973].

Gas gain measurements using the pulse matching method have to be corrected for the difference in rise times of pulses from the counter and the pulse generator, which are attenuated

differently by the amplifier shaping networks [Charles, 1972]. More details will be given in Chapter 4 as this method has been employed for the gas gain measurements reported in Chapters 5 and 6 of the present work.

2.4 Fluctuation in the Pulse Height

As mentioned in Section 2.3.1 above, the pulse height obtained from a proportional counter is strictly proportional to the deposited energy, and to the gas gain G , as long as the space charge due to the positive ions does not modify too much the electric field around the anode wire. As the energy deposited rises, the random variation of the signal will steadily become less significant. This trend will continue until the energy rises to such a value that new excitation processes become energetically possible. At this point the number of such new excitations which may be produced will be small, as each one requires much of the available energy, and statistical fluctuations in this number will again be relatively large [Gilmore, 1992]. The pulse height distribution from a proportional counter is affected by fluctuation in the initial number of electron-ion pairs produced by the X-ray photon absorption, and also by fluctuation in the gas multiplication process.

2.4.1 Fluctuation in Ionisation

The statistical fluctuation in the number of primary ion pairs produced and in the number of secondary electrons produced in the avalanche are factors which can significantly affect a proportional counter gas gain and energy resolution.

The electrons produced by the primary ionisation event become directly able to ionise more atoms in the counter gas. That is, each primary ionisation may produce an electron avalanche near the anode wire. If there are only a few ionisation events produced in the counter volume,

there will be no interaction between the avalanches caused by the primary electrons [Eichholz & Poston, 1979].

The fluctuations in the number of electron-ion pairs created in a volume of gas has been analysed by Fano (1947). The variance of this number n_0 can be given by:

$$\sigma_{n_0}^2 = Fn_0$$

where F is called the Fano factor, and it has values of ≤ 0.20 [Ribeirete *et al.*, 1983; Kase *et al.*, 1984] for most gases used in proportional counters. This equation can be re-written as:

$$\left(\frac{\sigma_{n_0}}{n_0} \right)^2 = \frac{F}{n_0} \quad (2.16)$$

If the number of ion produced was governed by Poisson distribution then F would equal unity.

2.4.2 Fluctuation in Gas Gain

The fluctuation in gas gain is subsequent to the fluctuation in the primary ionisation. The statistics of electron multiplication was first considered by Snyder ((1947) and then by Wijsman (1949), Legler (1955), and Kharitonov (1956).

Let A be the avalanche amplification, or number of electrons in the avalanche. Assuming that the probability of ionisation by an electron depends only upon the field strength and does not depend on the previous history of the electron, these authors showed that for large average avalanche amplifications ($\bar{A} > 100$), the distribution of the size of a single electron avalanche is of exponential form, and the relative variance of the avalanche size, $(\sigma_A / \bar{A})^2$, is equal to unity and usually denoted by f [Alkhazov, 1970].

The gas gain is the number of ion-electron pairs inside the avalanche divided by the number of electrons that started the avalanche. The multiplication could occur at any point along the path of electron; *i.e.* this process has a random nature, and the gas gain will not be constant but will show statistical fluctuations.

As shown in Section 2.3.1, avalanche multiplication can be described by using the Townsend coefficient α . The multiplication process may start with a single electron which ionises the gas atoms and then multiply further if the electric field is high enough. Therefore, the probability that the electron will multiply in distance dx can be given by $\alpha dx = \sigma_i N dx$, where N is the number of atoms per unit volume. The final distribution of pulse heights will be dominated by the early stages of the multiplication process, since the number of electrons later on will be so large that fluctuations will average out [Gilmore, 1992].

The charge, Q_c , created in the pulse on the anode wire can be assumed to be the sum of the charges created in each individual avalanche. The average gas gain, G , is given by:

$$G = Q_c / e n_0$$

or

$$Q_c = n_0 eG \tag{2.17}$$

Both n_0 and G are subject to inherent variation, therefore, the pulse amplitude from the counter is subject to fluctuation from pulse to pulse even in the case of equal energy deposition by the incident photon. The expected relative variance in Q_c can then be given [Knoll, 1979] by:

$$\left(\frac{\sigma_{Q_c}}{Q_c} \right)^2 = \left(\frac{\sigma_{n_0}}{n_0} \right)^2 + \left(\frac{\sigma_G}{G} \right)^2 \tag{2.18}$$

This can be written in terms of the variance of the single avalanche multiplication factor, A , as [Charles & Cooke, 1968; Alkhazov, 1970]:

$$\left(\frac{\sigma_{Q_c}}{Q_c}\right)^2 = \left(\frac{\sigma_{n_0}}{n_0}\right)^2 + \frac{1}{n_0} \left(\frac{\sigma_A}{A}\right)^2 \quad (2.19)$$

2.4.3 Energy Resolution

Although there are fluctuations in the initial number of e-ion pairs, and in the gas multiplication process, proportional counters are said to have a signal pulse height, at the counter output, proportional to the energy deposited by the incident photon.

The counter resolution, R , can be defined as:

$$R = \frac{FWHM}{\text{pulse height at the peak}} \times 100.$$

The overall resolution of a counter, R , can be expressed in form:

$$(R)^2 = (R_c)^2 + (R_s)^2 \quad (2.20)$$

where R_c is the counter energy resolution, and R_s is the counting system noise contribution which is typically negligible.

Provided all individual avalanches develop independently and there is no interaction between the primary ionisation and that resulting from the avalanche, the ultimate energy resolution of proportional counters can be obtained from Equation 2.19. Using Equations 2.7, 2.16, and the definition of f , in Equation 2.19, will result the following expression for proportional counter resolution [Alkhazov, 1970; Sipila, 1976]:

$$\left(\frac{\sigma_{Q_c}}{Q_c}\right)^2 = \frac{(F+f)W}{E_\nu} \quad (2.21)$$

here E_ν is the photon energy.

In case of a Gaussian distribution, the fwhm energy resolution of a proportional counter will then be given by:

$$\left(\frac{\sigma_{Q_c}}{Q_c}\right) = R = 2.35\sqrt{\frac{(F+f)W}{E_\nu}} \quad (2.22)$$

The relative variance, f , of the avalanche size depends on different parameters, such as anode wire diameter, and to improve energy resolution of the counter this factor should be reduced together with F and W . That is, the effect of the fluctuations on the energy resolution of proportional counters can be reduced by improving the efficiency of the ionisation mechanisms involved [Alkhazov, 1970].

The ionisation efficiency can be increased by means of the use of Penning mixtures [Penning, 1931; Sephton *et al.*, 1987] as will be discussed in the following section and in Chapter 5.

The fluctuations may be created by chemical reactions associated with the formation of avalanches. Such deterioration of performance occurs through deposits on old wires but also through the presence of small contamination of the counter gas [Blum & Rollandi, 1994].

To improve counter energy resolution, in addition to that the avalanche must be uniform and regular, the bias voltage must be stable, and the gas mixture must be also stable in composition (*i.e.* the gas should be highly pure). Other factors which affect energy resolution may include anode wire non-uniformity, electron attachment to impurities, and electronic noise.

2.5 Counter Gas Selection

The choice of gas mixture has a significant effect on the gas gain and energy resolution of proportional counters. The gas mixture should be selected to give as high a gain as possible. This reduces the need for a high electronic amplification, lowers the required operating voltage, and hence increases the breakdown threshold.

In principle, molecular gases can be used in proportional counters, as in ion chambers. Molecular gases are not preferred because they tend to capture electrons [Blum & Rollandi, 1994] hence reduce gas amplification and pulse height. Noble gases have zero electron affinity and low ionisation potential and hence high initial ionisation, *i.e.* they have low W . High gas gain, therefore, can be achieved using proportional counters filled with noble gases.

As mentioned in Section 2.2 above, in imaging proportional counters, any gas filling used has to have an adequate stopping power, which normally implies a high density. Therefore, although helium and neon have been used in proportional counters, their low mass make them unsuitable as gas filling especially for imaging purposes [Wolf 1974; Sipila, 1976]. Radon is the heaviest ($Z = 86$) of the noble gases but it is excluded because it is radioactive, an alpha particle emitter. Krypton has 15 isotopes and most of them are radioactive. Among these isotopes is ^{85}Kr which emits a high energy beta, making it unsuitable since it would increase the intrinsic counter radiation background [Peterson, 1975].

Figure 2.4 shows comparison of the cross-section for ionisation by collision of electrons with gas atoms for different noble gases, and clearly points out Xe, Kr, and Ar as the first choice. As xenon has an atomic number ($Z = 54$) larger than that of Argon ($Z = 18$), then it is considered to be the gas filling of choice in most applications [Christopherou *et al.*, 1979, 1980].

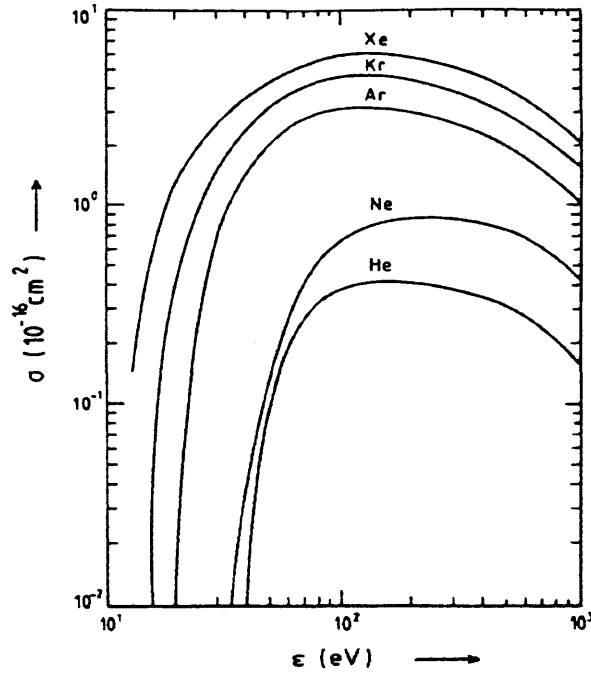


Figure 2.4: Cross section for ionisation by collision for electrons of energy ε in noble gases [Allkofer, 1969].

Xenon was selected in the present work to be the base gas for the different mixtures studied at different gas pressures up to 10 atm. As we are interested in X-ray photons of energies in the range 2-100 keV, xenon-based mixtures was expected to fulfil the requirements of an efficient and good performance counter for photons of energies in this range or higher. The detection efficiency comparison given by Manchanda *et al.* (1990) between a low-pressure xenon counter and an ultra-high-pressure argon counter is reproduced here in Figure 2.5.

2.5.1 Quenching Effect

As mentioned in Section (2.1) of this chapter, excited molecules of the counter gas may stabilise by emission of ultra-violet (UV) photons. These photons may not be always absorbed by the noble gases, and may be of sufficient energy to eject electrons from the cathode surface thereby creating further electron-ion pairs which may start additional secondary avalanches. That is, a noble gas is transparent to its UV photons emitted by the excited atoms. This process,

therefore, will be a source of gain fluctuation and will reduce the breakdown threshold of the counter. The work function of most common counter surface metals is less than 5 eV [Kaye & Laby, 1995].

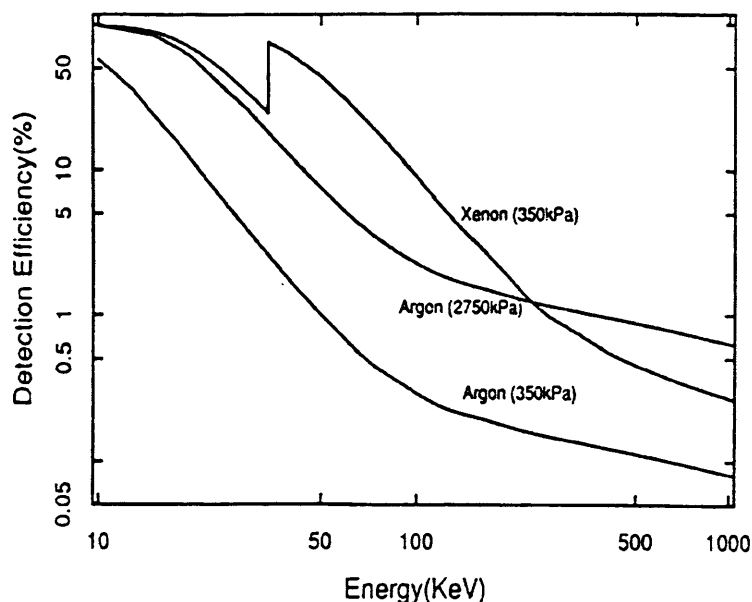


Figure 2.5: Detection efficiency of a xenon counter at ~ 3.5 atm pressure compared with an argon counter at ~ 3.5 and 27.5 atm pressures.

The problem has been solved by the addition of a small quantity of a polyatomic gas. These quenching gases, in general, are good absorbers of UV photons. This inhibits the extraction of further electrons from a metal surface by inert gases, and increases the breakdown threshold. Therefore, quenching gases reduce the mean free path of the noble gas photons and limit the extent of the discharge.

The excited molecules of the quench gas de-excite by either dissociation or by emitting one or more low energy visible or infrared photons, whose energy lies below the work function of the counter metal surfaces. The photo-ionisation threshold of some quench molecules can be found in Breskin *et al.* (1979).

Table 2.3 lists some quenching gases commonly used in proportional counters. The quench gas which should be selected should not be electronegative, and its lowest ionisation potential should be greater than the highest possible energy of the UV photons emitted by the noble gas atoms. The negative ions, if formed, have velocities close to those of the positive ions. Those negative ions could produce a spurious pulses in the counter.

Table 2.3: Properties of some common quenching gases

Gas	Molecular weight (g/mol)	Ionisation potential I (eV)	W (eV)
Argon	39.95	15.8	26.0
Methane	16.04	12.99	28.0
Carbon dioxide	44.1	13.68	33.0
Acetylene	26.04	11.4	25.7
Ethane	30.07	11.65	26.5
Propane	44.10	11.10	25.0
Isobutylene	56.11	9.30	20.9
Isobutane	58.12	10.67	23.0

Data are from Manchanda *et al.* (1990) and Christophorou (1971).

Mixtures of noble gases with hydrocarbons are commonly used in proportional counters but this type of mixture can limit the life of the counter [Turala & Vermeulen, 1982] because of the effect of quench gas polymerisation. This has a significant effect on the counter performance and could drastically reduce the gas gain of the counter and degrade its energy resolution [Dwurazny *et al.*, 1983].

Carbon dioxide has a relatively high ionisation potential (13.68 eV) compared with other common quench gases and, in addition to its low cost, has much lower danger of polymerisation [Faruqi, 1980].

Among the most common used gas mixtures in proportional counters are: Argon+10%Methane (CH₄), Argon+10%Ethanol, Ar+10% CO₂, or Argon+10% Isobutane (C₄H₁₀). Xenon has also been successfully used as the base gas in many areas of applications especially at high pressures (see Section 2.2 above). Common xenon mixtures are Xe+10%methane and Xe+5%CO₂, which was selected in the present work as a reference mixture.

For such gas mixtures, gas gain in the range of 10² to 10⁵ can be obtained, depending on the applied voltage. In general, gains of more than 10⁵ tend to saturate the counter so that all pulses are of similar size, and the energy dependence of the pulse height is lost. At this point the counter begins to function in the Gieger mode (Figure 2.3).

2.5.2 Penning Mixtures

Penning mixtures, *i.e.* mixtures of noble gases without a quenching agent, can provide high ionisation efficiencies which improve the energy resolution at low values of gas gain. The noble gas atom, X , may be excited by the incident X-ray photon to metastable excited energy levels. The Penning effect [Penning, 1931, 1934] takes place if the gas mixture contains another gas with an ionisation potential lower than the metastable excitation energy level of the first gas. The gas atom of the second type, Y , may be ionised rather than excited:



The Penning effect, therefore, reduces ionisation fluctuations in proportional counters, which means that proportional counters with Penning mixtures can give ionisation for much lower mean electron energies than are required in conventional quench mixtures, which results in higher gas gains at lower electric field, and hence an improvement in the counter energy resolution.

This has been proven experimentally to be true by many authors for different Penning mixtures [Sephton *et al.*, 1987; Agrawal & Ramsey, 1988; Agrawal *et al.*, 1989; Ramsey & Agrawal 1989; Bronic, 1995]. This was also shown in the present results reported in Chapter 5. At high values of gas gain, however, the lack of a quenching agent reduces the breakdown threshold and can lead to a degradation of energy resolution.

Much higher gains ($\sim 10^8$) have been reported by using special gas mixtures such as what has been called the “magic gas”- a mixture of Ar+Isobutane+Freon-13B1 [Bouclier *et al.*, 1970]. It is important in many applications to keep the energy resolution as good as possible if the gas gain is desired to be very high. In such gas mixtures very high gas gains require relatively very high applied voltages. For example, such special mixtures have been used in MWPCs and the applied voltage required to obtain an avalanche size of $\sim 10^6$ electrons was ~ 3 kV at atmospheric pressure [Koori *et al.*, 1984]. Operation at relatively high voltages increases the effect of self-induced space charge which in turn leads to poorer energy resolutions and finally the energy linearity of the counter will be lost.

As a conclusion, to achieve stable operation at high gas gain it is necessary that a quench gas is used in conjunction with the noble gas, and the choice of the quench gas is of significant importance.

2.6 The Effect of Counter Gas Pressure

As mentioned in Section 2.3 above, it is desired to use a low Z window material in the counter. At the same time the window should be made strong enough to resist the high pressure of the counter gas. This is one of the difficulties which usually arises in manufacturing large area high pressurised counters. This has been considered in the present work, and the MSPC used has been designed with a window which fulfil the requirements of being thin and able to resist high pressures up to ~ 11 atm, as described in Chapter 4.

Xenon has a very susceptibility to contamination with impurities such as Oxygen at reduced electric fields of less than 0.13 V/cm. Torr, and hence at high pressures [Sakurai *et al.*, 1991]. Therefore, xenon-based gas mixtures have to be very clean and pure at high pressures; a careful selection of the counter internal materials [Trow & Smith, 1992] becomes very important.

The work of Sakurai *et al.*(1991) has shown that methane-quenched gas fills were found to operate stably at gas gains up to 10^4 , regardless of pressure. These authors have found that the same was not true for pure xenon which would break down below this point for fills above 1 atm. Sakurai *et al.* also have reported that onset of breakdown in pure xenon occurred at progressively lower gas gains, as the pressure was increased.

Increasing the gas pressure in a gas counter will increase the density of the gas, *i.e.* bring the gas atoms closer to each other. This in turn increases the number of collisions the primary electrons make. That is, the mean free path and the mobility of the primary electrons will decrease as pressure increases. As Equation 2.2 shows, the drift velocity decreases with increasing gas pressure. As a result of the decrease in drift velocity of the primary electrons, the sensitivity of the counter even to small impurities will increase and hence the probability of electron loss to the formation of negative ions will be higher.

To keep the drift velocity unchanged, the drift field should be increased in proportion to the gas pressure. Keeping the drift velocity the same should produce the same total charge. At high anode voltages, the positive ions will still be able to create the same space charge with an electric field which could modify the anode electric field at low pressures. But the positive ion's electric field will be smaller than the increased drift field by the factor by which the pressure has been increased. Therefore the space charge effect at high pressures should exhibit a different behaviour [Blum & Rollandi 1994].

The self-induced space charge effect in proportional counters, has been found to increase with gas pressure as reported by Mori *et al.*(1982). This was taken into account in our work when gas mixtures were selected for operation at high gas pressures.

2.7 Multi-Wire Proportional Counters

The ionisation of the gas atoms in proportional counters is limited to a small region around the path of the incident photon. It is possible, therefore, to deduce some information about the position of any radiation entering the active region of the proportional counter. If the output charge pulse is taken from both ends of the central anode of a single wire proportional counter then there will be a difference in pulse height and rise time because of different resistance values through the anode wire in the two directions. The position sensitive signal is the ratio of the charge at one end to the sum of the charges from both ends. This method, as mentioned in Chapter 1, is called “charge division method” and it was first introduced in 1966 [Kuhlmann, 1966].

Another method was introduced by Borkowski & Kopp (1968). This method is based on the use of the pulse rise time instead of the magnitude of the charge, and the position signal is obtained from the rise time difference between the two pulses.

G. Charpak has introduced an imaging device by modification of the conventional cylindrical counter [Charpak *et al.*, 1968a, 1968b]. The Multi-Wire Proportional Counter (MWPC), which is sometimes called Charpak chamber, conventionally consists of a plane of equally spaced anode wires centred between two cathode planes, as shown in Figure 2.6, or between two arrays of wires as shown in Figure 1.2 of Chapter 1. Each wire could be considered as an independent proportional counter. For the mechanical construction of MWPC, one rule is to use a wire diameter of about 1% of the distance between anode wires to achieve sufficiently large electric field for gas multiplication, *e.g.* 20 μm diameter for 2 mm distance.

The length of the plateau, *i.e.* the region of electric field strength in which the chamber can be operated at full efficiency for minimum ionising photons and without breakdown, is determined by the gas multiplication and by the lower threshold of the amplifier following each wire, usually at about 200-500 μV [Kleinknecht, 1986]. The electric field, close to the anode wire, is roughly the same as in SWPC, but far away from the anode wire it takes a form which is shown in Figure 2.6.

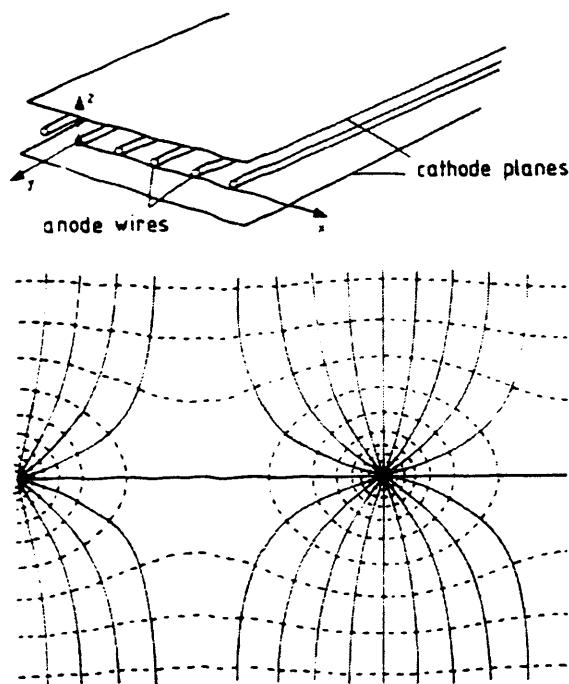


Figure 2.6: A schematic of an MWPC arrangement, and shape of electric field and equipotential lines in an MWPC [Erskine, 1972].

The gain of MWPC depends on the accuracy with which the electrode wires are aligned with each other. Small displacements of the anode wire, due to initial misalignments or electrostatic forces while under high voltage, can cause large gain variations across the detector plane and consequently degrade the energy resolution from that achievable with a SWPC. As an example, in a wire chamber with 25 μm anodes at 2 mm pitch, a displacement of 50 μm in a single anode will cause the gain on neighbouring anodes to vary by 20% [Ramsey, 1992].

Charges induced on the anode wires locate the position of the incident photon. The cathode planes could be made so that the pulses on them can also be used in determining the photon position. This is called the cathode readout proportional chamber.

The classical method is to make the cathodes in the form of an array of connected wires. The best way to extract accurate position information is to connect each cathode wire to a separate amplifier. This, of course, is difficult if a large number of cathode wires are used. Many different solutions, based on this configuration using the pulse amplitude, have been successfully introduced in this field. Among these configurations are the delay line readout [Grove *et al.*, 1970], RC line encoding [Fraser *et al.*, 1981a, 1981b], and the Graded Density readout [Mathieson *et al.*, 1980].

2.7.1 Graded Density Readout

A Graded Density readout element comprises [Mathieson *et al.*, 1980] a plane of wires of uniform pitch, connected electrically into two groups of wires, *A* and *B*. The connection (Figure 2.7) is made such that the density of wires connected to one output, *A*, decreases from left to

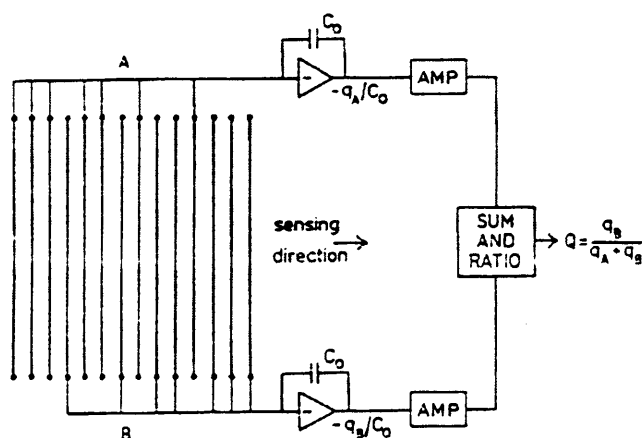


Figure 2.7: A schematic of a Graded Density cathode [Gilvin *et al.*, 1981].

right, and the density of wires connected to output B decreases from right to left. The charge q_A and q_B on each group will vary approximately linearly with position x , of the charge centroid across the electrode.

The position signal can be obtained as:

$$Q_x = q_B / (q_A + q_B) \tag{2.23}$$

In the absence of resistive noise, the principle noise contribution is from the preamplifiers and with suitable electronics this can be made very small [Fraser, 1989].

2.7.2 Disadvantages of MWPCs

Although MWPCs have been used successfully in many applications for more than twenty years, they have been reported to have some disadvantages which limit their performance. The main disadvantages of this type of counter is the limitation of the wire thickness and the wire spacing. This limits the spatial resolution of the counter and the count rate capability .

If the anode-cathode spacing is reduced this will shorten the ion collection time, and hence avoid the space charge build-up around the anode wires. However, below 1 mm wire spacing and below 2 mm anode-cathode gap, the MWPC becomes difficult to operate because of the electrostatic instabilities arising from the mechanical tolerances, unavoidable in detector construction with the iron solder technology [Bellazzini & Spezziga, 1994]. These drawbacks have been avoided in the new form of proportional counter called the Micro-Strip Proportional Counter (MSPC), which is discussed in the following chapter.

Chapter 3

Microstrip Proportional Chambers

In the previous chapter, a brief idea about the development of proportional counters to meet the demands of imaging was given. This chapter compares the MSPC with the MWPC in terms of operation, electric field distribution, and X-ray detection performance.

3.1 MSPCs Development

The original idea for the MSPC came from a desire to improve the qualities of the MWPC for neutron detection, in particular to increase the rate capability and the position resolution [Ramsey, 1992]. An MWPC consists of great number of thin anode wires assembled in a plane and mounted between two cathode plates. The high electric field strength necessary for avalanche amplifications in the gas is produced on the surface of the wires. A smaller wire spacing, however, causes the decrease of the field strength at the wire. In order to compensate for this loss, the applied voltage has to be increased, which, at below 1 mm wire spacing cause the operation of the counter to be difficult because of the electrostatic instabilities arising from the mechanical tolerances [Charpak & Sauli, 1984]. Even with larger wire spacing, it is difficult to ensure that the wires stay perfectly parallel under the action of the applied electric field and it is, therefore, a problem to maintain a uniform gas amplification over the entire sensitive area of the detector [Budtz-Jorgensen *et al.*, 1988].

Unlike MWPCs, the principle of MSPCs is that the anode and cathode electrodes are very narrow conductor strips. The field strength necessary to produce gas amplification is generated between neighbouring strips and by the voltage difference between the strips and the detector

cathode which can be at considerable distance. The MSPC is an ultraminiaturized version of the wire chamber, *i.e.* a proportional detector built with microelectronics technology. Drift and side electrodes define a region of collection of charges. Constructing such a chamber, with its strips on alternating potentials and at separations of a fraction of a millimetre, is only feasible provided these strips are fixed on an insulating substrate [Oed, 1988]. The application of the appropriate potentials on all the electrodes creates a proportional gas multiplication field [Bellazzini & Spezziga, 1994].

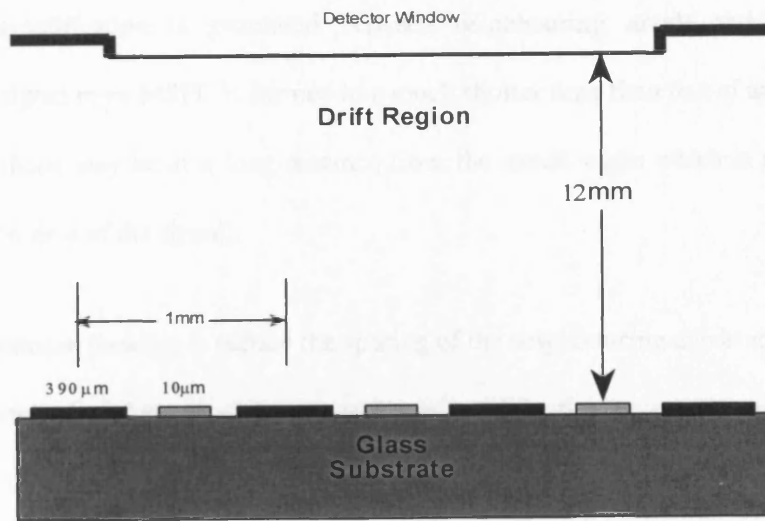
MSPCs, therefore, have been introduced as a new generation of position sensitive proportional counters to overcome some of the drawbacks which limit the use of MWPCs. Since their introduction in 1988, MSPCs have been considered among the most promising radiation detectors for many applications such as X-ray astronomy, high energy physics, nuclear physics and medical radiography.

In addition to their high energy and spatial resolution, due to the small spacing between electrodes, MSPCs have been proven also to have high counting rate capability. This is due partly to its fine pitch, which spreads the incoming flux over many electrodes, and partly to the very short ion collection time, which sharply reduces the space charge build-up [Budtz-Jorgensen, 1991]. However, systematic studies of high rate and long-term irradiation performance of MSPC show several types of instabilities in the chambers induced by the presence of the insulating support in the region of the avalanche [Alunni *et al.*, 1994].

3.2 Operating of MSPCs

Figure 3.1 is a schematic diagram of an MSPC. As mentioned above, this is a development of the MWPC design in which fine conducting strips on an insulating or partially insulating substrate

(a) Side View



(b) Plan View

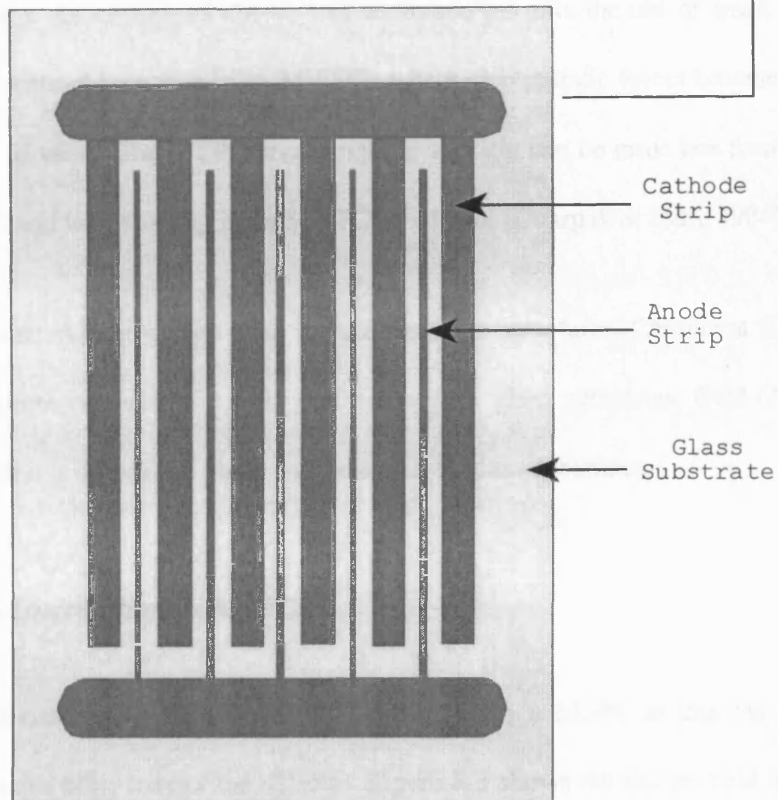


Fig. 3.1: The structure of an MSPC (not to scale). Dimensions shown are those of the Leicester detector, described in Chapter 4.

take the place of the conventional anode and cathode wires. The electric field necessary to produce gas amplification is generated between neighbouring anode and cathode strips. Therefore, the signal in an MSPC is formed in a much shorter time than that of an MWPC, where the detector cathode may be at a long distance from the anode wires which in turn results in a longer formation time of the signal.

If it is furthermore possible to reduce the spacing of the neighbouring anode and cathode strips to only a few multiples of the anode strip width, gas amplification takes place at a low potential difference.

The fine strip electrodes are usually laid down on the substrate by deposition using photolithography technology, with a precision of $\pm 0.2 \mu\text{m}$ or less, which offers very high spatial accuracy and uniformity. As mentioned above, this technique permits the use of small anode-cathode spacing which cannot be achieved in MWPCs where electrostatic forces become severe and disrupt the planes of wires. The MSPC anode-cathode spacing can be made less than $50\mu\text{m}$, while the smallest practical wire spacing in an MWPC is $\sim 1 \text{ mm}$ [Charpak & Sauli, 1984].

Different kinds of material have been used for the electrode structures. Chromium (Cr) and Aluminium (Al) are commonly used, since they adhere well to glass substrates. Gold (Au) has also been used although it is difficult to make it adhere well to glass substrates.

3.2.1 Electric Field Distribution in MSPCs

It is important to understand the electric field distribution inside a MSPC as this can help in predicting the performance behaviour of the detector. Figure 3.2 shows the electric field lines for a commonly used MSPC configuration. The applied electric potential alternates between the electrode strips so that the potential of the anode is positive relative to the adjacent cathodes and to the drift electrode (which can be the detector window).

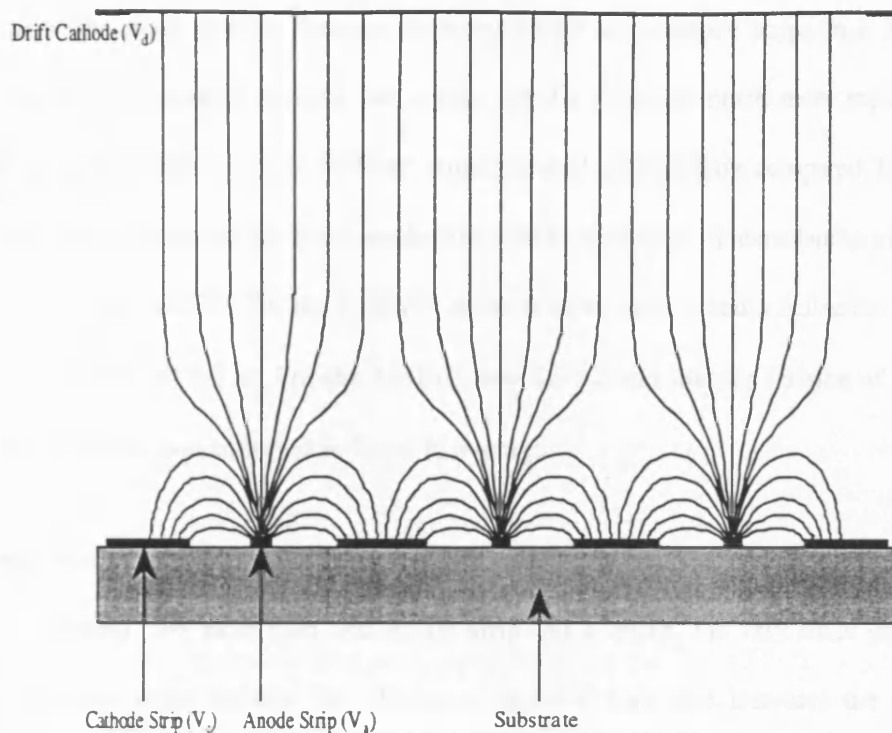


Figure 3.2: The electric field distribution in a MSPC [Bateman & Connolly, 1993a; Bellazzini & Spezziga, 1994].

Side electrode strips together with the drift electrode define the region of charge drift and collection. Such a configuration creates a proportional gas multiplication field, with the maximum value of the electric field near the edges of the anode and cathode strips. Thus, if electrons are ejected from the surface of the cathode, they might be multiplied in the high electric field region and cause the detector to breakdown.

3.2.2 Signal Development

The photoelectrons produced by photon absorption into active volume of the chamber will drift towards the strips under the influence of the applied electric field. In the avalanche region near the anode strips, electrons are collected by the anodes while the positive ions drift back mainly towards the adjacent cathodes inducing signals on both anodes and cathodes.

Because of the much smaller distance between anode and cathode strips in a MSPC, the positive ions in the avalanche around the anode will be collected much more rapidly by the neighbouring cathode than that in an MWPC. Angelini *et al.*(1993a) have compared, by means of a full Monte Carlo simulation, the time needed for a full collection of the avalanche charge in an MWPC, MSPC, and MGPC. For the MWPC, these authors have found a collection time of 84 μ s and for the MGPC of 9.2 ns. For the MSPC, they have found that the fraction of ions which go to the side cathodes was collected in 73 ns in average.

Another benefit from the small anode -cathode spacing is that the charge cloud will have a chance to be shared over more than one anode strip. As a result, the very small gap between anode and cathode strips reduces the effects of space charge and increases the count rate capability of the detector.

3.2.3 Substrate material

For stable operation of a MSPC care should be taken when selecting the substrate material. A variety of insulating materials have been used in fabricating the substrate. They can be loosely broken down into three groups: resistive glasses, ion implanted solids, and thin plastics [Ramsey, 1992]. Glass substrates have a very smooth surface which makes them particularly suitable for photolithography processing.

Most substrates exhibit the problem of charging up when positive ions reach the substrate surface. This modifies the electric field and produces time and rate dependent gain variations. This problem was encountered in the early work of Oed (1988), and was solved by applying a bias to the back of the MS plate similar to that of the anode strips, so that the positive ions on the front surface would be repelled- hence reducing the charging.

Since that time, attempts have been made by different groups to solve the problem. One of the most effective solutions is to use lower resistivity materials [Budtz-Jorgensen *et al.*, 1989; Gong *et al.*, 1994]. Semiconducting glasses [Oed, 1988; Bateman & Connolly, 1993a, 1993b; McMahon *et al.*, 1994] and different types of plastic [Bouclier *et al.*, 1992; Barasch *et al.*, 1992; Dixit *et al.*, 1994] are commonly used as substrates in MSPCs. Bouclier *et al.* (1992) have tested MSPCs manufactured on thin (100 μm) foil plastic supports, and reported that such chambers can be operated at large proportional gas gains ($\sim 10^4$) with reasonable energy resolution (better than 20% at 5.9 keV). The substrates they have used are Kapton and Tedlar which have quite different bulk resistivities, $\sim 10^{17}$ and 10^{14} $\Omega\text{-cm}$, respectively. Barasch *et al.* (1992) have studied ~ 50 different plastics and glasses to identify materials suitable for use as substrates in MSPCs. They have identified two particular plastics, BF Goodrich co-polyester ABS Cicolac and Mobay Texin polyurethane copolymer, which have a surface resistance of 10^{13} $\Omega\text{-cm}$.

Ion implantation is an effective technique when used in lowering the surface resistivity of quartz or silicon substrates to keep the gas gain of MSPC stable. Ion implanted quartz and silicon substrates have given encouraging results in terms of gain stability [Angelini *et al.*, 1992a, 1992b]. A difficulty with these type of substrate is that it cannot be easily made sufficiently thin to allow the manufacture of 2-dimensional readout based on induced charge on the rear of the substrate.

Plastic substrates are more flexible than those of glass and can be made much thinner and also in different geometries, but while glasses show problems connected with charging-up, the high surface resistance of plastic could lead to flux dependent charging effects. However, it is found that low resistivity glasses give better results. Corning 7740, a borosilicate glass with a resistivity of 10^8 $\Omega\text{-cm}$ was found to be ideally suited as a substrate [Budtz-Jorgensen *et al.*, 1989]. The MSPC results reported in Chapter 6 of the present work were obtained using a microstrip plate of this type.

3.3 Gas Gain in MSPCs

MSPC gas gain behaviour depends on the type of substrate used. The gas gain uniformity of MWPCs depends on the accuracy with which the electrode wires are aligned with each other. In MSPCs this is avoided because of their extremely precise pattern of metallisation. A one sigma gain variation of 1.1% over a 25 cm² MSPC with 0.8 mm pitch has been reported [Ramsey, 1992].

At high gas pressures in both MSPCs and MWPCs, higher voltages are required to produce gas gains of 10³ - 10⁴. It is therefore to be expected that substrate charging will become more serious. As mentioned above, the problem of substrate charging-up can be solved by applying a repulsion field to the rear of the microstrip plate [Oed, 1988], or by modification of the substrate material [Bishai *et al.*, 1995].

Therefore, apart from the substrate charging problem, the gas gain suppression noted in MSPCs prior to breakdown is probably due to the space charge effect although this effect has much less influence than in ordinary proportional counters. It is well known that the gas gain decreases and hence the energy resolution degrades in such situations in SWPCs and MWPCs [Sipila *et al.*, 1980; Mori *et al.*, 1982; Mathieson & Smith, 1992].

As the space charge effect can be reduced by a further reduction in the anode-cathode spacing, the maximum attainable gas gain will then be limited by breakdown between the anode and cathode strips. In ordinary gas detectors, breakdown depends mainly on the gas used, but in MSPCs it is also possible that the very high electric field at the microstrip electrodes' edges could easily cause such a breakdown. This commonly occurs in MSPCs at the tip of the cathode metallisation where they terminated at the anode end of the microstrip plate [Bateman & Connolly, 1993a].

The highest gas gain that can be attained before breakdown of the gas in a MSPC is a variable and unpredictable quantity [Bateman & Connolly, 1993a] lying in the range of about 10^3 - 10^4 . This range depends on the gas mixture used [Geijsberts *et al.*, 1992], the substrate type (thin layer or bulk conductivity), and the thickness [Pestov & Shekhtman, 1993], and shape of the electrodes [Duerdoth *et al.*, 1994]. An obvious option to improve MSPC performance in terms of the highest attainable gas gain is to use more quenching gas such as DME or Ethane (see Section 2.5 of Chapter 2). Another alternative is to design the cathode strip to have semi-circular ends. This method of electrode modification has been proposed and tested by Duerdoth *et al.* (1994) who have reported an increase of about 50 % in the maximum gas gain. Bouclier *et al.* (1994) and Salomon *et al.* (1994) have suggested other solutions include a method of passivating the MSPC with a very thin layer of Nickel Oxide Coating.

A recent study on the influence of geometrical parameters on the maximum gain that can be attained in a MSPC has been carried out by Bouclier *et al.*, (1995). These authors have confirmed that a single electron emission from the cathode is a precursor of discharge, particularly for gas mixtures with a high fraction of quencher. They have found that the maximum gain is obtained in a narrow range of cathode strip width and have suggested an optimum cathode width of 90-100 μm for a pitch of 200 μm .

Attempts have been made to derive gain formulae [Florent *et al.*, 1992] or to simulate the gain in MSPCs [Bellazzini & Spezziga, 1994; Schmidt *et al.*, 1994]. However, in order to predict the gas gain in a proportional counter, we should have a good knowledge of the electric field, which, in the case of MSPCs must be obtained numerically by integrating Laplace's transformation. For practical analysis of the behaviour of MSPCs, a simple approach is required, such that suggested by Bateman & Connolly (1993a). These authors have utilised a simple model derived for a cylindrical wire counter and ended with a semi-empirical gain formula which fits the behaviour of different types of flowing gas counter.

The application of SWPC gain formulae to MWPC [Tomitani, 1972] depends on the radial symmetry of the electric field. In the MSPC, there is no such radial symmetry and the transformation is not possible. Therefore, if the Diethorn formula (Equation 2.15 in Chapter 2) is to be applied to a MSPC, it will have to take account of the difference in MSPC geometry from that of a SWPC.

A rough approximation is to consider each anode strip as a single wire in a wire proportional counter with cathode radius equal to the spacing of anode-cathode centres. This approximation was used in the present work to predict the gas gain in the MSPC, as reported in Chapter 6.

3.4 Energy Resolution of MSPC

The work of Sakurai & Ramsey (1992) has shown that energy resolution of a single wire proportional counter can be improved from 8.1% to 7.0% if the anode wire radius is decreased from 100 μm to 12.5 μm . They have shown that proportional counters with thinner anode wires operate at stronger reduced electric fields than those with thicker anode wires.

Referring to Equation 2.21 in Chapter 2, the variance in gas multiplication, f , depends on the quantity $\chi = \alpha V_1 / E$, where α is the first Townsend ionisation coefficient, V_1 is the first ionisation potential of the gas, and E is the electric field strength [Alkhazov, 1970]. In order to reduce the uncertainty in the charge multiplication it is necessary to maximise the probability of ionisation taking place at each collision. This requires the value of χ to be large, which can be met by increasing the applied electric field [Sephton, 1981]. A thick anode wire has an electric field in the multiplication region much lower than that for very thin wire. For example, the estimated reduced field, in a wire cylindrical counter, at which an electron is initially multiplied to two electrons is 92 V/cm-Torr for a 12.5 μm anode and 45 V/cm-Torr for a 100 μm anode, at a gas gain of 100 in pure xenon fill gas [Sakurai & Ramsey, 1992]. Therefore, operating MWPCs at

high electric fields necessitates the use of very fine anodes and close anode to cathode spacing - the essential geometry of MSPCs.

Energy resolutions of < 11% at 5.9 keV and 5.5% at 22 keV have been reported by the PISA group using an MSPC with 3 μm anodes with Ar+Ethane mixture at atmospheric pressure [Angelini *et al.*, 1990]. MSPCs have also been used with xenon mixtures and exhibited excellent performance at pressures comparable with the atmospheric pressure. Energy resolutions of 7.2% and 6.2% for 22 keV X-rays using MSPCs with 25 and 8 μm anodes, respectively, in a Xe+2%Methane have been reported [Fulton *et al.*, 1992]. Another group has reported an energy resolution of 13.6 % for 5.9 keV X-rays using an MSPC of 8 μm anodes with Xe+10%CH₄ [Budtz-Jorgensen *et al.*, 1990].

As mentioned above, a consequence of the fine electrode structure in MSPCs is the reduction of the space charge effect. Energy resolution, then, is expected to be almost independent of gas gain. The 13.6 % energy resolution reported by Budtz-Jorgensen *et al.* (1990) has been measured at a gas gain of 3×10^3 and it degraded to only 14 % at a gas gain of 2×10^4 . Similar behaviour of the energy resolution was noted in the present work using an MSPC of 10 μm filled with Xe+5%CO₂ even at higher pressures up to 5 atm, as reported in Chapter 6.

3.5 Advantages of MSPCs

In conclusion, MSPCs have the following major advantages over MWPCs:

- 1- As the spacing between the strips is much smaller than the smallest wire spacing in MWPCs, it is possible to reach a correspondingly much better position resolution.
- 2- MSPCs have excellent energy resolution.

- 3- MSPCs can work properly at high gain values with little or no degradation in their energy resolution. In other words, the energy resolution is independent of gas gain.
- 4- MSPCs have high count rate capability, up to 10^7 count/sec.mm² has been reported [Angelini *et al.*, 1990; Bouclier *et al.*, 1994].
- 5- Many more gases can be employed in MSPCs than in any other kind of wire detector [Oed, 1988].
- 6- MSPCs can be operated at extremely low voltages. Only 500V was found to be required to achieve a gas gain of 10^3 [Ramsey, 1992]. Reduction of the applied potential reduces the electric field on the substrate surface which provides much safer operating condition in terms of the probability of dielectric breakdown.
- 7- MSPCs have a much faster signal development than for MWPCs, *i.e.* fewer space charge effects.
- 8- MSPCs are simple in their fabrication. It is in principle easy to rapidly replace any damaged parts including the electrode assembly. Furthermore, MSPCs can continue to be operated even if some electrodes have been accidentally broken.
- 10- The successful use of thin plastic substrates opened the door to a possibility of constructing cylindrical imaging detectors suitable for many applications such as X-ray astronomy.
- 11- The microstrip assembly is physically more durable than the thin wire planes of MWPCs. This is an important feature for long term MSPC operation.

However, in addition to the substrate charging up problem, MSPC performance, as any gas detector, depends on the gas properties and its pressure. As mentioned in the previous section, the

problem of substrate charging and space charge effect are expected to increase with increasing gas pressure because of the requirement for higher voltages.

The MSPC has been found to perform well at pressures up to ~ 6 atm, using Xe+10CH₄ gas mixture, without any measurable degradation in its energy resolution or instability in its gain behaviour [Minakov *et al.*, 1993; Angelini *et al.* 1993b]. Our results reported in Chapter 6 of the present work also demonstrate a stable behaviour for a MSPC with Xe+5%CO₂ at gas pressures up to 5 atm.

The limited maximum gain of MSPCs in addition to the desire to use as small pitch as possible for different objectives, have led to developments of MSPCs with different configurations. These developments include the micro-gap chamber [Angelini *et al.*, 1993a] and the microdot chamber [Biagi *et al.*, 1995] (see Section 1.1.1_e of Chapter 1). Figure 3.4 shows the electric field and equipotential lines for a micro-gap chamber compared with those in MWPCs and MSPCs.

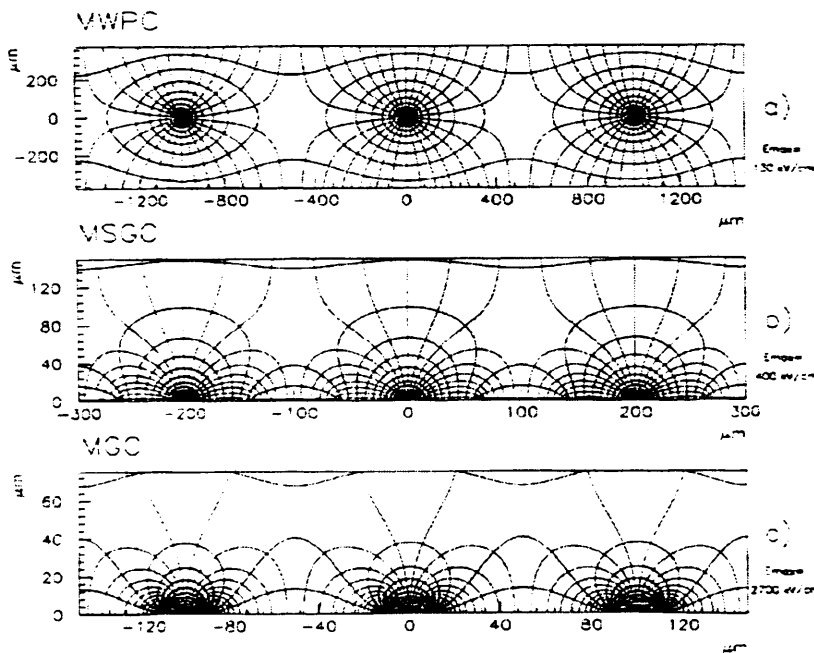


Figure 3.3: Electric field and equipotential lines for a MWPC, MSPC, and MGPC [Bellazzini & Spezziga, 1994].

Chapter 4

The Experimental Procedures for Gas Detector Evaluation

In the previous two chapters, a description of the principles of operating and the structures of SWPCs and MSPCs was given. This chapter gives a detailed description of the SWPC, the MSPC, and the counting electronics used in this work. The experimental work carried out on gas detectors was performed in two stages. The first stage was to evaluate the performance of an ordinary high pressure single wire proportional counter at different pressures up to 10 atm. The second stage was to build and test a high pressure MSPC, which was designed to operate as an imaging detector at high pressures. The first stage work enabled the Diethorn gas constants for the gas mixtures of interest to be determined and then used to calculate the predicted gas gain in the MSPC.

4.1 Detector Design

Both counters were designed in the Department of Physics and Astronomy at the University of Leicester. The electronic system used for this part of the work was the same for both the SWPC and the MSPC with the exception of the use of the additional high voltage supply for biasing the cathodes of the MSPC.

4.1.1 *The SWPC*

Figure 4.1 is a schematic which illustrates the main parts of the SWPC used in the present work. It was designed to be operated at pressures of > 10 atm. The main mechanical design parameters of the SWPC are listed in Table 4.1. As illustrated in Figure 4.1, the body of the counter, which

is mounted between two flanges, consists of two tubes; the first tube is made of stainless steel and the second tube is made of an aluminium alloy foil of 0.05 cm thick. The aluminium tube was slid and bonded into the stainless steel tube, which provides structure rigidity to the counter and allows it to withstand the high gas pressure. The counter wall thickness and the seals were designed to withstand pressures up to ~15 bar. The stainless steel tube is 12.5 cm long whereas the aluminium tube is 12.9 cm with 0.6 cm diameter. This represents a coaxial cathode which surrounds the 42.4 μm diameter anode wire. The anode wire is tightly clamped at both ends of the aluminium tube, and is connected at one end to a feedthrough to pass the signal to the counting electronics.

Seven slots were perforated in the surface of the stainless steel tube so that the aluminium alloy tube beneath these slots acts as a window of 0.05 cm thick. This thickness can easily be penetrated by ^{109}Cd X-rays with which most of the measurements in this work were carried out.

As very high voltage was expected to be applied on the anode wire, a good insulator was needed between the anode wire and the body of the counter; a KEL F (plastic) insulator was used for this purpose. A high voltage breakdown test was performed on the counter before it was attached to the filling rig.

The gas is introduced in the counter through the valve, and the counter seal against gas leak is provided by metal gaskets at both ends of the counter. The behaviour of the counter gas gain and energy resolution was investigated as a function of the anode voltage for the gas mixtures of interest at different gas pressures. The SWPC was leak tested to 10^{-8} torr l s^{-1} using the gas leak detector facility of the XRA group at the Department of Physics & Astronomy.

Prior to each refill with a new mixture, the counter and entire vacuum system were baked out down to a pressure of lower than 10^{-8} mbar at a temperature of 80 to 100°C for at least 3 days.

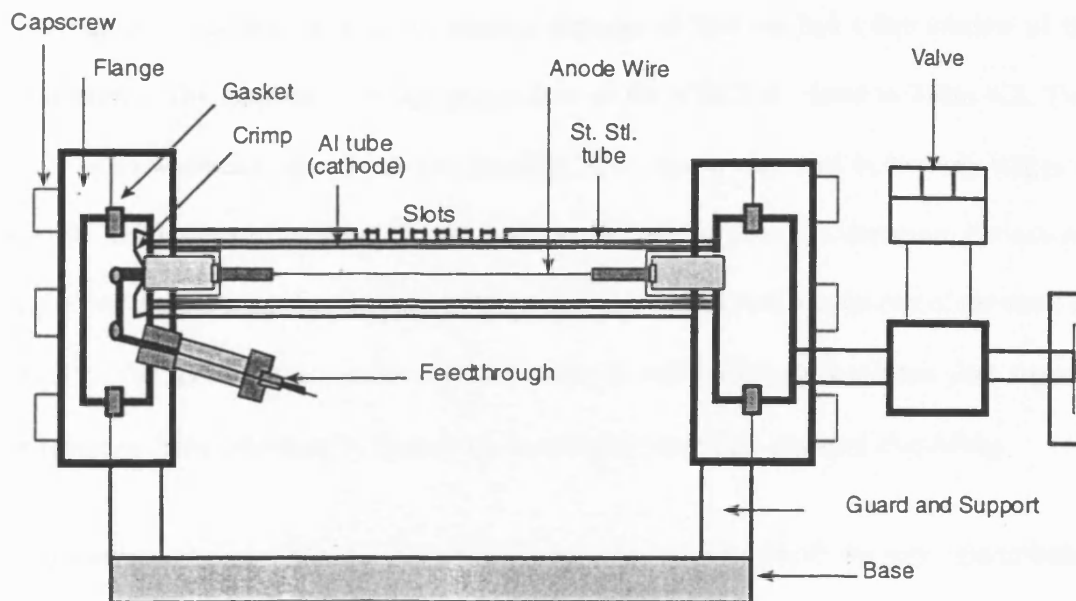


Figure 4.1: Schematic of the high pressure SWPC (by courtesy of J. Spragg).

Table 4.1: Description of the main mechanical design parameters of the SWPC.

Anode wire	stainless steel, 42.4 μm diameter
Cathode	aluminium alloy, 1.2 cm diameter
Window	aluminium alloy, 0.05 cm thick
Main tube length	12.9 cm
External body	stainless steel
Insulator	Kel-F

4.1.2 The MSPC

The Chamber where the microstrip (MS) plate was installed was designed and constructed earlier as an MWPC (see Figure 1.3 of Chapter 1). The body seals were of the knife-edge or “conflat” ultra-high vacuum type using a copper gasket. This chamber was modified for the present study by replacing all the multi-wire electrodes with the MS plate. A photograph of the chamber with the microstrip plate installed in is shown in Figure 4.2.

The stainless steel chamber with an internal diameter of 20.1 cm had a thin window of the same diameter. The mechanical design parameters of the MSPC are listed in Table 4.2. Two types of window material, aluminium and stainless steel sheets, were used in the early stages of this work. The stainless steel window was found much suitable than the aluminium for counter filling at pressures greater than 5 atm and was then selected to be used for the rest of the work on the MSPC. The stainless steel window was 25 μm thick and was attached to a top plate support to be protected from deforming by the excess internal pressure in the chamber after filling.

The feedthroughs are welded to the stainless steel body, and the whole was leak tight to better than 10^{-8} torr l s⁻¹. The chamber was leak tested using the leak detector, and then operated as a flow gas counter using Ar+5%CO₂. This mixture was supplied by BOC Ltd and was used to test the counter before it was sealed off and filled with the mixtures of interest.

Table 4.2: The mechanical design parameters of the MSPC

Anode-strip width	10 μm
Anode-strip pitch	10^3 μm
Cathode-strip width	390 μm
MS plate top to window	12.3 cm
Window	25 μm

The MS plate used, had 10 μm width anodes, 390 μm cathodes, and 1 mm anode pitch on a 7740 Corning glass substrate. The microstrip assembly was mounted in the chamber at distance of 1.23 cm from the window. The gas gain was set by biasing the anodes with respect to the adjacent cathodes, and the drift field was set by biasing these cathodes with respect to the window. All cathodes were connected together to an additional HV power supply to provide a drift field. More details of the chamber structure were given in previous works [Sims *et al.* 1981; Thomas, 1984].

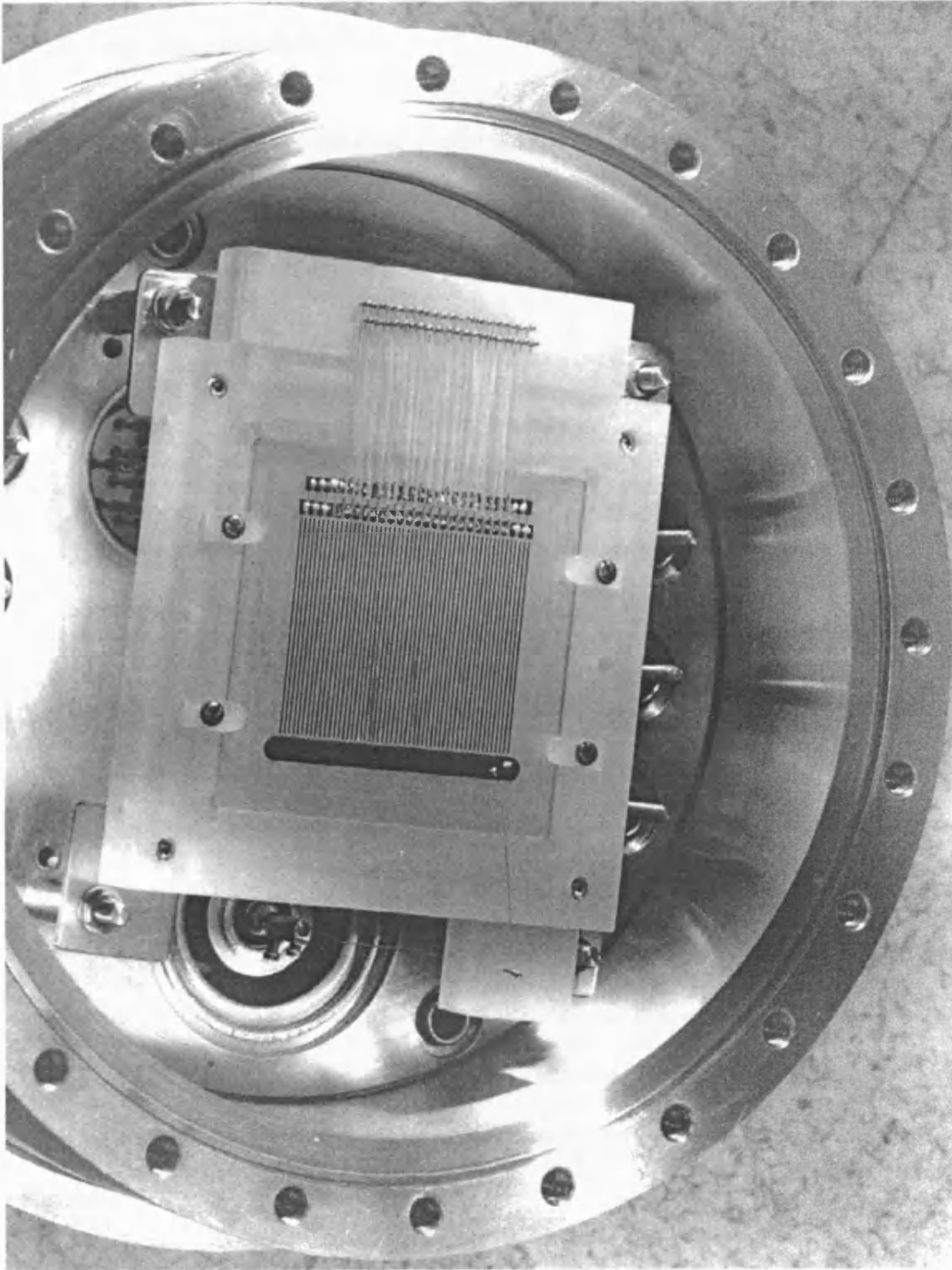


Figure 4.2: An internal view of the MSPC developed in the Department of Physics and Astronomy at the University of Leicester for the present work.

4.2 Gas Mixture Selection

As mentioned in the previous chapters, most studies on proportional counters have been carried out at atmospheric pressure, and Xenon was selected for the present work for the reasons discussed in Section 2.5 of Chapter 2, although it is more sensitive to very small gas impurities at high pressure.

The influence of the quench gas on energy resolution and gas gain is well known [Dwurazny *et al.*, 1983; Koori *et al.*, 1984; Kowalski *et al.*, 1992] and expected to be more significant at high pressures. The mixtures under study were: Xe+5%CO₂ , Xe-Ar (with different concentrations of argon), and Xe+5%Isobutylene (C₄H₈).

The selection of CO₂ was based on the facts that it is a low cost gas and has no polymerisation problems which effect the life of the chamber. It has a relatively high ionisation potential and hence is a conventional (non-Penning) quench gas. Carbon dioxide quench mixture has been found suitable for use in imaging proportional counters at 2 atm [Thomas *et al.*, 1982], whereas methane has been found to be of less quenching effect when used with xenon; a degradation in imaging proportional counters performance has been reported for such a mixture [Sims *et al.*, 1981; Thomas & Turner, 1983]. Therefore, a carbon dioxide quench mixture has been selected to be as a reference for comparison with other mixtures and to be examined at high pressures.

The behaviour of the SWPC at high pressure was investigated in the present work for different Xe-Ar mixtures to probe their feasibility at high pressures. The Penning mixture Xe+10% C₄H₈, has been studied at 1 atm [Agrawal & Ramsey, 1989] and been reported to exhibit a good performance in terms of gas gain and energy resolution. It was, therefore, selected in the present work to probe its behaviour at high pressures.

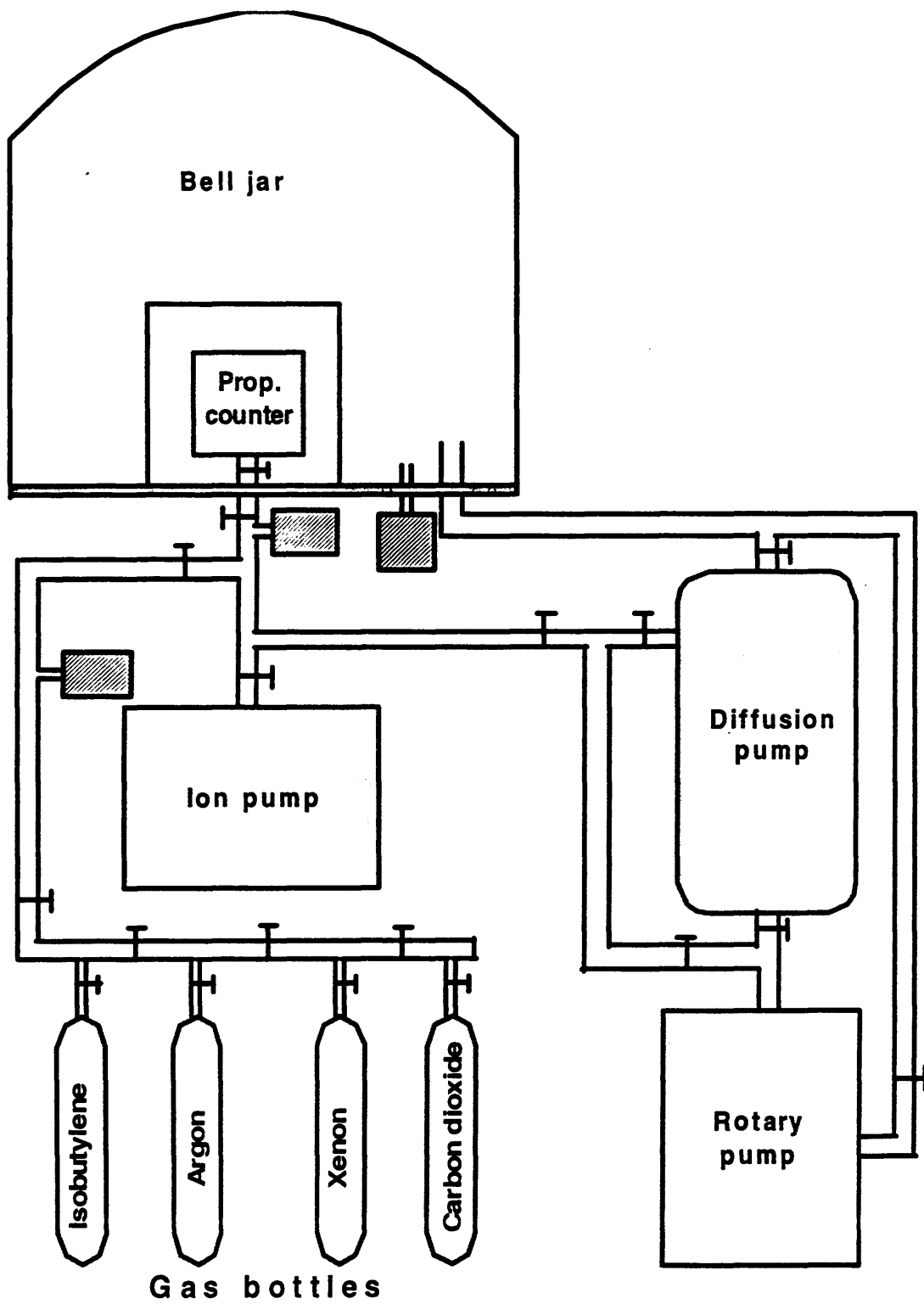
All gases used in this work were of research grade purity (~ 99.95%) supplied by BOC Ltd. They were introduced into the counters directly from the supplier containers without any further processing.

4.3 Counter Fill Procedure

Before each fill the same procedure was performed for both of the counters. The counters were evacuated using the pumping system shown in Figure 4.3. It consisted mainly of a rotary pump, a diffusion pump, an ion pump and a bell jar. Before the large counter was evacuated, the bell jar was pumped down to at least 0.1 mbar to protect the window of the counter from the high reverse pressure. Taking into account the small leak from the ring seal, the bell jar was pumped down each time to less than 10^{-6} mbar. This value of pressure was sufficient to keep the window safe, for at least 7 hours, from the high reverse pressure when the counter was evacuated and the bell jar was valved off. It happened, by accident, that it was left for more than 15 hours without causing any damage to the counter window.

In order to evacuate the counter, the bell jar was then valved off and the pipe system and the counter were evacuated. When a pressure of less than 6×10^{-7} mbar was reached the ion pump was operated. At counter pressure of less than 10^{-7} mbar heaters on the counter itself and on the piping system were turned on to increase the rate of outgassing.

The SWPC counter was baked at 80°-100° C for ~3 days, whereas the MSPC was baked for at least 7 days, depending on the counter status where sometimes it was extended to 12 days if, for any reason, the counter was opened to air. The temperature of the heaters surrounding the counter was controlled and monitored using two thermocouples. One was connected to a thermostat and the other to a Comark electronic thermometer. When the pressure had decreased again to less than 10^{-7} mbar, the heaters were turned off and the whole system was left to cool



 Pressure gauge
 Valve

Figure 4.3: The pumping system.

down to the room temperature. At room temperature, a pressure of less than 3×10^{-8} mbar was obtained in case of both counters. The counters then were ready for filling.

The gas mixtures were inserted into the counters using the partial pressure method. That is, we first introduce the minority gas filling and then valve off the detector. After evacuating the piping system, the majority gas filling is introduced in the counter so that, for example, 10 atm is achieved at 20° C.

After each fill the counter was left for at least half an hour before applying the high voltage. Large gas counters had been previously found to show an unstable behaviour if operated directly after filling [Turner, 1993]. This might be caused by the temperature difference between the electrodes and the gas being inserted.

4.4 Counting System Electronics

The pulse height distributions produced by the gas counters were obtained by detecting the signals created by the ^{109}Cd X-rays on the anode wire of the SWPC or on the anode strips of the MSPC. The pulse height distributions were studied with a counting system composed of commercially available NIM electronics modules.

The operating voltage of the SWPC was expected to be high at high gas pressure, as predicted by Diethorn formula [Diethorn, 1956]. For example, the predicted anode voltage required to obtain a gas gain of ~ 100 with $\text{Xe}+5\%\text{CO}_2$ at 10 atm is ~ 5.5 kV. This was calculated using the Diethorn gas constants ΔV and K obtained by Hendricks (1972) for the same gas mixture. Therefore, in the case of the SWPC, the Canberra 3106D (0-6 kV) bias supply was used. For the MSPC it was necessary to use a separate bias supply to provide the drift voltage needed to attract the electrons towards the avalanche region between the anode and cathode strips. This was obtained by connecting the Canberra 3002 (0-3 kV) bias supply to the cathode strips, where the

operating voltage of the MSPC was expected to be much lower than that of the SWPC as this has been previously shown by many other authors (see Chapter 3).

The X-ray signals received at the output of either counters were fed to the input of the charge sensitive preamplifier and then passed to the main amplifier for further shaping and amplification. The unipolar ($\tau = 4 \mu\text{s}$) or bipolar ($\tau = 6 \mu\text{s}$) output of the shaping amplifiers was then fed to the MCA to be stored and analysed.

Figure 4.4 illustrates a block diagram of the counting system used in this work. It consisted of the following components:

- 1- The power supplies: Canberra 3002 (0-3 kV), ORTEC 459 (0-5 kV), and Canberra 3106D (0-6 kV).
- 2- The preamplifier: Canberra 2006E.
- 3- The main amplifier: Canberra 2022 and ORTEC 571.
- 4- The oscilloscope: Telequipment D67.
- 5- The pulse generator: Tennelec TC 800 precision pulsar.
- 6- The Multichannel Analyser (MCA): A personal computer based MCA, Oxford PCA3.
- 7- The Digital Voltmeter: Schlumberger Solartron 7040.

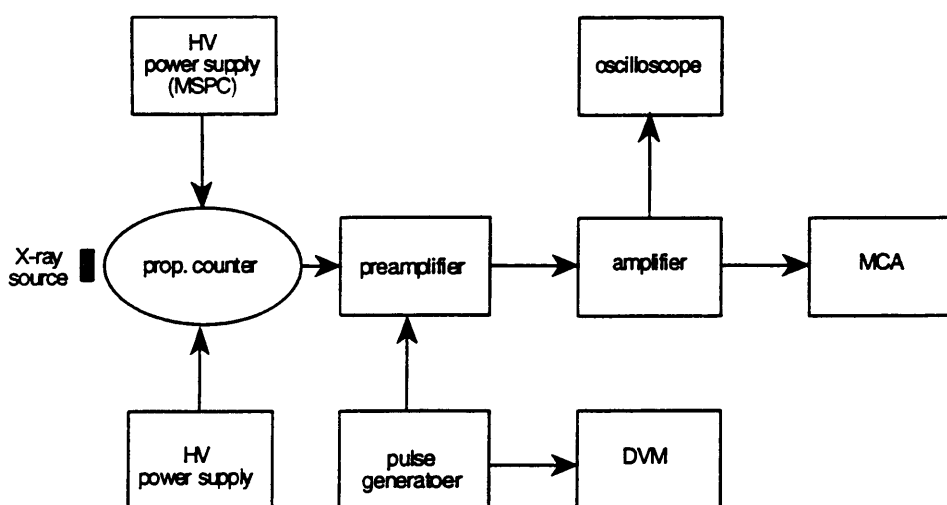


Figure 4.4: Electronics arrangement for the evaluation of the gas counter performance.

For calibrating the counting system a pulse generator was used. The preamplifier and main amplifier as well as the MCA were tested using a pulse of charge of 0.1 pC which ensured that each component had a linear response with charge.

In order to measure the gas gain using the pulse matching technique [Hendricks, 1973], a pulse generator, with the help of an oscilloscope and a digital voltmeter was used. The pulse generator was also used to measure the noise level at each anode voltage and its contribution to the counter energy resolution. These techniques are described in the following sections.

4.5 Counter Performance Measurement

Gas gain and energy resolution of the SWPC and MSPC were studied as functions of the applied potential and the gas pressure. For both counters, the same methods of measuring the gas gain and energy resolution were used.

4.5.1 Gas Gain Evaluation

The gas gain behaviour of the SWPC and MSPC was studied as a function of the applied voltage at different gas pressures. This was carried out for the different gas mixtures using the “pulse matching method” [Hendricks, 1973], and compared with predicted gas gain using the Diethorn formula [Diethorn, 1956].

It has been reported that measurements of gas gain can be in error by a factor of up to 10 depending on the methods of measurement [Kemshall *et al.*, 1969; Mathieson & Charles, 1969].

The “pulse matching method” is an old technique and was suggested by Rose and Korff (1941). The principle of this technique is to match the pulse height of the proportional counter charge output with a known charge created by a test pulse generator. That is if a known amount of charge Q_p created by a test pulse generator can be deposited at the input of a preamplifier in

of charge Q_p created by a test pulse generator can be deposited at the input of a preamplifier in parallel with the charge input from the detector, then by matching pulse heights of output signals from the main amplifier on an oscilloscope, it is possible to calculate the total charge Q generated in the detector. If W is known for the fill gas of the counter, the gas gain, G , can be determined directly [Hendricks, 1972].

If we rewrite Equation 2.4 as:

$$n = n_0 G \quad (4.1)$$

or:

$$Q = n e = n_0 e G = Q_0 G \quad (4.2)$$

The charge measured from the pulser, Q_p , can be written as:

$$Q_p = V_t C_t \quad (4.3)$$

where V_t is the pulser test voltage, and C_t is the preamplifier test input capacitance.

The gas gain, therefore, can be calculated by:

$$G = V_t C_t / Q_0 = V_t C_t / (h\nu/W)e^- \quad (4.4)$$

The predicted gas gains were determined first for a Xe+5%CO₂ mixture using the Diethorn formula (Equation 2.15 of Chapter 2). Before the measured gas gain was compared with theory, it had to be corrected for the “Ballistic Deficit effect”, *i.e.* the pulse attenuation by the amplifier network.

Pulses from the generator are step function type pulses because of their very short rise time ($\sim 0.02 \mu\text{s}$). This is much shorter than the collection time of the positive ions in ordinary proportional counters, which could be as long as tens of micro seconds. Because of this difference in rise time, the amplifier RC shaping networks will attenuate the pulses of the counter and generator differently. A shaping network of an equal integrating and differentiating time constants, τ , attenuates a step function by the factor $1/e$ ($= 0.368$).

We refer here again (see Section 2.1 of Chapter 2) to the theoretical analysis of Wilkinson (1950) and Sharp (1955) of the time development of the anode pulse from a cylindrical geometry proportional counter. The collected charge may be expressed as [Mathieson & Charles, 1969]:

$$v(t) = v_0 C_1 \log\left(1 + \frac{t}{t_0}\right) \quad (4.5)$$

where:

$$C_1 = 1/2 \log(b/a),$$

$$t_0 = a^2 / (4 C_1 V_a \mu^+),$$

and other terms have the same previous meanings. The parameters C_1 and t_0 can thus be calculated knowing the counter geometry, gas filling, and operating voltage.

Mathieson and Charles (1969) found that the pulse size (v_s) after shaping by equal RC integrating and differentiating networks of time constant τ was given by [Charles, 1972]:

$$v_s = v_0 C_1 [0.087 + 0.797 \log(\tau/t_0)] \quad (4.6)$$

Mathieson and Charles (1969) represented the attenuation ($f_{\text{max}} = v_s/v_0$) of the counter pulse, in the normal operating region of a proportional counter, as:

$$f_{\text{max}}/C_1 = 0.087 + 0.797 \log(\tau/t_0) \quad (4.7)$$

This equation has been verified by Gott and Charles (1969) for a variety of gas mixtures using a similar amplifier network to that assumed by Mathieson and Charles (1969). The correction factor which should be applied to the gas gain for such a case can then be written as $0.3679/f_{\max}$. The correction factor which should be applied to the gas gain measured with a pulse matching method takes into account the geometry of the counter as well as the gas pressure which is represented by the term μ^+ , the positive ion mobility.

In the present work, two shaping amplifiers were used because of a fault noticed in the ORTEC 571 amplifier during the work, then it was replaced by Canberra 2022. Therefore, two different shaping networks were used; the first network (the ORTEC amplifier) consisted of one *RC* differentiator and four *CR* integrators, using bipolar shaping with $6\mu\text{s}$ time constant. The other network (the Canberra amplifier) consisted of 1 differentiator and 2 integrators, using unipolar shaping with $4\mu\text{s}$ time constant.

The response of such amplifier networks to a step function of unit height has been evaluated by Fraser (1980) to be 0.195 for the first network and 0.271 for the other one. The responses of those networks to the pulses of the proportional counters were evaluated using Laplace transforms; a similar method to that adopted by Hendricks (1973) and later by Thomas (1984), which is described in the Appendix. The calculated correction factors which were applied to the measured gas gains in the SWPC are also given in the Appendix.

The positive ion mobilities used in these calculations for the different gas mixtures studied were estimated to be in the range $0.4\text{-}0.6\text{ cm}^2\text{ s}^{-1}\text{ V}^{-1}$. The mobility was assumed to remain constant with increasing pressure [Sood *et al.*, 1994] but the calculations were also checked assuming a changing mobility with pressure and the difference was found to be negligible.

In the case of the MSPC, the substrate charging-up effect on the counter gas gain were tested as this has been observed on most microstrip structures manufactured on insulating supports [Oed, 1988; Bouclier *et al.*, 1992; Bouclier *et al.*, 1993].

4.5.2 Energy Resolution Evaluation

Energy resolutions of the SWPC and MSPC were studied for 22 and 59.5 keV photon energies at different gas gains and pressures. The radioactive sources used were ^{109}Cd and ^{241}Am which were mounted on the counter stainless steel window support so that a few hundreds of counts per second were recorded.

The gas gain and energy resolution were measured mainly using ^{109}Cd source, therefore, 22.2 keV K_{α} and 26.2 keV K_{β} peaks should be presented in the pulse height spectrum. The two peaks individually were noted for the SWPC as well as for the MSPC although it was very difficult to analyse them separately.

For each gas fill, the level of the electronic noise was tested before and after biasing the counter. For each measurement of energy resolution, there was some contribution from the electronic noise, and the actual energy resolution of the counter was obtained as follows (see Section 2.4.3 of Chapter 2):

$$(\Delta E_C)^2 = (\Delta E_T)^2 - (\Delta E_N)^2 \quad (4.8)$$

where ΔE_C is the counter energy resolution

ΔE_T the total measured energy resolution

ΔE_N the electronic noise width.

The width of the electronic noise was obtained by means of the pulse generator signal selected to be on the same channel of the MCA as that of the X-ray signal.

Chapter 5

Results from the SWPC

In the previous chapter, the apparatus and methodology used for the gas counter work were described. This chapter presents the results obtained from the SWPC. The gas gain and the energy resolution of the SWPC were initially obtained at 2 atm pressure for comparison with other work and to predict the possible behaviour of the counter at higher pressures. The SWPC and MSPC (Chapter 6) were then studied at higher pressures for selected xenon-based mixtures using the same counting electronics. This chapter presents the results from the SWPC in terms of gas gain and energy resolution and explains the differences in counter behaviour at low and high gas pressures.

5.1 Gas Gain Measurements at Low Pressure

It is assumed in the measurements of gas gain and energy resolution of the SWPC that all secondary ionisation is produced by electron collisions with the gas atoms, *i.e.* the electron emission from the cathode surface caused by the UV photons is negligible. It is also assumed that secondary electron emission by positive ions at the cathode surface and electron recombination and attachment to neutral molecules are negligible.

The SWPC gain factors were measured using a ^{109}Cd X-ray source which emits X-rays with an energy of 22.2 keV. The measured gain factors were then corrected for the shaping attenuation and compared with the Diethorn formula [Diethorn, 1956] at different gas pressures. The Diethorn gas constants for the gas mixtures being studied were derived using the corrected measured gas gain, the gas pressure, and anode and cathode radii. The anode and cathode radii, a

and b , for the SWPC used were 21.4 μm and 0.6 cm respectively. The Diethorn gas constants were then used in estimating the predicted gas gain factors for the MSPC using the same Diethorn equation, as discussed in the next chapter.

The SWPC energy resolutions for the different gas mixtures under study were measured at 22.2 keV. Energy resolutions at 59.5 keV were also measured at selected gas gain values using an ^{241}Am source.

5.1.1 Gain in Xe+5%CO₂

The gain factor, G , which is the ratio of the output charge to the primary charge, varies exponentially with the anode voltage, V_a (see Chapter 2). This is predicted by the Diethorn equation which gives a straight line $G(V_a)$ relationship when plotted on a logarithmic scale.

The average energy, W , to form an electron-ion pair for this mixture has been given by Hendricks (1972) to be 21.7 eV. For the remainder of the work, W values for a particular mixture have been estimated using known W value for each gas component (see Table 2.3) in the mixture and calculating the number of primary electrons produced depending on the percentage of each gas component. For example, W for Xe+5%CO₂ was calculated for 22 keV incident energy as follows:

$$\text{number of ion pairs created} = \frac{22000}{22} \cdot 0.95 + \frac{22000}{33} \cdot 0.05 \approx 983$$

This corresponds to a W value of 22.4 eV compared with 21.7 eV obtained by Hendricks (1972).

Using the pulse matching technique discussed in Section 4.5 of the previous chapter, the observed (apparent) gain factor variation with anode voltage for Xe +5% CO₂ mixture at 2 atm pressure is shown in Figure 5.1a.

In order to calculate the predicted gas gain, Diethorn constants ΔV and K have to be calculated for each gas mixture used. At this stage of the work, *i.e.* at 2 atm pressure, we used the values of ΔV and K obtained for Xe+5%CO₂ mixture by Hendricks (1972) who calculated these constants using different experiments at pressures of 0.5 and 1 atm and found $\Delta V = 31.4$ V and $K = 3.66 \times 10^4$ V cm⁻¹ atm⁻¹.

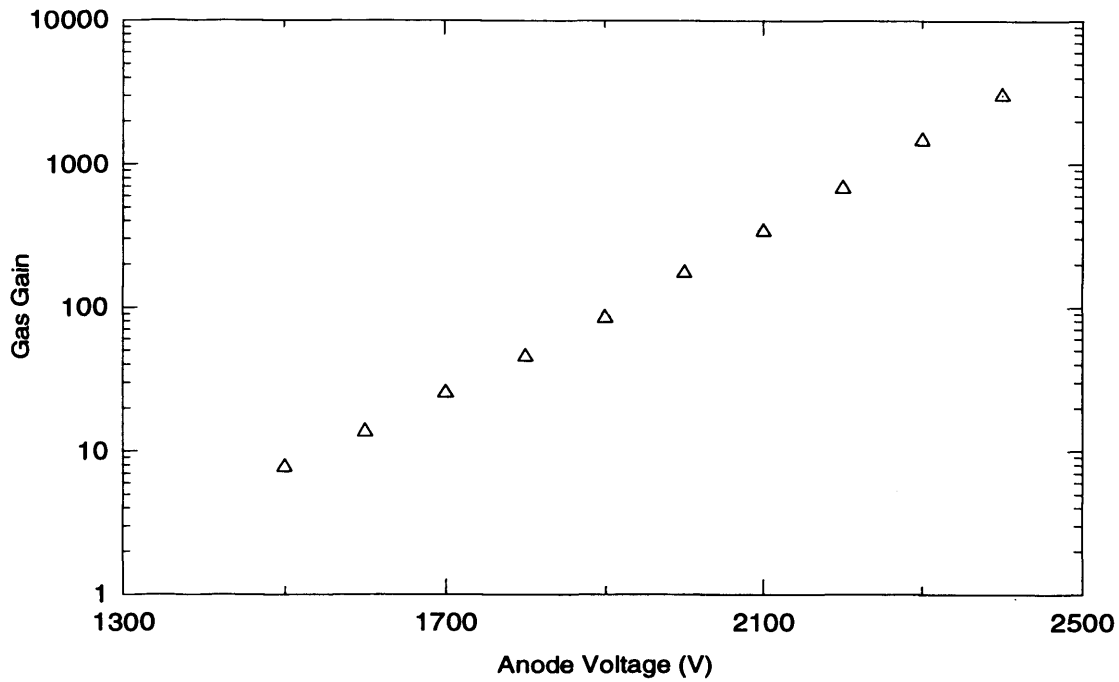
The corrected gas gain compared with the calculated values using the Diethorn equation is shown in Figure 5.1b. It is clear that the gas gain increases rapidly with anode voltage; for example, at high gains an increase of 50 V in the anode voltage could raise the gain by a factor of 2.

5.1.2 Gas Gain in Penning Mixtures

The Penning effect (see Section 2.5.2 of Chapter 2) takes place as a result of the fact that noble gas atoms can be excited to long lived metastable states. If the ionisation potential of the second gas is less than the metastable potential of the noble gas, the excited noble gas atoms may ionise the other gas atoms leading to an increased ionisation.

The first and second metastable energy levels of xenon are 8.3 and 9.4 eV respectively, and these for argon are 11.5 and 11.7 eV respectively [Kubota 1970; Bruckman *et al.*, 1983]. The Penning effect is strongest when the difference between the metastable energy level of the inert gas and the ionisation potential of the quench gas is at a minimum [Yamane, 1960; Ramsey & Agrawal, 1989].

(a)



(b)

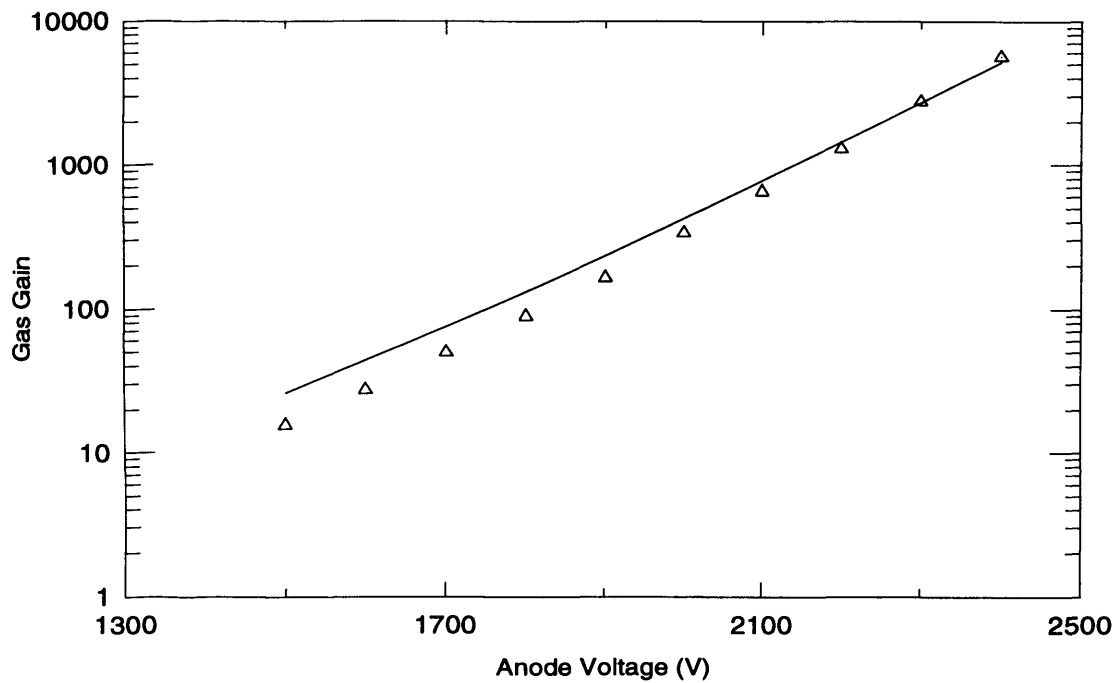


Figure 5.1: Gas gain as a function of the anode voltage of the SWPC using Xe+5%CO₂ at 2 atm pressure. (a) The apparent gas gain. (b) The corrected gas gain compared with the values calculated using the Diethorn equation with gas constants obtained by Hendricks (1972).

The ionisation potentials of carbon-dioxide (CO_2) and isobutylene (C_4H_8) are 13.78 and 9.35 eV, respectively [Christophorou 1971], therefore, Xe+5% CO_2 is a typical non-Penning mixture. In Xe+5% C_4H_8 , the Penning effect is induced by matching the first ionisation potential isobutylene to the second metastable energy of xenon (9.4 eV). This mixture has been studied at 1 atm pressure and has exhibited good performance at high gains (up to $\sim 10^4$) [Agrawal & Ramsey, 1989].

In the case of Xe-Ar mixtures, the ionisation potentials of argon and xenon are 15.80 and 12.15 eV, which means that the classical Penning effect is not expected to take place. These mixtures have been shown to exhibit a nonmetastable Penning effect which was first noted by Kubota (1970). This is most likely to happen in the case of Ar-based mixtures rather than Xe as can be revealed by the results reported in this chapter of the present work.

Gain factors for different Xe-Ar mixtures were obtained at 2 atm pressure; the gas gain variations with the anode voltage for those mixtures were compared with that of the Xe+5% CO_2 mixture. This comparison is shown in Figure 5.2.

The increase in gas gain, shown in Figure 5.2, occurs with increasing argon fraction in xenon, indicating an additional ionisation. As expected, this behaviour is not due to a classical metastable Penning effect, and may be explained by what is called the non-metastable Penning effect. It occurs when the xenon atoms collisionally de-excite the short-lived argon atoms in excited states lying above the principal metastable potentials of argon and become ionised [Agrawal & Ramsey, 1989].

The gas gain behaviour of the SWPC filled with Xe-Ar mixtures at constant anode voltages is shown in Figure 5.3 as a function of argon concentration. It is clearly seen that the gas gain

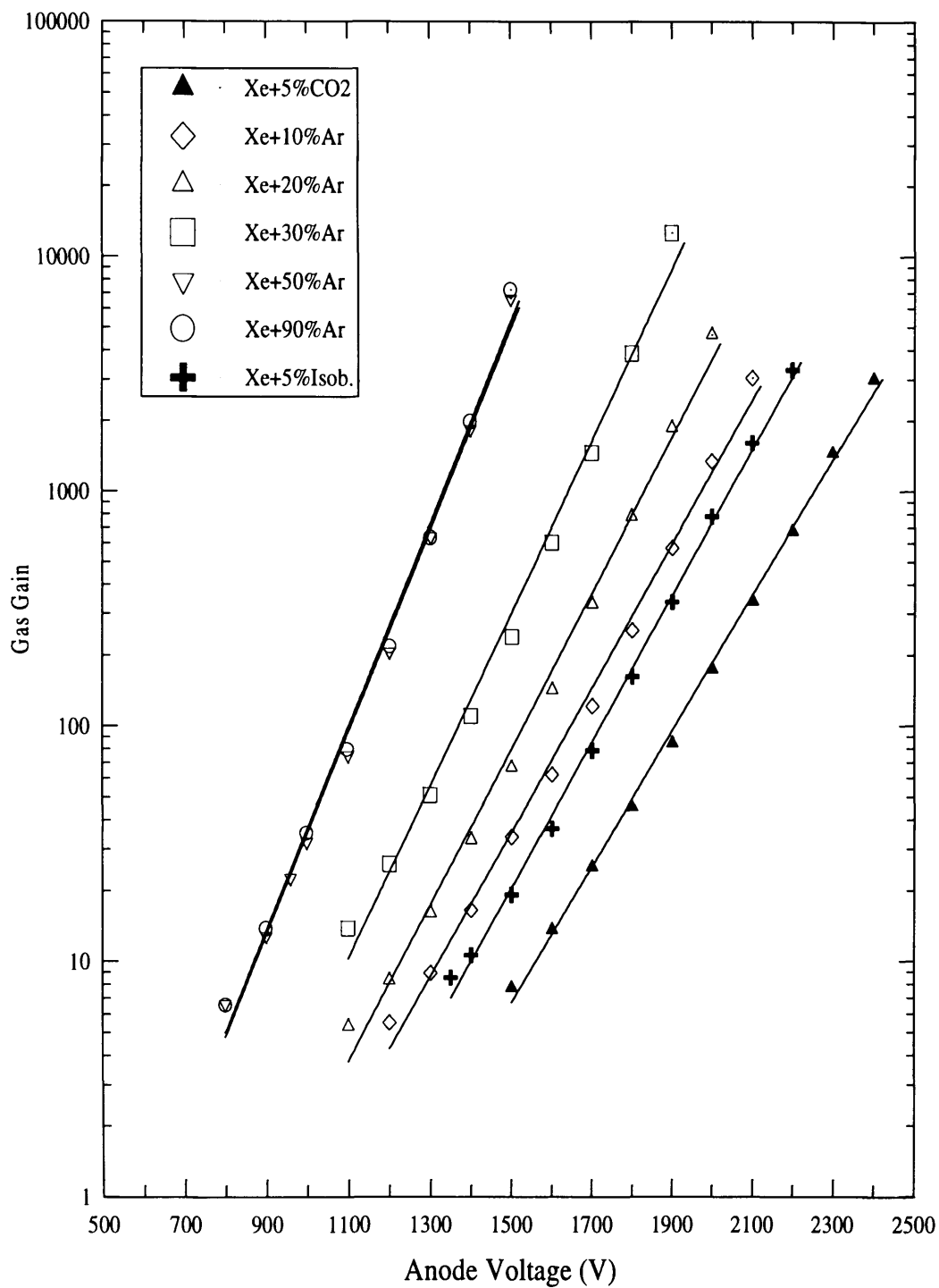


Figure 5.2: The apparent gas gain as a function of the anode voltage for the SWPC with different gas mixtures at 2 atm gas pressure. The solid lines are best fit to the measured points, obtained with the least squares method.

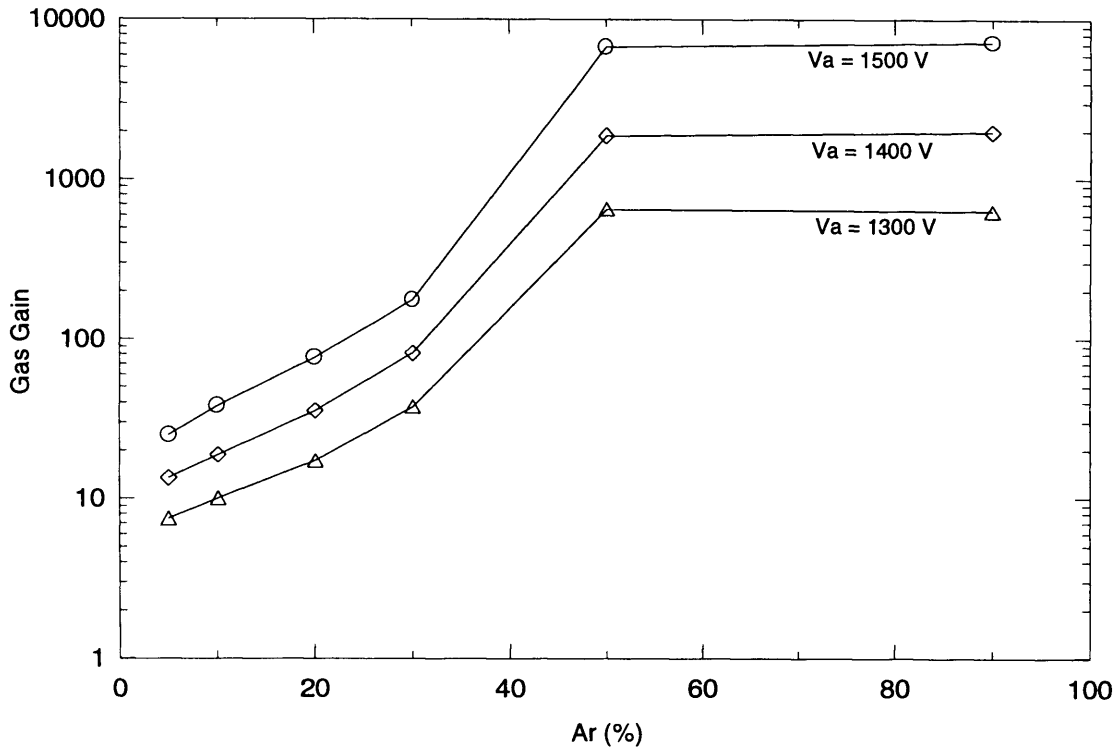


Figure 5.3: The gas gain variation with Argon concentration at constant anode voltages for Xe/Ar mixtures at 2 atm pressure.

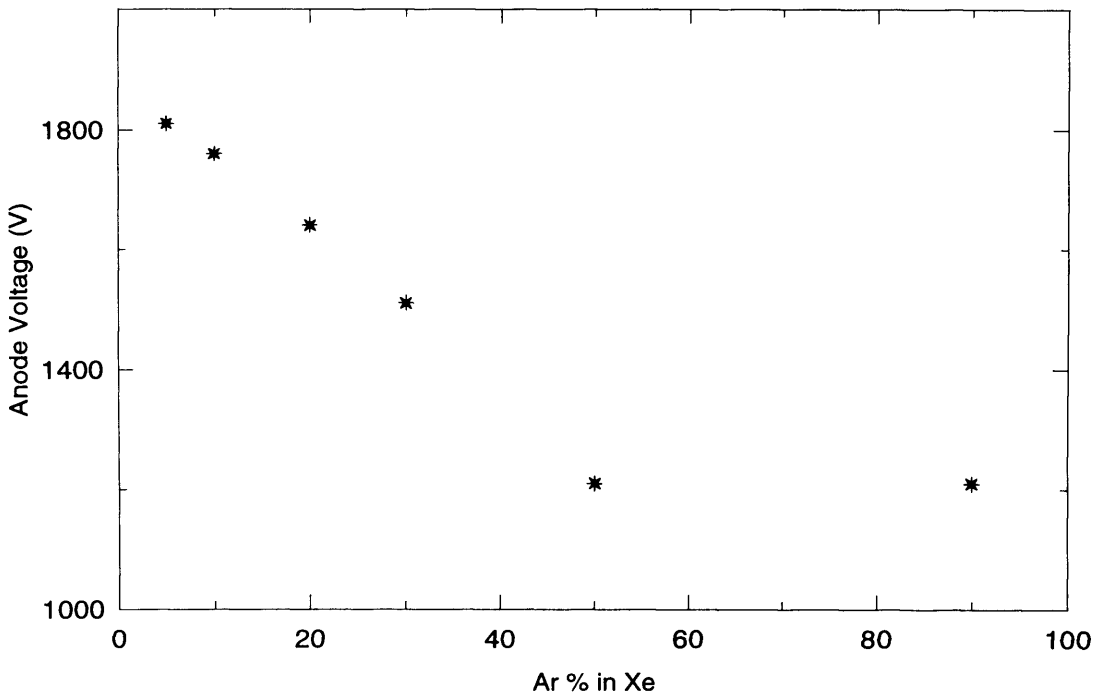


Figure 5.4: The anode voltage required to obtain a gas gain of 200 at 2 atm gas pressure for Xe/Ar Penning mixtures of different argon concentrations.

increases with increasing argon concentrations up to a certain level and then starts to slowly decrease. This agrees with the results obtained by Fuzesy *et al.* (1972) who studied an Argon-based mixture for MWPCs. These authors have reported the effect of increasing xenon concentration on the gas gain using Ar-Xe+7%CO₂ mixtures, where the gas gain is expected to be lower due to the presence of CO₂.

Figure 5.4 shows the effect of argon concentration in Xe-Ar mixtures in terms of the anode voltage required to obtain a gas gain of 200. The relatively low operating voltage of Xe-Ar proportional counters, compared to that of Xe-organic quench counters (Figure 5.2), in addition to their good energy resolution (as will be discussed later in Section 5.3), makes them a good choice for X-ray astronomy applications.

Moreover, the absence of organic quenches, which are usually connected with ageing problems in gas counters [Smith & Turner 1982], makes Xe-Ar mixtures very suitable for long-duration X-ray astronomy missions. Xe-Ar mixtures also have the advantage of providing enhanced detection efficiency for X-rays in the 10-30 keV band by a factor of ~3 compared to any argon-organic quench gas mixture [Agrawal *et al.*, 1989].

For high concentrations of Ar in Xe, it is obvious from the results above that high gas gain can be obtained at relatively low voltage. This is an important advantage for argon but as discussed in Chapter 2, argon proportional counters at low pressures have relatively low detection efficiency for photons with energies greater than ~5 keV. However, the comparison of Manchanda *et al* (1990), discussed in Section 2.5 of Chapter 2, made between detection efficiencies of counters with low-pressure xenon and ultra-high pressure argon has shown argon-based mixtures to be of less interest to us for the present work although xenon is much sensitive to impurities and is more expensive.

5.2 Gas Gain Measurements at High Pressures

The gas mixtures Xe+5%CO₂, Xe+5%C₄H₈, and Xe+20%Ar were studied at pressures 1, 2, 4, 6, 8 and 10 atm, using 22 keV X-rays from a ¹⁰⁹Cd X-ray source. The gas gain as a function of the anode voltage for the three mixtures at 2 atm pressure is shown in Figure 5.5. At high gas pressures the gas gain, or the electron multiplication process, will be affected (see Section 2.6 of Chapter 2) since the number of collisions of gas atoms with electrons, and with each other, depends on the gas density which increases with pressure at a constant temperature.

5.2.1 Gas Gain in The Xe+5%CO₂ Mixture

The apparent gas gain for Xe+5%CO₂ at 2 atm pressure was corrected for the amplifier pulse attenuation. The factor which is connected to pressure in the attenuation correction equation (see Appendix) is the mobility of the positive ions, μ^+ , (see Section 2.1 of Chapter 2). Sood *et al.*(1994) have assumed that since the reduced electric field, E/p , in a high pressure co-axial proportional counter is fairly low and also drops very significantly beyond a few mm from the anode wire due to the cylindrical geometry, mobility of the xenon positive ions can be considered constant even at high pressures. We have adopted this assumption in calculating the correction factors at high pressures for the different mixtures.

The apparent gas gain as a function of anode voltage at different gas pressures up to 10 atm for the Xe+5%CO₂, is shown in Figure 5.6. It can be seen from Figure 5.6 that the variation of the gas gain with anode voltage is much faster at low pressures than at high pressures. The gas gain is also plotted in Figure 5.7 as a function of the reduced electric field, E_d/p , for the same mixture (Xe+5%CO₂). Such a behaviour has been noted for different Xenon-based mixtures by

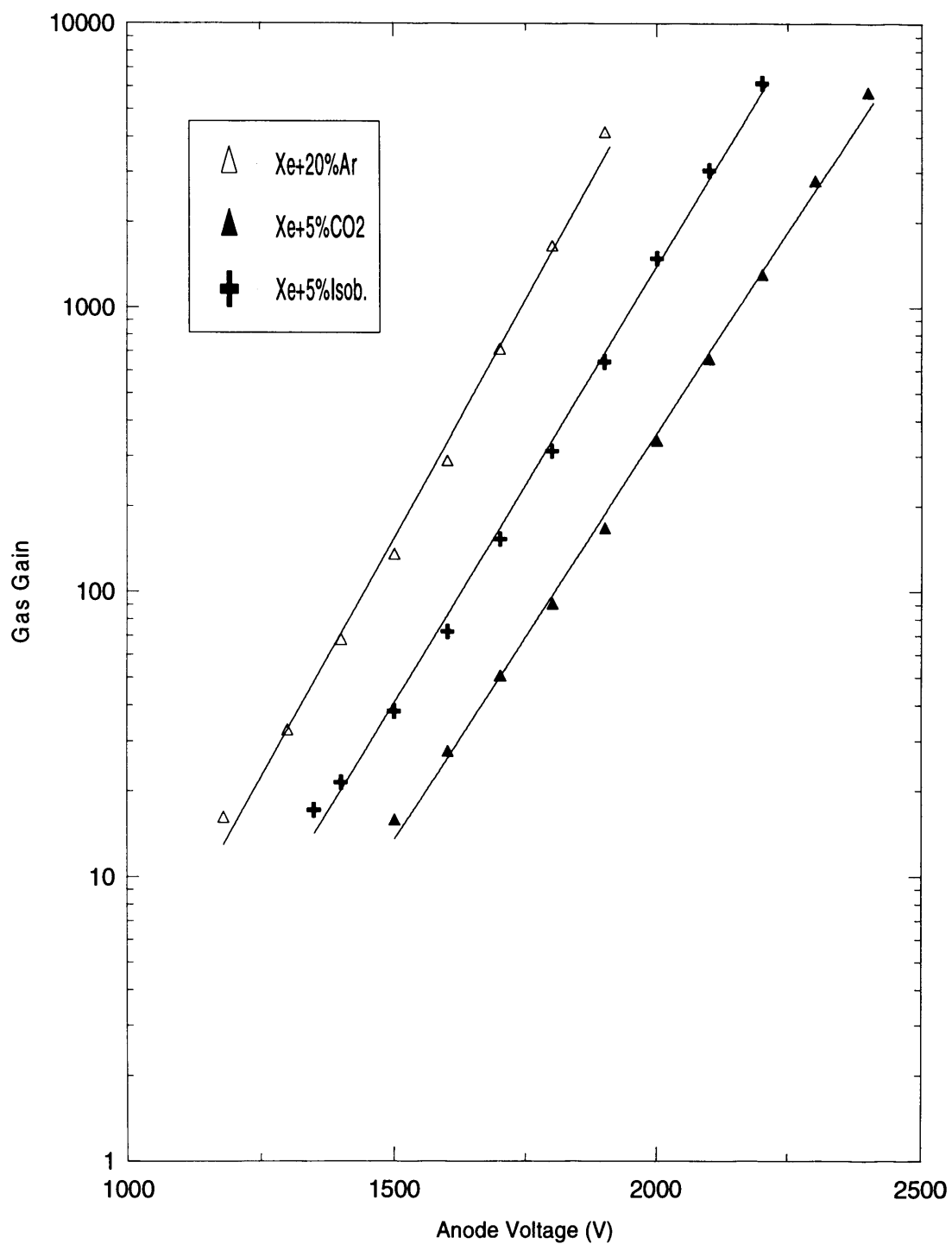


Figure 5.5: Apparent gas gain as a function of the anode voltage for the selected gas mixtures at 2 atm pressure. The solid lines are best fits to the curves obtained with the least squares method.

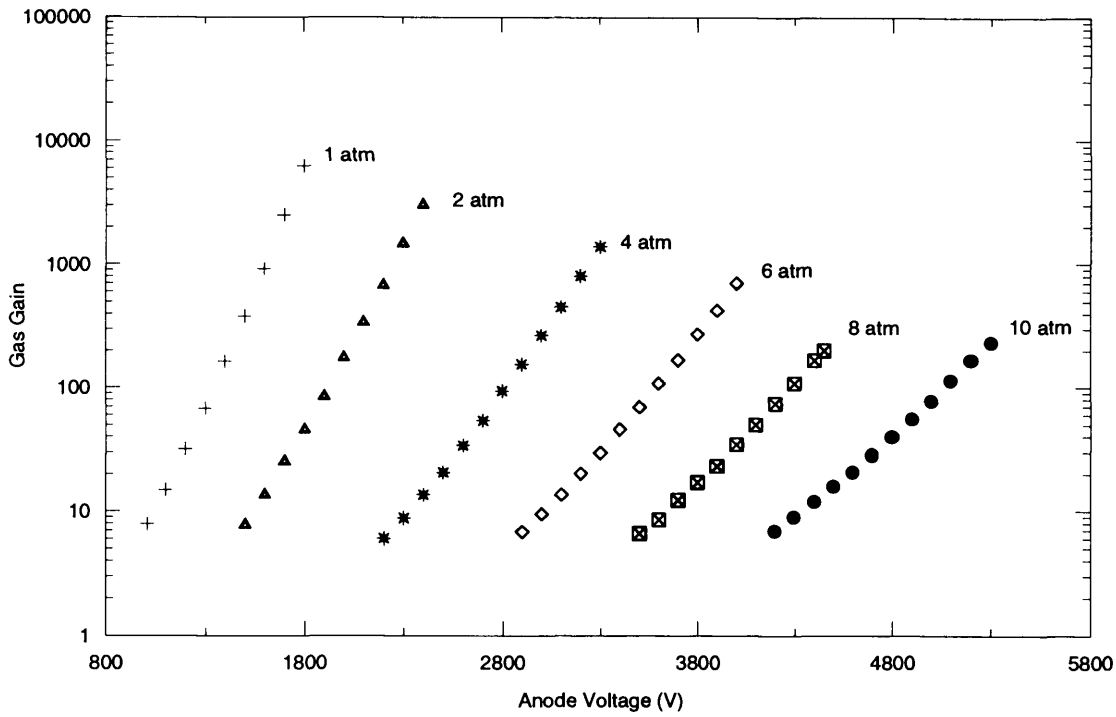


Figure 5.6: The apparent gas gain of the SWPC as a function of the anode voltage for Xe+5%CO₂ mixture at different gas pressures.

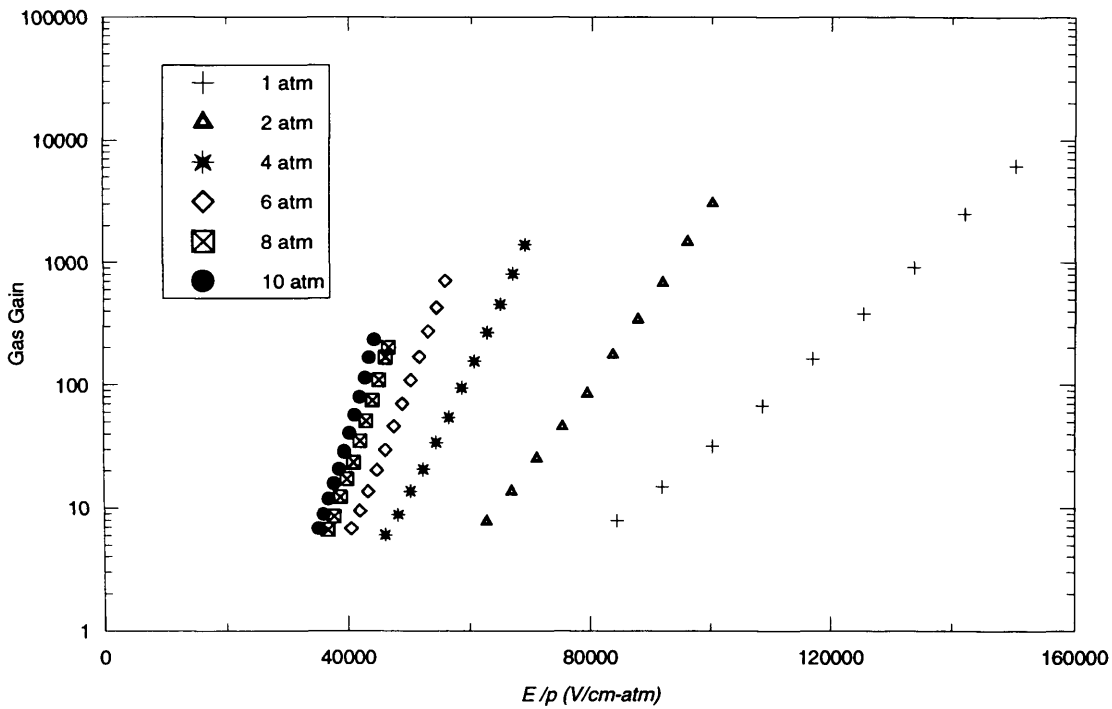


Figure 5.7: The apparent gas gain as a function of the E_d/p for the SWPC with Xe+5%CO₂.

Sakurai *et al.* (1991), Ye *et al.* (1993), and Sood *et al.* (1994). This has also been reported to be true for argon-based mixtures [Manchanda *et al.*, 1990; Ye *et al.*, 1993].

The rate at which the gas gain increases with the anode voltage at different pressures can be indicated by the change of the curve slope. The slope clearly decreases with gas pressure for the gain data plotted in Figure 5.6, as shown in Figure 5.8.

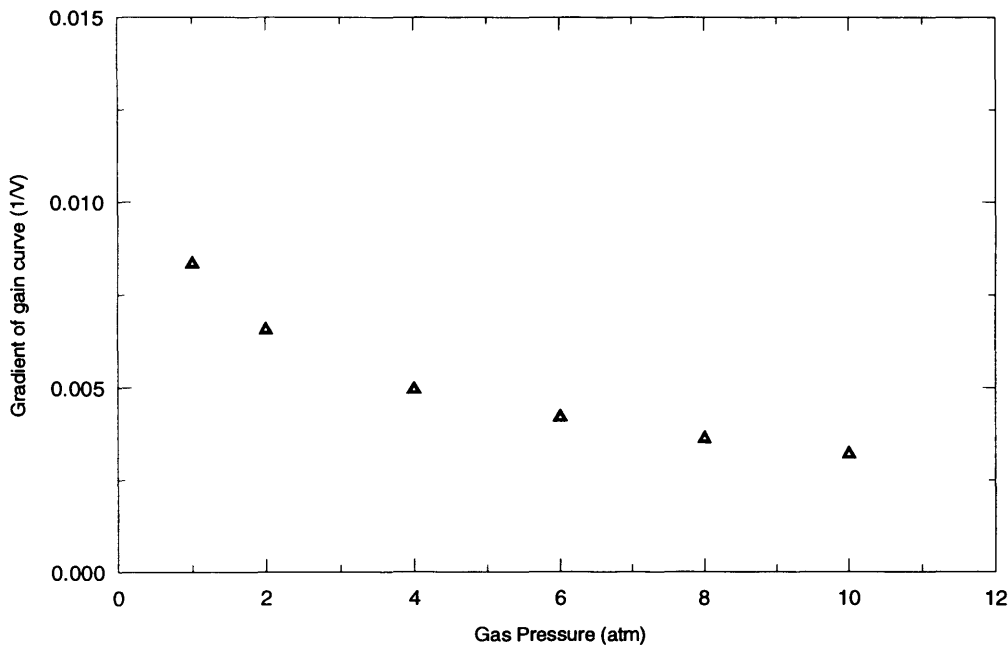
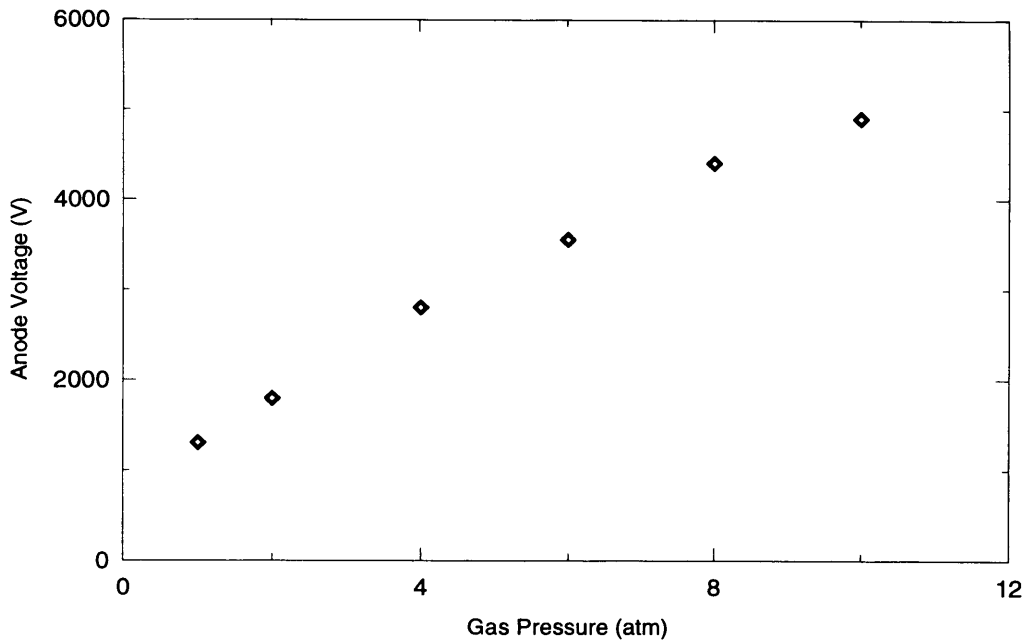


Figure 5.8: The slope variation with pressure for the gain data in Figure 5.6 for Xe+5%CO₂.

The variation of the anode voltage values required for a gas gain of 200 as a function of pressure is shown in Figure 5.9.

Most of the formulae proposed for predicting gas gain in conventional proportional counters (see Section 2.3.1 of Chapter 2) have assumed the form for α/p as a function of E/p [Aoyama, 1985]. These formulae have been proposed as linearized functional forms based on the following semi-empirical formula which describes a non-linear functional dependence of α on the gas pressure and the applied electric field:



Figur 5.9: The anode voltage required to obtain a gas gain of 200 for the Xe+5%CO₂ mixture at different pressures up to 10 atm.

$$\alpha = pA \exp\left(\frac{-Bp}{E}\right) \quad (5.1)$$

where A and B are constants depend on the gas filling, p is the gas pressure, and E is the electric field.

The Townsend ionisation coefficient has been calculated and measured in xenon over a large range of E/p [Hayashi, 1983]. As expected from Equation 5.1, the functional form of α/p has been found to be non-linear as shown in Figure 5.10, reproduced here from Hayashi (1983).

Recently, Zasawny (1997) has confirmed the validity of Equation 5.1 and obtained the same functional dependence as that shown in Figure 5.10. This author has reported values for the parameters A and B for variety of gas mixtures including Xe+5%CO₂, where A and B have been calculated to be $8.78 \times 10^2 \text{ cm}^{-1} \text{ atm}^{-1}$ and $1.33 \times 10^5 \text{ V cm}^{-1} \text{ atm}^{-1}$, respectively, for E/p in the range $6.5 \times 10^4 - 1.4 \times 10^5 \text{ V. cm}^{-1} \text{ atm}^{-1}$.

Figure 5.10 also reveals that at higher gas pressures, electron multiplication commences in regions of lower reduced electric field.

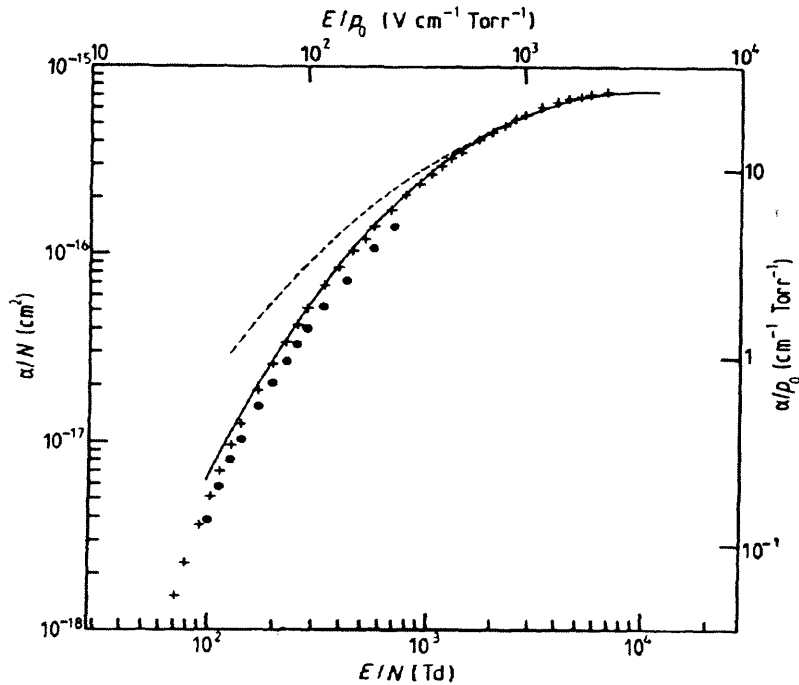


Figure 5.10: Townsend ionisation coefficient α in xenon. (+) experimental by Kruithof (1940), (•) experimental by Bhattacharya (1976), (--) and (–) theoretical by Hayashi [Hayashi, 1983].

Therefore, one cannot expect that, for a given counting gas mixture, the Diethorn equation will fit all the gain curves at all pressures with a single pair of ΔV and K values [Fraser, 1996].

The Diethorn gas “constants” ΔV and K were obtained by “averaging” over the range of pressures 1-10 atm. The pressure dependence of these constants will be discussed later in Section 5.4.

Rewriting the Diethorn equation in the form:

$$\frac{\ln G \ln(b/a)}{V} = \frac{\ln 2}{\Delta V} \ln \left[\frac{V}{p a \ln(b/a)} \right] - \frac{\ln 2}{\Delta V} \ln K \quad (5.2)$$

Equation 5.2 can be rewritten in terms of the reduced electric field, $S_a = E_a / p$, at the surface of the anode wire, as:

$$\frac{\ln G}{p a S_a} = \frac{\ln 2}{\Delta V} \ln S_a - \frac{\ln 2}{\Delta V} \ln K \quad (5.3)$$

where $S_a = \frac{V_a}{p a \ln(b/a)}$ and G is the actual gas gain.

If the quantity on the left of the Equation 5.2 or 5.3 is plotted against the natural logarithm of the quantity in brackets on the right, a straight line of slope $[\ln 2 / \Delta V]$ and intercept $[-\ln 2 (\ln K / \Delta V)]$ should result [Diethorn, 1956].

Hendricks (1972) has calculated ΔV and K for Xe+5%CO₂ from gas gain data at 0.5 and 1 atm pressures. In the present work, these “constants” were obtained at pressures up to 10 atm, *i.e.* for much lower E/p values.

The straight line relationship given by Equation 5.2 is shown in Figures 5.11a,b for the results obtained using Xe+5%CO₂ mixture at pressures up to 10 atm. By applying least squares fitting to the data, we calculated values of ΔV and K from the curve slope and intercept, respectively.

The gas gain was corrected for the amplifier network pulse attenuation with two assumptions; ion mobility is constant or decreases with increasing gas pressure. The Diethorn gas “constants” ΔV and K , calculated from Figures 5.11a and 5.11b by assuming constant and variable ion mobility, were found to be almost the same.

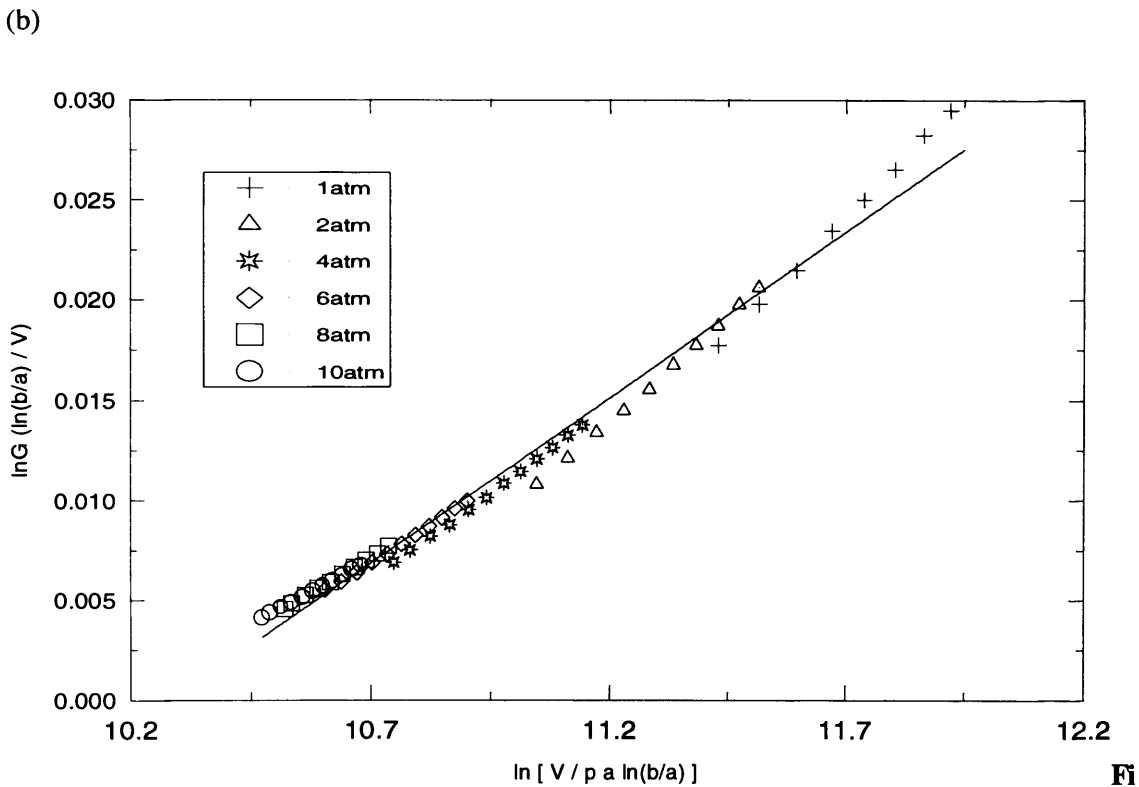
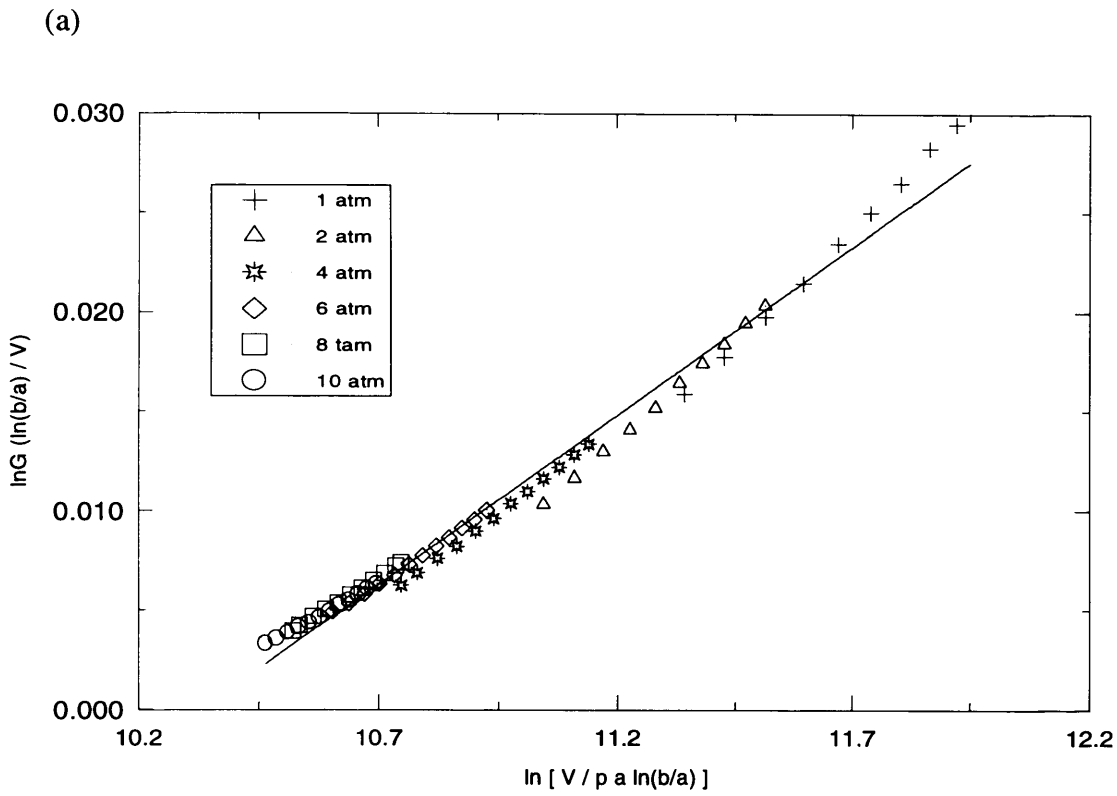


Figure 5.11: Diethorn equation plot for the SWPC filled with Xe+CO₂. (a) for μ^+ assumed to be constant ($0.4 \text{ cm}^2 \text{ s}^{-1} \text{ V}^{-1}$). (b) for μ^+ changing with pressure.

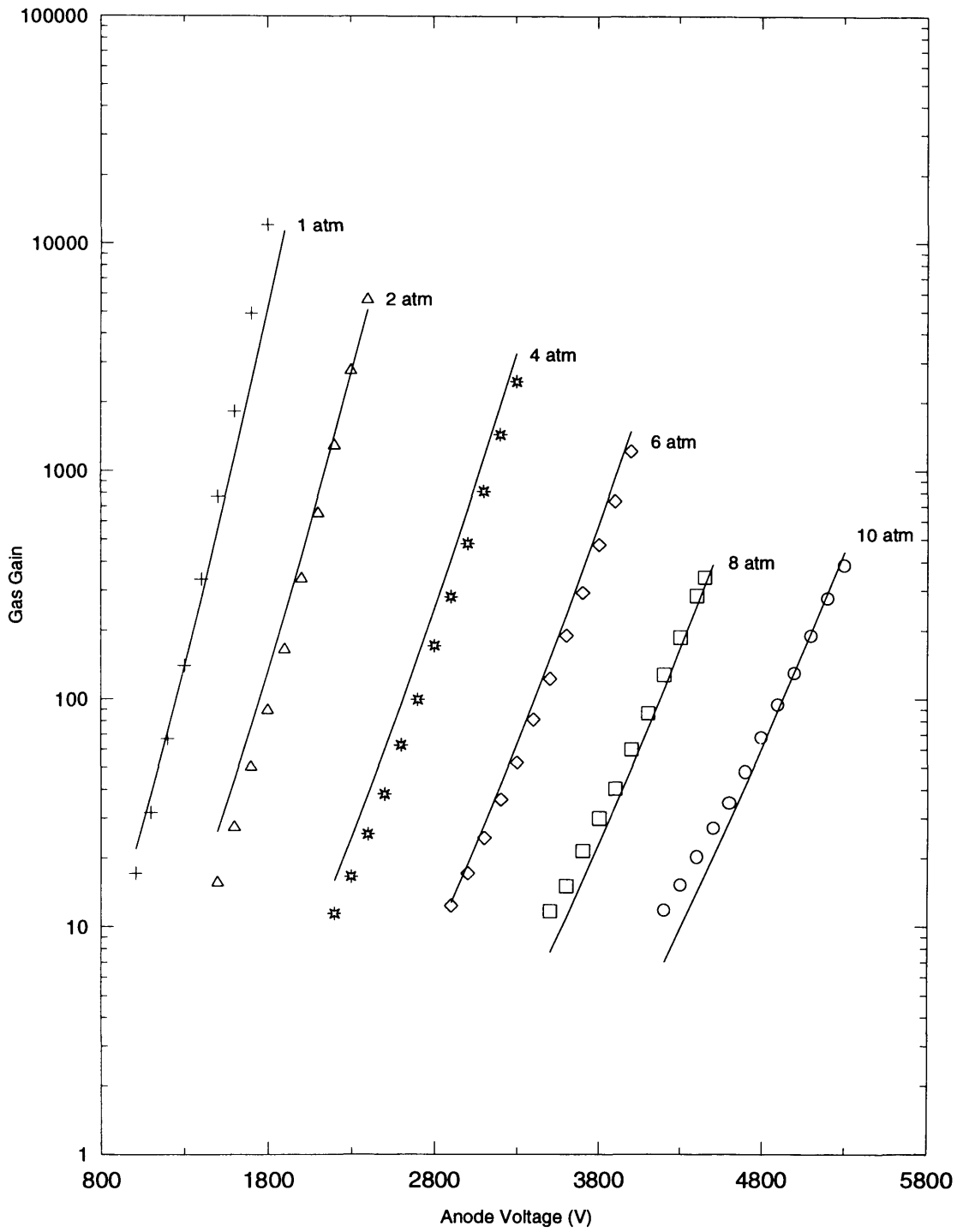


Figure 5.12: Gas gain as a function of the anode voltage compared with the calculated gain using the Diethorn equation for Xe+5%CO₂.

The corresponding values of the gas constants for the Xe+5%CO₂ mixture calculated from Figure 5.11a, averaged over pressures 1-10 atm, are:

$$\Delta V = 41.60 \text{ V} ,$$

$$K = 3.01 \times 10^4 \text{ V cm}^{-1} \text{ atm}^{-1}$$

whereas those obtained by Hendricks (1972) are: $\Delta V = 31.4$ and $K = 3.66 \times 10^4$ which indicates that these “constants” are pressure dependents.

The reduced electric field, S_a , depends on the anode voltage, gas pressure, and the anode and cathode radii, whereas the parameters ΔV and K were stated by Diethorn (1956) to be independent of E and p .

The gas gain as a function of the anode voltage is shown in Figure 5.12 as compared with the calculated value using the pressure dependent Diethorn gas constants. The experimental gas gain values were limited at each pressure by the point just below the breakdown threshold, which could be predicted by the broadening of the X-ray spectrum and by worsening of the energy resolution. This is crucial if the counter gas fill is pure xenon where quenching is absent [Sakurai *et al.*, 1991].

The self-induced space charge effect (see Chapter 2) could be partially responsible for the noticeable increase in gas gain at high pressures. If the gas pressure is increased, then to have the same gas gain, the applied anode voltage has to be increased. The electron and positive ion velocities will remain the same as before. The positive ions will however produce the same space charge around the anode wire which is smaller compared with the increased drift potential by the factor by which the pressure was increased [Blum & Rollandi, 1994]. This will modify the electric field in the counter in such a way that the gas gain will be higher than what is to be expected from the Diethorn equation.

5.2.2 Gas Gain in The Xe+5%C₄H₈ Mixture

Similar gain behaviour was also found in the case of the Xe+5%C₄H₈ mixture, taking into account the Penning effect which results from matching the second metastable state of xenon with the ionisation potential of Isobutylene and results an increase in the gas gain. As this mixture was found to give higher gains at 2 atm than the Xe+5%CO₂, the value of K was expected to be smaller than that for Xe+5%CO₂; as consistent with the Diethorn equation. ΔV was also expected to be smaller as revealed from the experimental results of Wolff (1974).

Figure 5.13 shows the apparent gas gain as a function of the anode voltage for the Xe+5%C₄H₈ mixture at pressures up to 10 atm. The points on the plot at 10 atm were not included because no reasonable pulse height distribution was obtained due to unexpected high level noise from the counter. The gas gain for the mixture is shown in Figure 5.14 as a function of the reduced electric field.

Although very high gas gains were obtained at high pressures using the Xe+5%C₄H₈ mixture, the energy resolution was found to be very poor compared to the Xe+5%CO₂ mixture at pressures higher than 4 atm, as will be discussed in Section 5.3.

The constants, ΔV and K , for the Xe+5%C₄H₈ mixture were calculated from Figure 5.15 using gas gains at different pressures, as before. The “averaged” values of the Diethorn gas constants over all pressures (1-8 atm) were found to be:

$$\Delta V = 32.73 \text{ V,}$$

$$K = 3.08 \times 10^4 \text{ V cm}^{-1} \text{ atm}^{-1}.$$

The predicted gas gain by the Diethorn equation, using the calculated constants above, for the Xe+5%C₄H₈ mixture is plotted together with the actual gas gain in Figure 5.16.

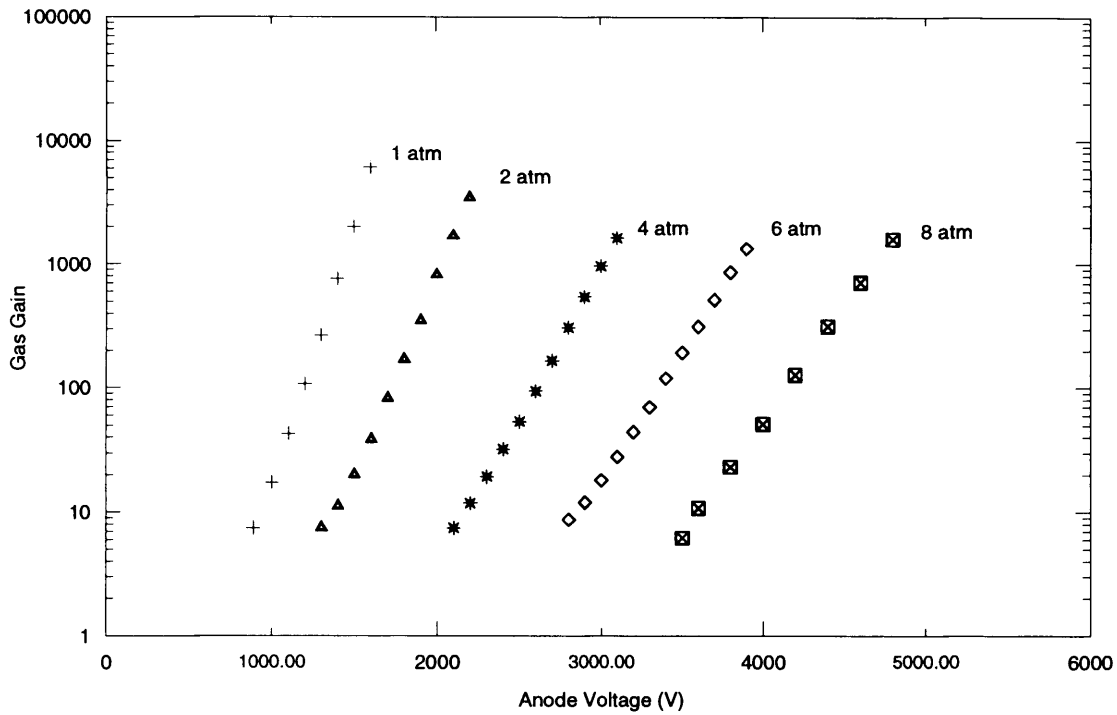


Figure 5.13: The apparent gas gain of the SWPC as a function of the anode voltage for Xe+5% C₄H₈ mixture at different gas pressures.

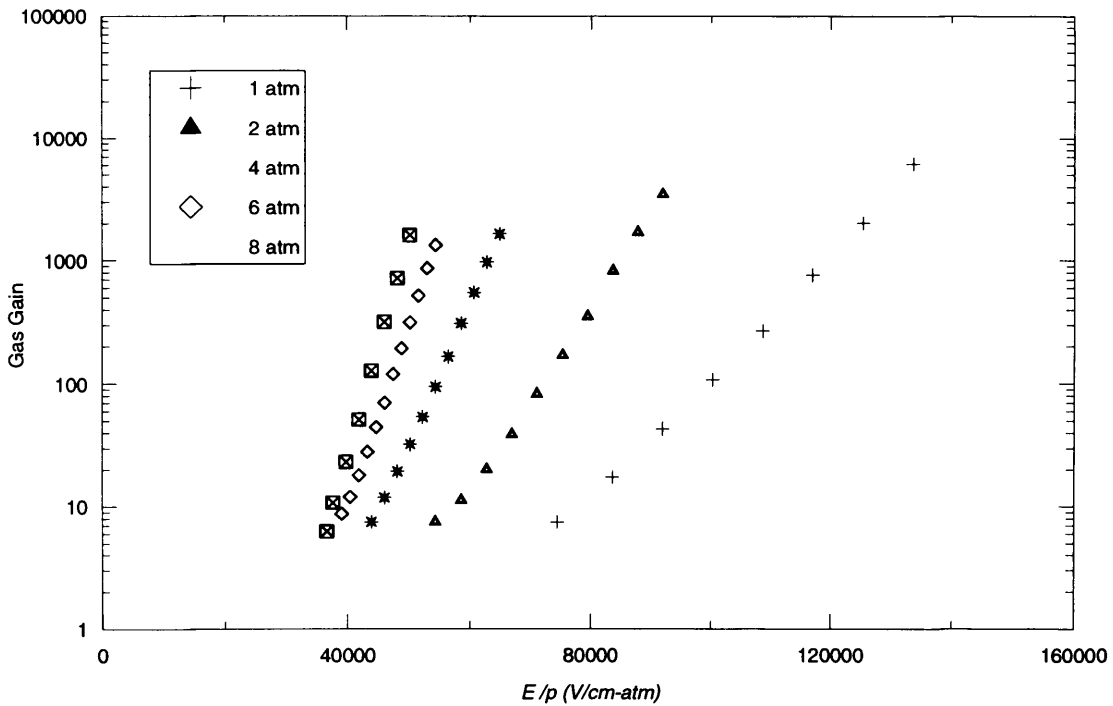


Figure 5.14: The corrected gas gain as a function of the reduced electric field E_a / p for the SWPC with Xe+5% C₄H₈.

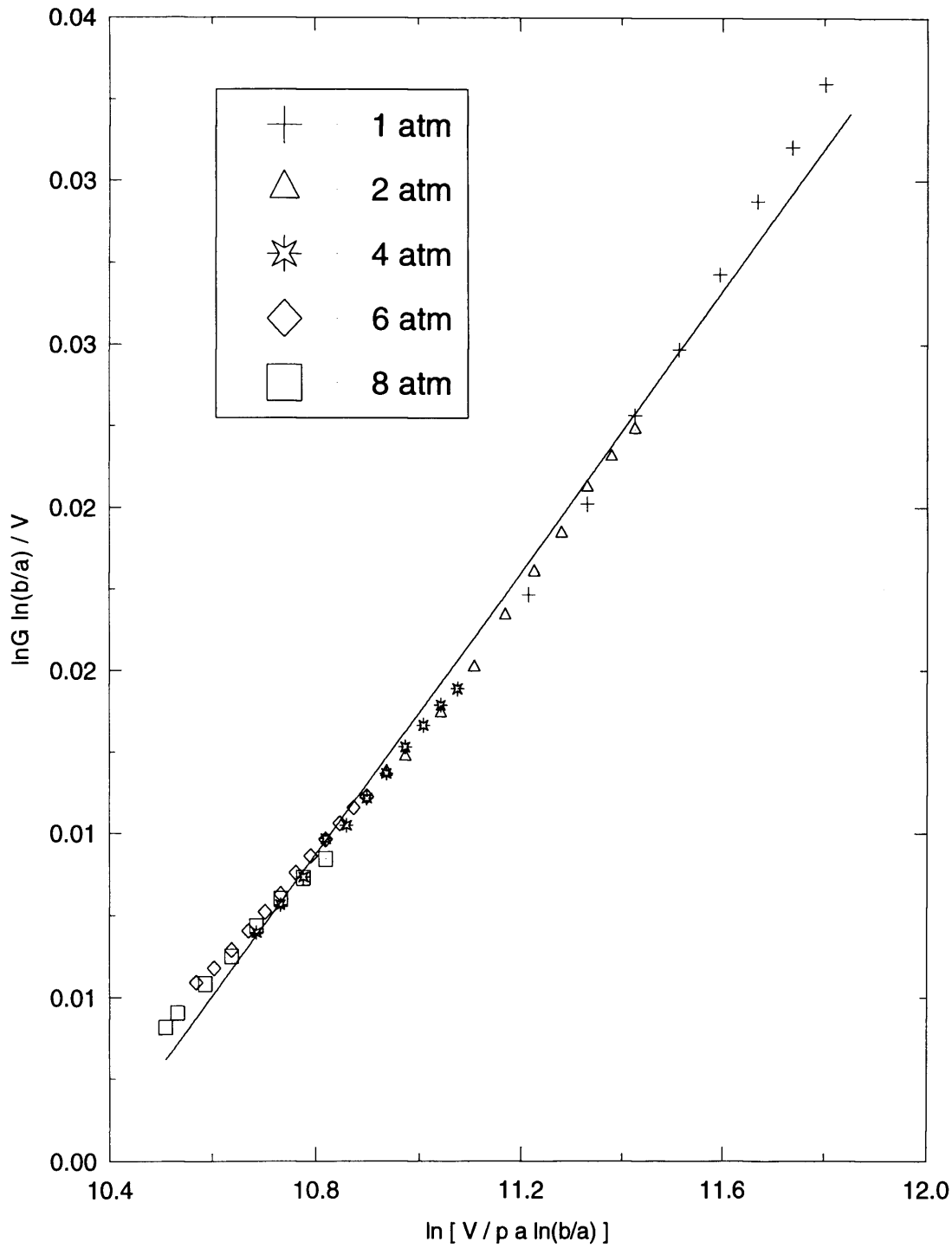


Figure 5.15: A straight line relationship between the corrected gas gain and the reduced electric field for using the Diethorn equation for the SWPC filled with Xe+5% C_4H_8 .

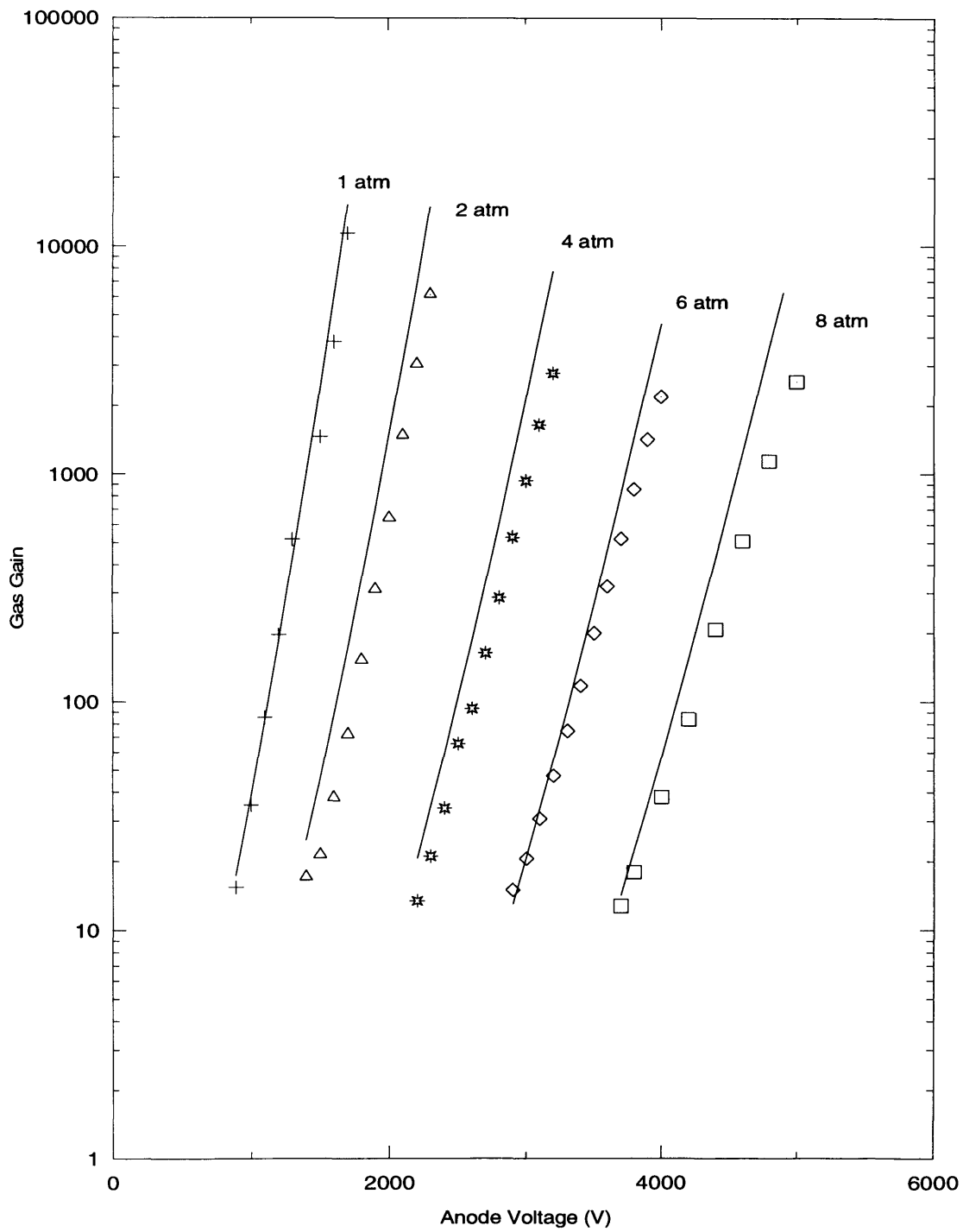


Figure 5.16: The corrected gas gain as a function of the anode voltage compared with the calculated using the Diethorn equation for Xe+5% C₄H₈.

5.2.3 Gas Gain in The Xe+20%Ar Mixture

The Xe-Ar mixtures were found to give the highest gas gain at lower operating voltages, with better energy resolutions. The existence of Argon in the mixture increases the gain, as shown in Figure 5.2 of Section 5.1.2.

This effect will be more significant at high pressures because the excitation efficiency of xenon increases with pressure [Sakurai *et al.*, 1991] which in turn increases the non-metastable Penning effect, *i.e.* increases the gas gain. On the other hand, as a result of the absence of quenching the maximum gas gain threshold will be reduced (see Chapter 2).

We experienced two breakdown events in the counter for the Xe+20%Ar mixture at a gas gain of ~ 1000 at 10 atm. As a result of these breakdown events, the anode wire had to be changed every time. The breakdown in the counter may be related to lack of quenching of UV photons emitted by the excited Xe atoms. The liberated electrons from the cathode walls could contribute to the ionisation process together with Xe and Ar atoms causing the counter to lose its proportionality and breakdown. Figure 5.17 is an SEM photograph showing a section of the “old” anode wire which was replaced after a breakdown event.

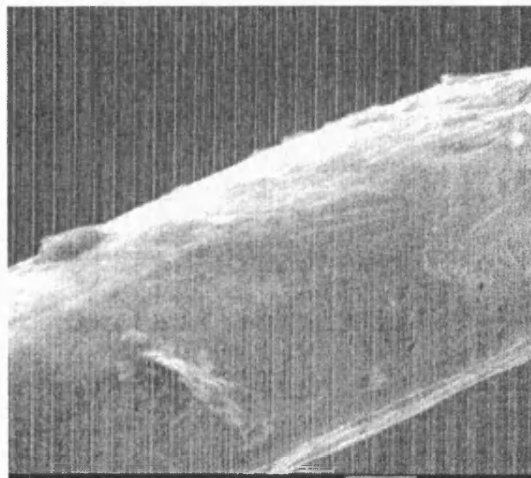


Figure 5.17: A section of the 42.4 μm diameter anode wire.

Figure 5.18 shows the apparent gain as a function of the anode voltage for the Xe+20%Ar mixture at different pressures up to 10 atm. The results of this mixture show similar behaviour, for the gas gain with voltage and pressure, to that of the other mixtures, but with more tendency to be linear. The same data is shown in Figure 5.19 as a function of the reduced electric field.

Apart from its lower maximum gain threshold, the Xe+20%Ar mixture has shown better performance than the other gas mixtures under study. This includes a lower operating voltages and good energy resolution. The energy resolution, as will be discussed later, does not degrade much with pressure as in case of the other mixtures.

These advantages, in addition to its higher detection efficiency over Ar-based mixtures [Manchanda *et al.*, 1991], make it suitable for many applications taking into account its sensitivity to small amounts of impurities which needs more care in counter construction.

Figure 5.20 shows the straight line relationship plotted to give the value of the Diethorn “constants” ΔV and K for the Xe+20%Ar mixture. The corresponding pressure averaged values in this case were found to be as:

$$\Delta V = 37.60 \text{ V},$$

$$K = 2.10 \times 10^4 \text{ V cm}^{-1} \text{ atm}^{-1}.$$

The corrected gas gain for the Xe+20%Ar mixture is shown in Figure 5.21 as a function of the anode voltage together with the calculated gain using the Diethorn equation. The plot shows better agreement than the other mixtures.

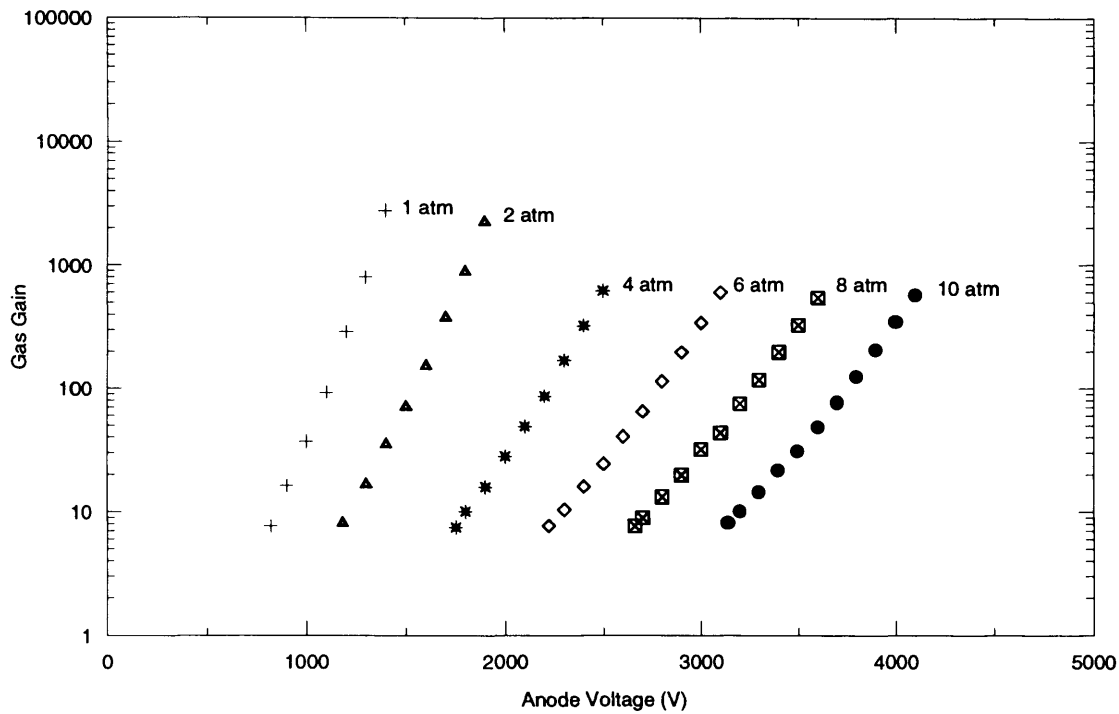


Figure 5.18: Apparent gas gain of the SWPC as a function of the anode voltage for Xe+20%Ar mixture at different gas pressures.

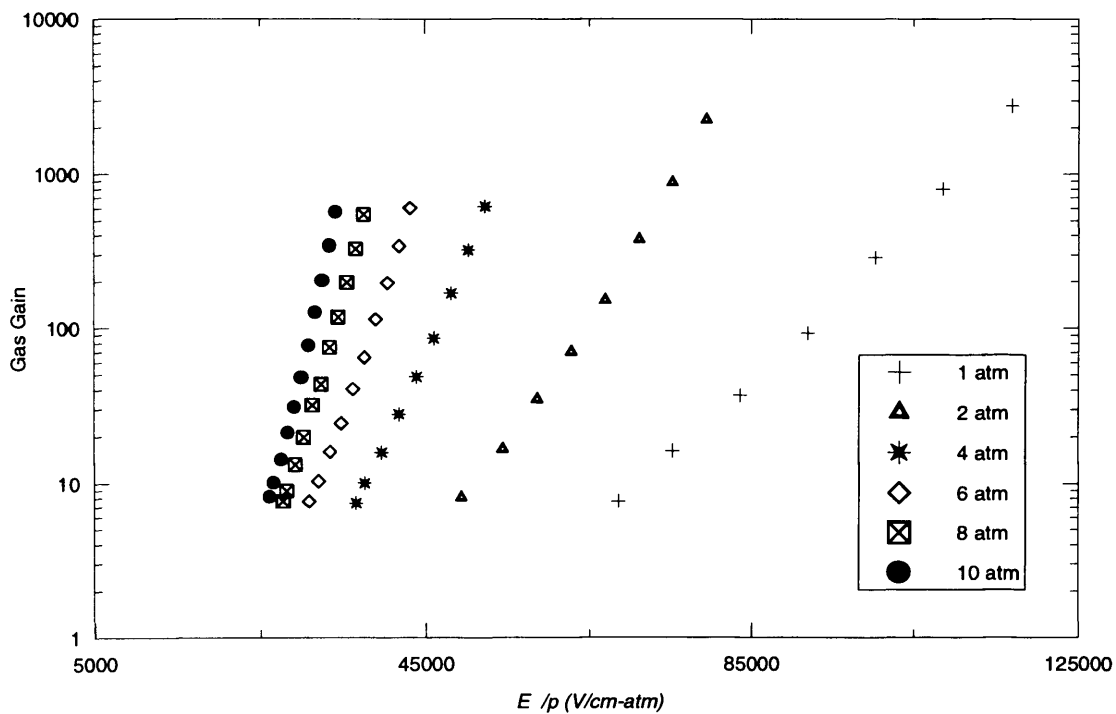


Figure 5.19: Apparent gas gain as a function of the reduced electric field for the Xe+20%Ar mixture.

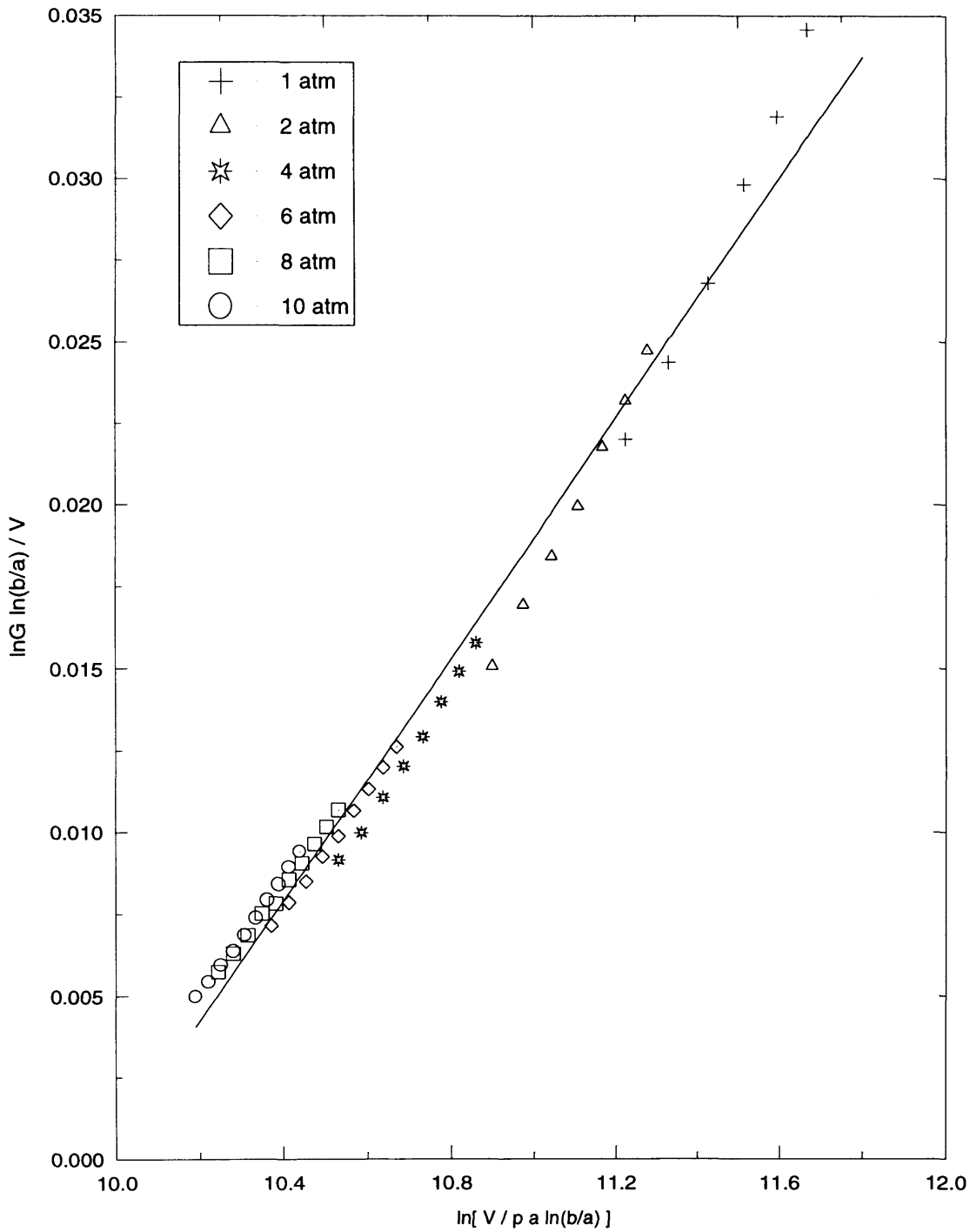


Figure 5.20: A straight line relation between the corrected gas gain and the reduced electric field for using the Diethorn equation for the SWPC filled with Xe+20%Ar.

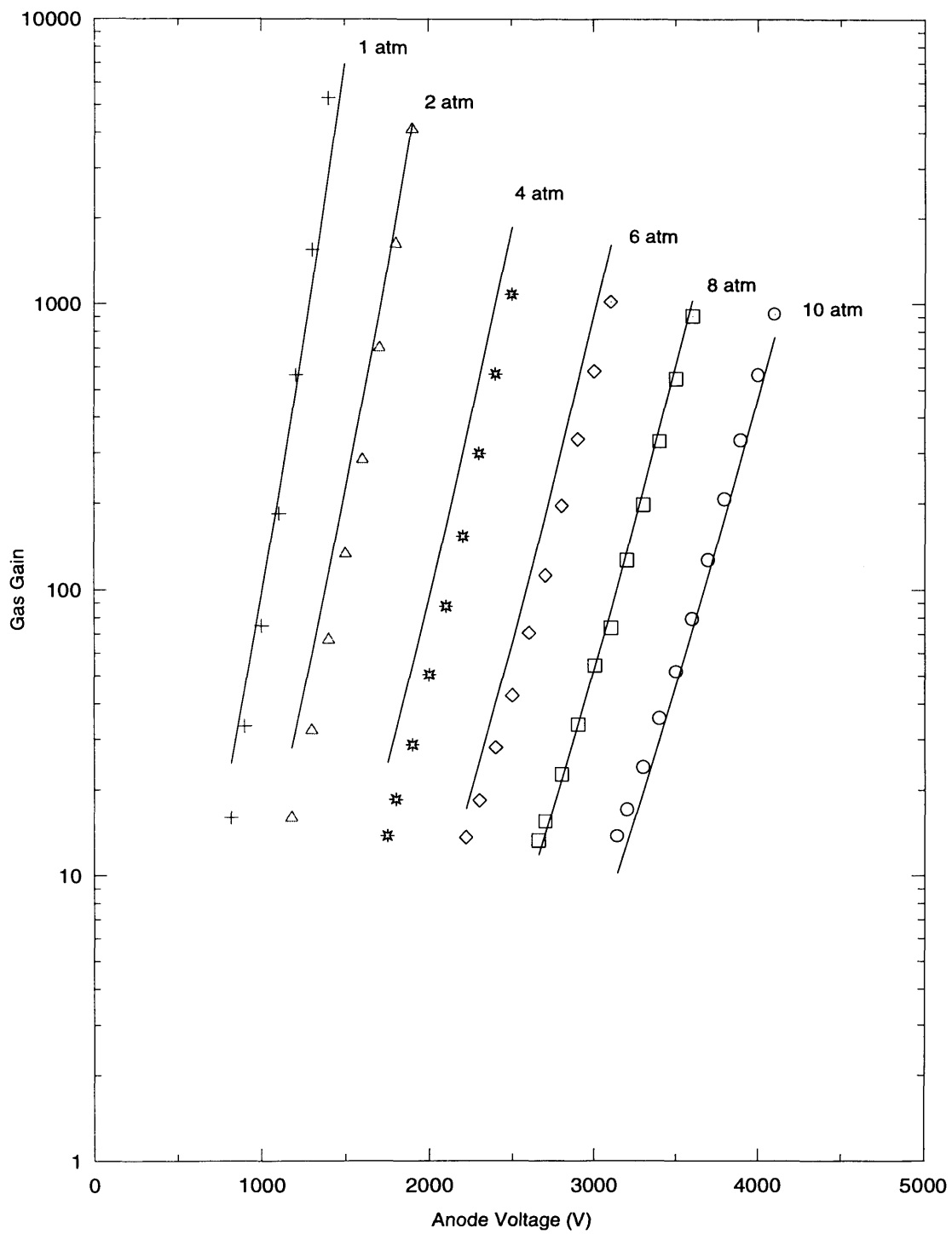


Figure 5.21: The corrected gas gain as a function of the anode voltage compared with the calculated gain using the Diethorn equation for Xe+20%Ar.

5.3 Energy Resolution

A proportional counter performance may be affected by a number of factors which increase with pressure. Among those factors are increase of the excitation processes, the increase of sensitivity to impurities, and the increase of dependence on anode wire uniformity. This section discusses the possible parameters causing the worsening of the energy resolution of the SWPC at high pressures.

5.3.1 *The Effects of Ionisation and Excitation*

In Section 2.4 of Chapter 2, it was shown that the energy resolution of a proportional counter is a function of the incident energy and of the fluctuations in the ionisation and multiplication processes. The increase in fluctuations at high pressures is caused probably by weaker strength of the reduced electric, as noted in Section 5.2 of the present chapter, which in turn will effect the Townsend ionisation coefficient, modify the multiplication process, increase the statistical fluctuations, and hence affect the counter energy resolution [Alkhazov, 1970].

The size of the primary electron cloud also decreases with increasing pressure and hence could make the energy resolution strongly dependent on the uniformity of the anode wire, as will be discussed below in Section 5.3.2.

Energy resolutions obtained for the SWPC with different Xe-Ar Penning mixtures were found to be better than those of Xe+5%CO₂ and Xe+5%C₄H₈. The measurements of SWPC energy resolution for the Xe+5%CO₂ mixture at 2 atm pressure and a gas gain of 200 show that the energy resolution at an energy of 22.2 keV was 8.9%. As the gas gain was increased to values above 10³, the energy resolution degraded rapidly. At the same gas gain, pressure, and photon energy, the energy resolution of the counter with Xe+5%Ar was 7.9%. This indicates one more

important advantage of the non-metastable Penning effect besides the higher gas gain obtained for such mixtures, as noted in Section 5.1.2.

On the other hand, the energy resolution of the counter with Xe-Ar mixtures at 2 atm pressure was found to improve with the increase of argon concentration. This is shown in Figure 5.22 for 22.2 keV ^{109}Cd photons of a gas gain of ~ 200 . These measurements were taken with the “old” anode wire. The energy resolutions at 10% and 90% argon concentrations were 7.7% and 6.7% respectively, which was expected to be a result of the non-metastable Penning effect, mentioned in the previous section. In addition, for Xe-Ar mixtures with majority argon gas, the UV photons produced by the excited xenon atoms are reduced and hence the effect of secondary electron emission from the cathode surface is reduced.

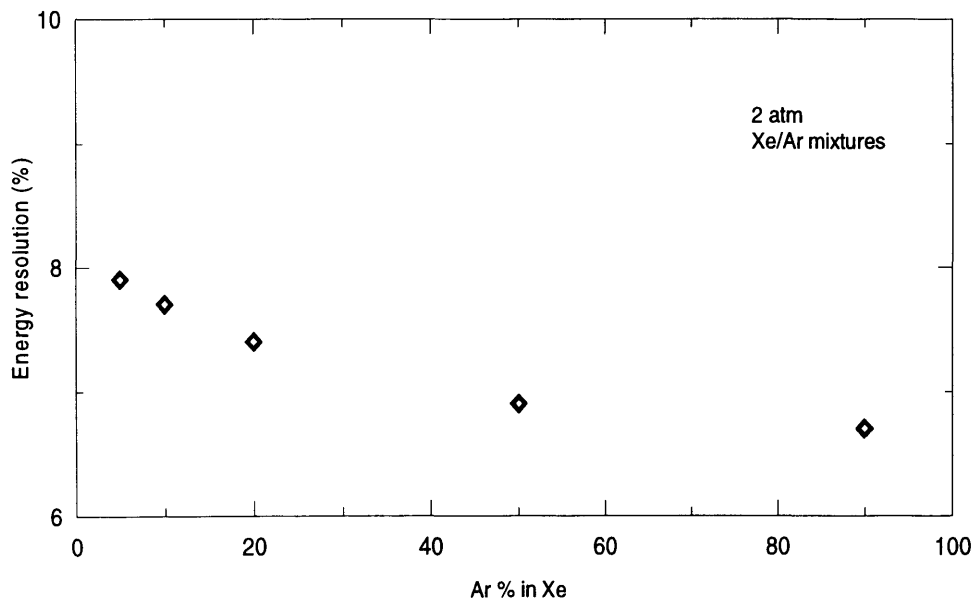


Figure 5.22: Energy resolution as a function of argon concentration in xenon at pressure of 2 atm and gas gain of ~ 200 for 22.2 keV X-rays.

Pulse height distributions recorded by the SWPC, with a new anode wire, obtained from a ^{109}Cd source for the mixtures under study at 2 and 10 atm pressures are shown in Figures 5.23, 5.24, and 5.25. These pulse height spectra were obtained at a gas gain of ~ 200 . The energy

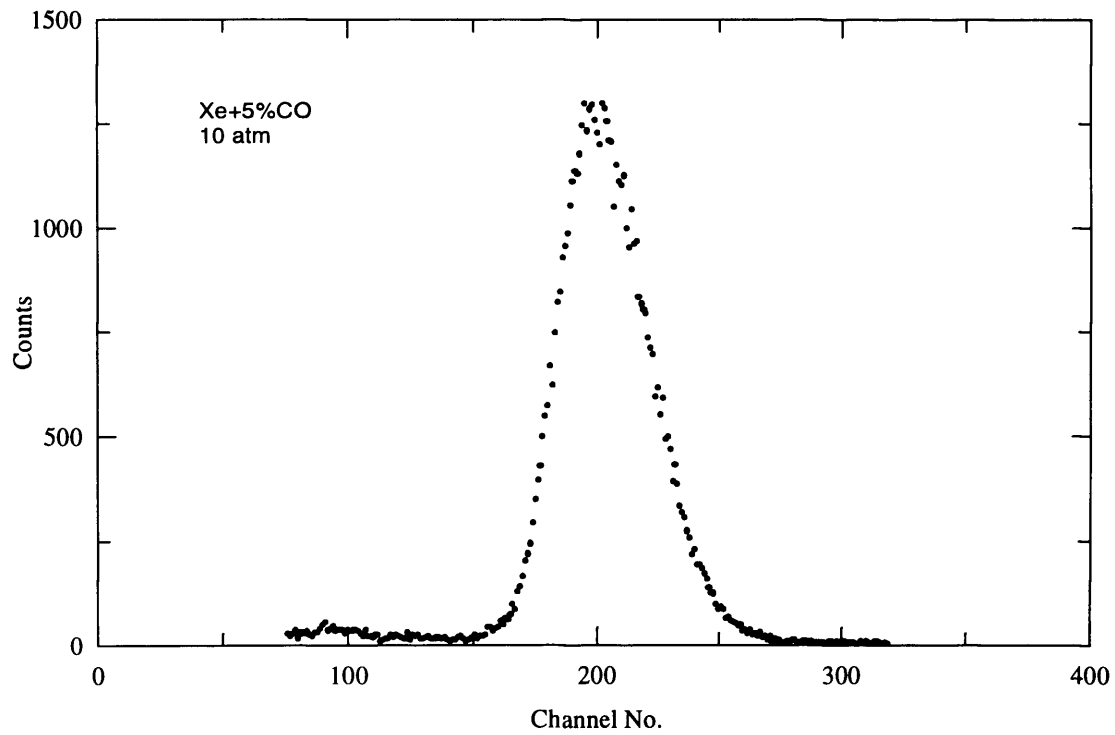
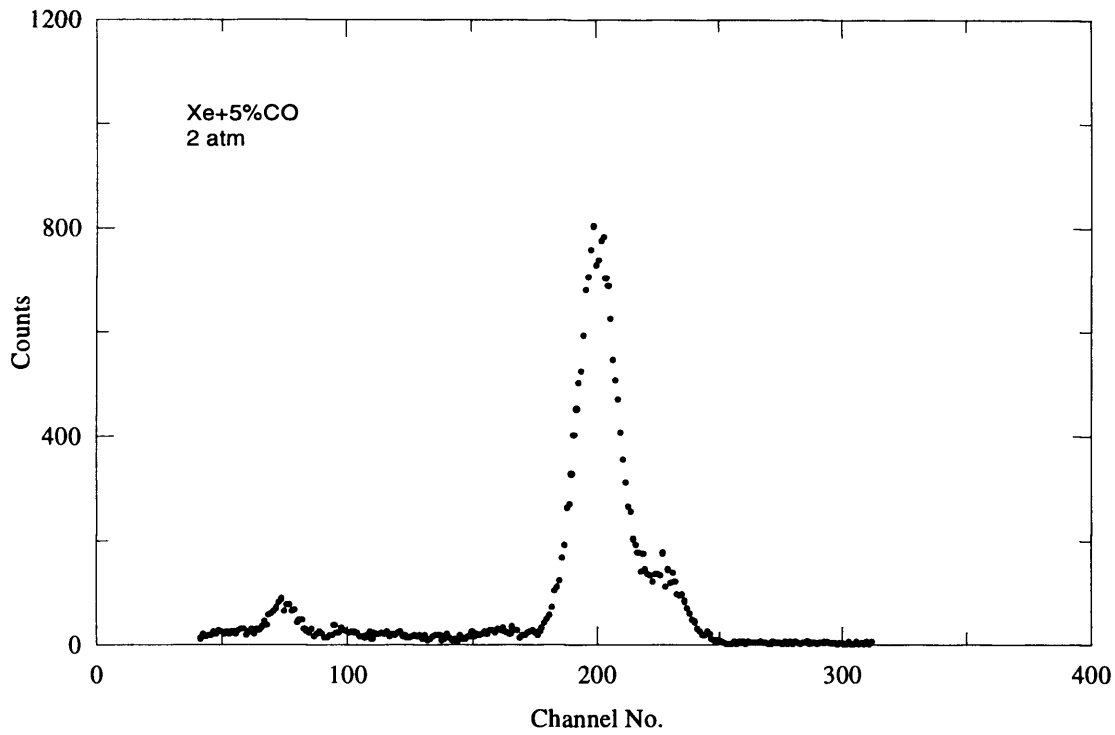


Figure 5.23: Pulse height distribution obtained by the SWPC for Xe+5%CO₂ at pressures 2 atm and 10 atm and a gas gain of ~200 for 22 keV X-ray photons.

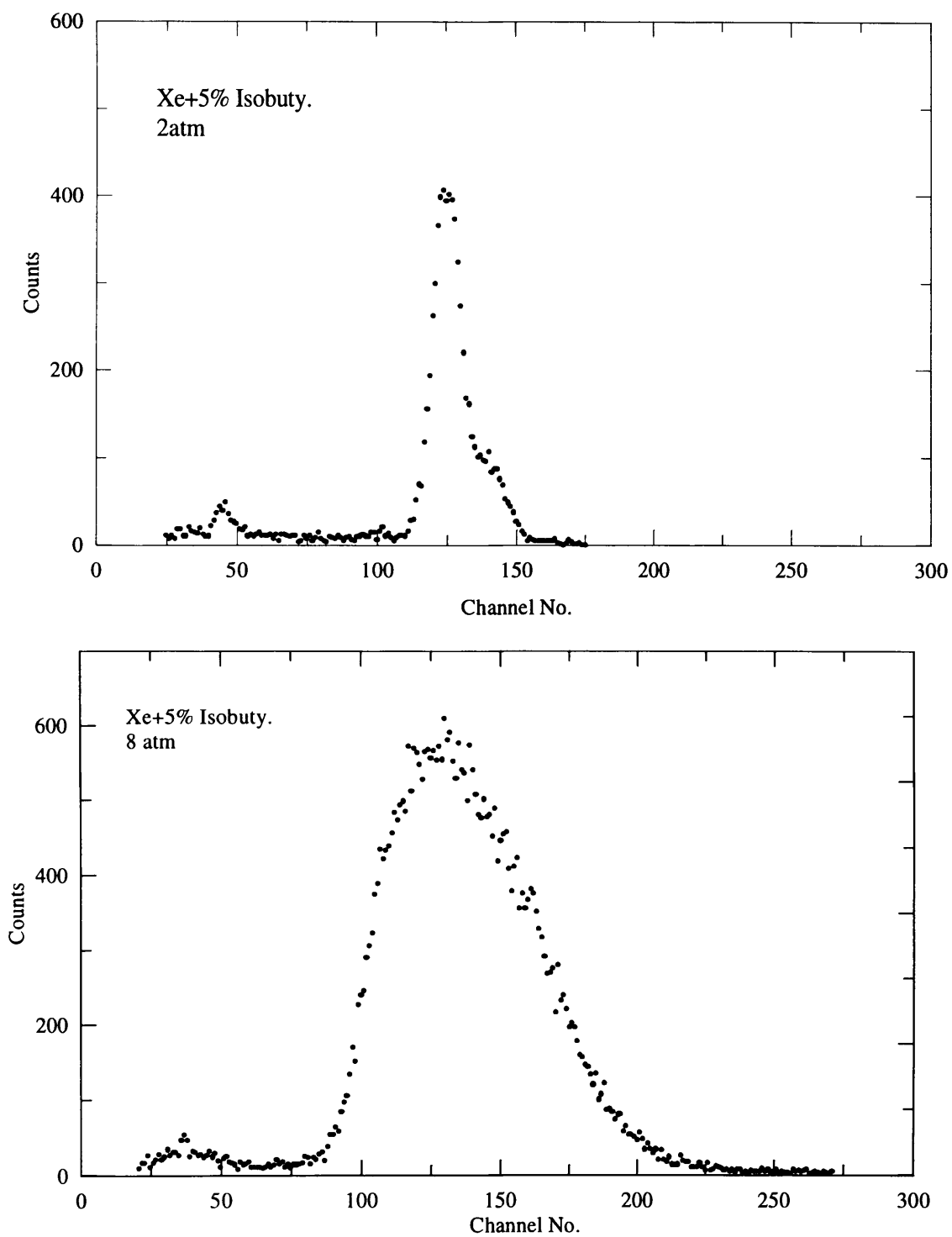


Figure 5.24: Pulse height distribution using the SWPC with Xe+5% C_4H_8 at pressures 2 atm and 8 atm and a gas gain of ~ 200 for 22 keV X-ray photons.

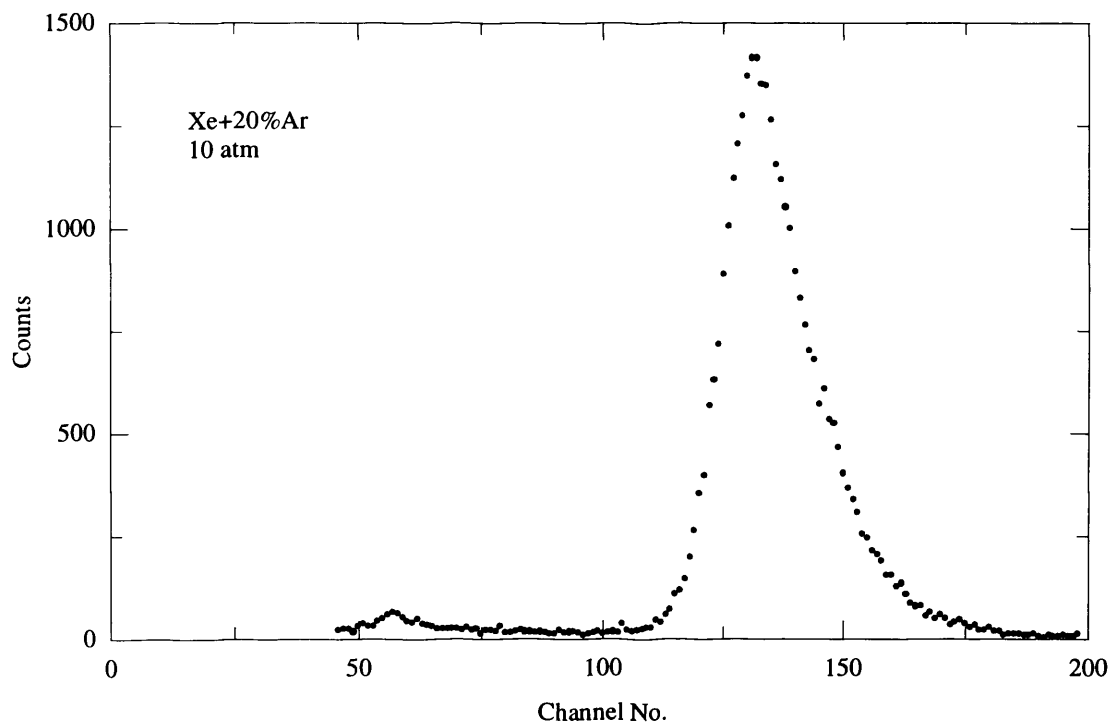
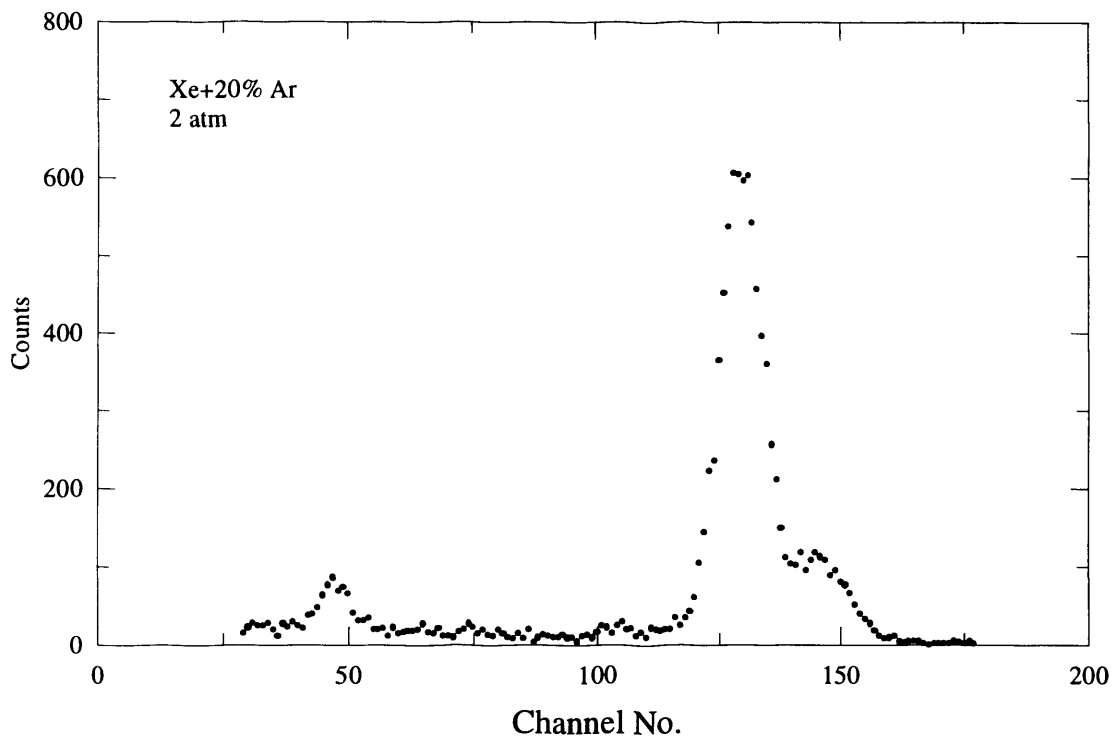


Figure 5.25: Pulse height distributions obtained by the SWPC using Xe+20%Ar at pressures 2 and 10 atm and a gas gain of ~ 200 for 22 keV X-rays.

resolutions displayed in the figures for Xe+5%CO₂, Xe+5%C₄H₈, and Xe+20%Ar were 8.9, 8.5, and 6.4%, respectively, at 2 atm pressure.

In the spectra shown, it is clear that the SWPC at 10 atm pressure was unable to distinguish the K_α (22.2 keV) and K_β (25 keV) peaks. At 2 atm, the counter has shown a slightly improvement in its behaviour with Xe+5%C₄H₈ compared to that with Xe+5%CO₂. The behaviour of the counter with Xe+20%Ar was found to be the best in terms of energy resolution.

It has been reported by Sood *et al.* (1994) that the energy resolution of a Xe-CH₄ counter at 13.5 atm showed a faster degradation for gas gains above 10³ than at 1 atm, and this behaviour has been explained by these authors to be due to the change in the operating region from limited proportional to Geiger, set off by the large number of UV photons released as a result of the xenon molecules' de-excitation.

As mentioned earlier, at high pressures the counter was found to operate at a weaker reduced electric field E/p . This will also contribute in increasing excitation events in the gas relative to ionisation which in turn results in greater avalanche fluctuations and hence inferior energy resolution.

The results obtained for the gas mixtures under study, show that the energy resolution of the SWPC degrades with increasing gain at constant pressure and with increasing pressure at constant gain. The corresponding energy resolutions at 10 atm for the mixtures Xe+5%CO₂, Xe+5%C₄H₈, and Xe+20%Ar were found to be 26.1, 55.2, and 16.0% respectively.

The variation of energy resolution with pressure as well as with gas gain for these mixtures is shown in Figures 5.26, 5.27, and 5.28. These figures show clearly the degradation of energy resolution at high gas gains as well as at high pressures with different proportion for each mixture.

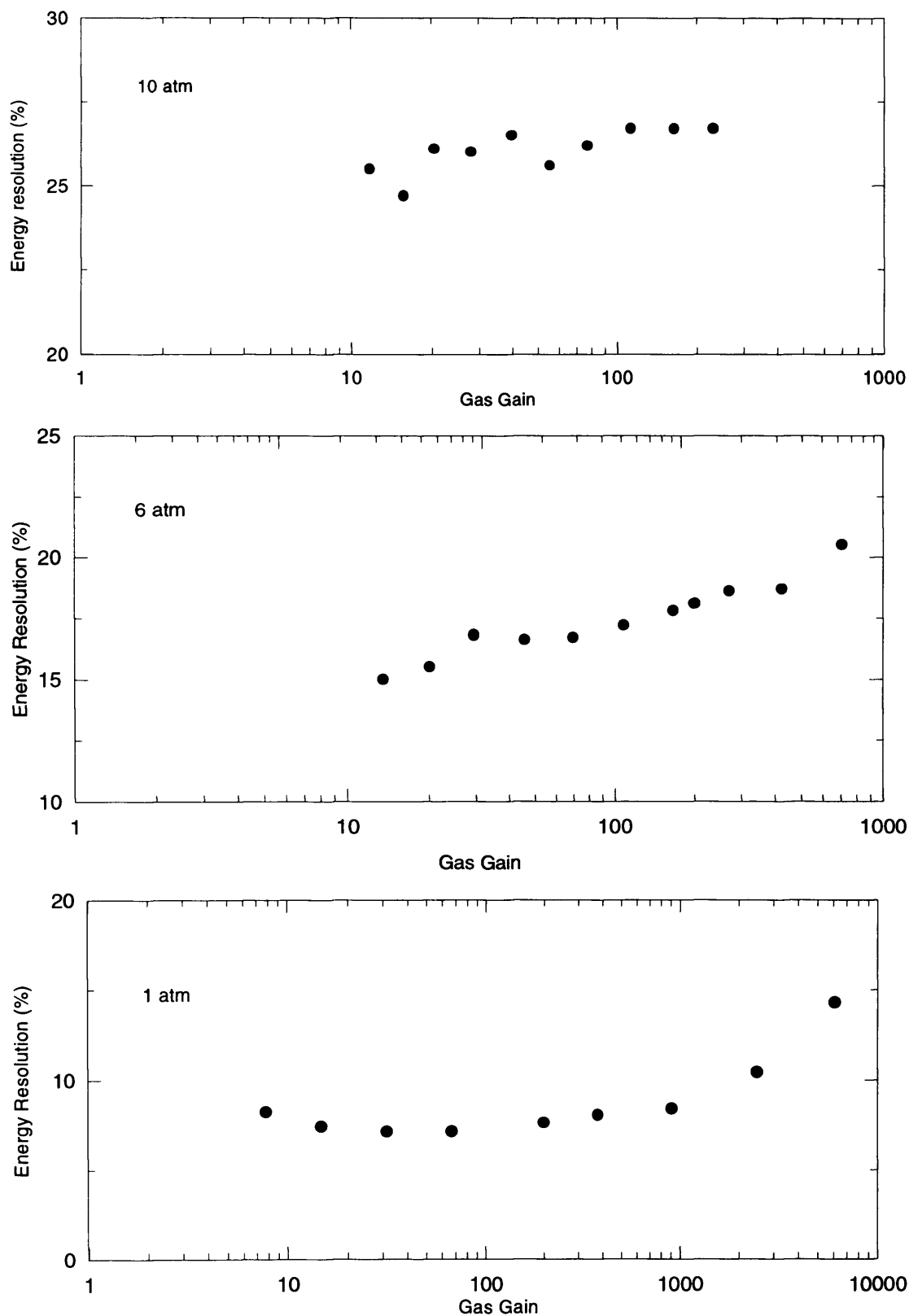


Figure 5.26: Energy resolution of the SWPC as a function of gas gain for the Xe+5%CO₂ mixture at pressures 1, 6, and 10 atm.

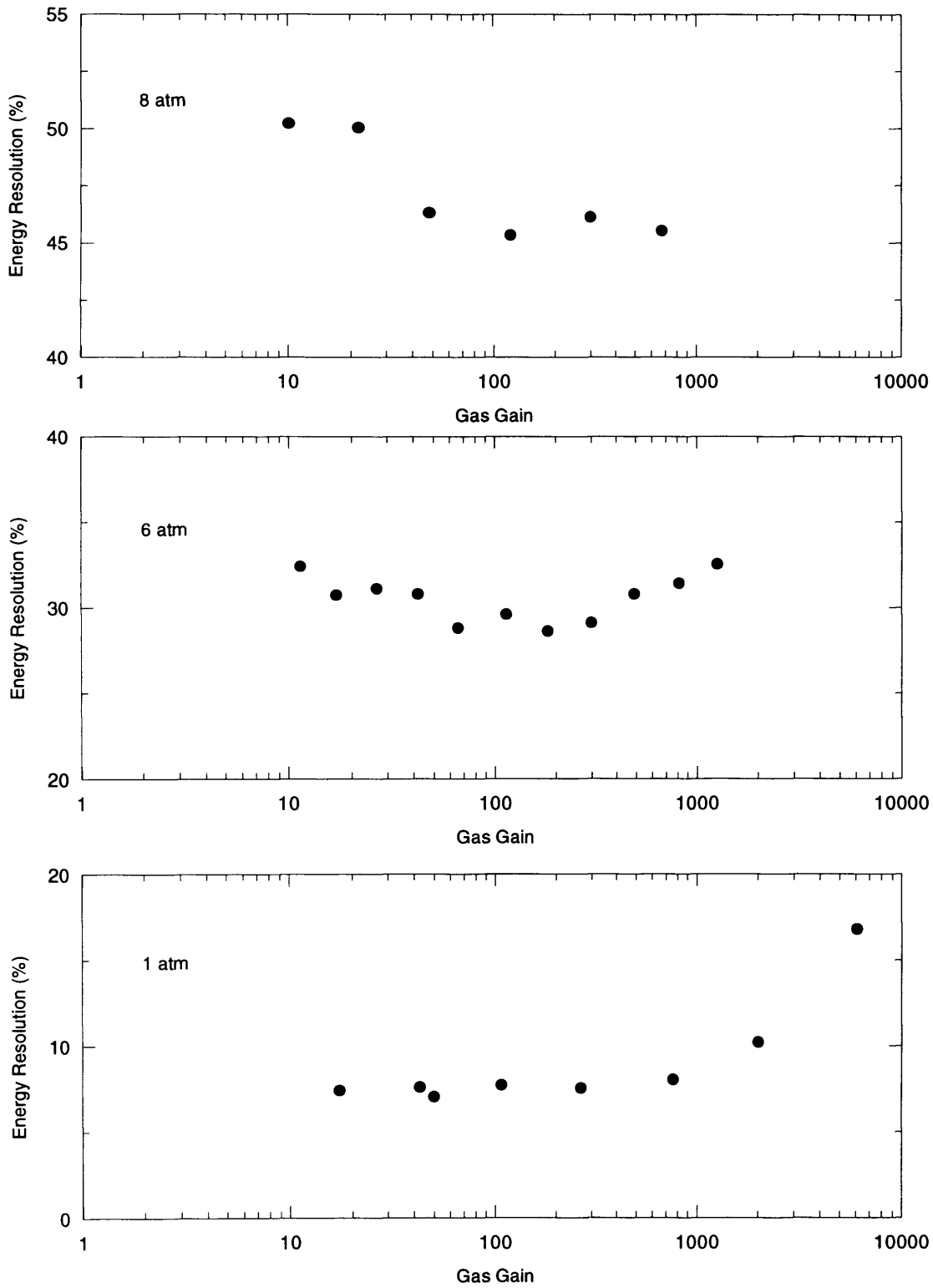


Figure 5.27: Energy resolution of the SWPC as a function of gas gain using Xe+5% C_4H_8 mixture at pressures 2, 6, and 8 atm.

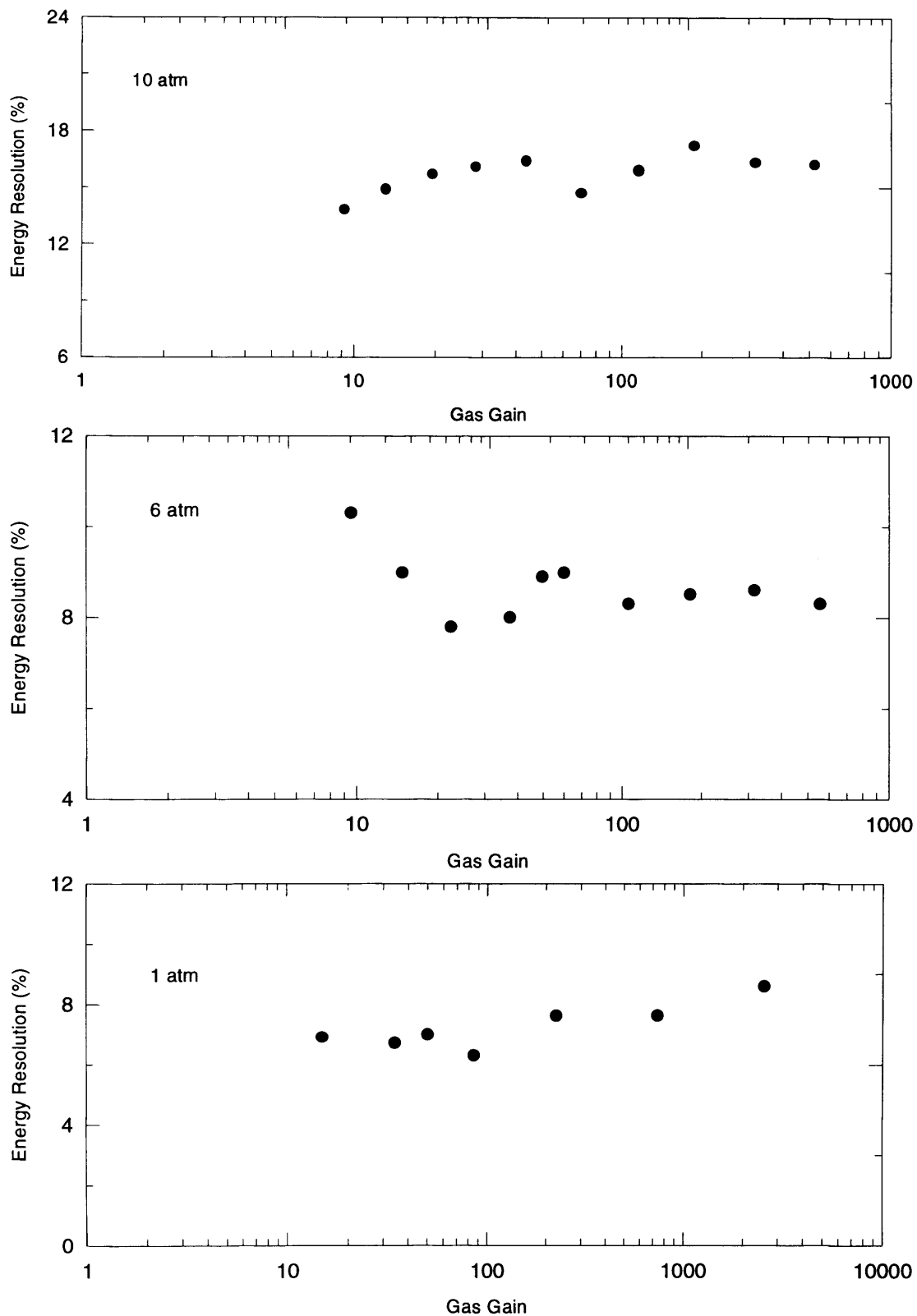


Figure 5.28: Energy resolution of the SWPC as a function of gas gain using Xe+20%Ar mixture at pressures 2, 6, and 10 atm.

We will assume, as in Section 5.2, that for the same gas gain at different gas pressures, the amount of the space charge will be the same while its effect at higher pressure will be less by a factor of which the pressure was increased. As a consequence of this, we may refer the energy resolution deterioration at high gains at a constant gas pressure to be mainly due to the self-induced space charge effect.

From the plots of energy resolution versus gas gain, the space charge effect appears to have a notable effect on the energy resolution at gas gains above 900. On the other hand, at a constant gas gain, the effect of the induced space charge on the energy resolution will be negligible at high pressures if we accept that the space charge does not increase with increasing pressure.

5.3.2 The Effect of Anode Wire Uniformity

One possible explanation for the degradation of the SWPC energy resolution at high pressures is that the dependence of energy resolution on the anode wire uniformity increases with pressure. This has been reported by Sakurai *et al.* (1991) using pure xenon. The concept they have proposed as a possible explanation is that with increasing gas pressure the range of the primary photoelectron decreases and hence the initial charge cloud becomes smaller. Furthermore, the resulting electron cloud is also affected by its diffusion in proportion to $1/\sqrt{p}$, where p is the gas pressure.

pressure. The average size of the electron cloud at the anode wire surface can be expressed as [Sakurai *et al.*, 1991]:

$$A = \frac{\sqrt{A_0^2 + 2Dtp}}{p} \quad (5.4)$$

where A_0 is the size of the primary electron cloud, D the diffusion constant at 1 atm, and t is the

drift time. Therefore, the size of the electron avalanche will be smaller at high pressures in comparison with the anode wire dimensions. Sakurai *et al.* (1991) have estimated the size of electron cloud when projected to the anode wire surface in pure xenon, to be 5 μm at 1 atm and 0.6 μm at 10 atm. Their estimation has been made considering an electron cloud, from 22 keV X-rays, travelling in pure xenon gas to the anode wire from a point 3.5 mm from the anode. Values for the range of electrons in xenon have been given by Berger & Seltzer (1964) and Bateman *et al.* (1975), and values for the diffusion coefficient have been given by Peisert & Sauli (1984) and Sipila (1976).

Therefore, the dependence of gas gain on anode uniformity is expected to be much more sensitive at higher pressures. The comparison made between our measurements using an old and a new anode wires showed clearly the increasing dependence of energy resolution on the anode wire uniformity with increasing pressure. The old wire was a heavily used one, and the energy resolution of the counter obtained with that wire was worse at high pressures in comparison to that with the new one. This is shown in Figure 5.29 where the increasing difference gap can be clearly noticed at pressures above 4 atm. This can only be related to the difference between the two wires in terms of the surface uniformity. Those measurements were taken at a gas gain of ~ 50 with Xe+5%CO₂ using a ¹⁰⁹Cd X-ray source, which was always placed at the same position with respect to the window of the counter.

The counter was found to show a good energy response which was accompanied with an improvement in the energy resolution. This good response was found for the Xe+5%CO₂ and Xe+20%Ar mixtures at pressures of up to 8 atm, and for Xe+5%C₄H₈ at pressures of up to 4 atm. The energy response of the counter was tested by observing the behaviour of the counter at gas gains of ~ 50 or 200 for the 59.5 keV X-rays, from an ²⁴¹Am source, and the 22.2 keV X-rays from a ¹⁰⁹Cd (see Table 5.1).

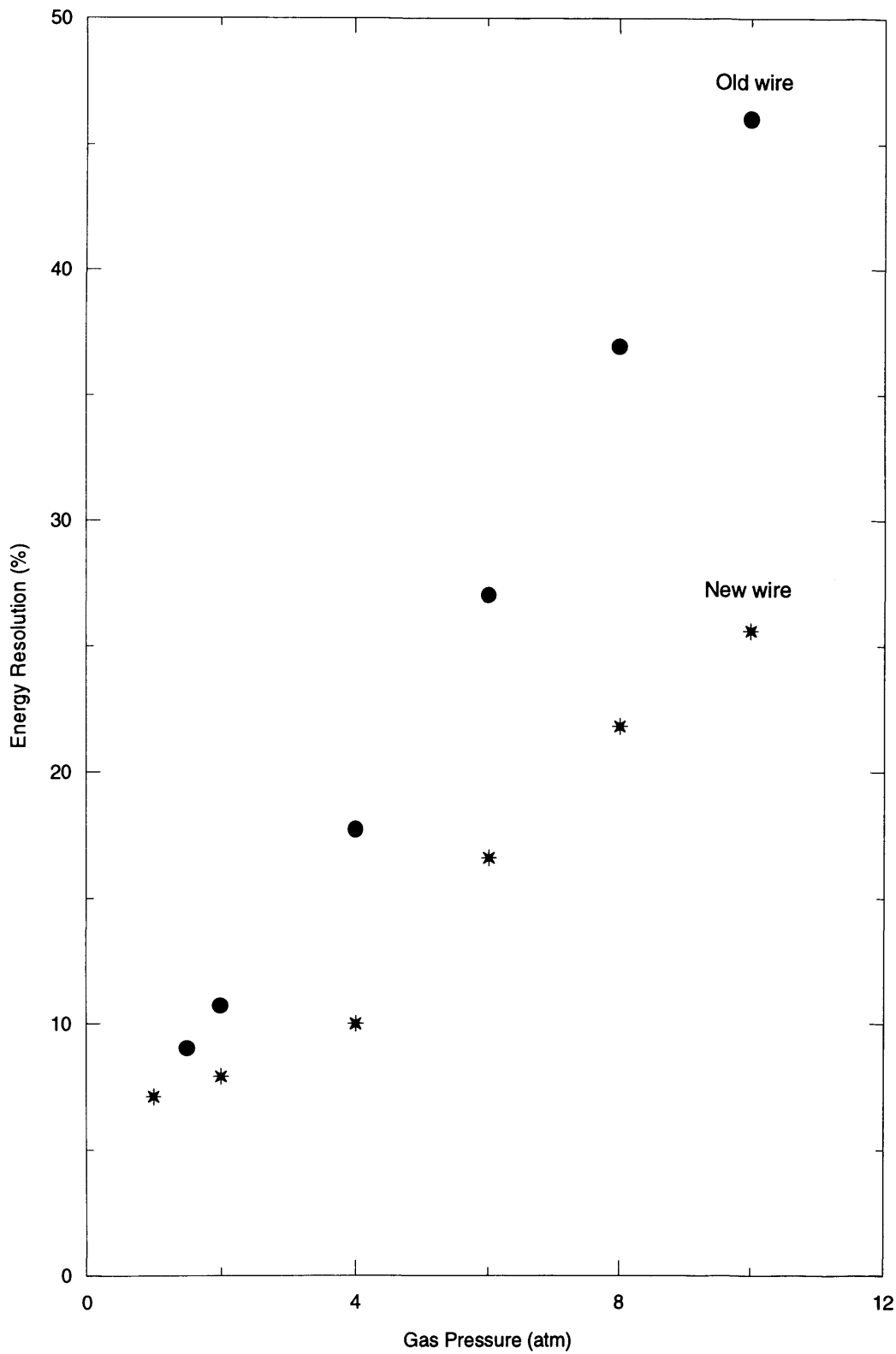


Figure 5.29: Energy resolution measured for the SWPC with old and new anode wire at gas gain of ~ 50 using $\text{Xe}+5\%\text{CO}_2$ at different pressures.

The worse energy resolution of the Penning mixture Xe+5% C_4H_8 was not expected. This mixture was found to exhibit the worst energy resolution at high pressures in comparison with the other mixtures. The counter with this mixture was found to perform well for pressures up to 6 atm.

The following table lists the SWPC energy resolutions obtained for 22.2 and 59.5 keV X-rays for the studied mixtures at different gas pressures.

Table 5.1: Energy resolutions of the SWPC using different mixtures at different pressures for X-rays of ^{109}Cd and ^{241}Am .

Pressure (atm)	Xe+5% CO_2		Xe+20% Ar		Xe+5% C_4H_8	
	(%)		(%)		(%)	
	22.2 keV $G=200$	59.5 keV $G=200$	22.2 keV $G=200$	59.5 keV $G=50$	22.2 keV $G=200$	59.5 keV $G=50$
1	7.6	4.9	6.0	4.0	7.6	4.7
2	8.9	6.9	6.4	4.3	8.5	5.8
4	12.3	9.0	6.5	5.8	18.0	13.8
6	18.1	14.7	8.5	5.8	29.0	24.3
8	22.4	19.7	9.4	7.2	46.0	—
10	26.1	29.5	16.0	—	55.2	—

In conclusion, a possible reason for the degradation of energy resolution of the SWPC at high pressures is the increasing number of excitation events compared to ionisation which in turn increases UV photons emitted from the excited Xe atoms leading to loss of the counter proportionality and hence inferior energy resolution. This will also lower the maximum gain threshold prior to discharge specially with Penning mixtures.

5.4 Pressure Dependent Diethorn Gas Parameters

In the previous sections we calculated the Diethorn gas “constants” to have single values approximately averaged over 1 to 10 atm pressures. That is, we assumed that ΔV and K remain constants with increasing pressure and are characteristic constants of the gas used.

In fact, close inspection of the Diethorn’s data [Diethorn, 1956] reveals that ΔV and K could not be the same for each individual gas pressure. Practically, we found in the present work that the Diethorn gas “constants” are pressure dependents. If the Diethorn gas constants are calculated for each pressure value, then, as shown in Figure 5.30, it can be seen that ΔV increases with pressure, whereas K decreases.

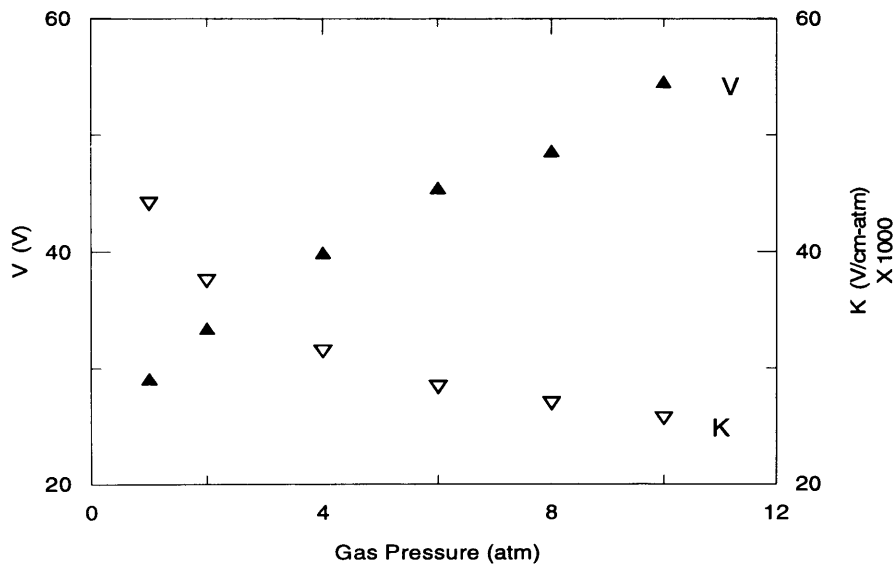


Figure 5.30: The calculated Diethorn gas “constants” for Xe+5%CO₂ as functions of the gas pressure.

Diethorn (1956) defined K as E_0 / p , where E_0 is a critical value for the electric field at which the avalanche commences, and ΔV as the potential difference through which an electron has moved in covering the distance between successive ionising events.

The distance, d , between successive ionising events is actually the reciprocal of the first ionisation Townsend coefficient (*i.e* $1/\alpha$). We can, therefore, write:

$$\Delta V = Ed = E\left(\frac{1}{\alpha}\right) \quad (5.5)$$

$$\Delta V = \frac{E}{p}\left(\frac{1}{\alpha/p}\right) \quad (5.6)$$

In Section 5.2.1, it was mentioned that α/p is non-linearly dependent on E/p as shown in Figure 5.10 of Hayashi (1983). This also has been shown by Sakurai *et al.* (1991) and recently by Zastawny (1997).

Equation 5.6 can be rewritten using Equation 5.1 as:

$$\Delta V = \frac{E}{p}\left(\frac{1}{A \exp[-B/(E/p)]}\right) \quad (5.7)$$

which shows that ΔV increases with pressure which was confirmed here practically (Figures 5.30 and 5.31).

Figures 5.31 and 5.32 show that the Diethorn gas factors ΔV and K depend on both the gas type and pressure, and the behaviour of these “constants” is clearly almost the same for the gas mixtures studied.

Figure 5.32 shows that mixtures which exhibited higher gas gains are characterised by smaller K , which has already been confirmed by Wolff (1974). This figure also show that with increasing pressure, the avalanche commences at lower reduced electric field further closer to the anode wire.

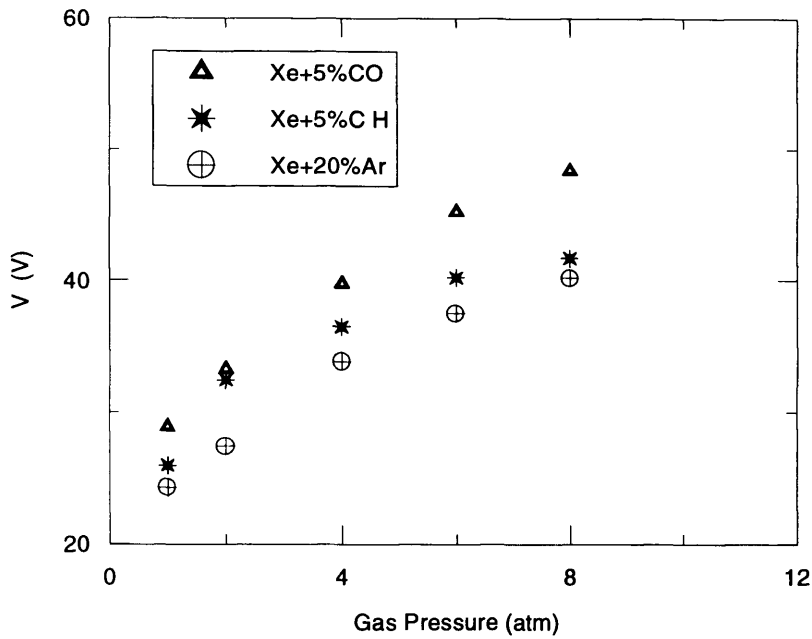


Figure 5.31: The calculated ΔV as a function of gas pressure for the mixtures under study.

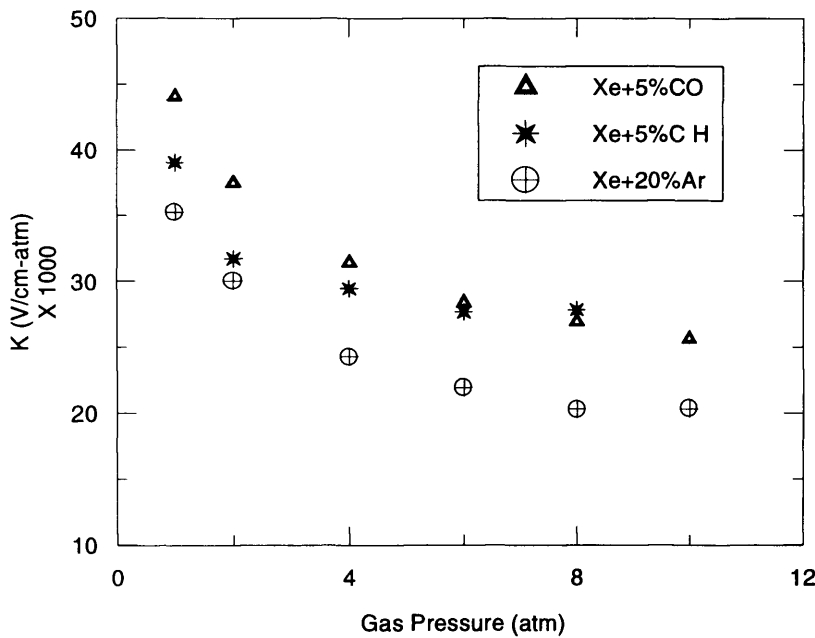


Figure 5.32: The calculated K as a function of gas pressure for the mixtures under study.

As will be discussed in Chapter 6, the thinner the anode wire the higher the electric field around it. At a constant pressure, the point at which the avalanche commences is expected to depend on the anode wire dimensions and type of the gas. Using Equation 2.4 of Chapter 2 and

the K values obtained at each gas pressure, we estimated the critical field radius, or the electron multiplication onset point, for the SWPC with the gas mixtures under study:

$$K = E_0 / p = V_a / [r_0 \ln(b/a)] \quad (5.8)$$

The calculated critical radius r_0 was estimated at a gas gain of 200 in the SWPC, which has an anode radius, a , of $21.2 \mu\text{m}$. The results are shown in Figure 5.33, which reveals that the

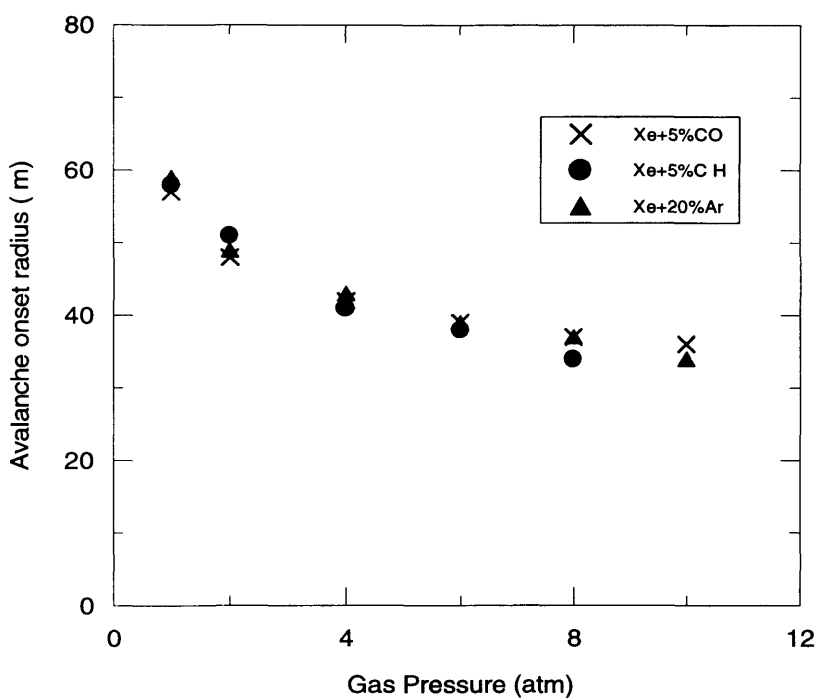


Figure 5.33: The critical radius (or the avalanche onset point) as a function of the gas pressure

avalanche, or electron multiplication, onset point does not strongly depend on the gas used, *i.e.* it is expected to depend mainly on the counter geometry, as will be discussed in Section 6.3.2 of Chapter 6. The radius r_0 decreased from $58 \mu\text{m}$ at 1 atm to $34 \mu\text{m}$ at 10 atm.

Chapter 6

Performance of a High Pressure MSPC

Performance of the MSPC was studied at pressures up to 5 atm using Xe+5%CO₂, although the results were limited by a technical difficulties and leak problems which resulted in a series of breakdown events. This finally caused serious damage to the two identical MS plates used in this work. This chapter presents the results describing the MSPC performance in terms of gas gain and energy resolution using Xe+5%CO₂ at pressures up to 5 atm. At the end of the chapter a comparison is made with the SWPC.

6.1 Gas Gain Measurements

The gas gain and energy resolution of the MSPC, operated with Ar+5%CO₂ as a flow gas counter at atmospheric pressure, were measured for ¹⁰⁹Cd X-rays to test the counter before it was filled with xenon mixtures and sealed off. The counter performed well in terms of gas gain stability and energy resolution (Section 6.2). Figure 6.1 shows the gas gain as a function of the anode voltage where the cathodes were kept grounded. The gas gain was relatively high as expected from Ar-based mixtures.

As mentioned in Chapter 3, ions produced in the avalanche can attach to the surface of the insulating substrate resulting in charge build up and modification of the electric field around the electrode strips, which in turn causes gas gain drift. The short-term change in gas gain of MSPCs after application of voltage, has been observed for most MS structures manufactured on insulating supports, with a time constant that does not seem to depend on irradiation rates. However, this kind of gain instability is absent in MSPC with electronically conductive substrate

[Bouclier *et al.*, 1993; Pestov & Shekhtman, 1994]. The time needed for a MSPC to stabilise has been noted to differ from MS structure to another; *e.g.* a 1 minute period has been noted to be required for a Pestov P9 semiconducting glass [Bateman & Connolly, 1993a].

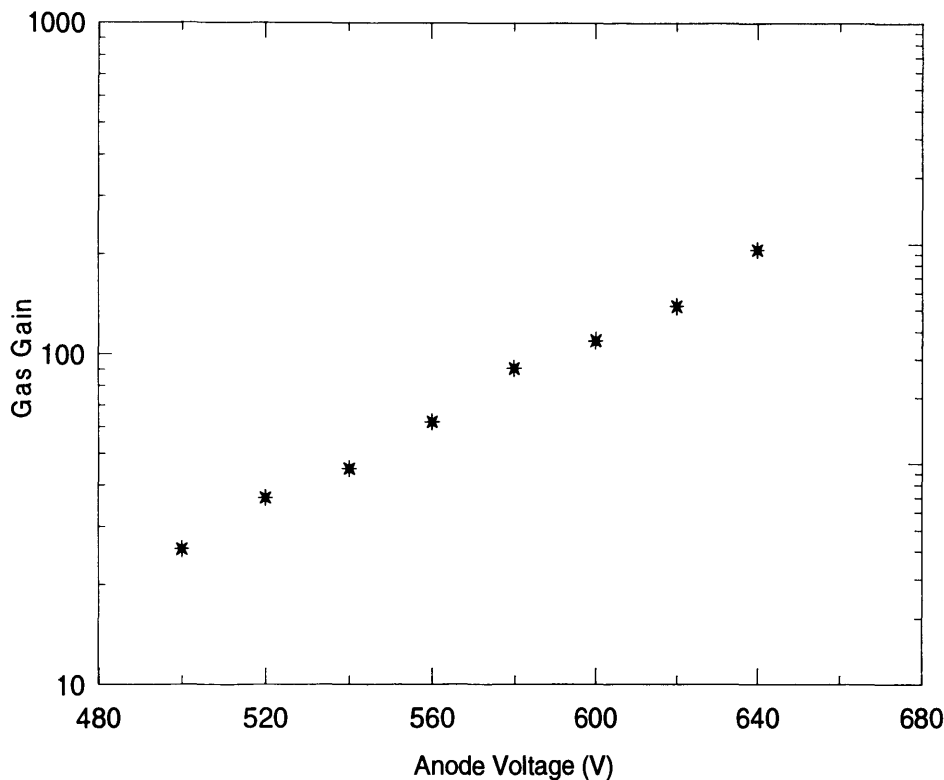


Figure 6.1: Gas gain as a function of the anode voltage for the MSPC operated as a flow gas counter at atmospheric pressure using Xe+5%CO₂. The cathodes were grounded.

This effect was noted in our measurements as a rapid gas gain change with time directly after the application of the high voltage. Figure 6.2 shows the variation of gas gain with time for different values of applied voltage at 2 atm pressure. The counter gas gain needed at least 30 min to stabilise, and after that no gain variations were noted and the counter worked well. The counter was left at a constant voltage (800 V) for a period of about 13 hours, and the gas gain was found to be quite stable.

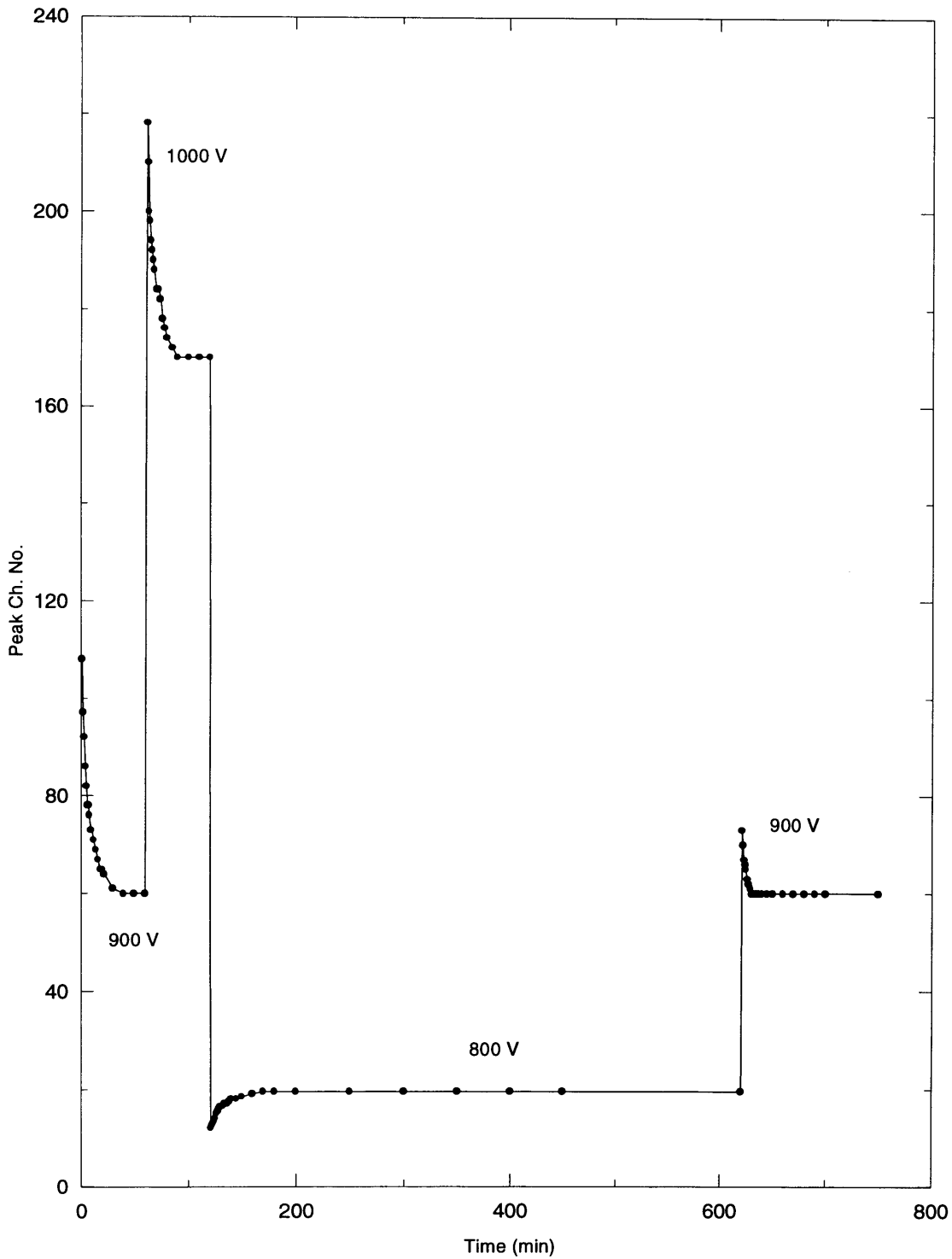


Figure 6.2: The gas gain variation with time due to MS plate charging-up effect using Xe+5%CO₂ at 2 atm pressure. The cathode voltage was set at 0 V.

Referring to Figure 6.2, in case of charging (*i.e.* increasing anode voltage), the gas gain $G(t)$ was gradually “decaying” according to the equation:

$$G(t) = G_0 e^{-t/\tau} + G_1 \quad (6.1)$$

where, $G_0 = G_2 - G_1$, G_1 is the gas gain value before applying a further voltage, G_2 is that after stabilisation, τ is the time constant.

On the other hand, in case of dis-charging (*i.e.* decreasing anode voltage), the gas gain was gradually rising according to the equation:

$$G(t) = G_0 (1 - e^{-t/\tau}) + G_1 \quad (6.2)$$

The time constant, τ , in both cases was about 9 min.

Figure 6.3 shows the variation of gas gain with the anode-cathode potential difference ($V_a - V_c$) at different cathode potentials and different gas pressures up to 5 atm. This figure reveals a similar behaviour for gas gain as for the SWPC (Section 5.2 of Chapter 5); with the exception that, at a constant pressure, gas gain changes more rapidly with bias.

The Diethorn gas constants obtained in Section 5.2.1 of chapter 5 were used here to estimate the effective cathode radius in the MSPC. By using those gas constants, the measured gain, and the applied voltage we were able to solve the Diethorn equation for b (cathode radius in SWPC), where the anode radius, a , was assumed to be half of the anode strip width (5 μm). The values obtained for b at 2 atm pressure and different gas gains indicate that the corresponding cathode radius for the MSPC could be assumed to be the distance between anode and cathode width

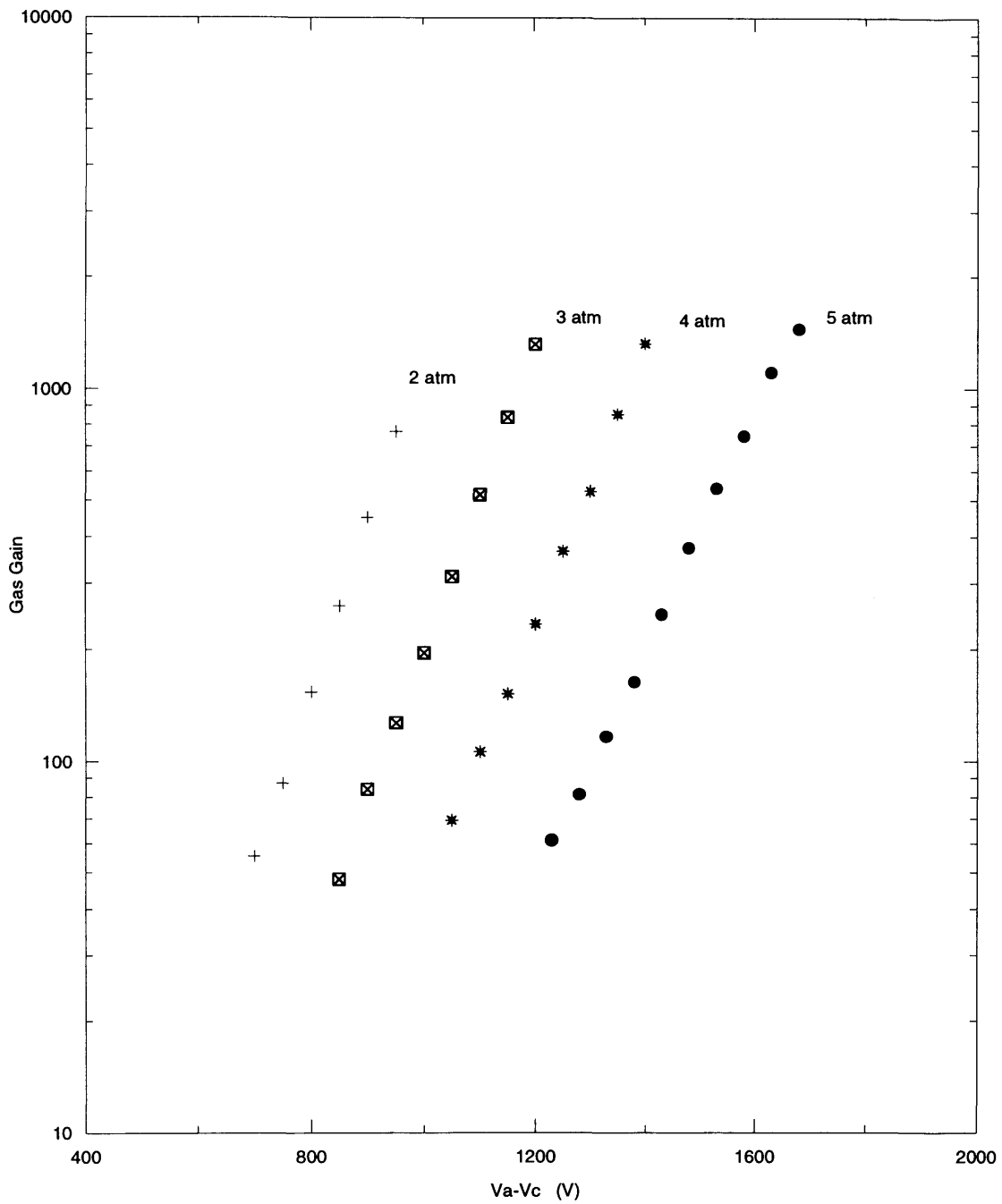


Figure 6.3: Measured gas gain as a function of the potential difference ($V_a - V_c$) for the MSPC using Xe+5%CO₂ at different gas pressures.

centres, which, for our MS plate, is 505 μ m. Thus, MSPC gas gains are approximately calculable using established SWPC formulae and the obvious parameters of the SWPC pattern.

Accepting this finding enabled us to use the procedure, previously used for the SWPC, to calculate Diethorn gas constants ΔV and K from the MSPC data. Figure 6.4 shows the Diethorn equation “straight line” plot using the MSPC gain data. It is clear from Figure 6.4 that the gas gain of the MSPC has a different behaviour from that of SWPC in terms of its rate of change with pressure, as will be discussed in Section 6.3.

The calculated Diethorn gas constants for each gas pressure are given in Table 6.1. The value of K seemed to be constant with pressure which indicates, from the definition of K ,

Table 6.1: Diethorn gas constants calculated from Xe+5%CO₂ MSPC gain data.

Gas Pressure (atm)	ΔV (V)	$K \times 10^{-4}$ (V cm ⁻¹ atm ⁻¹)
2	34.80	3.94
3	37.22	3.90
4	39.75	3.90
5	44.06	4.02

that avalanche in the case of the MSPC begins almost at the same E/p for different gas pressures, at least up to 5 atm. The Diethorn constants were used to calculate the predicted gas gain at each gas pressure which was then compared with measured gain as shown in Figure 6.5. The gain is also plotted in Figure 6.6 as a function of the reduced electric field (E_a/p) at the edge of the anode strip. The electric field, E_a , was estimated using Equation (2.3) at $r=a$.

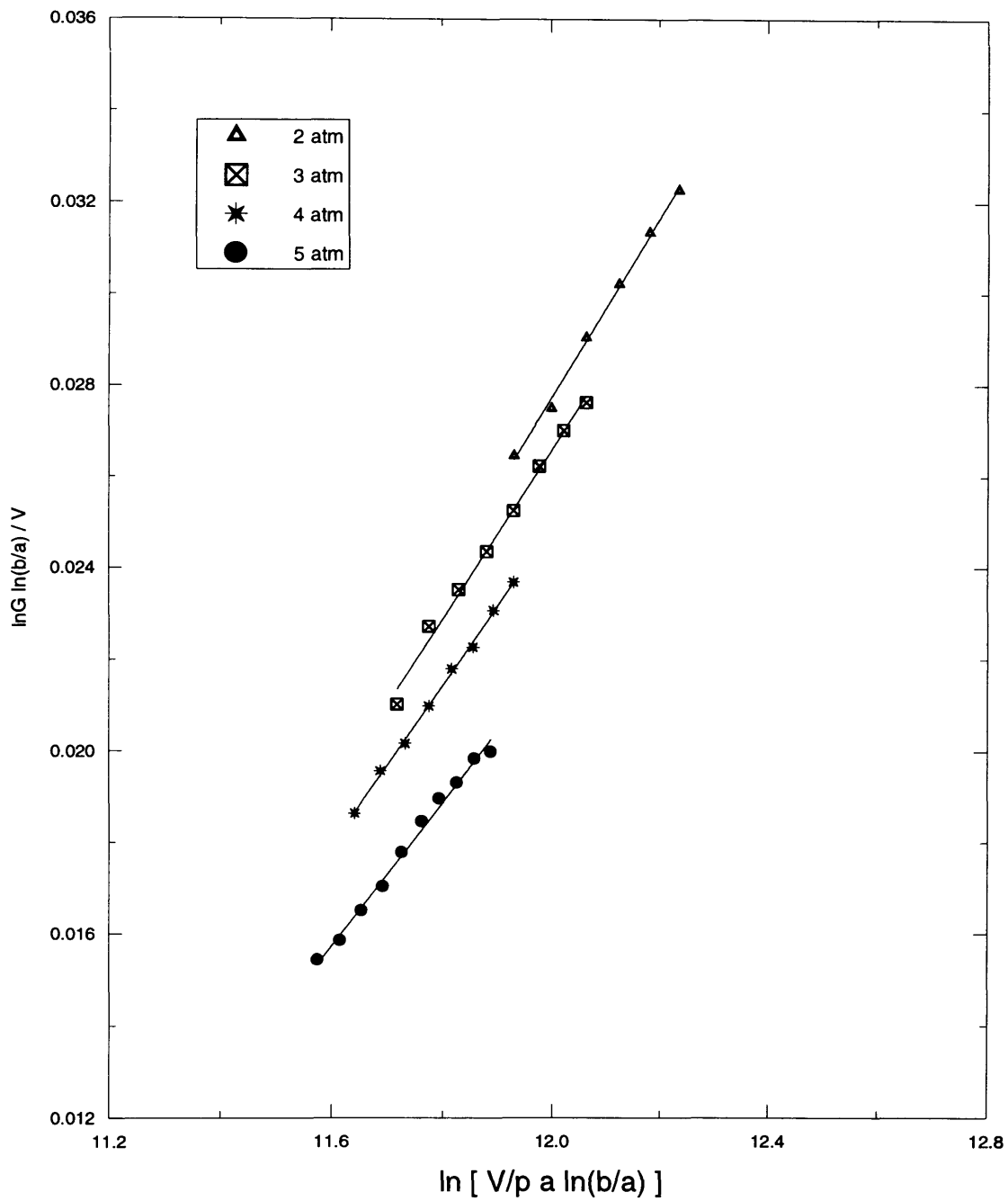


Figure 6.4: Diethorn plot (straight line relation) for the MSPC gas gain using Xe+5%CO₂ at different pressures.

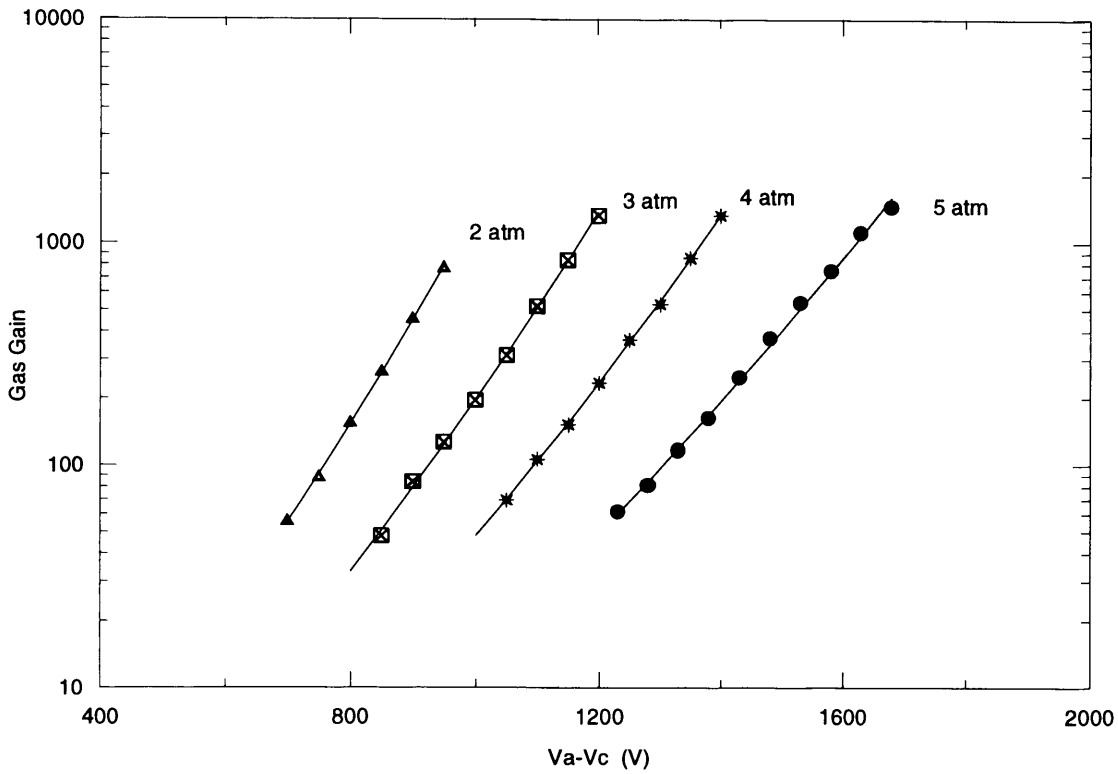


Figure 6.5: The measured gas gain as a function of anode-cathode potential difference ($V_a - V_c$) for the MSPC using Xe5%+CO₂ at different pressures compared with the calculated gas gain (solid lines) using the Diethorn parameters given in Table 6.1.

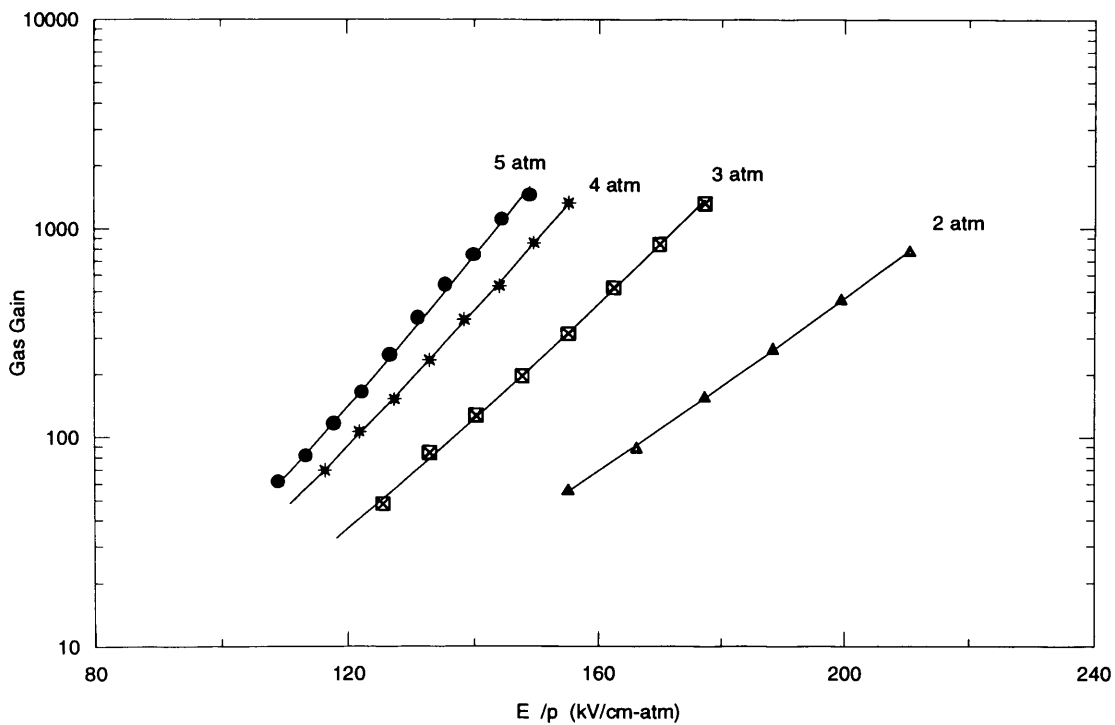


Figure 6.6: The measured gas gain compared with the calculated as a function of the reduced electric field (E_a/p) for the MSPC using Xe+5%CO₂ at different pressures.

6.2 Energy Resolution Measurements

Figure 6.7 shows variation of the energy resolution with the gas gain for the MSPC operated as a flow gas counter with Ar+5%CO₂. At a gas gain of ~ 150, the energy resolution was found to be ~ 7.9%. This was an indication of satisfactory MSPC operation at least at atmospheric pressure.

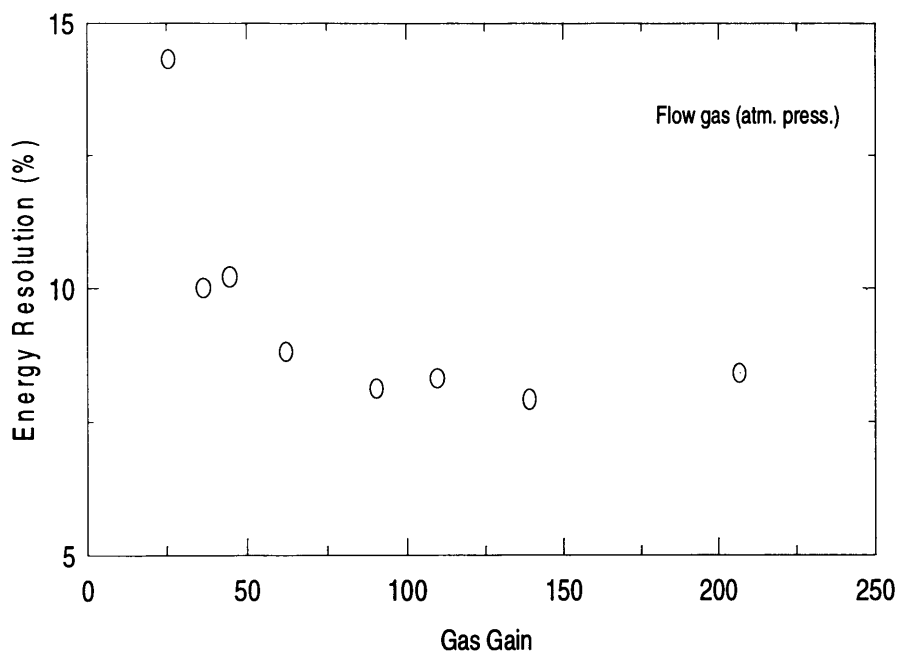


Figure 6.7: Energy resolution as a function of MSPC gas gain. MSPC operated as a flow gas counter using Ar+5%CO₂ at atmospheric pressure.

The MSPC was first operated as a sealed counter with Xe+5%CO₂ at 1.5 atm and was found to have nearly a stable energy resolution of ~9.2 % at gas gains of 200 up to 10³ for 22.2 keV X-rays.

The energy linearity of the MSPC was also checked at 1.5 atm using the radioactive sources ⁵⁵Fe, ¹⁰⁹Cd, and ²⁴¹Am (Figure 6.8). The energy resolutions for the principal peaks were found to be 22.2, 9.6, and 8.2% respectively at a gas gain of ~100.

At a pressure of 2 atm and gas gain of ~ 200 , the energy resolutions at 22.2 and 59.5 keV were found to be 11.6% and 7.1%, respectively. The approximate corresponding theoretical values using Equation 1.4 [Fraser, 1989] are $\sim 7.4\%$ and 4.5% , respectively.

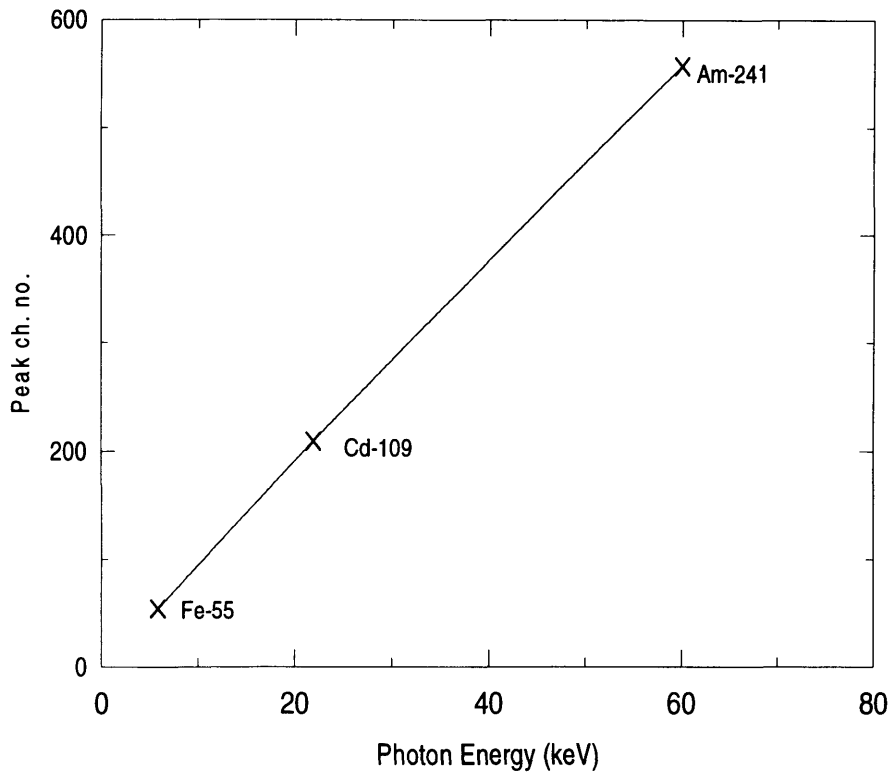


Figure 6.8: The MSPC response for 5.9, 22.2, and 59.5 keV X-rays using Xe+5%CO₂ at 1.5 atm pressure.

Because of the expected short rise time of a signal from a MSPC, the effect of the shaping amplifier time constant (see 4.5.1 of Chapter 4) on the energy resolution was tested. Energy resolution at 22.2 keV was measured for different time constants at a gas gain of ~ 1200 and gas pressure of 2 atm and is shown in Figure 6.9. The energy resolution measured at time constant of 6 μs was found to be the best. Therefore, it was decided to use this value for the rest of our measurements with the MSPC.

The very small area of anode strips compared with that of the cathode strips make it necessary to apply an additional potential to the cathodes so that the primary and secondary electrons,

produced by the X-ray photons, can all be attracted to the avalanche region. As shown in Figure 6.10, the energy resolution was found to improve with increase of the cathode voltage (V_c) at a constant anode-cathode potential ($V_a - V_c$). This results in a better energy resolution which becomes more important at high gas pressures. At higher gas pressures, the cathode voltage was selected so that the drift field was proportional to the increase in pressure.

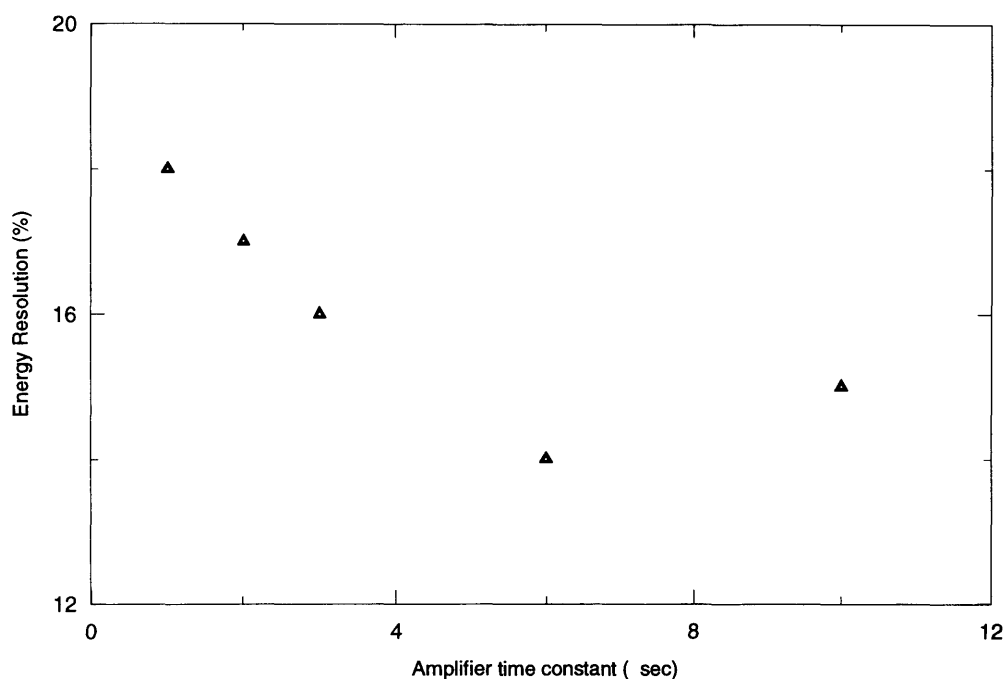


Figure 6.9: Variation of the observed MSPC energy resolution with the amplifier time constant at gas gain of ~ 1200 and pressure of 2 atm.

As noted in Chapter 3, the advantage of the small anode-cathode spacing in a MSPC is to reduce the effect of self-induced space charge, which is the main factor affecting the energy resolution in wire chambers at high gas gains. Our measurements on the MSPC energy resolution confirm this advantage in practice, where the counter was operated at relatively high gas gains without a notable degradation in its energy resolution. This is clear in Figure 6.11 which shows that the MSPC energy resolution remains constant for gas gains at least up to 1400. Therefore, the energy resolution of a MSPC could be said to be independent of gas gain at constant pressure.

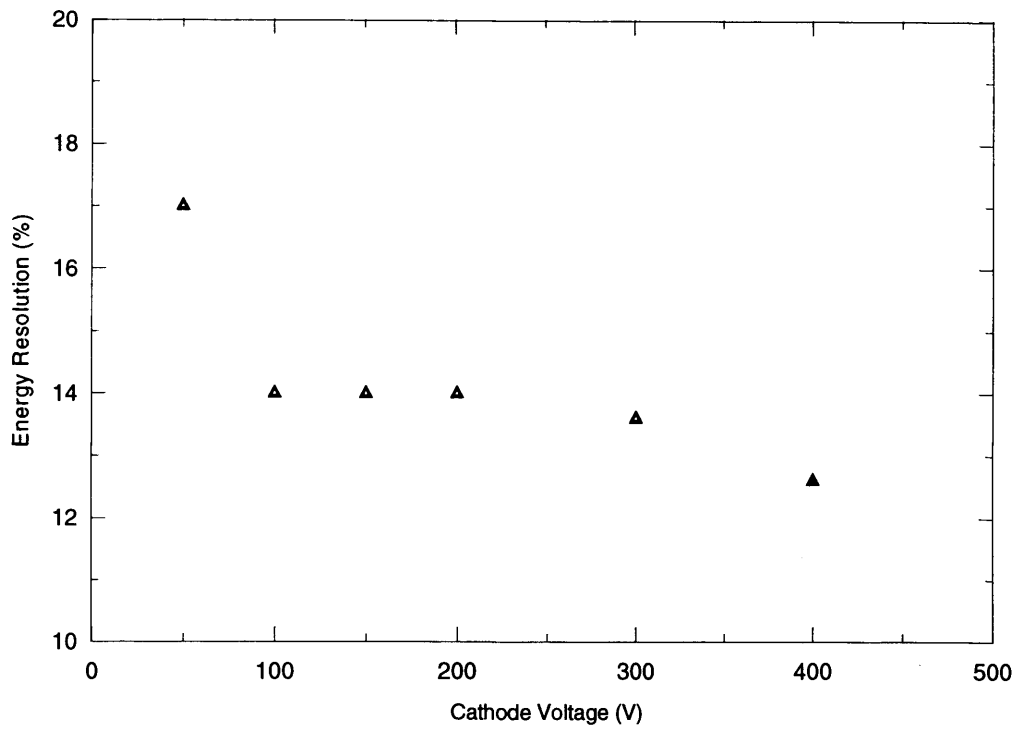


Figure 6.10: Variation of the observed MSPC energy resolution with the cathode voltage (V_c) at gas gain of ~ 400 ($V_a - V_c = 900$ V).

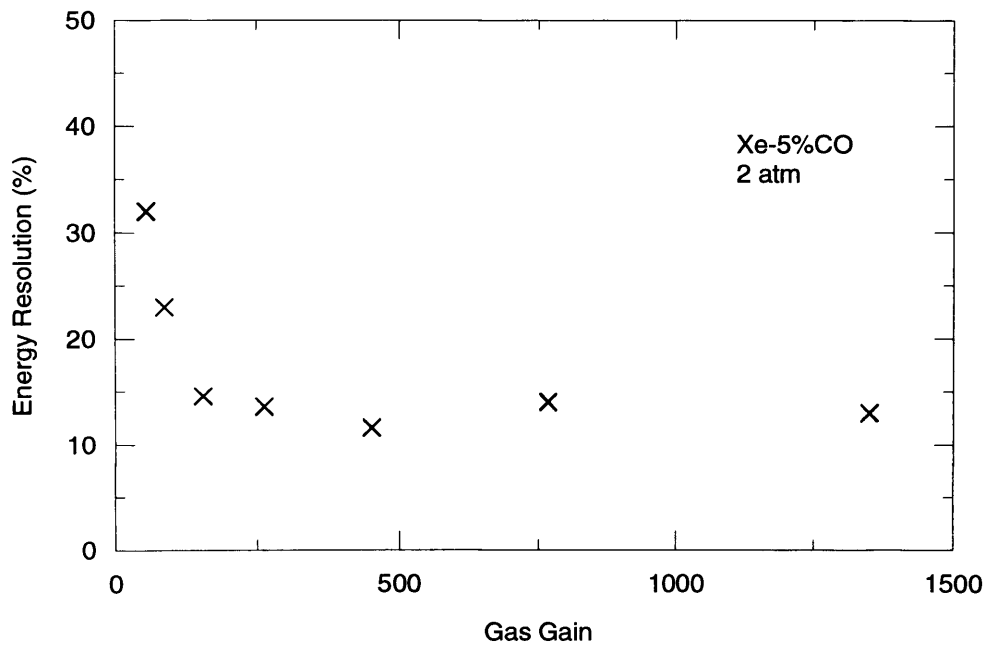


Figure 6.11: MSPC energy resolution (for ^{109}Cd X-rays) as a function of gas gain using Xe+5%CO₂ at 2 atm pressure.

Figure 6.12 illustrates the MSPC pulse height distributions obtained for a Xe+5%CO₂ mixture at 1 and 5 atm pressures. The variation of energy resolution with gas gain at pressure 2, 4, and 5 atm is shown in Figure 6.13.

Figures 6.12 and 6.13 clearly display the deterioration of energy resolution with increasing pressure. This deterioration of energy resolution at high pressures can not be related to the effect of anode nonuniformity, which could be significant in the case of an SWPC or MWPC. This is simply because of the very fine and precise structure of the anode strips of a MSPC.

As noted in Chapter 5, in the case of the SWPC, the deterioration of the energy resolution with increasing pressures was probably due to the increase of excitation events compared to the frequency of ionisation in xenon (Section 5.2 of Chapter 5). This could be the situation in the case the MSPC, although it is also possible to suspect the level of gas purity, given the larger size of the counter.

It has been reported for a Xe+2%CH₄ SWPC [Sakurai *et al.*, 1991] that the change in energy resolution with pressure cannot be due to impurities at the part per million (ppm) level, and at 5atm gas pressure the addition of 16 ppm of oxygen had no measurable effect on the energy resolution. Therefore, the increasing sensitivity of Xenon gas to impurities with increasing pressure could be a possible explanation of our results only if the impurity level in the mixture was relatively high. This was not checked and the gases were assumed to have the level of purity (99.95%) indicated by the supplier [BOC].

The deterioration of the energy resolution could not be due to the nature of the Xe+5%CO₂ mixture because the same behaviour was also found in the cases of the other mixtures in the SWPC (see Chapter 5). In recent work [Fraga *et al.*, 1996] carried out with an MSPC using Xe+14%CO₂ at pressures up to 6 atm, a very poor counter performance has been reported; no

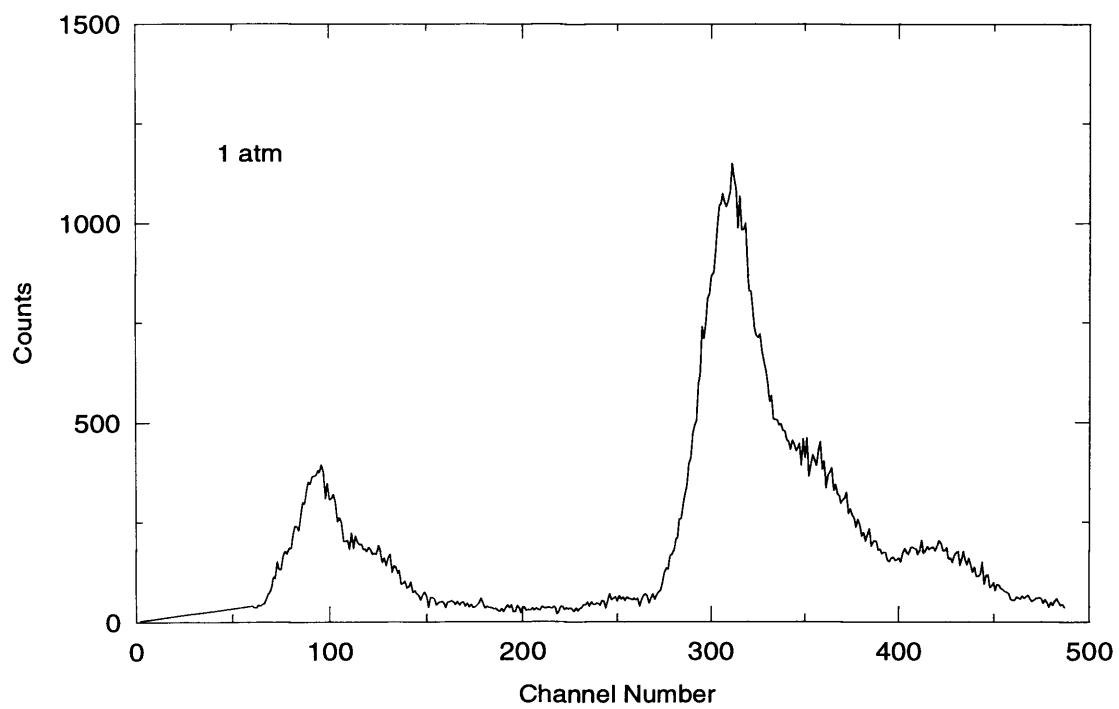
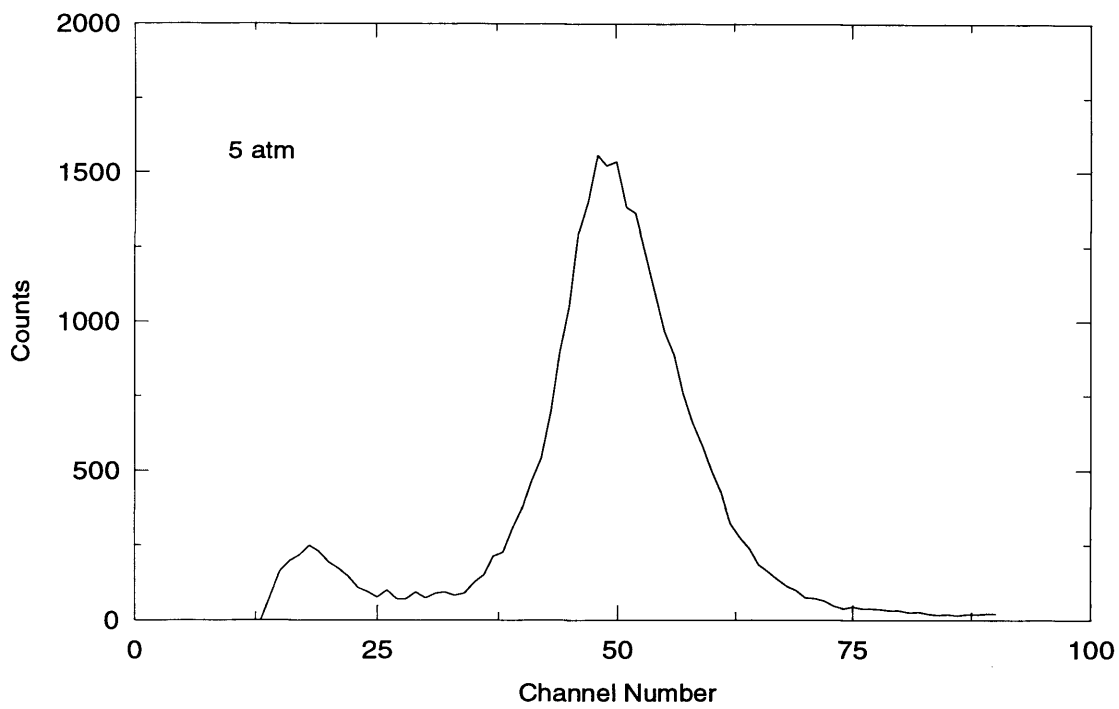


Figure 6.12: MSPC pulse height distributions for ^{109}Cd X-rays using Xe+5%CO₂ at 1 and 5 atm pressures.

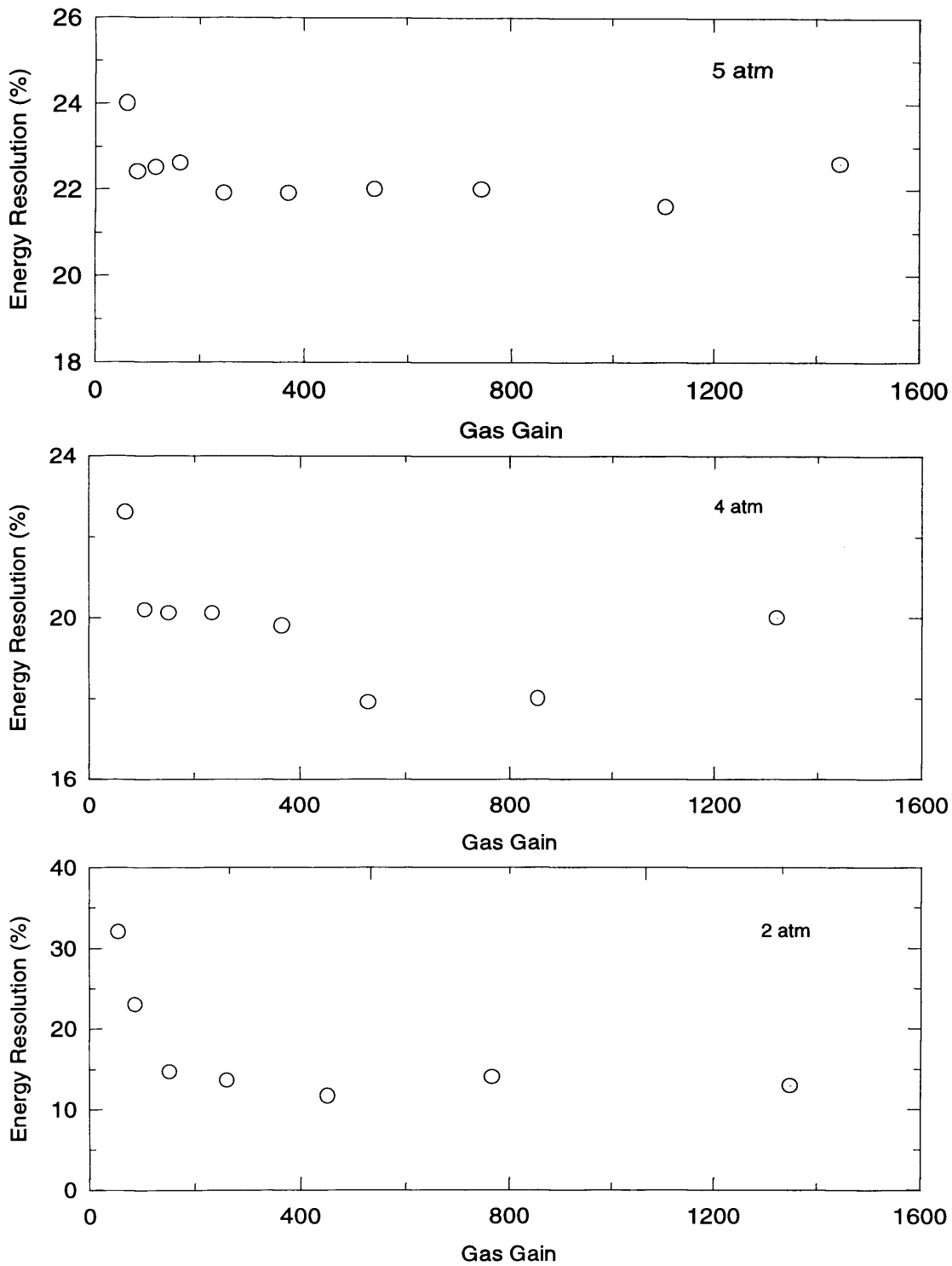


Figure 6.13: MSPC energy resolution as a function of gas gain using Xe+5%CO₂ at different pressures for ¹⁰⁹Cd X-rays.

analysable spectrum was obtained. The results of Fraga *et al.* (1996) may indicate that the Carbon-dioxide concentration (14%) is a probable reason for the poor performance of the MSPC they have used, since they have reported 15% energy resolution at 22 keV for Xe+10%CO₂ using an MGPC.

Figure 6.14 shows a pulse height spectrum which we were able to obtain for ²⁴¹Am X-rays from the MSPC in its worst condition after a series of breakdown events. All attempts to acquire a better spectrum for ²⁴¹Am X-rays after that time were unsuccessful. This indicates one of the most important advantages of MSPCs of being able to operate reasonably with a partially damaged electrode structure which is not true in the case the wire proportional counters.

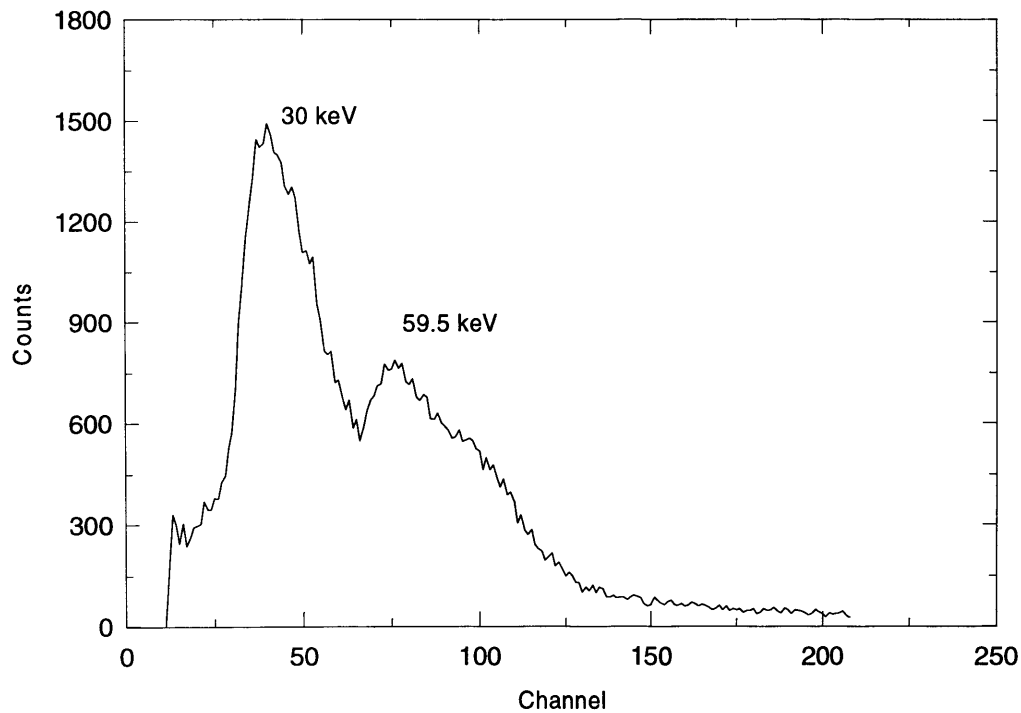


Figure 6.14: Pulse height spectrum of ²⁴¹Am X-rays obtained with the MSPC using a Xe+5%CO₂ mixture at 6 atm pressure (most of the anode strips were damaged).

An energy resolution of 17.9% at 59.5 keV was measured with the MSPC at 5 atm pressure, and the behaviour of energy resolution with gas gain at the same pressure is shown in Figure 6.15.

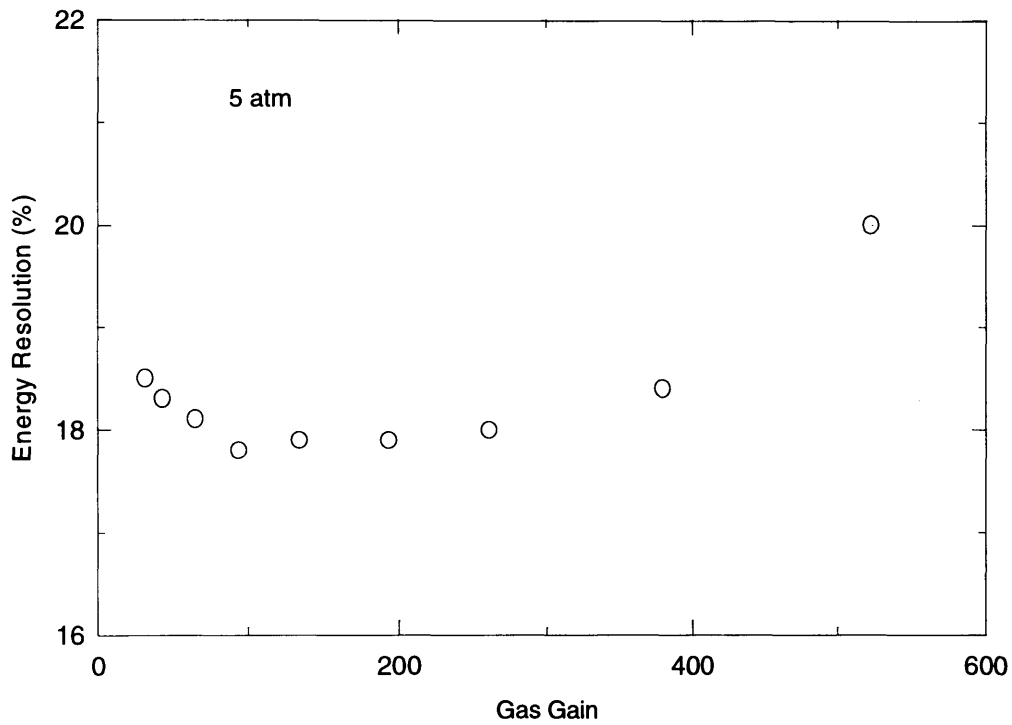


Figure 6.15: MSPC Energy resolution as a function of gas gain of using Xe+5%CO₂ at 5 atm pressure for ²⁴¹Am X-rays.

6.3 Comparison with the SWPC

This comparison is based on measurements obtained for the SWPC using Xe+5%CO₂ at pressures of up to 6 atm (presented in Chapter 5) and those obtained for the MSPC using the same mixture at pressures up to 5 atm.

6.3.1 Gas Gain

The dependence of gas gain on the applied voltage for both counters was found to be similar in terms of proportionality. In the case of the MSPC the dependence is stronger; the gas gain was found to change faster with voltage. That is the gradient (slope) of the gas gain vs voltage curve is larger. Figure 6.16 shows the variation of gas gain with voltage at 2 and 4 atm pressures for both counters.

The higher MSPC gas gains are due to the very high electric field strength which can be obtained near the anode strips of the MSPC by applying a much lower voltage than that required with the SWPC. The electric field at the edge of the anode strip can be estimated using Equation 2.3 for an anode voltage of 1 kV to be $4.33 \times 10^5 \text{ V cm}^{-1}$, corresponds to $8.35 \times 10^4 \text{ V cm}^{-1}$ for the SWPC, *i.e.* it is ~ five times greater in the case of the MSPC. The gas multiplication in the MSPC, therefore, occurs in a region of stronger reduced electric field than for the SWPC, and hence more ionisation events are possible (Equation 5.1 of Chapter 5) which produce higher gas gains.

Figure 6.17 reveals that with increasing pressure, the MSPC exhibits less degradation of the slope of the gas gain curve. This indicates less non linearity of the avalanche dependence on gas pressure in MSPC. The SWPC was found to operate at lower reduced electric field, E/p , at high pressures, as noted in Chapter 5. The MSPC exhibited the same behaviour but with less degradation of the slope of the gain curve.

Figure 6.18 shows clearly the difference in behaviour of the SWPC and MSPC in terms of gas gain linearity with pressure. This figure is a combination of the data previously displayed in Figure 5.11 and 6.4 at selected pressures up to 6 atm. The figure shows that both the slope ($\ln 2/\Delta V$) and the intercept $[(\ln 2/\Delta V) \ln K]$ are changing with pressure.

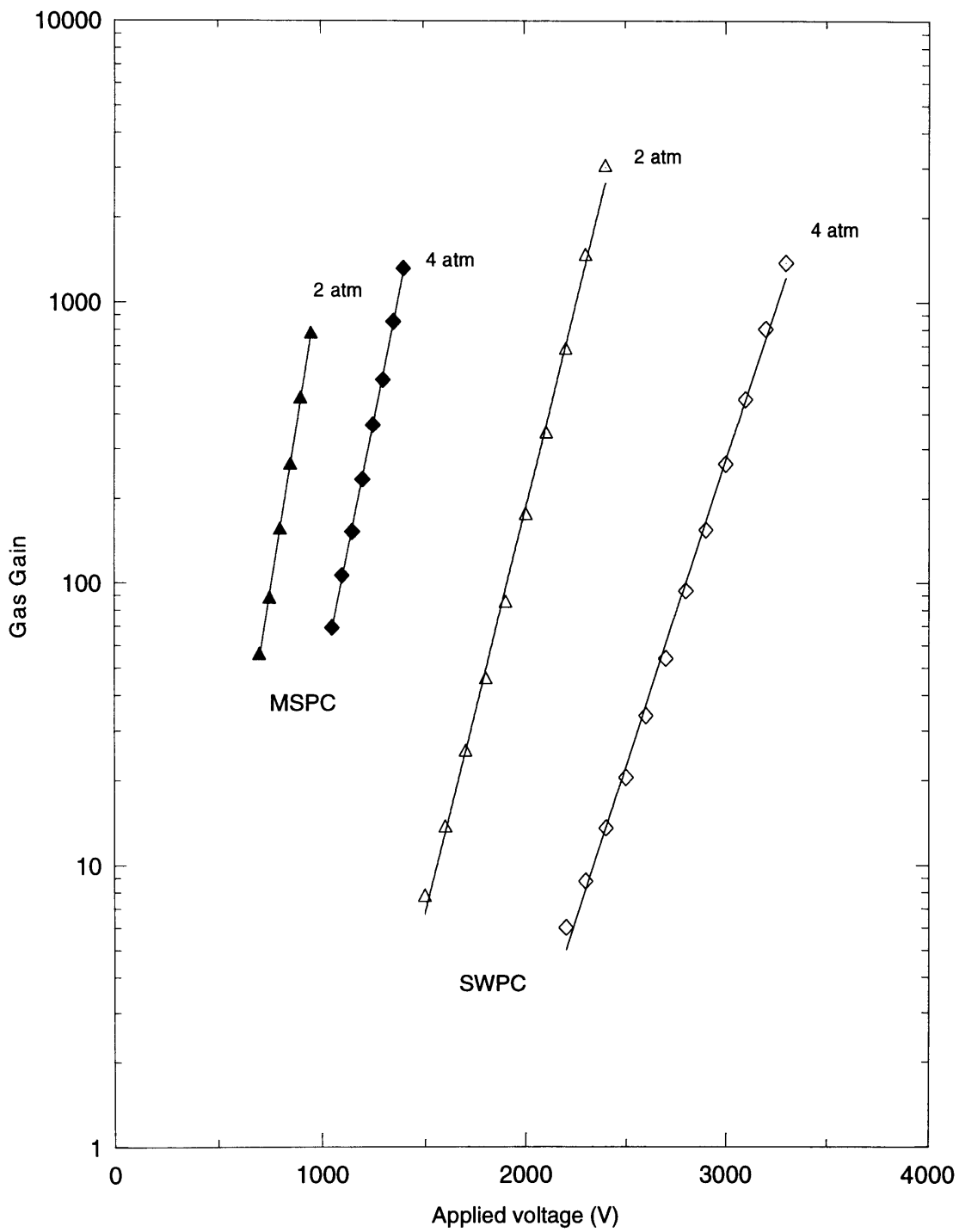


Figure 6.16: Gas gain as a function of applied voltage for both the SWPC and the MSPC using Xe+5%CO₂ at 2 and 4 atm pressures.

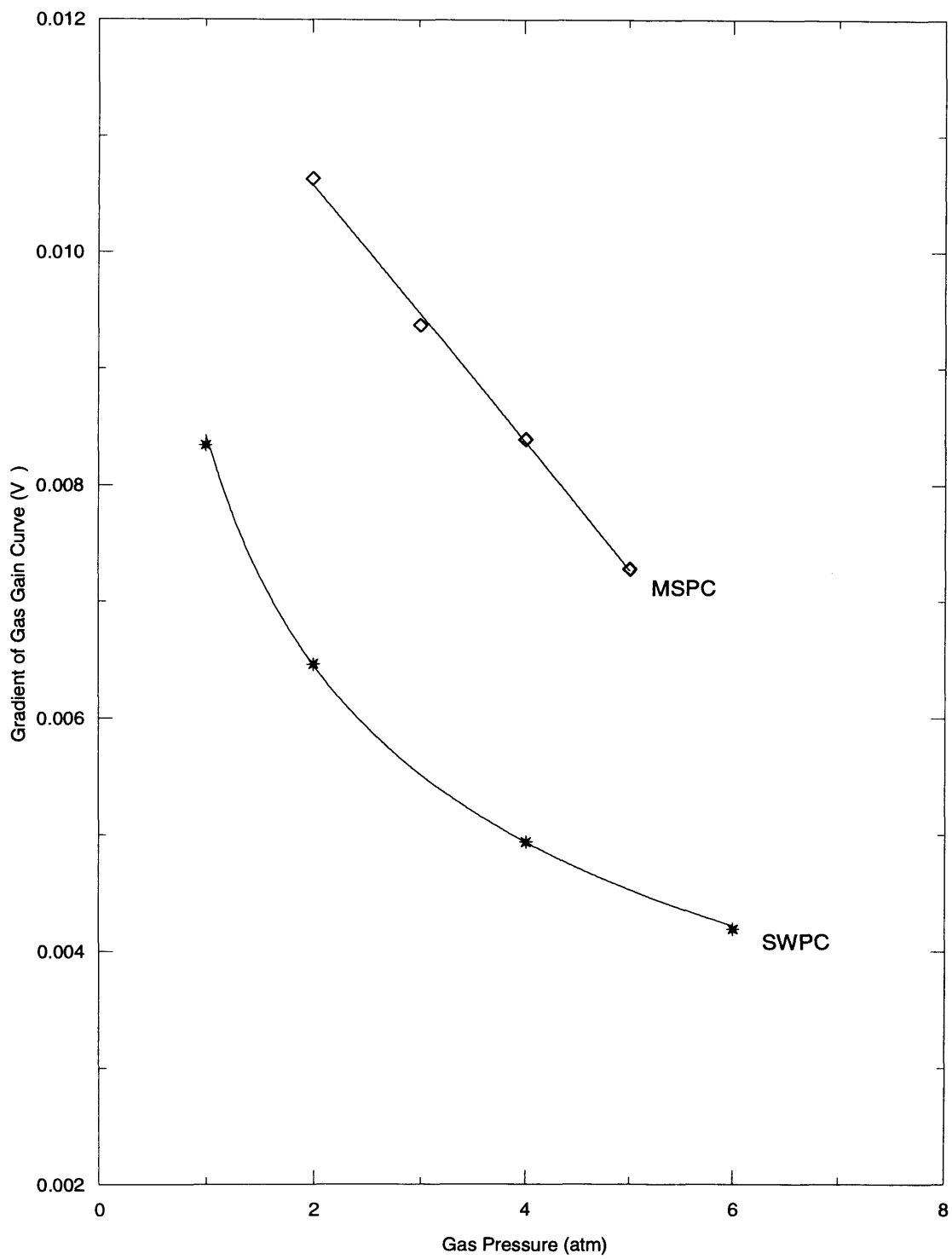


Figure 6.17: Variation of the gradient of the gas gain curves from data of Figure 5.7 and Figure 6.3.

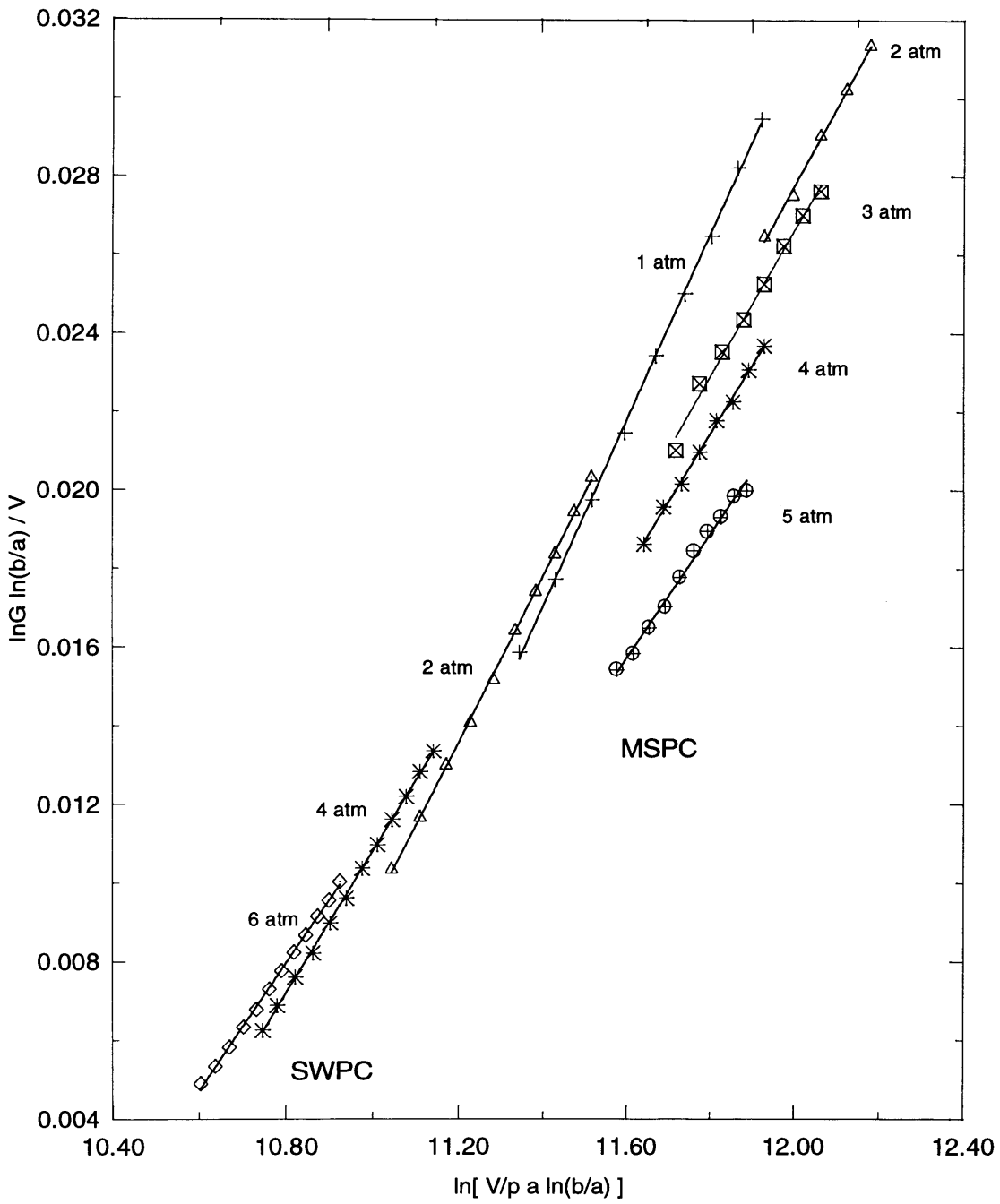


Figure 6.18: Diethorn plot for the MSPC and SWPC gas gains using Xe+5%CO₂ at different pressures.

Low operating voltage is one of the most important published features of MSPCs, and was confirmed by the performance of the MSPC studied in this work. We found in Chapter 5 that Xe+5%CO₂ mixture gives the lowest gain in comparison with the other mixtures. It was possible with the MSPC to have a high gain using this mixture with a low potential difference.

The required potential difference for a gas gain of $\sim 10^3$ in the SWPC was ~ 2250 V at 2 atm, whereas in the MSPC the same gas gain was obtained with only ~ 980 V. The same gain at 4 atm was obtained with ~ 3250 V in the SWPC and with ~ 1380 V in the MSPC. A comparison of the potential difference required to obtain a gas gain of ~ 200 for the SWPC and the MSPC is shown in Figure 6.19.

The results shown in Figure 6.19 indicate that the MSPC works much better than SWPC with Xe+5%CO₂ at high pressures, and it is expected to obtain much higher gas gain with lower operating voltages by using a Penning mixture.

6.3.2 The Diethorn Parameters

As shown above and in Chapter 5, the rate of change gas gain with the applied voltage is slower at higher pressure, *i.e.* at lower reduced electric field (E/p). That is, the ionisation efficiency decreases with increasing pressure.

Figure 6.20 shows that ΔV obtained for both the SWPC and MSPC has the same behaviour and almost the same value. This is consistent with the definition of this parameter which reveals that it is geometry independent.

It is already reported [Sakurai *et al.*, 1992; Tokarai *et al.*, 1994] that proportional counters with thinner anode wires operate at a stronger reduced electric (E/p) field than for thicker ones.

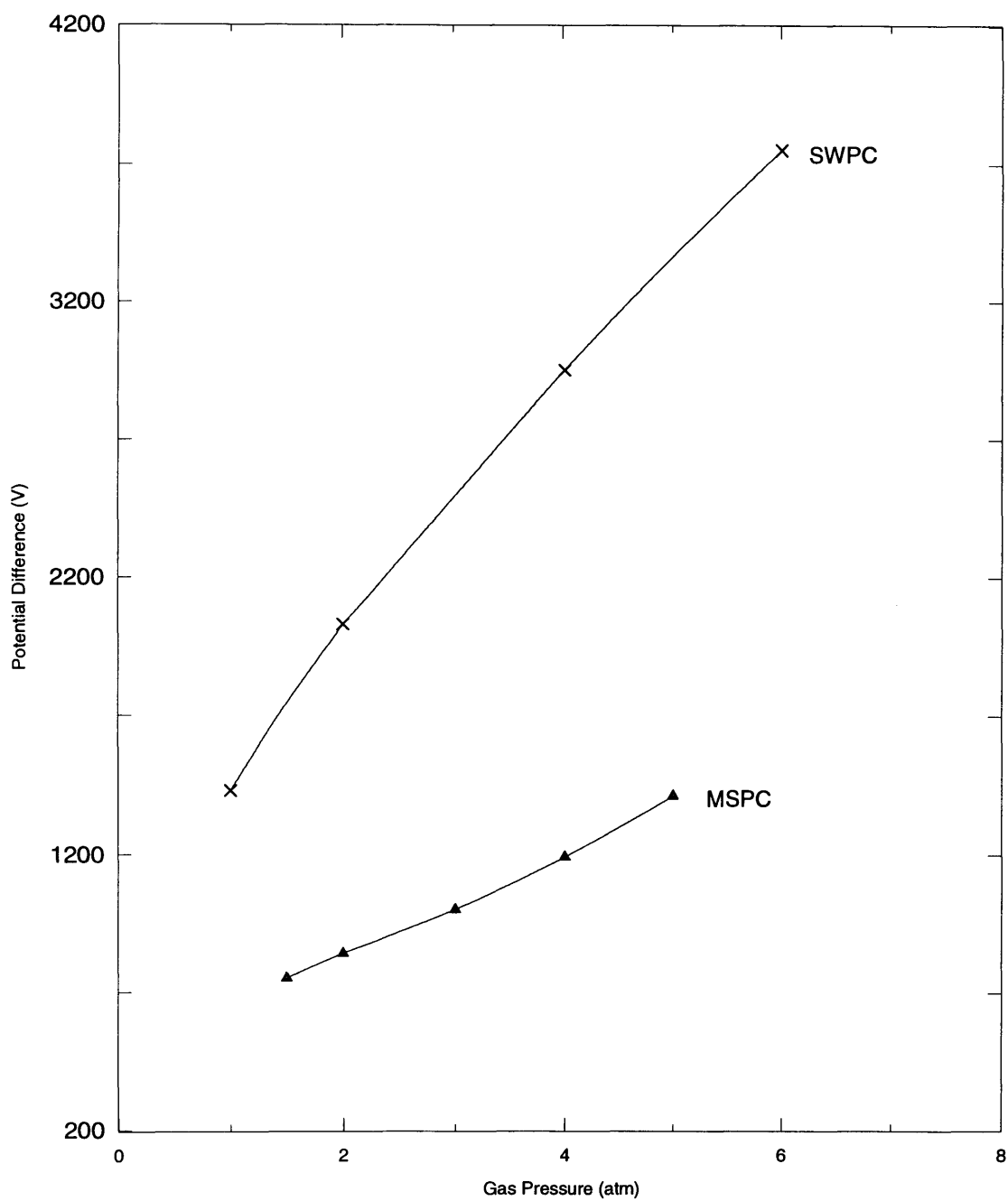


Figure 6.19: Pressure dependence of the voltage needed to obtain a gas gain of ~ 200 in the SWPC using Xe+5%CO₂.

At a constant pressure, K is expected to be larger for thinner anode diameters, and at a constant anode diameter, K is expected to be smaller for higher pressures.

As calculated in the previous section, electric field around the anode strip of the MSPC is about 5 times stronger than that of the SWPC. This, as mentioned above, explains the higher gas gain obtained for the MSPC which is due to operation at higher E/p which means higher α/p .

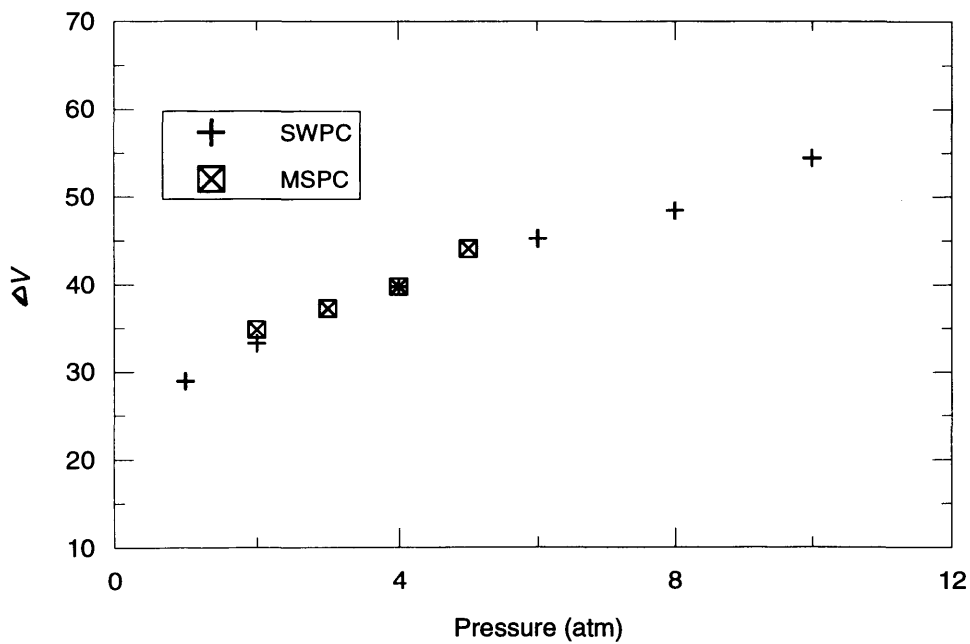


Figure 6.20: The variation of ΔV with pressure for the SWPC and MSPC.

Figure 6.21 shows the variation of the Diethorn gas parameter K with gas pressure for both of the counters. If the curves in the Diethorn plot shown in Figure 6.18 was extrapolated down to $\ln V/pa \ln(b/a) = 0$, as shown in Figure 6.22, we can find that both of the Diethorn parameters ΔV and K are similarly changing with pressure for both of the cases but with much slower rate for K in the case of the MSPC. That is, for thinner anode wires the dependence of K on pressure is lesser.

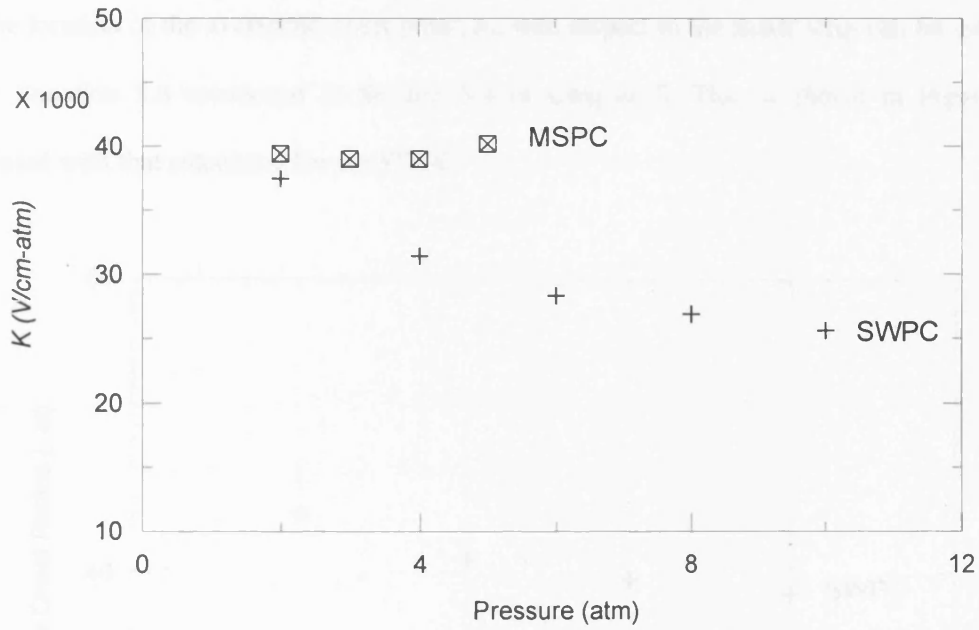


Figure 6.21: The variation of K with gas pressure for the SWPC and MSPC.

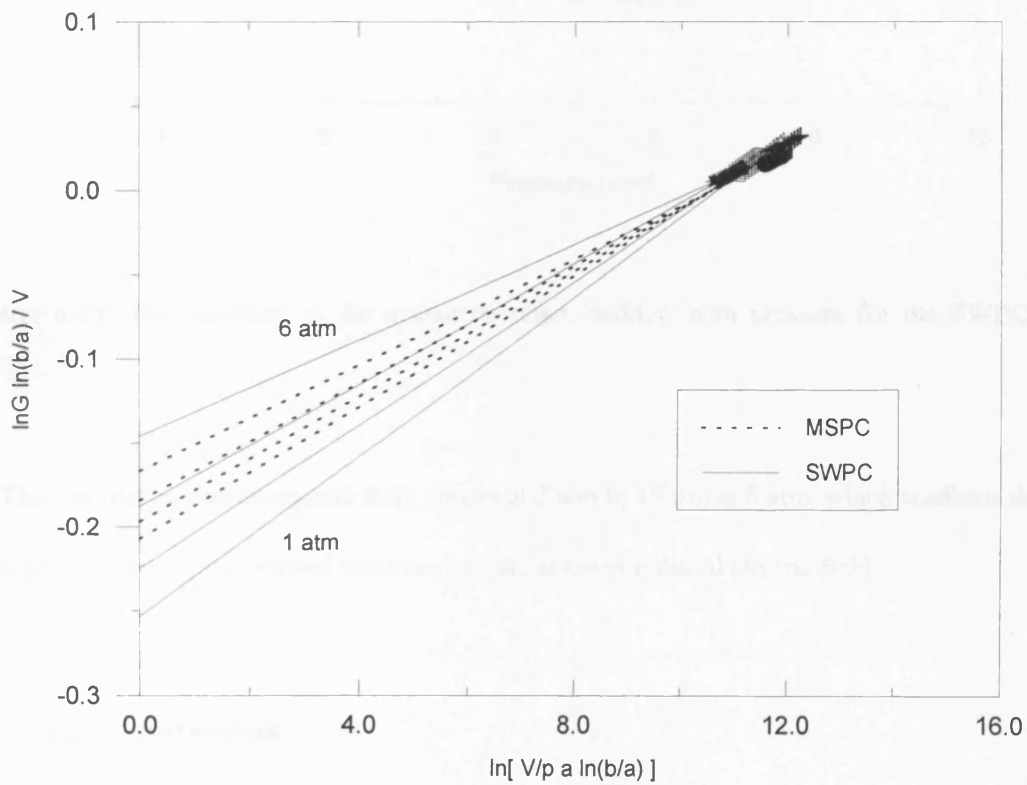


Figure 6.22: The Diethorn plot (Figure 6.18) showing the variation of the Diethorn gas parameters, ΔV and K with pressure.

The location of the avalanche onset point, r_0 , with respect to the anode strip can be estimated using Equation 5.8 mentioned in Section 5.4 of Chapter 5. This is shown in Figure 6.23 compared with that calculated for the SWPC.

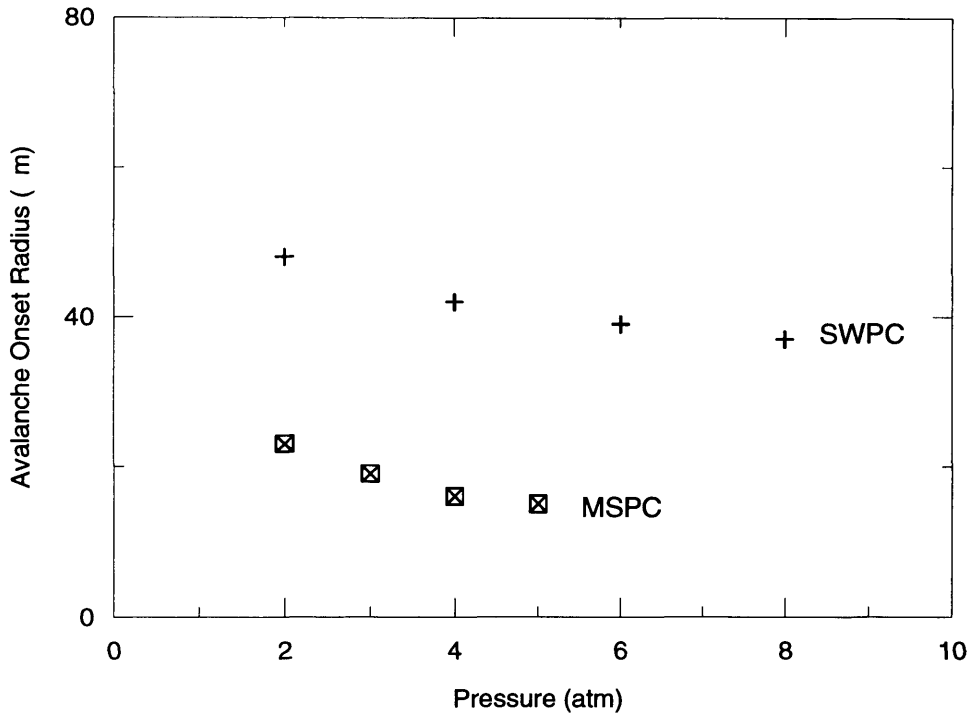


Figure 6.23: The variation of the avalanche onset “radius” with pressure for the SWPC and MSPC.

The “radius” r_0 was decreased from 23 μm at 2 atm to 15 μm at 5 atm, which confirms that at high gas pressures, proportional counters operate at lower reduced electric fields.

6.3.3 Signal Formation

Positive ions have to travel a distance of 0.6 cm to reach the cathode surface in the SWPC, whereas they need to travel only ~ 0.04 cm to be collected by the cathode strip in the MSPC. Thus, the small gap between anode and cathode in the MSPC permits a faster transit for the positive ions which in turn results in a fast signal compared to that of the SWPC.

The gas gain was measured for both counters using the pulse matching method (see Chapter 4) It was found in case of the MSPC that the pulse attenuation correction factor almost equals unity. Therefore, no correction was applied to the gas gain in case of the MSPC.

6.3.4 Breakdown Effect

The special structure of the MSPCs, discussed in Chapter 3, make it possible to operate them safely and reasonably even in the case of loss of most anode strips.

Breakdown in proportional counters is mainly caused by discharge which can be initiated by electrons ejected from the cathode and multiplied in the region of the high electric field near the anode. This will limit the maximum gas gain of the counter which is affected by many factors including the gas mixture in use and the size of the counter electrodes.

The breakdown which dramatically affected the SWPC performance took place with Xe+20%Ar at 10 atm pressure. The gas gain was $\geq 10^3$ whereas at 2 atm pressure gas gain of 2.6×10^3 was obtained safely with an energy resolution of 8.6%, which indicates an increase of breakdown probability at high pressures in the absence of quenching.

After the breakdown, the SWPC was tested at 10 atm and found to show gas gain variation from one point to the other along the length of the anode wire. This was tested by changing the position of ^{109}Cd source with respect to the entrance window. The energy resolution for ^{109}Cd X-rays was found to be ~22% near both ends of the wire and ~40% near its middle, compared to a value of 16% before the breakdown.

In the MSPC, breakdown events could take place in the region between the anode and cathode strips, particularly at the ends of the cathodes where the electric field is at its maximum.

Using a MS plate which was heavily used, with many damaged strips, an energy resolution of 12.5% at a gas gain of $> 10^3$, was measured for the Xe+5%CO₂ mixture at 2 atm in comparison with 11.9% at the same gain and pressure but with a good MS plate. As mentioned before, this is an advantage over the wire counters which has been confirmed here.

6.3.5 Energy Resolution

The variation of energy resolution with pressure for the MSPC compared with that of the SWPC is shown in Figure 6.24. The worsening of the energy resolution with pressure in both counters was discussed earlier.

As the results of the MSPC energy resolution were obtained at pressures up to 5 atm only, we can say formally that the energy resolution of the MSPC is worse than that of the SWPC at pressures of up to 5 atm. We note from Figure 6.24, however, that the energy resolution of the MSPC gets worse with increasing pressure faster than that of the SWPC. The behaviour of the energy resolution of the MSPC could be related to the existence of some impurities in the mixture where the counter becomes more sensitive to impurities at higher pressures. This is also may be due to the decrease of the ionisation efficiency relative to the excitation which becomes significant in Xe mixtures as discussed earlier in Chapter 5.

The influence of impurities becomes more significant if the drift region is relatively large, increasing the number of electron collisions before the charge cloud reaches the multiplication region. The number of collisions increases with pressure and results in a degradation in the counter resolution. The drift region in the MSPC is the distance from the entrance window to the electrode strips, which was 1.2 cm, compared with the cathode radius of the SWPC which was 0.6 cm.

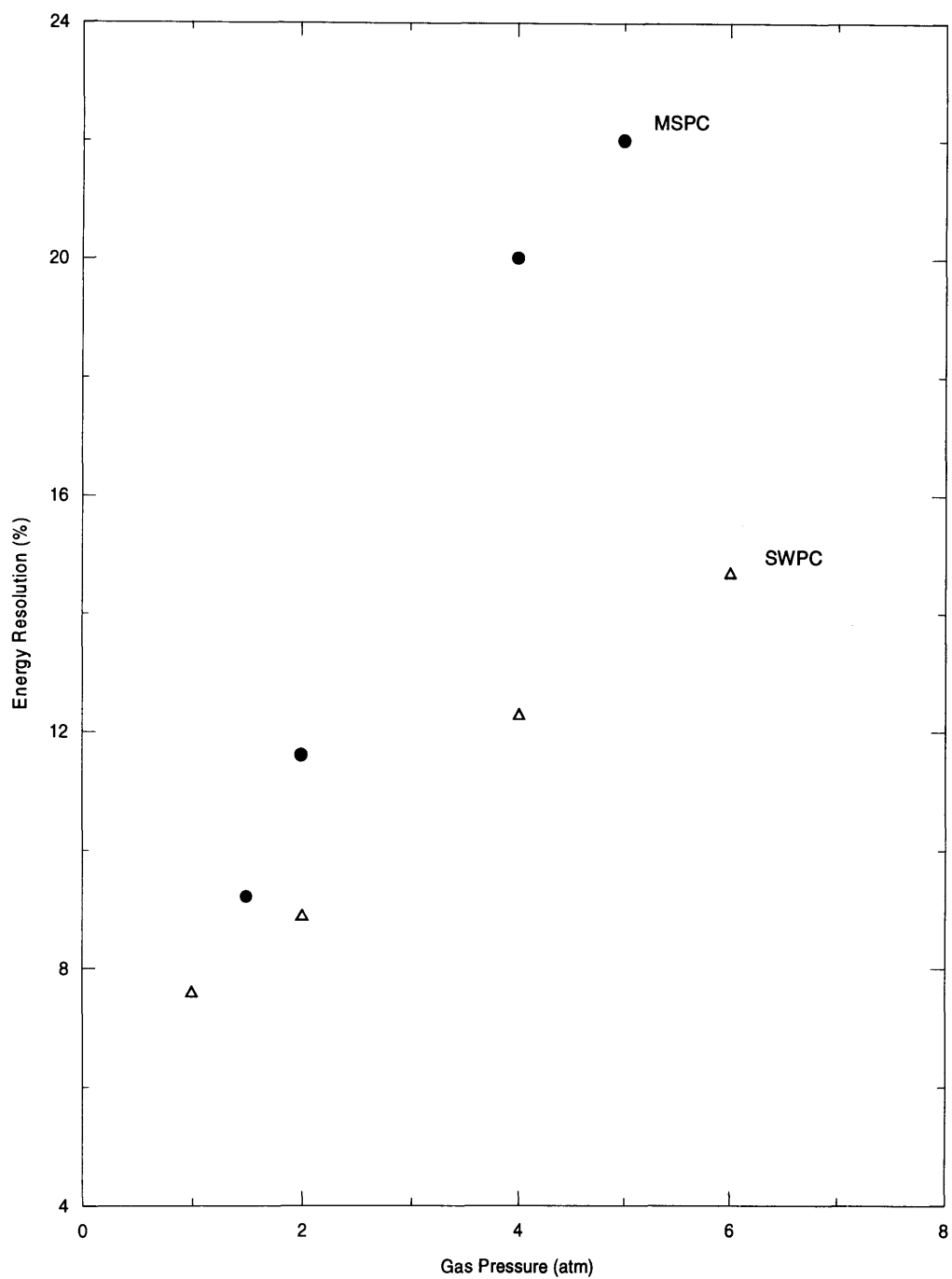


Figure 6.24: Comparison of the energy resolution of the SWPC and the MSPC for ^{109}Cd X-rays using $\text{Xe}+5\%\text{CO}_2$ at different pressures.

From the results of the MSPC we can find that at 1.5 atm the counter was able to distinguish between the ^{109}Cd lines as in the case of the SWPC, whereas at 5 atm the resolution was worse but the counter was found to have higher efficiency for the ^{241}Am X-rays (59.5 keV). This was checked by monitoring the count rate in each experiment.

Chapter 7

Thermal Neutron Imaging Using MCPs

7.1 Introduction

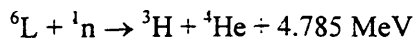
Some background about MCPs was given in Chapter 1. In this chapter, more details are given on MCPs' operational principles and on the work carried out on MCPs as thermal neutron imaging detectors. Two contrasting techniques are described; the first method involves direct neutron detection within a special channel plate structure containing lithium and/or boron. The second method involves the detection, using MCPs of standard glass composition, of the internal conversion electrons from a thin gadolinium foil.

MCPs are very widely used for the high resolution imaging of charged particles and energetic photons. Spatial resolution approaching the pitch ($\sim 12\text{-}15\ \mu\text{m}$) of the hexagonally packed microchannel array can be achieved over image areas of $10 \times 10\ \text{cm}^2$ [Murray & Chappel, 1985].

Thermal neutrons can be detected by MCPs via the "conversion" of neutrons to charged particles. One of these techniques is to incorporate ^6Li or ^{10}B in the MCP glass. That is to employ an (n, α) reaction, such those of Equations 1.2 and 1.3 of Chapter 1, to take place and to use the alpha particles to produce secondary electrons. Another technique, employed in the present work, is based on the use of gadolinium foil as a converter, as will be discussed below.

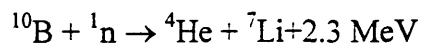
In a previous work [Fraser and Person, 1990], it was reported that it might be possible to adapt for thermal neutron imaging the MCP multiplier technology developed for imaging in X-

ray astronomy. These authors have considered, both theoretically and experimentally, the use of a MCP structure containing lithium. The charged products of the reaction:



have ranges in lead glass which are a few times the septal thickness of conventional microchannel plate structures. The triton and alpha particle ranges match to the MCP dimensions in a way that produces a high avalanche initiation probability without introducing large spatial uncertainty. For the lithium-containing MCP glass used by the authors, Li_2O was only a minor fraction (~ 1 mole %) and the estimated thermal neutron detection efficiency was low-only 0.21% in plates of thickness $L= 1.5$ mm. Nevertheless, it seemed possible that the production of lead glasses with much higher ${}^6\text{Li}$ concentrations might produce a thermal neutron detector combining useful efficiency and channel-pitch-limited spatial resolution.

In the same reference [Fraser and Person, 1990], the authors also proposed that borate glasses, utilising the reaction [Equation 1.3 in Chapter 1]:



should be considered in any future attempt to produce a neutron sensitive channel plate glass composition.

Section 7.2 of this chapter reports the results of a study carried out at Galileo Electron-Optics into the possibility of producing precisely a neutron sensitive MCP glass. The problem is not simple one, since essential multiplier properties such as high gain and stability must not be compromised by the introduction of the neutron sensitive elements. Furthermore, any neutron-sensitive MCP glass will have to closely resemble existing industry standards in terms

of its viscosity and softening point in order to be manufacturable using existing fibre drawing equipment.

The rest of the chapter describes the experimental study carried out at Leicester into an alternative pulse counting MCP-based detector, modelled on the film-based image intensifier of Chalmerton (1973), which uses gadolinium foil as the neutron converter. Measurements of detection efficiency, pulse height resolution and imaging properties the detector system are presented.

7.2 Operating Principles of MCPs

As mentioned in Chapter 1, an MCP is an array of $\sim 10^7$ packed miniature electron multipliers, fabricated from a slightly conductive glass which have common diameter. Each channel can be considered as an independent, continuous-dynode photomultiplier, as shown in Figure 7.1. The opposite faces of the plate are coated with a conducting film and serve as electrodes with which to apply a high voltage across the plate. As the glass is conductive it acts as a resistive potential divider and gives a uniform potential drop along the channels.

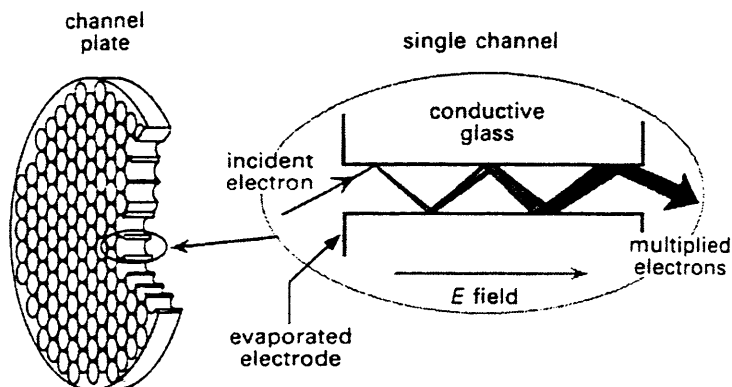


Figure 7.1: A microchannel plate electron multiplier [Gilmore, 1992]

Because MCPs only operate stably at pressures below $\sim 10^{-5}$ torr, measurement of the fundamental physical properties, gain, quantum detection efficiency, dark noise,..etc., can only be made in specialised test chambers constructed to ultra-high-vacuum standards [Fraser, 1989].

7.2.1 Gain Factor

Any charge which is produced in a channel is accelerated along it by the applied field between the two surfaces of the plate and will eventually strike the wall to emit further charge which is again accelerated along the channel. As the channels are very narrow, with a diameter which could be as small as 6 μm , the electrons will collide with the wall many times in their passage through the channel and can give a large multiplication, up to 10^4 .

The gain factor is the ratio of the output charge (final number of electrons) to the primary charge. The gain factor depends mainly on the voltage between the two surfaces of the MCP, the length-to-diameter ratio (L/D) of the channels, and the secondary emission coefficient of the wall material. The mechanism limiting MCP pulse gain in saturated operation is generally believed to be positive wall charging.

Zeroth-order calculations [Loty, 1971; Leonov, *et al.* 1980] based on the wall charge model predict a saturated gain dependence for a single MCP:

$$G \propto V_0 D (L/D)^{-1}$$

The following semi-empirical equation relates the peak gain G_C of a two-stage chevron detector (see next section) to the gains of its constituent front (F) and rear (R) plates [Fraser *et al.*, 1983]:

$$G_C = G_F^{1-r} G_R N_C \quad (7.1)$$

where N_C is the number of channels in the rear MCP illuminated by the charge cloud emerging from the front plate. Here, r is a parameter related to the channel diameter; r has the value 0.6 for plates with 12.5 μm diameter channels [Fraser *et al.*, 1983; Smith & Allington-Smith 1986] and the value 0.8 for 25 μm channels. An expression analogous to Equation 7.1 has been derived by Siegmund *et al.* (1985) to describe the operation of three-stage multipliers [Fraser, 1989].

7.2.2 MCP Chevron Configuration

The MCP is subject to breakdown produced by positive ion feedback when the gain is too high, as are proportional counters. When the gain exceeds $\sim 10^4$, positive ions released when the electrons strike the tube walls may eventually strike the photocathode, releasing more electrons.

This effect may be reduced by bending the channels or by using two MCPs in a chevron arrangement [Colson *et al.* 1973], as the one used in the present work (Figure 7.2 b). The channels in the two plates are at different angles, so that there is no longer a straight path for positive ions through the whole amplification section. The gap between the plates may be several tens or hundreds of micrometers. A gain of $>10^7$ is possible with such configurations [Wiza, 1979].

If an accelerating potential is applied between a two plates in chevron, there is less time for the charge cloud from the first plate to spread radially, and fewer channels in the second plate are excited. As a result the amplitude distribution of the signal becomes narrower [Medvedev,, 1994].

7.3 Incorporation of Neutron-Sensitive Elements Into MCP Lead Glass

Detection with such methods is based on utilising (n, α) reactions using ^6Li or ^{10}B . Both the (n, α) cross section and natural abundance of ^{10}B are higher than the corresponding figures for ^6Li (3837 b and 18.8%, compared to 940 b and 7.5%).

7.3.1 Lithium Incorporation in a MCP

Lithium is not commonly used in glass formulation at other than low levels. The most common reason for incorporation of lithium into MCP glass is its powerful fluxing abilities. Addition of small amount ($\sim 1\%$ by weight) can substantially reduce the high temperature viscosity of a glass. At high concentrations, the presence of lithium in silicate glasses leads to high rates of devitrification. The primary uses for high-lithium-content glasses are as glass-ceramics (e.g. Corningware [Fishwick, 1974]) and as laser hosts [Miniscalco, 1991].

In the later area, composition with up to 27 mole % Li_2O have been commercially produced. These glasses, however, are not of sufficient stability to be of interest for channel plate production. Glasses with a high lithium content also exhibit poor chemical durability, particularly when exposed to acids. A final problem is that the gain of any MCP multiplier for which lithium was the predominant alkali metal constituent would be expected to be low, because of the relatively high work function of the metal (2.5 eV, compared with 2.2 eV for potassium) for secondary electron emission.

7.3.2 Boron Incorporation into an MCP

The incorporation of boron, rather than lithium, into MCP glass would produce, weight for weight, a more efficient thermal neutron detector. Fortunately, the prospects for boron-based neutron sensitive MCPs are also rather brighter.

Boron oxide is a network former; pure glassy B_2O_3 is easy to prepare but is extremely hygroscopic. The incorporation of other oxides such as SiO_2 or Al_2O_3 leads to the formation of stable, durable glasses over a wide compositional range. In borosilicate glasses, up to 20 mole % boron oxide can readily be incorporated, particularly when alkali metals are added to reduce viscosity. Such borosilicate glasses (e.g. Pyrex) are not immediately useful for MCP manufacture because of their lack of reducible constituents.

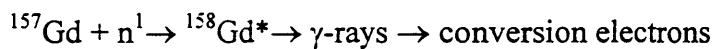
Ternary lead borosilicates and lead lithium borates have also been widely studied. Stable glasses with up to 35 mole% B_2O_3 [Bansal & Doremus, 1986] and as much as 90 mole% ($B_2O_3 + Li_2O$) [Sugira *et al.*, 1964; Bobkova, 1971] exist, with physical properties quite similar to those of conventional MCP glasses. The chemical durability of these glasses is not well-documented but may be expected to be far inferior to those of existing MCP formulations.

Quaternary alkali lead borosilicates are also stable over a significant range of boron oxide content but have been extensively studied. This compositional space is promising for the development of neutron-sensitive devices. It should be possible to fabricate reasonably durable, hydrogen reducible glasses containing multiple alkali metal ions where the sum of boron and lithium oxide fractions exceeds 25 mole%.

The thermal neutron detection efficiency of a 1 mm thick MCP containing 10 mole% of naturally-occurring B_2O_3 would be approximately 13%, assuming a standard MCP open area fraction of 63% and an effective atomic weight for the glass of 90.

7.4 Gadolinium Foil Method

Gadolinium foil was first suggested as a thermal neutron detection medium over fifty years ago [Amaldi *et al.*, 1939]. Since then it has been used in film contact radiography [Harms & McCormack, 1974] and as the neutron sensitive element in gas proportional chambers [Jeavons *et al.*, 1978; Director *et al.*, 1978]; with silicon surface barrier detectors [Feigl & Rauch, 1968] and PIN photodiodes [Aoyama *et al.*, 1992]; as an (n, γ) converter with mercuric iodide single crystals [Melamud *et al.*, 1983] and in the early MCP-intensifier experiments of Chalmerton [Chalmerton, 1973]. The reactions taking place in the case of natural gadolinium are [Crawford, 1992]:



Neutron capture by ^{155}Gd (14.73% of the naturally occurring metal) and ^{157}Gd (15.7%) results in the emission of gamma rays and internal conversion electrons from the excited states of ^{156}Gd and ^{158}Gd . The thermal neutron capture cross sections of ^{155}Gd and ^{157}Gd are 61,000b and 254,000 b respectively, leading to a value of 49,000 b for foils, such as those considered below, of the natural composition. The full complexity of the gadolinium emission spectra is described elsewhere [Groshev *et al.*, 1962].

The cross-section of Gadolinium for neutrons differs from the E^{1-2} capture cross-sections of ^{10}B and ^6Li , as it is based on a resonance at 0.031 eV. Technically, this means that Gd foils will be better in discriminating slow neutrons against a background of fast neutrons which can also be further improved if used with a suitable neutron moderator [Raouf, 1990].

The principal electron energies are summarised, for example, by Harms & McCormack (1974) and are reproduced here in Table 7.1. The total electron emission probability per

Table 7:1: Conversion electron emission probabilities P_e (electron/100 neutron) for natural gadolinium [Harms & McCormack, 1974]

	Energy (keV)	P_e
Contributions from ^{156}Gd	39	4.19
	81	4.97
	88	1.16
	149	0.84
	191	0.30
	246	0.02
Contributions from ^{158}Gd	29	9.82
	71	26.8
	78	6.17
	131	3.41
	173	1.46
	180	0.31
	228	0.40

neutron capture is high (59.9 %) and dominated by the emission at 29 and 71 keV, which together contribute some 60 % of the total electron flux from an irradiated natural Gd foil. According to Melamud *et al.* [Melamud *et al.*, 1983], the principle gamma ray lines are: 199.4, 897.0, 944.0, 961.8, 977.2, and 1186.5 keV, with emission probabilities, P_γ , equal to 0.095, 0.065, 0.105, 0.074, 0.041, and 0.108 respectively. The total gamma ray emission probability is therefore 0.488 per absorbed neutron.

A number of authors have used basic atomic data to compute a conversion efficiency-vs-foil thickness function, $F(T)$. According to Jeavons *et al* (1978), for a natural Gd foil operation in transmission, $F(T)$ has a maximum value 0.13 electrons/neutron for an optimum thickness $T= 5$

μm when irradiated by $2A$ (0.02 eV) neutrons. This optimum thickness is confirmed by the measurements of Feigl and Rauch (1968) and by the independent calculations of Chalmeton (1973) for 300K thermal neutrons. The work of Chalmeton (1973) predicts a maximum yield $F(T) = 0.16$ electrons/neutron. A 5 μm thick natural gadolinium foil absorbs 52% of any normally-incident thermal neutron flux.

Although 20 % of natural gadolinium is radioactive ^{152}Gd , with a half-life for alpha emission of 1.1×10^{14} years, the resultant background from a 5 μm thick foil is negligible in all practical applications. The estimated excess background from this source in the MCP/Gd experiments described in the following sections of this chapter is ~ 0.002 counts per second, a factor ~ 1000 below the MCP intrinsic background.

7.5 Detector Set-up

This work was carried out using one of the University of Leicester X-ray Astronomy group MCP facilities. The MCP/Gd neutron detector arrangement; the MCPs, vacuum chamber, and neutron source are schematically illustrated in Figure 7.2. The MCPs used are of standard glass composition, and were used in a chevron configuration. Some details of the MCPs are given in Table 7.2. The commercial 25 mm^2 Gd foil [supplied by Goodfellow Metals Ltd.] was of 5 μm thickness. It was placed at ~ 0.6 mm distance from the MCPs and was supported on a thick copper block. The electrical contact to the MCPs is via three gold-plated copper electrodes. The Gd foil and the MCPs are contained inside a high vacuum chamber with the neutron source mounted outside the vacuum chamber vertically above the MCP.

The resulting conversion electrons are incident on the first MCP with some divergence because of the space between the foil and the MCP. These electrons are received as an

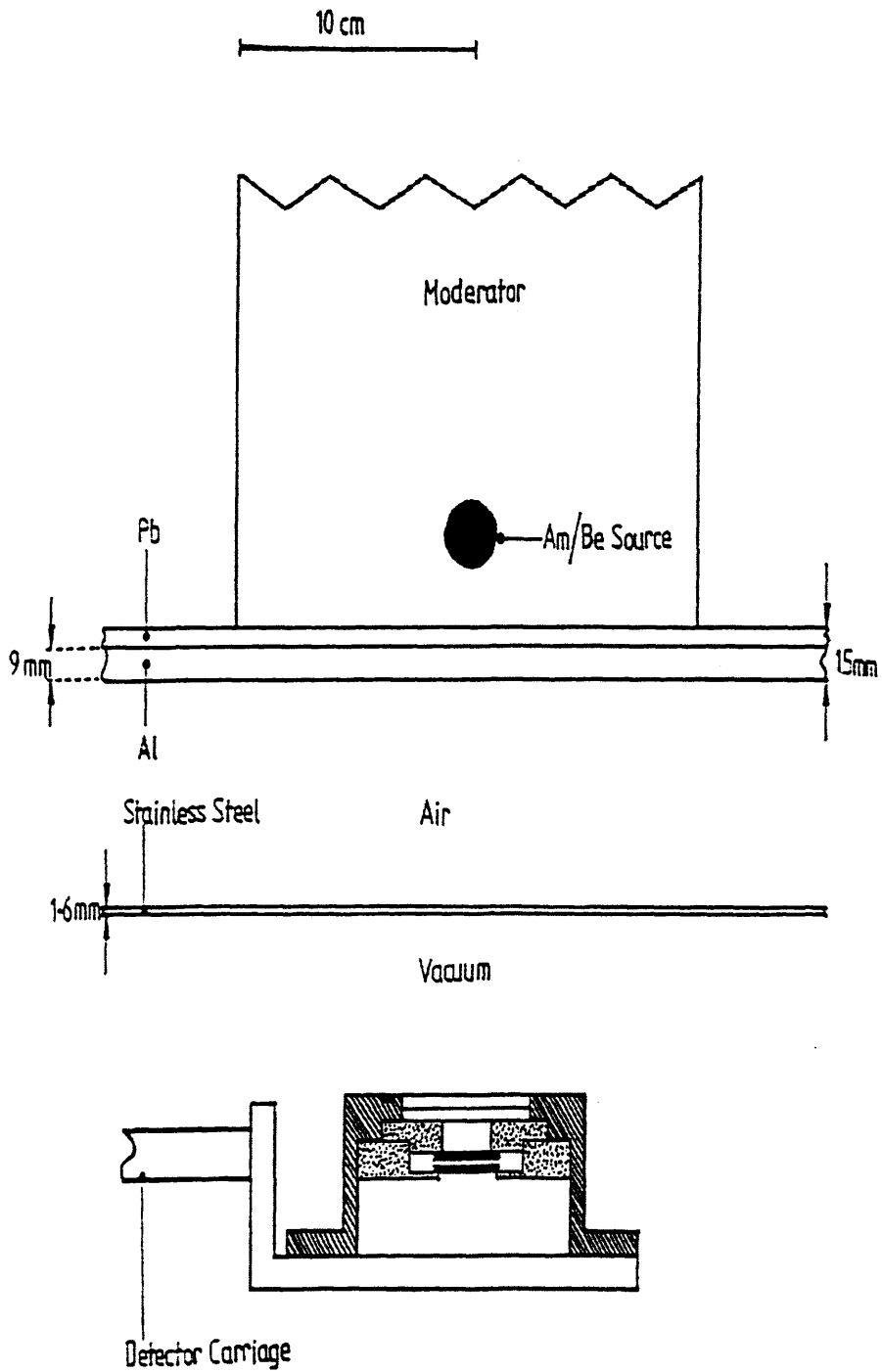


Figure 7.2: Experimental arrangement for neutron measurements showing the MCP, vacuum chamber, and neutron source.

avalanches on the readout element which is a graded density array from which the foil image is obtained using a suitable computer. Figure 7.3 shows a schematic cross section of the MCP/Gd assembly.

7.5.1 Gamma Ray Rejection

An ^{241}Am -Be neutron source of activity of 10.68 GBq in its paraffin wax moderator was mounted directly above the detector vacuum chamber on a 9 mm thick aluminium support plate. The air gap between the source and the 1.6 mm thick stainless steel wall of the detector vacuum chamber was 3.5 cm wide; the total separation of source and detector was 15.5 cm.

In order to suppress, or attenuate, the source gamma ray flux accompanied with neutrons, a 6 mm layer of lead sheet was placed between the neutron source and the MCP assembly. Another 1.2 mm layer of lead sheet was placed around the wax moderator to attenuate any gamma rays emitted horizontally, with a small gap being left to accommodate the neutron source pole.

The magnitude of the scattered neutron and gamma-ray fluxes which arise, under isotropic neutron irradiation, in the particular MCP detector body (mainly PCTFE plastic and stainless steel), stainless steel vacuum housing, and lead shield against environment gamma rays, were not amenable to priori estimation. It was recognised, however, that since the MCPs were

Table 7.2: lists details of the MCPs used in the present work.

Plate diameter	36 mm
Thickness	1 mm
Channel diameter	12.5 μm
Pitch	15 μm
Channel bias	13 degrees
Active area	30 mm

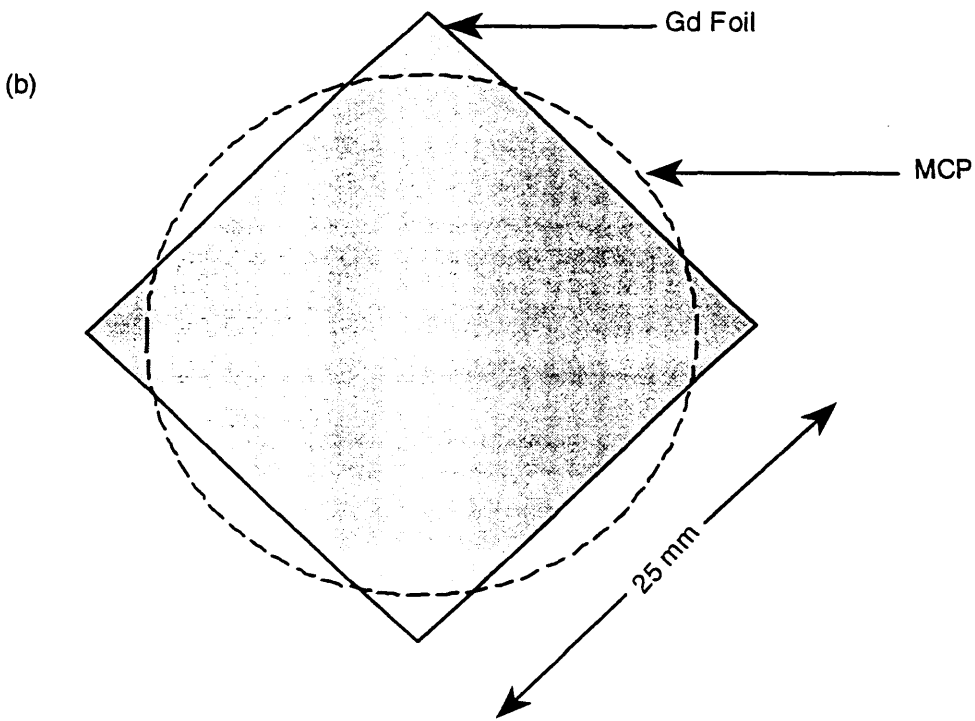
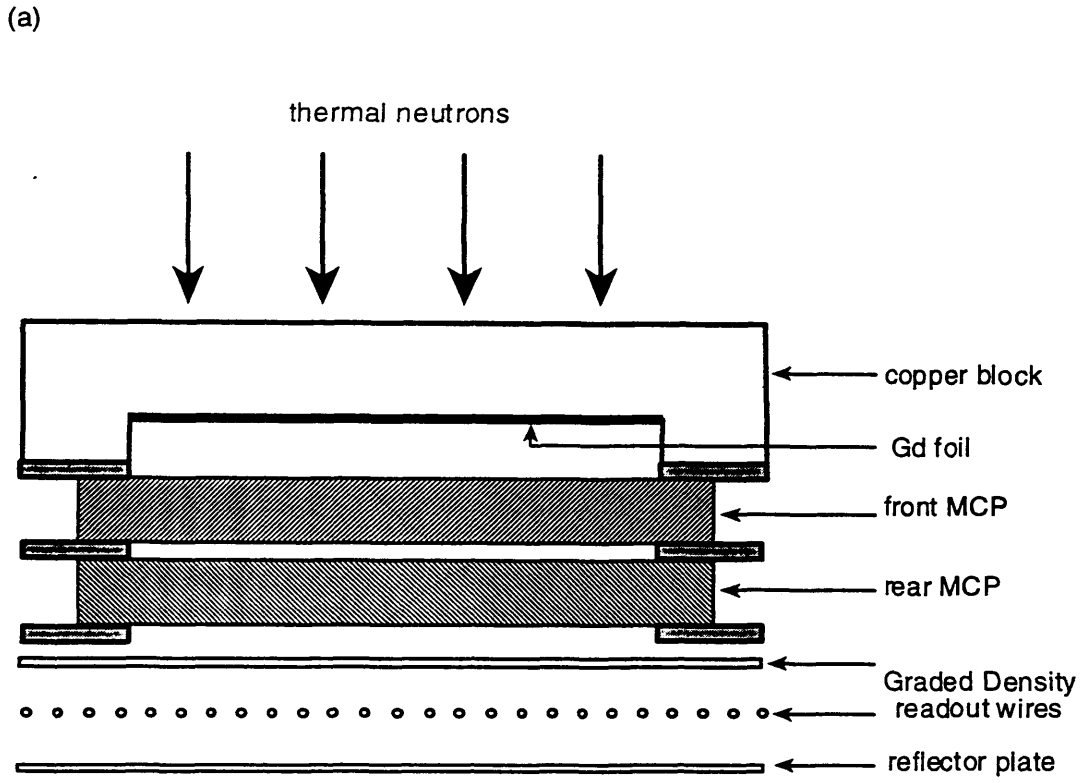


Figure 7.3: (a) Schematic cross section of MCP/Gd detector. (b) Extent of Gd foil.

crosssurrounded by a much greater mass of detector housing and vacuum chamber, a large background of (n, γ) events might be observed for all MCPs. Furthermore, the PCTFE plastic components of the detector body contains chlorine (as CF₃Cl), which has a large (n, γ) cross section [Fraser & Pearson, 1990].

7.5.2 Predicted Detection Efficiency

The thermal neutron detection efficiency, Q_n , of the MCP/Gd detector may be found by multiplying the foil conversion efficiency $F(T)$ by an MCP electron detection efficiency appropriately averaged first over the energies of Table 7.1 and second over the angular distribution with which the betas strike the input MCP of the two-stage “chevron” multiplier.

Using the 10-300 keV electron detection efficiency data of Babenkov *et al.* (1986) and assuming a $\cos\theta$ distribution of emission angles, we obtain an upper limit based on the Jeavons (1978) 2A yield of:

$$Q_n = 0.065 \text{ counts/incident neutron}$$

close to Chalmerton’s estimate (0.06), based on earlier, less complete MCP electron detection efficiency data.

The hard X-ray (energy $E_\nu > 100$ keV) quantum detection efficiency of microchannel plates has been measured by number of authors [Bateman, 1977; Dolan & Chang, 1977; Shilov *et al.*, 1987] to lie between one and two percent. Adopting the higher limit, we estimate the MCP gamma ray count rate resulting from neutron absorption in a 5 μm thick natural Gd foil to be 0.0025 counts/incident neutron, a factor of ~ 25 less than that the β -mediated rate Q_n .

Whereas neutron-induced gamma rays will be absorbed throughout the MCP bulk [Fraser & Pearson, 1990], internal conversion electrons may initiate avalanches in the channel plate

Whereas neutron-induced gamma rays will be absorbed throughout the MCP bulk [Fraser & Pearson, 1990], internal conversion electrons may initiate avalanches in the channel plate structure close to the positions of neutron absorption in the Gd foil. Using the formulae of Tabata *et al.* (1972), the ranges of 29, 71, and 173 keV electrons were estimated in a homogenous layer of MCP lead glass to be 3.8, 14.3, and 57 μm , respectively. Thus, for an ideal MCP/Gd detector system, with the foil in direct contact with the input MCP surface [Chalmeton, 1973], we would expect spatial resolution close to the ultimate channel-pitch-limited performance alluded to above in Section 7.1 and probably undistinguished from that of a direct detection system based on lithium and/or boron-containing glass. For the initial measurements described below, the gadolinium-MCP gap chosen conservatively to be 0.6 mm wide. The Gd foil was supported on a thick copper block, as shown in Figure 7.3 a.

7.6 Results and Discussion

Assuming source isotropy, and accounting for the neutron attenuation in the intervening aluminium, lead, stainless steel and copper layers, the estimated neutron flux at the gadolinium foil was $118 \text{ neutrons.cm}^{-2}.\text{s}^{-1}$. Measurements were made with the detector unattended over two separate ~ 65 hours periods, with 1300 V across each plate and with an electron-accelerating potential difference of 200 V across the 160 μm interplate gap.

Under irradiation, the measured MCP/Gd count rate was 80.6 s^{-1} . With the gadolinium foil removed, repeat measurements using a “dummy” copper block and the same MCP high voltage settings produced a “background” count rate, due to neutron interactions in the detector body, of 58.0 s^{-1} .

Correcting for the incomplete coverage of the detector active area by the Gd foil (Figure 7.3b), the count rate arising from interactions in the foil was then obtained to be $3.9 \text{ cm}^{-2}.\text{s}^{-1}$.

Experimentally, therefore, we estimate an intrinsic neutron-detection efficiency:

$$Q_n = 3.9 / 118 = 0.033 \text{ counts/incident neutron}$$

about a factor of two less than the predicted above.

Figure 7.4a compares the output pulse height spectra measured with and without the gadolinium foil. The accumulation time for both spectrums was 54,000 sec. The former spectrum is clearly peaked, as shown in Figure 7.4b. The peak obtained consists of pulses (due to Gd betas) originating at the input surface of the front MCP and developing through the full potential difference of the multiplier stack.

The spectrum also shows the presence of a “two-electron” peak at approximately twice the modal gain, arising from avalanches in two spatially-separated channels of the front MCP. Such a peaked pulse height distribution is clearly advantageous in discriminating against (n, γ) events originating in the massive detector body and surrounding vacuum chamber. As noted above, gamma ray interactions with MCPs take place throughout the plate bulk and so give rise to quasi-exponential pulse height distributions.

Figure 7.5 shows the image of the gadolinium foil obtained under neutron irradiation. As expected from Figure 7.3 b, the image takes the form of a “square with rounded corners”. The horizontal and vertical linear features in the image are artefacts caused by the differential non-linearity of the Graded Density readout element. Each x- and y-axis pixel corresponds to 74 microns in the detector plane. An upper-limit measure of the MCP/Gd spatial resolution was obtained by studying the count rate transition at the straight edges of this field. In principle [Fraser *et al.*, 1988], the (rms) detector resolution Δx can be estimated from the positions at which the count rate per pixel has fallen to 75 % and 50 % of the plateau value.

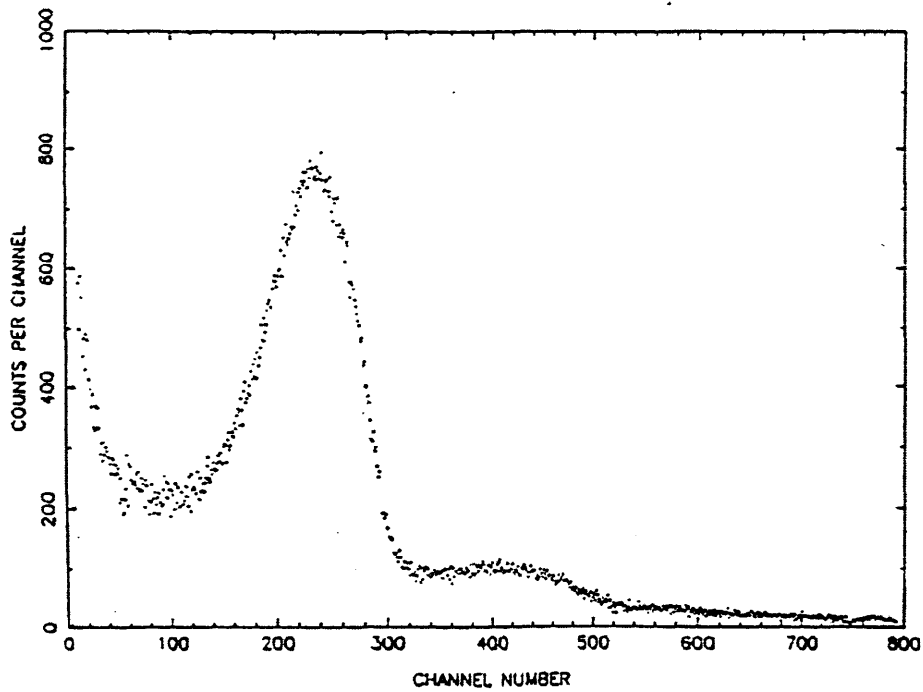
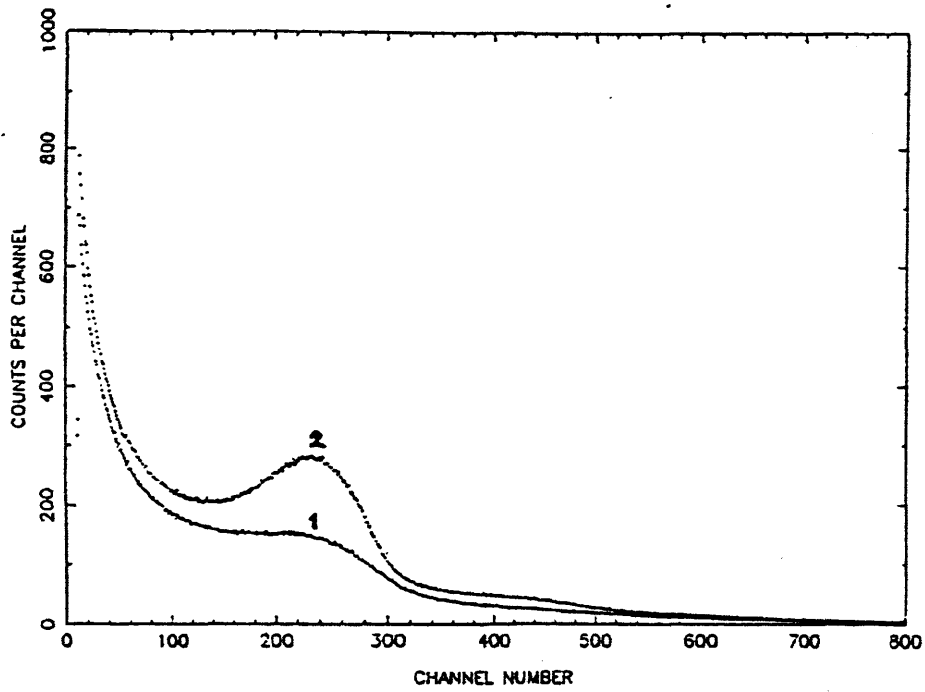


Figure 7.4: Detector pulse height distributions: (a)- represents the pulse height under irradiation, where spectrum 1 is the background (no Gd foil) and spectrum 2 is the Gd foil spectrum; (b)- represents pulse height spectrum of gadolinium beta events, obtained by subtracting spectrum 2 from 1 of figure (a).

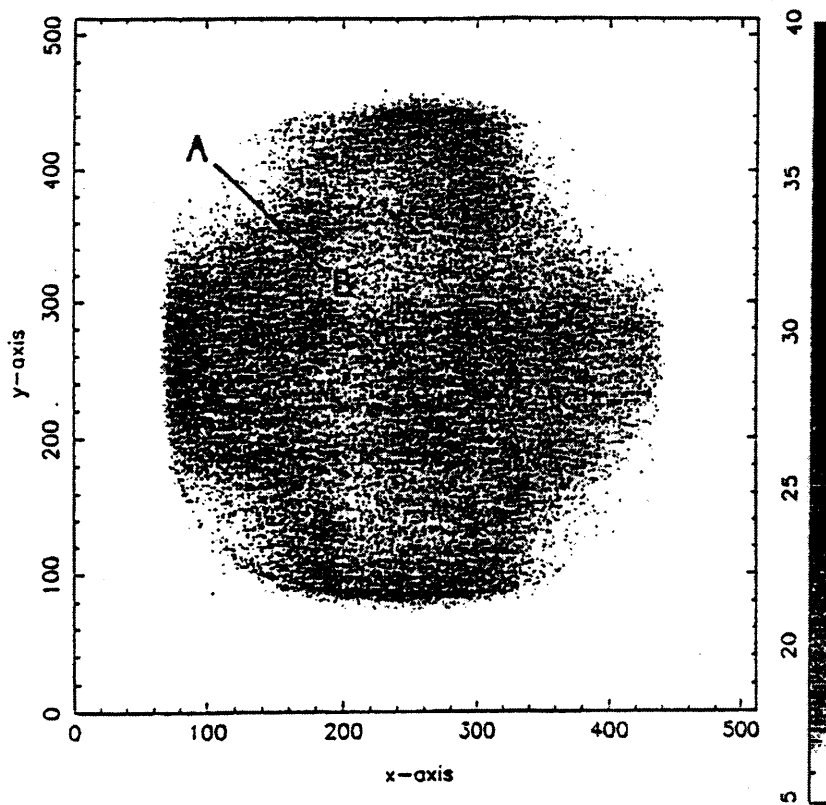


Figure 7.5: Image of Gd foil obtained under thermal neutron irradiation.

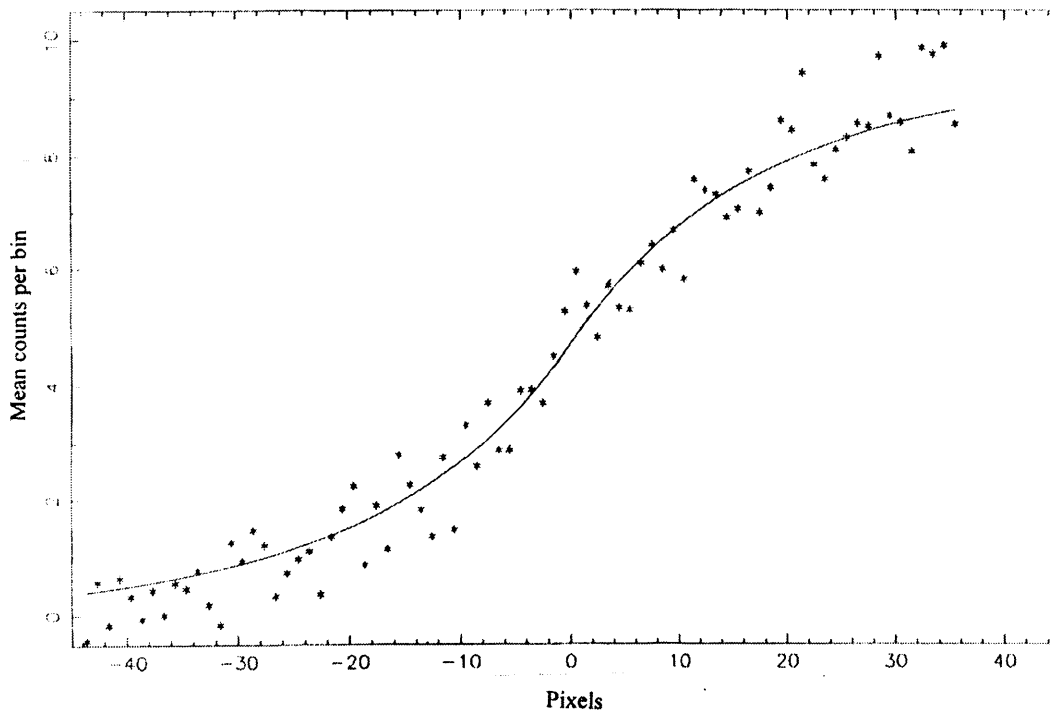


Figure 7.6: Cut across image of Figure 7.5 in the direction AB.

By best fitting to the data using the following exponential edge response function (ER) [Fraser, 1996] to the image slice AB in Figure 7.5:

$$ER = 0.5 \exp(\lambda x) \quad x < 0$$
$$= 1 - 0.5 \exp(-\lambda x) \quad x > 0,$$

the fwhm line spread function spatial resolution Δx derived from such a fit is simply:

$$\Delta x = 1.386 / \lambda$$

and:

$$\lambda = 0.057 / \text{pixels (by averaging over all the four cuts of the image in Figure 7.5)}$$

and with a 74 micron pixel size, we obtain an average spatial resolution:

$$\Delta x = 1.82 \text{ mm fwhm.}$$

We originally calculated this value to be 2.8 mm [Fraser *et al.*, 1992] and the difference between the two values was actually due to using a different methods for calculating the resolution, and we believe that the above method is the proper one.

This figure is likely to be a gross overestimate of the actual detector response, given : (i)- the isotropic nature of the irradiating source and (ii)- the fact that it was recovered from the extremities of the imaging area, where the electronic resolution of the Graded Density readout is poorest. The resolution obtained can be affected by many factors such as divergence of electrons, the isotropic neutron source, noise arising from the electronics: readout, preamplifiers, ..*etc.*

Chapter 8

Summary and Conclusions

This chapter gives an overall summary of the results obtained, which are presented in Chapters 5, 6, and 7. Conclusions regarding both parts of the thesis are given together with suggestions for future work.

8.1 An Overall Summary

8.1.1 *The High Pressure Xe Gas Counters*

(a) *The SWPC results*

Performance of a conventional SWPC was investigated at pressures up to 10 atm using several Xe-based mixtures: Xe+5%CO₂, as a reference mixture, Xe+5%C₄H₈, and Xe-Ar (with different Ar concentrations). The SWPC performance investigations were carried out in terms of gas gain and energy resolution.

The results, which were presented in the first part of Chapter 5, show that Xe-Ar Penning mixtures offer better performance than the other mixtures. Increasing concentration of argon showed an increase in the gas gain together with an improvement in the energy resolution.

Using the Diethorn equation [Diethorn, 1956], the predicted gas gain of the SWPC at different gas pressures was calculated and then compared with the measured gas gain. The Diethorn gas constants ΔV and K were obtained for the mixtures Xe+5%CO₂, Xe+5%C₄H₈, and Xe+20%Ar, by employing the attenuation-corrected measured gas gain in the Diethorn formula at pressures

up to 10 atm. The calculated gas constants were then compared with gains obtained using our constants which were also calculated for Xe+5%Isobutylene and Xe+20%Ar.

The SWPC was investigated at high pressures using the three mixtures. The Penning mixture Xe+20%Ar was found to exhibit the best performance although the maximum gain threshold was noticed to decrease with pressure. Energy resolutions for 22.2 keV photons obtained with this mixture at a gas gain of 200 and pressures of 2 and 10 atm, were 6.9% and 16%, respectively. The mixture Xe+5% C_4H_{10} was found to perform competitively well at pressures up to 6 atm but got worse in terms of energy resolutions at higher pressures. The energy resolution for this mixture varied from 8.5% at 2 atm to 55.9% at 10 atm.

(b) The MSPC results

The performance of a glass substrate MSPC was investigated using Xe+5%CO₂ at pressures up to 5 atm. The results, which are presented in Chapter 6, have confirmed some already known features of MSPCs, in addition to revealing some interesting properties connected with their operation at high pressures.

Gas gain variation with potential difference ($V_a - V_c$) was found to change with increasing gas pressure in a slower way than in the case of the SWPC.

Energy resolutions at 1.5 and 5 atm pressure and 200 gas gain were ~9 % and 22 % , respectively, and were found to be nearly stable for gas gains of up to $\sim 1.2 \times 10^3$, unlike those of the SWPC, where the energy resolutions, for example, at 2 atm pressure changed from 8.9 % at gas gain of 200 to ~12% at 10^3 .

An approximation was used to compare the measured gas gain of the MSPC with the predictions of the Diethorn equation. This was based on a rough estimation of the effective cathode radius of a MSPC, where Diethorn gas constants, obtained using the SWPC, with the

other known parameters of the MSPC were substituted into the Diethorn equation. This resulted in a value for an effective cathode radius of approximately the spacing between width centres of the anode and cathode strips.

8.1.2 Thermal Neutron Imaging with a MCP

The use of lead glass MCPs for the imaging of thermal neutrons was considered. Two contrasting techniques were described. The first method involves direct thermal neutron detection within a special channel plate structure containing lithium and/or boron. The constraints of the glass chemistry on the maximum neutron detection efficiency were reviewed.

The second method involves the detection, using MCPs of standard glass composition, of the internal conversion electrons from a thin gadolinium foil. The first measurements of the detection efficiency, pulse height resolution and imaging properties of pulse-counting MCP/Gd detection system were presented.

The experimental estimated intrinsic neutron detection efficiency was 0.033 counts/incident neutron, about a factor of 2 less than the predicted value. The average value obtained for the spatial resolution was 1.8 mm fwhm.

8.2 Conclusions and Suggestions for Future Work

This work is a new contribution, particularly in the field of high pressure Xe gas MSPCs and in the field of thermal neutron detection and imaging using MCPs. Results in this work are concerned with investigations of the most important characteristics which control the choice of a radiation detector such as detection efficiency, gas gain, energy resolution, and spatial resolution. Conclusions from the present work are summarised below:

8.2.1 Gas Counter Performance

- It was found that a SWPC filled with Xe-Ar mixtures provided some important advantages over Xe-CO₂- and Xe-C₄H₈-filled devices. These advantages include higher gas gain, better energy resolution and lower operating voltage
- At 2 atm gas pressure, the SWPC with Xe+5%CO₂ and Xe+5% C₄H₈ performed almost the same although a Xe+5% C₄H₈ mixture was found to offer slightly higher gas gains.
- A SWPC filled with Xe-Ar mixtures has the disadvantage of lower maximal attainable gains compared with Xe-CO₂ and Xe-C₄H₈ mixtures. The maximum attainable gain of the SWPC with Xe+20%Ar was found to decrease with increasing pressure.
- The Diethorn formula was experimentally tested and found to be invalid at high gas pressures up to 10 atm, when using Diethorn gas constants ΔV and K , derived at pressures of only 1-2 atm. In other words, the Diethorn gas “constants” were found to be pressure dependent.
- It was confirmed practically, that ΔV was not affected by the counter geometry since it had the same value in both cases (the SWPC and MSPC) for the same gas mixture. On the other hand, K was confirmed to be geometry dependent.
- The Penning mixture Xe+5%C₄H₈ was found to exhibit worse behaviour at high pressures (above 4 atm) compared to Xe-CO₂ and Xe-Ar mixtures.
- The energy resolution dependence on anode wire uniformity of the SWPC was found to increase with increasing gas pressure. This probably was due to the decrease of the avalanche size compared with the anode wire diameter.
- MSPCs can be operated at high pressures, at least up to 5 atm with Xe+5%CO₂, and exhibit stable gas gains and reasonable energy resolutions, regardless of the short term gas gain variations.

- The MSPC was found to operate at voltages of at least a factor of 2 lower than those of the SWPC.
- The results obtained for the MSPC with Xe+5%CO₂ mixture confirmed that MSPCs can be an attractive alternative to the MWPC, in particular because of their high rate capability which can be expected as a result of its much lower space charge effect. This can be deduced from the stable energy resolution obtained at a wide range of gas gains.
- As a result of the fine structure of the MSPC, *i.e.* the very small anode width and anode-cathode spacing, the gas gain and energy resolution of the MSPC were expected to improve compared to that of the SWPC. As expected, the gas gain was remarkably improved but not the energy resolution.
- The energy resolution of the MSPC was expected to be better than that of the SWPC. It was found that energy resolution at ~ 1 atm for both counters was almost the same. At higher pressures, the energy resolution of the MSPC was found to be worse. Furthermore, as the pressure was increased, the energy resolution of the MSPC degraded faster. The main suspect factors causing this unexpected behaviour of the MSPC are the purity level of the gas mixture together with the relatively long drift region.

For future work on SWPC and MSPCs we would recommend the following:

- (a)- An improvement in counter construction and filling procedures has to be made to avoid outgassing and gas contamination, which become more significant in pressurised sealed counters.
- (b)- Further study on Xe-C₄H₈ and Xe-CO₂ mixtures at high pressures seems to be necessary using lower concentrations of C₄H₈ and CO₂.
- (c)- The angular dependence of a MSPC performance will be necessary for future X-ray imaging work.

- (d)- The drift distance in the MSPC used in the present work was quite long (1.2 cm), and should be decreased to a minimum value to improve the counter energy resolution.
- (e)- Although proportional counters have the advantage of large signal-to-noise ratio, it is sometimes necessary to study the counter performance at very low gas gains, which will encounter the existence of relatively high levels of electronic noise. Thus, the use of lower noise electronics will be very useful.
- (f)- More studies on gas physics seem to be necessary to further understand and explain the different processes which affect the behaviour of high pressurised gas counters.
- (g)- If the maximum attainable gas gain is to be increased in SWPCs and also in MSPCs, then testing further Xe-based mixtures is advisable.

8.2.2 Thermal Neutron Imaging

- It was shown that a simple combination of a low-cost commercial gadolinium foil with standard microchannel plates produces a pulse-counting thermal neutron detector with useful efficiency, inbuilt discrimination against gamma ray background and (potentially) very high spatial resolution.
- The direct detection method proposed in the work of Fraser & Pearson (1990) and studied further in Section 7.3 of Chapter 7, may yield much higher neutron detection efficiency and still higher spatial resolution, but requires capital investment to produce a viable neutron-sensitive MCP glass. Recently, a low cost thermal neutron detector using individual multipliers constructed from new B-glass is being tested at University of Leicester, UK [Pearson, 1997] and at National Institute of Standards and Technology (NIST), USA [Feller, 1997]. The detector was constructed by Nova Scientific Inc.

- Irrespective of detection mechanism, a careful study of MCP detector construction is required in order to minimise (n, γ) background rates.

As mentioned in Section 7.6 of Chapter 7, the spatial resolution obtained was likely to be a gross overestimate of the actual detector response, given that the isotropic nature of the irradiating source and the fact that it was recovered from the extremities of the imaging area, where the electronic resolution of the Graded Density readout is poorest.

We would, therefore, recommend for future work that a parallel input neutron beam is used, and to place the Gd foil in contact with the input MCP. More important, the readout performance has to be improved.

Appendix

A.1 Calculation of the Attenuation Correction Factor

The attenuation correction factor was calculated by assuming that the pulse response of the preamplifier is ideal, and that the attenuation of the pulse is due to the shaping amplifier only. The equation derived below was used to calculate the correction factor required to evaluate the actual gas gain in the SWPC. No correction was applied to the measured gas gain in the case of the MSPC.

The shaping amplifier employed for measurements with the SWPC consisted of one integrator and two differentiators using a unipolar shaping with 4 μ s time constant. The response of such a shaping system to a step function of unit height has already been evaluated by Fraser (1980) to be a pulse of 0.271 height.

As mentioned in Section 4.5.1 of Chapter 4, the anode pulse of a cylindrical proportional counter may be expressed as a function of time, t , by (Equation 4.5):

$$q(t) = q_0 C_1 \ln\left(1 + \frac{t}{t_0}\right) \quad \text{A.1}$$

where q_0 is the initial charge,

$$t_0 = a^2 / (4 C_1 V_a \mu^+),$$

$$C_1 = 1/2 \ln(b/a),$$

a and b are the anode and cathode radii, V_a is the anode voltage, and μ^+ is the mobility of the positive ions.

Using Laplace transform, the response of the preamplifier to a current pulse can be written as $1/S.C_f$, where C_f is the feedback capacitance. Therefore, the input voltage pulse to the main shaping amplifier will be, in the Laplace transform domain,:

$$V_0(S) = i(S) / S \cdot C_f \quad \text{A.2}$$

Differentiating Equation A.1 will result current $i(t)$:

$$i(t) = q_0 C_1 / (t + t_0)$$

and in Laplace transform domain [Abramowitz & Stegun, 1970]:

$$i(S) = q_0 C_1 \cdot \exp(S t_0) \cdot E_1(S t_0) \quad \text{A.3}$$

Substituting for $i(S)$ into Equation A.2 gives:

$$V_0(S) = (q_0 C_1 / S \cdot C_f) \exp(S t_0) \cdot E_1(S t_0) \quad \text{A.4}$$

The output pulse of the shaping amplifier is given by multiplication of the input pulse by the amplifier transfer function. Therefore, the output pulse of the amplifier is given by:

$$V(S) = V_0(S) \cdot H(S) \quad \text{A.5}$$

where $H(S)$ is the transfer function in the Laplace domain.

The transfer function of a shaping filter with n differentiation and m integration, has been shown by Fraser (1980) to be:

$$H(S) = \frac{S^n \omega_0^m}{(S + \omega_0)^{n+m}} \quad \text{A.6}$$

where $\omega_0 = 1/T_a$ and T_a is the time constant.

For the present work, therefore, $V(S)$ will be given by Equation A.5 as:

$$V(S) = \frac{q_0 C_1}{C_f} \exp(S t_0) \cdot E_1(S t_0) \cdot \frac{\omega_0^2}{(S + \omega_0)^3} \quad \text{A.7}$$

The inverse of Laplace transform of the above equation, utilising the convolution integral is given by:

$$V(t) = \frac{q_0 C_1 \omega_0^2}{C_f} \int_0^t \left(\frac{1}{\tau + t_0} \right) \frac{(t - \tau)^2}{2!} \exp[-\omega_0(t - \tau)] d\tau \quad \text{A.8}$$

This equation was solved numerically using a computer, and the input data needed for SWPC are the anode voltage, time constant, positive ion mobility, and anode and cathode radii. The positive ion mobility, which indicates the dependence of Equation A.8 on pressure, was assumed to be constant (see Chapter 5). The correction factor was calculated using two estimated values for the mobility: 0.4 and 0.6.

The pulse attenuation correction factors calculated for each voltage are listed in Tables A.1 and A.2.

Table A.1: The correction factor calculated for different anode voltages using Equation A.8 at 4 μ s time constant and $\mu^+ = 0.4$.

Anode Voltage (V)	Correction Factor	Anode Voltage (V)	Correction Factor
1010	2.179	3300	1.786
1100	2.142	3400	1.778
1200	2.109	3500	1.77
1300	2.079	3600	1.763
1400	2.053	3700	1.755
1500	2.029	3800	1.748
1600	2.008	3900	1.741
1700	1.986	4000	1.735
1800	1.967	4100	1.729
1900	1.95	4200	1.723
2000	1.933	4300	1.717
2100	1.918	4400	1.711
2200	1.904	4450	1.708
2300	1.89	4500	1.705
2400	1.877	4600	1.699
2500	1.865	4700	1.694
2600	1.853	4800	1.689
2700	1.842	4900	1.684
2800	1.832	5000	1.679
2900	1.822	5100	1.675
3000	1.812	5200	1.67
3100	1.803	5300	1.665
3200	1.795		

Table A.2: The correction factor calculated using Equation A.8 for different anode voltages at 4 μ s time constant and $\mu_+ = 0.6$.

Anode Voltage (V)	Correction Factor	Anode Voltage (V)	Correction Factor
1000	2.029	2900	1.714
1100	1.996	3000	1.705
1200	1.967	3100	1.697
1300	1.942	3200	1.689
1400	1.918	3300	1.682
1500	1.897	3400	1.674
1600	1.877	3500	1.668
1700	1.859	3600	1.661
1800	1.842	3700	1.655
1900	1.827	3800	1.648
2000	1.812	3900	1.642
2100	1.799	4000	1.636
2200	1.786	4100	1.631
2300	1.774	4200	1.625
2400	1.763	4300	1.62
2500	1.752	4400	1.615
2600	1.741	4500	1.610
2700	1.732	4600	1.605
2800	1.723		

References

- Abramowitz, M. and Stegun, A. “*Hand Book of Mathematical Functions*”, Dover Publications, Inc., (1970).
- Agrawal, P. C. and Ramsey, B. D., *Proc. of Nuclear Science Symposium*, Orlando, Florida, USA, 1988.
- Agrawal, P.C., Ramsey, B.D., and Weisskopf, M.C. *Nucl. Instr. Meth.* **A277** (1989) 557.
- Akande, W. *Rev. Sci. Instr.* **63**, No. 10 (1992) 4354.
- Alkhazov, G.D. *Nucl. Instr. Meth.* **89** (1970) 155.
- Allkofer, O.C. “*Spark Chambers*”, Thiernig Verlag, Munchen (1969).
- Alunni, L., Bouclier, R., Fara, G., Garabatos, Ch., Manzin, G., Million, G., Ropelewski, L., Sauli, F., Shekhtman, L.I., Daubie, E., Pingot, O., Pestov, Yu. N., Busso, L., and Costa, S. *Nucl. Instr. Meth.* **A348** (1994) 344.
- Amaldi, F. and Rasetti, F. *Ricerca Sci.* **10** (1939) 115.
- Angelini, F., Bellazzini, R., Berz, A., Massai, M.M., Raffo, R., Spandre, G., and Spezziga, M.A. *Nucl. Instr. Meth.* **A335** (1993 a) 69.
- Angelini, F., Bellazzini, R., Berz, A., Massai, M.M., Spandre, G., Torquati, M.R., Bouclier, R., Gauden, J., and Sauli, F. *IEEE Trans. Nucl. Sci.* **37**, No. 2 (1990) 112.
- Angelini, F., Bellazzini, R., Bosisio, L., Brez, A., Massai, M.M., Perret, A., Spandre, G., and Torquati, M.R. *Nucl. Instr. Meth.* **A323** (1992 a) 229.
- Angelini, F., Bellazzini, R., Bosisio, L., Brez, A., Massai, M.M., Spandre, G., and Torquati, M.R. *Nucl. Instr. Meth.* **A314** (1992 b) 450.
- Angelini, F., Bellazzini, R., Brez, A., Mossai, M.M., Spandre, G., Torquati, M.R., and Shekhtman, L. *Physica Medica* **IX**, No. 2-3 (1993 b) 59.

- Aoyama, T. *Nucl. Instr. Meth.* **A234** (1985) 125.
- Aoyama, T., Oka, Y., Honda, K., and Mori, C. *Nucl. Instr. Meth.* **A314** (1992) 590.
- Asam, A.R. *Opt. Eng.* **17** (1978) 640.
- Aschenbach, B., Brauninger, H., Briel, U., Brinkmann, W., Fink, H., Heinecke, N., Hippmann, H., Kettenring, G., Metzner, G., Ondrusch, A., Pfeffermann, E., Predehl, P., Reger, G., Stephan, K.H., Trumper, J., and Zimmermann, H.U. *Space Science Rev.* **30**, No. 1-4 (1981) 569.
- Babankov, M.I., Zhadanov, V.S., and Starodubov, S.A. *Nucl. Instr. Meth.* **A252** (1986) 83.
- Bansal, N. and Doremus, R. “*Handbook of Glass Properties*”, Academic Press (1986).
- Barasch, E.F., Bowcock, T.J.V., Demroff, H.P., Elliott, S.M., Howe, M.R., Lee, B., Mazumdar, T.K., McIntyre, P.M., Pang, Y., Smith, D.D., Wahl, J., Wu, Y., and Yue, W.K. *Nucl. Instr. Meth.* **A315** (1992) 170.
- Bateman, J.E. and Connolly, J.F. *Rutherford Appleton Laboratory report RAL-93-090* (1993a).
- Bateman, J.E. and Connolly, J.F. *Rutherford Appleton Laboratory report RAL-93-096* (1993b).
- Bateman, J.E. *Nucl. Instr. Meth.* **144** (1977) 537.
- Bateman, J.E., Waters, M.W., and Jones, R.E. *Rutherford Lab Report RL-75-140* (1975).
- Bellazzini, R. and Spezziga, M.A. *della Societa Italiana di Fisica* (1994).
- Berger, M.j. and Seltzer, S.M. “*Tables of Energy Loses and Ranges of Electrons and Positrons*”, *NASA SP-3012* (1964).
- Bhattacharya, A.K. *Phys. Rev.* **A13** (1976) 1219.
- Biagi, S.F. and Jones, T.J. *Nucl. Instr. Meth.* **A361**, No.1-2 (1995) 72.
- Biagi, S.F., Bordas, J., Duxbury, D., Gabathuler, E., Jones, T.J., Kiourkos, S. *Nucl. Instr. Meth.* **366** (1995) 76.

- Bishai, M.R., Gerndt, E.K.E., Shipsey, I.P.J., Wang, P.N., Bagulya, A.V., Grishin, V.M., Negodaev, M.A., and Geltenbort, P. *Nucl. Instr. Meth.* **A365** (1995) 54.
- Blum, W. and Rolandi, L. “*Particle Detection with Drift Chambers*”, Springer-Verlag, (1994).
- Bobkova, N. *Stekloobrasynye Sistemy: Novye Stekla na ikh Osnove* (1971) 95.
- Borkowski, C.J. and Kopp, M.K. *Rev. Sci. Instr.* **39** (1968) 1515.
- Bouclier, R., Capeans, M., Garabatos, C., Manzin, G., Million, G., Ropelewski, L., Sauli, F., Temmel, T., Shekhtman, L., Nagaslaev, V., Pestov, Yu., and Kuleshov, A. *Nucl. Instr. Meth.* **A365** (1995) 65.
- Bouclier, R., Charpak, G., Domcovski, Z., Sauli, F., Coignet, G., and Flugge, G. *Nucl. Instr. Meth.* **88** (1970) 149.
- Bouclier, R., Florent, J.J., Gaudaen, J., Million, G., Ropelewski, L., and Sauli, F. *IEEE Trans. Nucl. Sci.* **39**, No. 4 (1992) 650.
- Bouclier, R., Garabatos, C., Manzin, G., Sauli, F., Shekhtman, L., and Temmel, T., Della Mea, G., Maggioni, G., Rigato, V., Logachenko, I. *IEEE Trans. Nucl. Sci.* **41**, No. 4 (1994) 821.
- Breskin, A., Charpak, G., Demierre, C., Majewski, S., Policarpo, A., Sauli, F., and Santiard, J.C. *Nucl. Instr. Meth.* **143** (1977) 29.
- Breskin, A., Charpak, G., Majewski, S., Melchart, G., Peterson, G., and Sauli, F. *Nucl. Instr. Meth.* **161** (1979) 461.
- Bronic, I.K. *Radiation Protection Dosimetry* **61**, No. 1-3 (1995) 263.
- Buckman, S.J., Hammond, P., King, G.C., and Read, F.H. *J. Phys. B: At. Mol. Phys.* **16** (1983) 4219.
- Budtz-Jorgensen, C. *Rev. Sci. Instr.* **63**, No. 1 (1992) 648.
- Budtz-Jorgensen, C., Bahnsen, A., Christensen, F.E., Mohl Madsen, M., Olesen, C., and Schnopper, H.W. *Proc. “EUV, X-Ray, and Gamma-Ray Instrumentation for Astronomy II” SPIE* **1549** (1991) 429.

- Budtz-Jorgensen, C., Bahnsen, A., Madsen, M.M., Olesen, C., Jonasson, P., Schnopper, H.W. *Nucl. Instr. Meth.* **348**, No. 2-3 (1994) 496.
- Budtz-Jorgensen, C., Bahnsen, A., Olesen, C., Madsen, M.M., Jonasson, P., and Schnopper, H.W. *SPIE Proc.* **1344** (1990) 91.
- Budtz-Jorgensen, C., Madsen, M.M., Jonasson, P., Schnopper, H.W., and Oed, A. *Proc. "X-Ray Instrumentation in Astronomy II" SPIE* **982** (1988) 152.
- Budtz-Jorgensen, C., Madsen, M.M., Jonasson, P., Westergaard, N.J., Bahnsen, A., Schnopper, H.W., and Oed, A. *Proc. "EUV, X-Ray, and Gamma-Ray Instrumentation for Astronomy and Atomic Physics" SPIE* **1159** (1989) 236.
- Castelli, C.M. and Fraser, G.W. *Nucl. Instr. Meth.* **376**, No. 2 (1996) 289.
- Chalmeton, V. "Neutron Radiography", *Acta Electronica* **16** (1973) 73.
- Charles, M.W. and Cooke, B.A. *Nucl. Instr. Meth.* **61** (1968) 31.
- Charles, M.W. *J. Phys.* **E5** (1972) 95.
- Charles, M.W., *Journal of Physics E: Sci. Instr.* **5** (1972) 95.
- Charpak, G. and Sauli, F. *Ann. Rev. Nucl. Part. Sci.* **34** (1984) 285.
- Charpak, G., Bouclier, R., Bressani, T., Favier, J., and Zupancic, C. *Nucl. Instr. Meth.* **62** (1968 a) 262.
- Charpak, G., Bouclier, R., Bressani, T., Favier, J., and Zupancic, C. *Nucl. Instr. Meth.* **65** (1968 b) 217.
- Christopherou, L.G., Maxey, D.V., McCorkle, D.L., and Carter, J.G. *Nucl. Instr. Meth.* **171** (1980) 491.
- Christopherou, L.G., McCorkle, D.L., Maxey, D.V., and Carter, J.G. *Nucl. Instr. Meth.* **163** (1979) 141.
- Christopherou, L.G. *Atomic and Molecular Radiation Physics*, Wiley-Interscience (1971).
- Colson, W.B., McPherson, J., and King, F.T. *Rev. Sci. Instr.* **44**, No. 12 (1973) 1694.

- Convert, P. and Forsyth, J. (editors) "Position Sensitive Detection of Thermal Neutrons", *Academic Press*, 1983.
- Crawford, R. *SPIE* "Neutrons, X Rays, and Gamma Rays" **1737** (1992) 210.
- Curz, R., Reinartz, R., Widdau, S., Schelten, J., Scholz, A., and Schafer, W. *Nucl. Instr. Meth.* **A273** (1988) 273.
- Cuzin, M. *Nucl. Instr. Meth.* **A253** (1987) 407.
- Damerell, C.J., Farley, F., Gilman, A., and Wickens, F. *Nucl. Instr. Meth.* **185** (1981) 33.
- Delaney, C.F.G. and Finch, E.C. "Radiation Detectors", *Clarendon Press*, 1992.
- Diethorn, W., *US Atomic Energy Commission Report NYO-6628* (1956).
- Director, B., Kaplan, S., and Perez-Mendez, V. *IEEE Trans. Nucl. Sci.* **NS-25** (1978) 358.
- Dixit, M.S., Oakham, F.G., Armitage, J.C., Dubeau, J., Karlen, D., Stuart, G.C., Taylor, S.C., Shipsey, I., Johnson, E., and Greenwald, A. *Nucl. Instr. Meth.* **A348** (1994) 365.
- Dolan, k.W. and Chang, J. *Proc. SPIE* **106** (1977) 178.
- Duerdoth, I., Snow, S., Thompson, N., and Lumb, N. *Nucl. Instr. Meth.* **A348** (1994) 356.
- Dwurazny, A., Jelen, K., and Zarebska, E. R. *Nucl. Instr. Meth.* **217** (1983) 301.
- Dwurazny, A., Jelen, K., and Zarebska, E.R. *Nucl. Instr. Meth.* **217** (1983) 301.
- Eichholz, G.G. and Poston, J.W. "*Principles of Nuclear Radiation Detection*", Ann Arbor Science (1979).
- Erskine, G.A. *Nucl. Instr. Meth* **105** (1972) 565.
- Fano, U. *Physical Review* **17**, No. 1 (1947) 26.
- Faruqi, A.R. *IEEE Trans. Nucl. Sci.* **NS-27** (1980) 644.
- Favata, F., Smith, A., Bavdaz, M., and Kowalski, T.Z. *Nucl. Instr. Meth.* **A294** (1990) 595.
- Feigl, B. and Rauch, H. *Nucl. Instr. Meth.* **61** (1968) 349.
- Feller, W.B. Private communication (1997).

- Fishwick, J. “*Applications of Lithium in Ceramics*”, Cahners, Boston (1974).
- Florent, J.J., Gaudaen, J., Ropelewski, L., and Sauli, F. *CERN report PPE/92-78* (1992).
- Fraga, F.A.F., Fraga, M.M.F.R., Marques, R.F., Margato, L.M.S., Goncalo, J.R.M.S., and Policarpo, A.J.P.L. *Proc. of 4th International Conference on Position-Sensitive Detectors*, Manchester (1996).
- Fraser, G W , “*X-ray Detectors in Astronomy*”, Cambridge University Press (1989).
- Fraser, G.W. “*Position Encoding for Imaging X-ray Detectors*”, PhD thesis, University of Leicester (1980).
- Fraser, G.W. and Pearson, J.F. *Nucl. Instr. Meth.* **A293** (1990) 569.
- Fraser, G.W. *Nucl. Instr. Meth.* **350**, No. 1-2 (1994) 368.
- Fraser, G.W. *Proc. of the Inter.Workshop on Superconducting Tunnel Junctions for X-ray Detection*, Napoli, (1990) 1.
- Fraser, G.W., Barstow, M.A., and Pearson, J.F. *Nucl. Instr. Meth.* **A273** (1988) 667.
- Fraser, G.W., Lees, J.E., Pearson, J.F., and Barstow, M.A. *Nucl. Instr. Meth.* **A310** (1991) 292.
- Fraser, G.W., Mathieson, E., and Evans, K.D. *Nucl. Instr. Meth.* **180** (1981 b) 269.
- Fraser, G.W., Mathieson, E., Evans, K.D., Lumb, D.H., and Steer, B. *Nucl. Instr. Meth.* **180** (1981 a) 255.
- Fraser, G.W., Pearson, J.F., Al-Horayess, O.S., Feller, W.F., and Cook, L. *Proc. “Neutrons, X-rays, and Gamma rays: Imaging Detectors, Material Characterisation Techniques and Applications”*, San Diego, 1992, *SPIE* **1737-31** (1992) 298.
- Fraser, G.W., Pearson, J.F., Smith, G.C., Lewis, M., and Barstow, M.A. *IEEE Trans. Nucl. Sci.* **NS-30** (1983) 455.
- Fraser, G.W., Private Communication (1996).
- Fulton, M.A., Kolodziejczak, J.J., and Ramsey, B.D. *SPIE* **1743** (1992) 125.

- Fuzesy, R.Z, Jaros, J., Kaufman, L., Marriner, J., Parker, S., Perez-Mendez, V., and Redner, S. *Nucl. Instr. Meth.* **100** (1972) 267.
- Gabriel, A. *et al.*, *Advances in Space Research* **15**, No. 7 (1995) 63.
- Garg, K.C. *IETE Technical Review* **9**, No. 4 (1992) 301.
- Garg, S.P., Murthy, K.B.S., and Sharma, R.C. *Nucl. Instr. Meth.* **336**, No. 1-2 (1993) 200.
- Garg, S.P., Murthy, K.B.S., and Sharma, R.C. *Nucl. Instr. Meth.* **357**, No. 2-3 (1995) 406.
- Gatti, E. and Rehak, P. *Nucl. Instr. Meth.* **225** (1984) 608.
- Geiger, H. and Rutherford, E., *Phil. Mag.* **24** (1912) 168.
- Geijsberts, M., Hartjes, F.G., Pannekoek, J.G., Schmitz, J., Udo, F. *Nucl. Instr. Meth.* **A313** (1992) 377.
- Gilmore, R. “*Single Particle Detection and Measurement*”, Taylor & Francis (1992).
- Gilvin, P., Mathieson, E., and Smith, G. *IEEE Trans. Nucl. Sci.* **NS-28**, No.1 (1981) 835.
- Gong, W.G., Wieman, H., Harris, J.W., Mitchell, J.T., Hong, W.S., and Perez-Mendez, V. *IEEE Trans. Nucl. Sci.* **41**, No. 4 (1994) 980.
- Goodfellow Metals Ltd., Cambridge Science Park, Cambridge CB4 4DT, England.
- Gott, R. and Charles, M.W. *Nucl. Instr. Meth.* **72** (1969) 157.
- Groshev, L.V., Demidov, A.M., Ivanov, V.A., Lutsenko, V.N., and Pelekhov, V.I. *Bull. Acad. Sci. USSR Phys. Ser.* **26** (1962) 1127.
- Grove, R., Lee, K., Perez-Mendez, V., and Sperinde, J. *Nucl. Instr. Meth.* **89** (1970) 257.
- Gruber, D., Blanco, P.R., Heindl, W.A., Pelling, M.R., Rothschild, R.E., and Hink, P.L. *Astronomy & Astrophysics Supplement Series* **120**, No. 4 SISI (1996) C641.
- Hailey, C.J., Ku, W.H.M., and Vartanian, M.H. *Nucl. Instr. Meth.* **213** (1983) 397.
- Harms, A.A. and McCormack, G. *Nucl. Instr. Meth.* **118** (1974) 583.
- Hayashi, M. *J. Phys. D: Appl. Phys.* **16** (1983) 581.

- Hendricks, R.W. *Nucl. Instr. Meth.* **102** (1972) 309.
- Hendricks, R.W. *Nucl. Instr. Meth.* **106** (1973) 579.
- Henize, K.G. *Sky and Telescope* **70**, No. 1 (1985) 5.
- Hoftiezer, J.H., Mutchler, G.S., Buchanan, J.A., Madigan, W.P., and Philips, G. C. *Nucl. Instr. Meth.* **147** (1977) 465.
- Israel, G.L. *Astrophysical J.* **474**, No. 1, pt. 2 (1997) L53.
- Janesick, J.R. and Blouke, M.M. *Sky and Telescope* **74** (1978) 238.
- Jeavons, A.P., Ford, N.L., Lindberg, B., and Sachot, R. *Nucl. Instr. Meth.* **148** (1978) 29.
- Kase, M., Akioka, T., Mamyoda, H., Kikuchi, J., and Doke, T. *Nucl. Instr. Meth.* **227** (1984) 311.
- Kaye, G.W.C. and Laby, T.H. “*Tables of Physical and Chemical Constants*”, Longman (1995).
- Kemshall, C.D., Beauchamp, K.G., and Benjamin, P.W. *Nucl. Instr. Meth.* **68** (1969) 153.
- Kharitonov, V.M. *Pribory i Tekhn. Eksperim.* **3** (1956) 45.
- Khristov, L.G. *Dokl. Bulg. Akad. Nauk* **10** (1947) 453.
- Klanner, R. *Nucl. Instr. Meth.* **A235** (1985) 209.
- Kleinknecht, K. “*Detectors for particle radiation*” Cambridge University Press (1986).
- Knoll, G. F., “*Radiation Detection and Measurement*”, Wiley (1979).
- Koori, N., Oda, S., Kawamura, K., Fujiwara, M., Nagayama, K., Takeda, N., Fujita, Y., Katayama, I., Morinobu, S., Yamazaki, T., and Ikegami, H. *Nucl. Instr. Meth.* **220** (1984) 453.
- Kowalski, T. *Nucl. Instr. Meth.* **A243** (1986) 501.
- Kowalski, T.Z. and Stopczynski, A.R. *Nucl. Instr. Meth.* **A323** (1992) 289.
- Kowalski, T.Z. *Nucl. Instr. Meth.* **A234** (1985) 521.
- Kruithof, A.A. *Physica* **7** (1940) 519.

- Kubota, S. *Journal of Physical Society of Japan* **29**, No. 4 (1970) 1017.
- Kuhlmann, W.R., Lauterjung, K.H., Schimmer, B., and Sistemich, K. *Nucl. Instr. Meth.* **40** (1966) 118.
- Lees, J. E. “*An Investigation of Soft X-ray Imaging and Polarimetry*”, PhD thesis, University of Leicester (1989).
- Legler, W. *Z. Physik* **140** (1955) 221.
- Leo, W. R. “*Techniques for Nuclear and Particle Physics Experiments*”, Springer-Verlag (1994).
- Leonov, N., Tyutikov, A., and Shishatskii, N. *Instr. Exp. Tech.* **22** (1980) 200.
- Loty, C. *Acta Electronica* **14** (1971) 107.
- Manchanda, R.K., Ye, Z., and Sood, R.K. *Nucl. Instr. Meth.* **292** (1990) 373.
- Mathieson, E. and Charles, M.W. *Nucl. Instr. Meth.* **72** (1969) 155.
- Mathieson, E. and Smith, G.C. *Nucl. Instr. Meth.* **A316** (1992) 246.
- Mathieson, E. *Nucl. Instr. Meth.* **A249** (1986) 413.
- Mathieson, E., Smith, G.C., and Gilvin, P.J. *Nucl. Instr. Meth.* **174** (1980) 221.
- McMahon, T., Wilson, J., Jones, T., Duerdoth, I., Lumb, N., Baines, J., Botterill, D., Edgecock, R., English, R., Payne, B., Bignall, P., Crone, G., and Esten, M. *Nucl. Instr. Meth.* **A348** (1994) 361.
- Medvedev, M.N. *Instruments and Experimental Techniques* **37**, No. 1, pt. 1 (1994) 1.
- Melamud, M., Burshtein, Z., Levi, A., and Schieber, M.M. *Appl. Phys. Lett.* **43** (1983) 275.
- Minakov, G.D., Pestov, Yu. N., Prokopenko, V.S., and Shekhtman, L.I. *Nucl. Instr. Meth.* **A326** (1993) 566.
- Miniscalco, W. *J. Lightwave Tech.* **9** (1991) 234.
- Mori, C., UNO, M. and Watanabe, T. *Nucl. Instr. Meth.* **196** (1982) 49.

- Murray, S.S. and Chappell, J.H. *Proc. SPIE* **597** (1985) 274.
- Oed, A. *Nucl. Instr. Meth.* **A263** (1988) 351.
- Ohashi, T., Ebisawa, K., Fukazawa, Y., Hiyoshi, K., Horii, M., Ikebe, Y., Ikeda, H., Inoue, H., Ishida, M., Ishisaki, Y., Ishizuka, T., Kamijo, S., Kaneda, H., Kohmura, Y., Makishima, K., Mihara, T., Tashiro, M., Murakami, T., Shoumura, R., Tanaka, Y., Ueda, Y., Taguchi, K., Tsuru, T., and Takeshima, T. *Pubs. Astro. Soc. of Japan* **48**, No. 2 (1996) 157.
- Ouseph, P. “*Introduction to Nuclear Radiation Detectors*”, Plenum Press (1975).
- Peacock, A., Andresen, R., Manzo, G., Taylor, B. *Space Sci. Rev.* **30** (1981) 525.
- Pearson, J.F., Private communication (1997).
- Peisert, A. and Sauli, F. *Drift and Diffusion in Gases: A Compilation*, CERN **84-08** (1984).
- Penning, F.M. *Phil. Mag.* **11** (1931) 961.
- Penning, F.M. *Physica* **1** (1934) 1028.
- Pestov, Yu. and Shekhtman, L. *BINP* **93-59** (1993).
- Pestov, Yu.N. and Shekhtman, L.I. *Nucl. Instr. Meth.* **A338** (1994) 368.
- Peterson, L.E. *Ann. Rev. Astr. Astrophys.* **13** (1975) 423.
- Policarpo, A.J.P.L., Alves, M.A.F., Dos Santos, M.C.M., and Carvalho, M.J.T. *Nucl. Instr. Meth.* **102** (1972) 337.
- Policarpo, A.J.P.L., Alves, M.A.F., Salet, M., Leite, S.C.P., and Dos Santos, M.C.M. **118** (1974) 221.
- Ramsey, B.D. and Agrawal, P.C. *Nucl. Instr. Meth.* **A278** (1989) 576.
- Ramsey, B.D. *Proc. SPIE* “*EUV, X-Ray, and Gamma-Ray Instrumentation for Astronomy III*” **1743** (1992) 96.
- Ramsey, B.D., Apple, J.A., Austin, R.A., Dietz, K.L., Minamitani, T., Kolodziejczak, J.J., Weisskopf, M.C. *Nucl. Instr. Meth.* **A383** (1996) 424.

- Raouf, M.A, Al-Soraya, A.M., and Al-Horayess, O.S. *Nucl. Instr. Meth.* **290**, No. 1 (1990) 208.
- Ribeirete, M.M.F, Policarpo, A.J.P.L., Salete, M., Leite, S.C.P., Alvis, M.A.F., and de Lima, E.P. *Nucl. Instr. Meth.* **214** (1983) 561.
- Ricci, D., Israel, G.L., and Stella, L. *Astronomy & Astrophysics* **299**, No. 3 (1995) 731.
- Rice-Evans, P. “*Spark, Streamer, Proportional and Drift Chambers*”, The Richelieu Press (1974).
- Rose, M.E. and Korff, S.A. *Phys. Rev.* **59** (1941) 850.
- Rutherford, E. and Geiger, H., *Proc. Roy. Soc.* **A81** (1908) 141.
- Sakurai, H., and Ramsey, B.D. *Nucl. Instr. Meth.* **A313** (1992) 155.
- Sakurai, H., Ramsey, B.D., and Weisskopf, M.C. *Nucl. Instr. Meth. A* **307** (1991) 504.
- Salomon, M., Armitage, J., Dixit, M., Fraser, W., Lam, D., and Oakham, G. *IEEE Trans. Nucl. Sci.* **41**, No.4 (1994) 817.
- Sanada, J. *Nucl. Instr. Meth.* **196** (1982) 23.
- Sauli, F. *CERN 77-09* (1977).
- Sauli, F. *Nucl. Instr. Meth* **A323** (1992) 1.
- Scarsi, L. *Astronomy & Astrophysics Suppl. Ser.* **97**, No. 1 (1993) 371.
- Schieber, M. and van den Berg, L.. eds. “Proc. 5th inter. workshop on HgI₂ nuclear radiation detectors”, *Nucl. Instr. Meth.* **213** (1983).
- Schmidt, S., Werthenbach, U., and Zech, G. *Nucl. Instr. Meth.* **A344** (1994) 558.
- Sephton, J.P. “*Fluctuation Phenomena in the Proportional counter*”, PhD thesis, University of Leicester (1981).
- Sephton, J.P., Turner, M.J.L., and Leake, J.W. *Nucl. Instr. Meth.* **A256** (1987) 561.
- Sharp, J. “*Nuclear radiation detectors*”, Methuen (1955).

- Shilov, A.L., Ershov, L.S., Ivanov, V.N., Il'Chenko, A.V., Morgovskii, L. Ya., and Tyutikov, A.M. *Instr. Exp. Tech.* **30** (1987) 538.
- Siegmund, O.H.W., Coburn, K., and Malina, R.F. *IEEE Trans. Nucl. Sci.* **NS-32** (1985) 443.
- Simon, D.G., deKorte, P.A.J., Peacock, A., and Bleeker, J.A.M. *Proc. SPIE* **597** (1985) 190.
- Sims, M.R., Thomas, H.D., and Turner, M.J.L. *IEEE Trans. Nucl. Sci.* **NS-28**, No. 1 (1981) 825.
- Sims, M.R., Thomas, H.D., Turner, M.J.L., *Nucl. Instr. Meth.* **199** (1982) 597.
- Sipila, H. *Nucl. Instr. Meth.* **133** (1976) 251.
- Sipila, H. *Nucl. Instr. Meth.* **133** (1976) 251.
- Sipila, H., Vanha-Honko, V., and Bergovist, J.
- Smith, A. and Bavdaz, M. *Rev. Sci. Inst.* **63**, No. 1 (1992) 689.
- Smith, A. and Turner, M.J.L. *Nucl. Instr. Meth.* **192** (1982) 475.
- Smith, A., Peacock, A., and Kowalski, T.Z. *IEEE Trans. Nucl. Sci.* **NS-34**, No. 1 (1987) 57.
- Smith, A.D. and Allington-Smith, J.R. *IEEE Trans. Nucl. Sci.* **NS-33** (1986) 295.
- Smith, G.C., Pearson, J.F., and Mathieson, E. *Nucl. Instr. Meth.* **192** (1982) 383.
- Snyder, H.S. *Phys. Rev.* **72** (1947) 181.
- Soltau, H., Holl, P., Kemmer, J., Krisch, S., Vonzanthier, C., Hauff, D., Richter, R., Brauniger, C., Shwaab, G., Strudr, G., Trumper, J., Kendziorra, E., and Kramer, J. *Nucl. Instr. Meth.* **377**, No. 2-3 (1996) 340.
- Sood, R.K., Manchanda, R.K., and Ye, Z. *Adv. Space Res.* **11**, No. 8 (1991) 421.
- Sood, R.K., Manchanda, R.K., and Ye, Z. *Adv. Space Res.* **11**, No. 8 (1991) (8) 421.
- Sood, R.K., Ye, Z., and Manchanda, R.K. *Nucl. Instr. Meth. A* **344** (1994) 384.
- Sugaira, T., Murakami, K., Tanaka, H., and Akimoto, H. *Yogyo Kyokai Shi.* **72** (1964) 71.
- Sumner, T.J., Rochester, G.K., and Hall, G. *Nucl. Instr. Meth. A* **273** (1988) 701.

- Swinbanks, D. *Nature* **326**, No. 6111 (1987) 322.
- Tabata, T., Ito, R., and Okabe, S. *Nucl. Instr. Meth.* **103** (1972) 85.
- Tait, W.H. “*Radiation Detection*” Butterworths (1980).
- Tanaka, Y. *Pubs. Astro. Soc. of Japan* **36**, No. 4 (1984) 641.
- Thomas, H.D. “*The use of Xenon in Position Sensitive Proportional Counters*”, PhD thesis, University of Leicester (1984).
- Thomas, H.D. and Turner, M.J.L. *Nucl. Instr. Meth.* **221** (1984) 175.
- Thomas, H.D. and Turner, M.J.L. *IEEE Trans. Nucl. Sci.* **NS-30**, No. 1 (1983) 499.
- Thomas, H.D., Sims, M.R., and Turner, M.J.L. *IEEE Trans. Nucl. Sci.* **NS-29** (1982) 148.
- Tokanai, F., Sakurai, H., Noma, M., Gunji, S., Ueno, H., Anzai, T., Kato, F., and Hoshina, T. *IEEE Trans. Nucl. Sci.* **41**, No. 4 (1994) 1042.
- Tomitani, T. *Nucl. Instr. Meth.* **100** (1972) 179.
- Townsend, J.S. “*Electricity of gases*”, Clarendon Press, Oxford (1915).
- Trow, M. and Smith, A. *Rev. Sci. Instr.* **63**, No. 1 (1992) 693.
- Tsoufanidis, N. “*Measurement and Detection of Radiation*”, Hemisphere Publishing Corporation; McGraw-Hill Series in Nuclear Engineering (1983).
- Turala, M. and Vermeulen, J.C. *CERN EP/82-79* (1982).
- Turner, M.J.L. and Thomas, H.D. *Publ. Astron. Soc. Japan* **41** (1989) 345.
- Turner, M.J.L., Private communication (1993).
- Ubertini, P., Bazzano, A., Cocchi, M., Lapadula, C., and Sood, R.K. *Astrophysical J.* **386**, No. 2, pt. 1 (1992) 710.
- Uozumi, Y., Sakae, T., Matoba, M., Ijiri, H. and Koori, N. *Nucl. Instr. Meth.* **A324** (1993) 558.
- Ward, A.L. *Phys. Rev.* **112** (1958) 1852.
- Weisskopf, M. *Proc. SPIE* **597** (1985) 228.

- Wijsman, R.A. *Phys. Rev.* **75** (1949) 833.
- Wilkins, S.W., Stephenson, A.W., Nugent, K.A., Chapman, H., and Steenstrup, S. *Rev. Sci. Instrum.* **60** (1989) 1026.
- Wilkinson, D. “*Ionisation Chambers and Counters*” Cambridge University Press (1950).
- Williams, A. and Sara, R.I. *Inter. J. Appl. Rad. Isotopes* **13** (1962) 229.
- Winkler, C. *Astronomy & Astrophysics Supplement Series* **120, No. 4 SISI** (1996) C637.
- Wiza, J.L. *Nucl. Instr. Meth.* **162** (1979) 587.
- Wolff, R. *Nucl. Instr. Meth.* **115** (1974) 461.
- Yamane, M. *Journal of Physical Society of Japan* **15, No. 6** (1960) 1076.
- Ye, Z., Sood, R.K., Sharma, D.P., Manchanda, R.K., and Fenton, K.B. *Nucl. Instr. Meth.* **A329** (1993) 140.
- Zastawny, A. *J. Sci. Instr.* **43** (1966) 179. *Nucl. Instr. Meth.* **176** (1980) 381.
- Zastawny, A. *Nucl. Instr. Meth.* **A385** (1997) 239.
- Zombeck, M.V., David, L.P., and Harnden, F.R. *Proc. “EUV, X-ray, and Gamm-Ray Instr. Astr. VI”, SPIE* **2518-25** (1995).